UNIVERSITY OF
BIRMINGHAM

OPTIMIZATION AND CONTROL OF A DUAL-LOOP EGR SYSTEM IN A MODERN DIESEL ENGINE

BY
YUNFAN ZHANG

A THESIS SUBMITTED TO
THE COLLEGE OF ENGINEERING AND PHYSICAL SCIENCE OF
THE UNIVERSITY OF BIRMINGHAM

DOCTOR OF PHILOSOPHY

Department of Mechanical Engineering
School of Engineering
College of Engineering and Physical Science
The University of Birmingham

July 2018

ABSTRACT

This thesis is devoted to the study of intelligent optimization algorithm and advanced control methods for the air path in a light duty automotive diesel engine.

The conventional manual engine calibration methods are reaching their limits due to the strong nonlinearity, coupling effects and delay in the diesel engine's air path. There is a demand to simplify this process and reduce the time consumption. In this thesis, an intelligent transient calibration method is proposed, which is a model-based optimization approach using the chaos-enhanced accelerated particle swarm optimization (CAPSO) algorithm. The real-time model in the simulation platform developed in this study is validated and used as the virtual engine to conduct the co-simulation with the algorithm. The optimization variables are controller parameters of the PI-based controllers for the dual-loop EGR (DLEGR) and variable geometry turbocharger (VGT). The optimization objects are the tracking performance of the engine MAP, MAF and LPEGR fraction and the optimization results are sent to the engine test bench via ETAS INAC. The engine experiments show that the proposed method can successfully locate the global optimal results of the controller parameters during the engine transients under various working conditions. The engine dynamic response is improved and a measurable reduction of engine fuel consumption is achieved.

The model predictive control (MPC) is selected for the controllers of DLEGR and VGT in the air-path of the diesel engine. The control objects are the engine boost pressure and EGR mass flow which must be regulated during engine transients. Both the TMPC and the Neural Network MPC (NMPC) approach are investigated. Compared with the conventional PID controller, the MPC-based controllers show better reference trajectory tracking performance. The overshoot and settling time of the control objects are successfully reduced, which lead to reduced emissions in the engine transients. In addition, the fuel economy of the engine is improved. These two controllers both achieve the same level of reference trajectory tracking and fuel consumption reduction. The real-time capability of the proposed TMPC and NMPC controller are validated on the HIL test platform and the test results show that the response of the actual controller is close to the offline simulation results. The signal lag is negligible and acceptable, which means the proposed controllers could be implemented on the real engine.

ACKNOWLEDGEMENT

First and foremost, I would like to express my sincerely appreciate to my supervisor Professor Hongming Xu for his guidance and support throughout my PhD study. I would also like to thank my second supervisor Dr. Oluremi Olatunbosun for his encouragement and help. In addition, valuable advice from Professor Akabar Ghafourian and Professor Miroslaw L. Wyszynski. Special thanks are due to Ben Neaves and his team at Jaguar Land Rover for their continuous support and advice. Without this support and advice, completion of the work in this thesis would not have been possible.

I acknowledge the support from Advantage West Midlands and European Regional Development Fund, Jaguar Land Rover, Shell Global Solutions, AVL and Cambustion. Without their testing equipment and technical advice, I could not finish my PhD study.

Great thanks should go to the team of laboratory technicians- Carl Hingley, Jack Garrod, Lee Gauntlett and Peter Thornton- for their support with respect to all test facility matters. I am also grateful to post-doctoral research fellows and former PhD students in the lab, Dr. Guoxiang Lu, He Ma, Cheng Tan, Jianyi Tian, Arumugam Sakunthalai Ramadhas, Dai Liu, Changzhao Jiang, Chongming

Wang and Wei Zhang, for their generous help and technical support. I also acknowledge the advice from Mrs. Janet Hingley in thesis writing. This thesis was partly copy edited for conventions of language, grammar and spelling by Janet's Proofreading Service.

Special thanks belong to my friends and colleagues at the University of Birmingham: Quan Zhou, Ziyang Li, Ji Li, Yuanzhuo Mei, Tawfik Badawy, Sohiel Zeraati Rezaei, Olalere Rafiu Kayode, Aawishkar Dharmadhikari, Lewis Parry, Scott Cash and Carlo Coratella for their great support in my study and social life.

Finally, I would like to express my sincere gratitude to my family and my girlfriend from the bottom of my heart for their unconditional support and encouragement. I am so lucky to have them during my PhD study. It is impossible for me to get this degree without their understanding and companion.

CONTENTS

LIST OF PUBLICATIONS

1. ***Yunfan Zhang***, Guoxiang Lu, Hongming Xu*, Ziyang Li. “Tunable model predictive control of a turbocharged diesel engine with dual loop exhaust gas recirculation”, *Proceedings of the Institution of Mechanical Engineers, Part D: Journal of Automotive Engineering.* (in press, available online from October 2017)

2. ***Yunfan Zhang***, Quan Zhou, Ziyang Li, Ji Li, Hongming Xu*. “Intelligent Transient Calibration of a Dual-loop EGR Diesel Engine using Chaos-enhanced Accelerated Particle Swarm Optimization Algorithm”, *Proceedings of the Institution of Mechanical Engineers, Part D: Journal of Automotive Engineering*. (in press, available online from May 2018)

3. Quan Zhou, ***Yunfan Zhang***, Ziyang Li, Ji Li, Hongming Xu*, Oluremi Olatunbosun. “Cyber-Physical Energy-Saving Control for Hybrid Aircraft-Towing Tractor based on Online Swarm Intelligent Programming”, *IEEE Transactions on Industrial Informatics*. (in press, available online from December 2017)

4. Guoxiang Lu, ***Yunfan Zhang***, Hongming Xu*, Ziyang Li, Ben Neaves. “Multiple Model Predictive Control for Diesel Engines with Dual Loop Exhaust Gas Recirculation”, 3rd Biennial International Conference on Powertrain Modelling and Control, PMC 2016, Loughborough, UK.

5. Ziyang Li, Ji Li, Quan Zhou, ***Yunfan Zhang***, and Hongming Xu*, “Intelligent Air/Fuel Ratio Control Strategy with a PI-like Fuzzy Knowledge Based Controller for GDI Engines”, Proceedings of the Institution of Mechanical Engineers, Part D: Journal of Automobile Engineering. (in press, available online from June 2017)

6. Yunfan Zhang, Quan Zhou, Ziyang Li, Ji Li, Hongming Xu*, “Nonlinear Model Predictive Control of a Dual-loop EGR Diesel Engine”. (Prepare to Submit)

LIST OF ABBREVIATIONS

APSO	Accelerated Particle Swarm Optimization
BSFC	Brake Specific Fuel Consumption
CAC	Chare Air Cooler
CI	Compressed Ignition
CO	Carbon Monoxide
DOC	Diesel Oxidation Catalytic
DOE	Design of Experiments
DPF	Diesel Particulate Filter
ECU	Engine Control Unit
EGR	Exhaust Gas Recirculation
F&E	Filling & Emptying
FMEP	Friction Mean Effective Pressure
GA	Genetic Algorithm
HCCI	Homogeneous Charge Compression Ignition
HIL	Hardware-In-the-loop
HPEGR, HP, hpegr	High Pressure loop EGR
IC	Internal Combustion
IMEP	Indicated Mean Effective Pressure

I/O	Input/output
LPEGR, LP, lpegr	Low Pressure loop EGR
LTC	Low Temperature Combustion
MAF	Mass Air Flow
MAP	Manifold Absolute Pressure
MBC	Model-Based Calibration
MIMO	Multiple-Input-Multiple-output
MPC	Model Predictive Control
NARX	Nonlinear AutoregRessive network with eXternal inputs
NEDC	New European Driving Cycle
NMPC	Neural Network Model Predictive Control
PCCI	Premixed Charged Compression Ignition
PM	Particulate Matter
PMEP	Pumping Mean Effective Pressure
PSO	Particle Swarm Optimization Algorithm
QP	Quadratic Programming
RCCI	Reactivity Controlled Compression Ignition
RDE	Real Driving Emissions
SCR	Selective Catalytic Reduction
SI	Spark Ignition
SISO	Single-Input-Signe-output

SQP	Sequential Quadratic Programming
THC	Total Hydrocarbon Emissions
TMPC	Tuneable Model Predictive Control
VGT, vgt	Variable Geometry Turbocharger
VVA	Variable Valve Actuation
VVT	Variable Valve Timing
WLTP	Worldwide Harmonized Light vehicles Test Procedures

LIST OF SYMBOLS

A	Effective area of the valve
A_{hpegr}	HPEGR valve position
A_{hpegr}	LPEGR valve position
A_{vgt}	VGT rack position
C	Discharge coefficient
c_p	Specific heat ratio
I_{turb}	Turbo Charger inertia
M	Mass flow rate
N_{eng}	Engine Speed
P, p	Pressure
PR	Pressure ratio
Q	Quantity
Q_{LHV}	Lower heat value of diesel
R	Ideal gas constant
R_{egr}	Total EGR rate
R_{LP}	LPEGR fraction
ref	Reference value

T	Temperature
V	Volume
γ	Specific heat ratio
η	Efficiency
β	Attraction parameter
α	Convergence parameter
ρ	Convergence factor
|| ||	Euclidean distance

Symbols used as suffixes

amb	Ambient Condition
c, comp	Compressor
cyl	Cylinder
d	Displacement volume
ds	Downstream
em	Exhaust manifold
exh	Exhaust
fuel	Fuel Injection
HP, hp	HPEGR valve
im	Intake Manifold
LP, lp	LPEGR valve
max	Maximum

min	Minimum
set, sp	Setpoint
us	Upstream

LIST OF FIGURES

LIST OF TABLES

CHAPTER 1 INTRODUCTION

Internal combustion engines have been the most widely used power supplier for vehicles in the last century (Takashi Suzuki, 1997). The vehicles with alternative powertrain such as electricity, hybrid and fuel cell have been developed rapidly in the recent decades. But the drawbacks such as the limited power storage, high cost and system stability still inhibit their wide utilization on the market (Hannan et al., 2014). Meanwhile, numerous emerging technologies have been invented and applied to modern internal combustion engines. So it is forecasted that the internal combustion engines would still play an important role as the power supplier of vehicles even in the 21st century (Kalghatgi, 2018).

1.1 Background

1.1.1 Environmental Protection and Energy Scenario

The environmental protection has drawn the public's attention in recent years especially the greenhouse gas emissions as it affects the global environment dramatically. The figure below shows the proportion of the global greenhouse gas. The carbon dioxide (CO2) occupies 65% of it and the fossil fuel is the main contributor. The statistical analysis points out the transportation section accounts

for 28% of the whole CO2 generation. The majority of the greenhouse gas from transportation section is resulting from the combustion of petroleum-based products(“Sources of Greenhouse Gas Emissions US EPA,” n.d.). Focusing on the vehicles, the CO2 emissions of the internal combustion engines must be reduced.

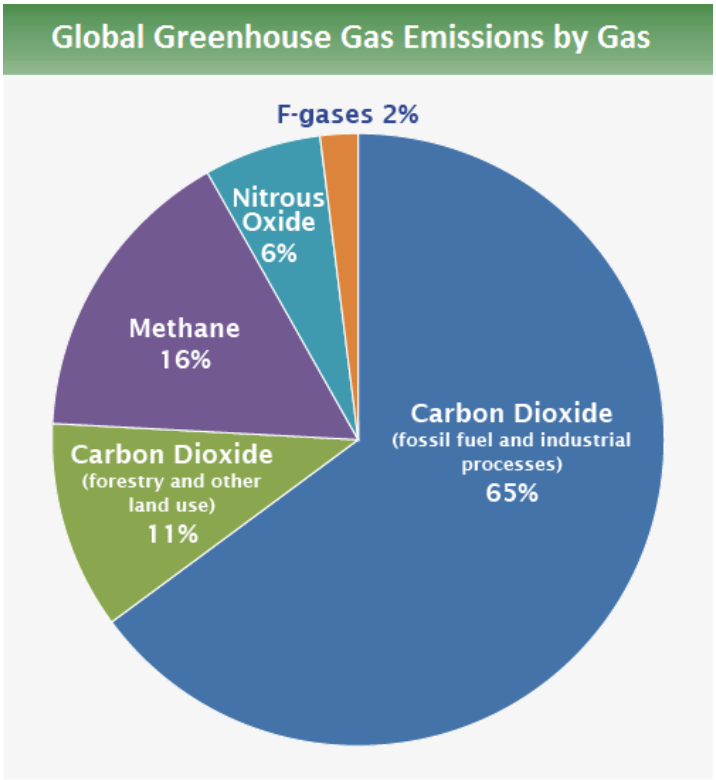

Figure 1-1 Proportion of Global Greenhouse Gas Emissions(“Global Greenhouse Gas Emissions Data | Greenhouse Gas (GHG) Emissions | US EPA,” n.d.)

To meet the demand of CO2 reduction, the authorities have established CO2 limits for internal combustion engines and launched policies to encourage the development of electric vehicles (Yang Zifei, 2014). The EU has declared the average CO2 generation of passenger cars would be limited to 95g/km by 2020. The percentage of internal combustion engines on vehicles would be shrunk to

59% in 2030 based on the projection from the EU parliament's committee. But internal combustion engines are still adopted in the vast hybrid systems (Gurney et al., 2009). All these factors make it extremely essential for internal combustion engines to obtain more optimal fuel economy. Fortunately, compared with gasoline engines, diesel engines achieve higher thermal efficiency due to their higher compression ratio and lean fuel combustion(Bonilla et al., 2014). These characteristics make the diesel engine a competitive candidate to meet required CO2 demands with the help of emerging engine technologies.

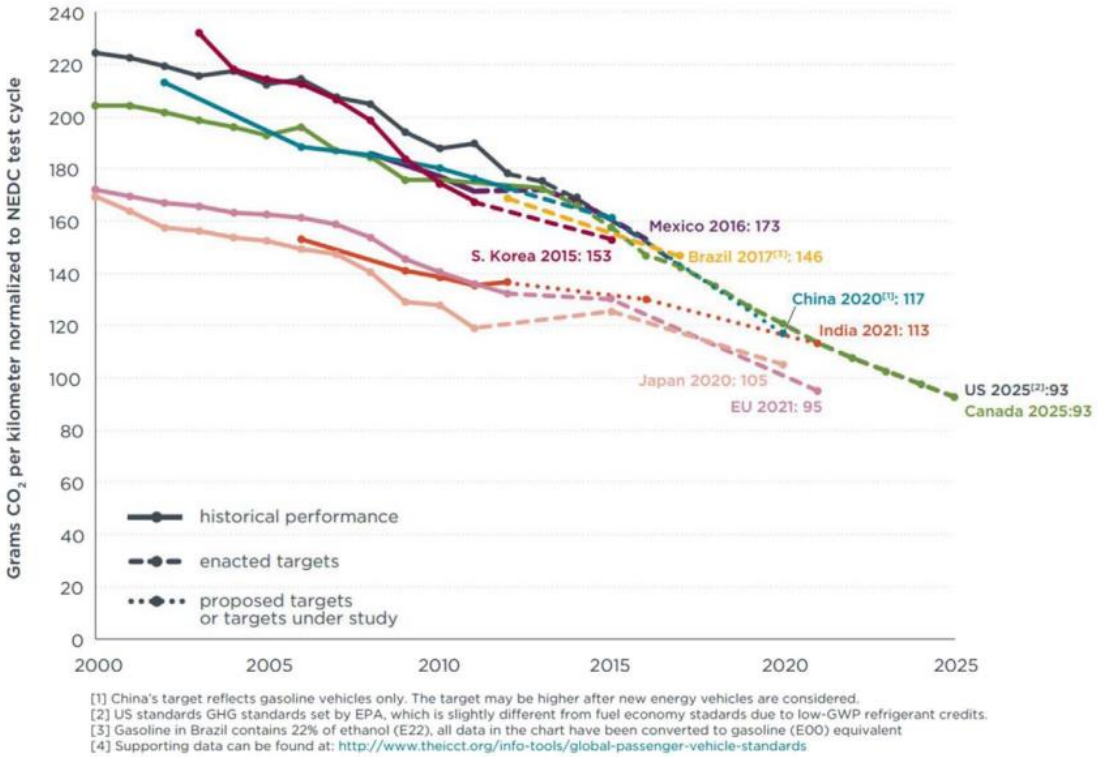

Figure 1-2 Global CO2 Regulation for Passenger Cars in NEDC Cycle, g/km (Enang and Bannister, 2017)

1.1.2 Challenges for Diesel Engine Emissions

As the environmental protection is more and more important, the internal combustion engine is continuously required to reduce the engine out emissions. The pollution caused by the vehicles with diesel engines are concerned by the public and the authority since the Volkswagen scandal erupted in September 2015 (“How VW tried to cover up the emissions scandal - BBC News,” n.d.). The NOx and PM emission are the major challenges for diesel engine. There is a risk that the diesel engines will be abandoned in light-duty vehicles.

The emission legislation for light-duty diesel engines in European Union was firstly proposed in 1992, which involved gaseous emissions such as carbon dioxide (CO), nitrogen oxides (NOx) and total hydrocarbon (THC). The engine particulates are also included. The detailed information of the EU emission standard for light-duty diesel vehicles is shown in the table below.

Table 1-1 EU Emission Standard for Light Duty Diesel Vehicles (DELPHI, 2017)

Stage	Year	CO	HC+NOx	NOx	PM	PN
		g/km				*/km
Euro 1	1992	2.72 (3.16)	0.97 (1.13)	-	0.14	-
Euro 2, IDI	1996	1.0	0.7		0.08	-
Euro 2, DI	1996	1.0	0.9	-	0.10	-
Euro 3	2000	0.64	0.56	0.50	0.05	-
Euro 4	2005	0.50	0.30	0.25	0.025	-
Euro 5a	2009	0.50	0.23	0.18	0.005	-
Euro 5b	2011	0.50	0.23	0.18	0.005	6.0×10^{11}
Euro 6b	2014	0.50	0.17	0.08	0.005	6.0×10^{11}
Values in brackets are conformity of production (COP) limits						

It could be observed that all engine emissions have shrunk massively. The engine NOx is limited in the EURO 3 emission standard. The latest EURO 6 standard is 84% smaller when compares with EURO 3 standard. The particulate mass is reduced by 80% when compares the EURO 6b and EURO 4 standard. Apart from the mass-based limitation on particulates, the limitation of particulate number appears since the EURO 5b standard. All these changes bring extra challenges for diesel engines to survive in the market.

The previous engine research on emissions mainly focuses on steady states conditions. However, the engine transient operations are the majority in real driving scenarios. The fuel economy and emission generation are deteriorated seriously when compared with the steady state calibrations (Heuwetter et al., 2014). So the new European driving cycle (NEDC) is adopted as the standard driving cycle since EURO 4 standard to simulate the transient scenarios and

evaluate emissions (Rakopoulos and Giakoumis, 2009). To cover a wider engine operation range and get close to the real-world driving conditions, the worldwide harmonized light vehicles test procedure (WLTP) is proposed. This test cycle is already utilized for EURO 6d, which makes it more difficult for manufacturers to pass the emission test (DELPHI, 2017). In the future, the real-world driving emissions would be considered in the emission standard. So, it is necessary to further explore the potential of diesel engines on emission reduction, especially in transient conditions. The detailed review about engine transient studies, test cycles and real-world driving emissions would be shown in chapter 2 (literature review).

1.1.3 Development of Diesel Engines

To overcome the above-mentioned challenges, modern diesel engines become more efficient and cleaner with the help of advanced technologies invented in the past decades. As mentioned above, the major requirements on future diesel engines are better fuel economy and less emission generation. The figure below demonstrates a typical modern light-duty diesel engine with featured designs and equipment.

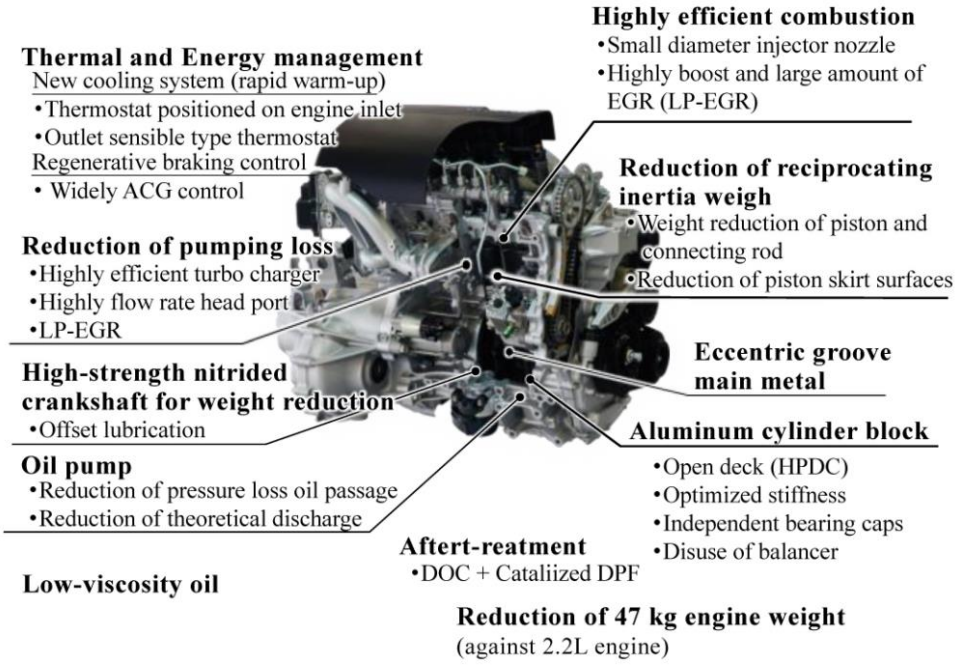

Figure 1-3 Technologies for Modern Diesel Engine (Nishio et al., 2013)

The engine contains a high-pressure common-rail direct injection system and injector nozzles are designed into small-diameter to optimize the fuel spray so that the combustion efficiency is improved. A VGT (variable geometry turbocharger) is adopted to enhance the compressor performance. Other than conventional single loop EGR (exhaust gas recirculation), a dual-loop EGR (HPEGR and LPEGR) system is installed in the engine's air path. The engine NOx and pumping loss can be reduced simultaneously. In terms of aftertreatment devices, the diesel oxidation catalyst (DOC) can convert HC and CO into harmless products effectively. The DPF (diesel particulate filter) could decrease more than 95% of particulates at the engine's tailpipe (Johnson, 2008). Due to the strict emission legislation, the selective catalyst reactor (SCR) is also added

to the exhaust pipe to further reduce the NOx emission (Haga et al., 2015). Besides, improvements in engine material, mechanical design, engine manufacture etc. are beneficial for achieving ultra clean and high efficiency. To cope with more and more engine components, engine control units (ECU) with powerful computational ability are developed, which lead to an increasing demand for engine calibration methods and control methods.

To obtain the optimal performance, engine variables and controller parameters should be calibrated. This process is defined as the engine calibration or optimization which is very important for the engine development. But the calibration process is also very time consuming and requires large costs. There is strong demand for fast and efficient engine optimization methods. Since the engine is a typical multi-input-multi-output (MIMO) system, the optimization method should also handle the multiple objects simultaneously, especially overcome the trade-off effects.

With the increased complexity of diesel engines, the difficulty of optimal engine control during transient conditions has increased dramatically. It is found that the conventional PID control strategy based on look-up tables has met its limitation when dealing with high non-linearity and coupling effects such as the engine's air path (Lu et al., 2016). But fortunately, the rapid development of the engine ECU provides the computational capability and allows the use of other control methods.

Many emerging control strategies including fuzzy logic control (R.S.Wijetunge et al., 2000), robust control (Langthaler and Re, 2008), neural network control (Hafner et al., 2000) and model predictive control (Borhan et al., 2015) have been proposed and implemented in diesel engine successfully. The future engine control strategy should shift from non-model-based control to model-based control. To further improve the diesel engine's performance, the controllers of modern diesel engines should contain both feedback control (FB) and feed-forward control (FF). As it is shown in figure 1-4, it is achieved by constrained

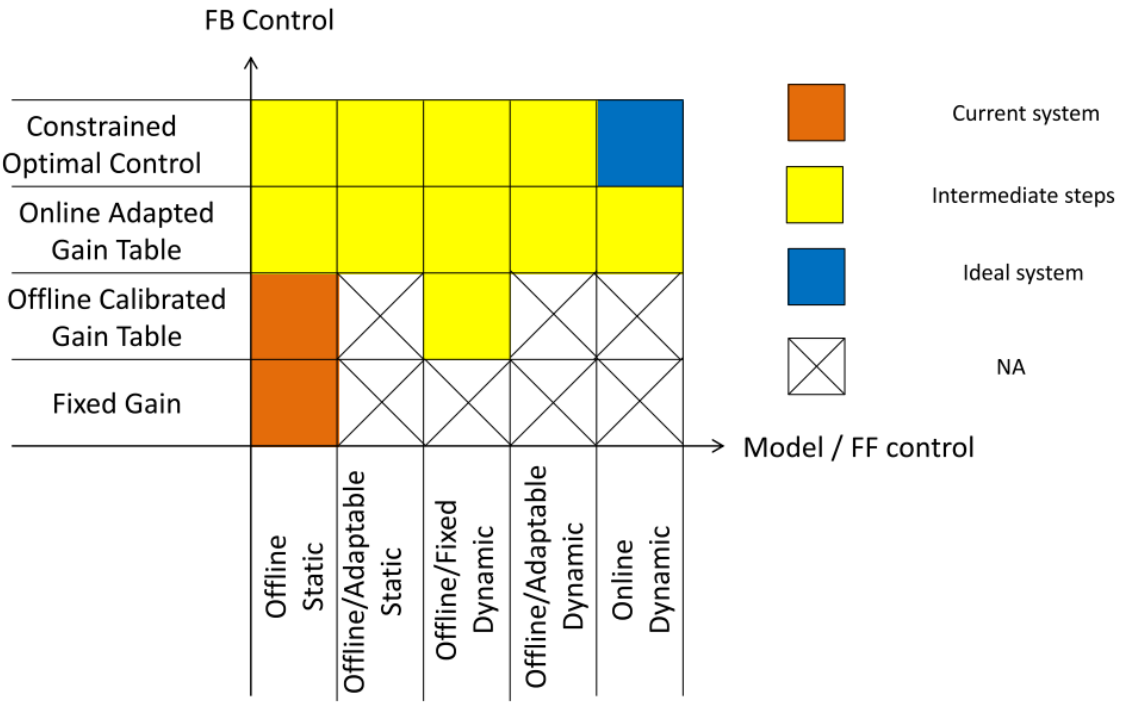

Figure 1-4 Control for Optimal Engine Performance (Wang, 2018)

1.2 Thesis Objectives

The main objectives of the thesis are the optimization and control of the diesel engine's air path with dual-loop EGR. The purpose is to improve the diesel engine's transient performance (accurate trajectory tracking of the engine parameters with less overshoot and shorter setting time) and reduce the engine 's fuel consumption. It is to be achieved by developing intelligent transient calibration algorithm and investigating advanced model-based controllers. The specific targets of the study are listed:

- To commission the transient engine test bench at the University of Birmingham for the research on engine control.

- To develop the real-time control-oriented model of the diesel engine's air path as the simulation platform for the research activities in the thesis.

- To create the intelligent transient calibration method based on the natural-inspired evolutionary algorithm and validate the calibration results via engine tests.

- To build controllers based on model predictive control (MPC) methods for the air path of the diesel engine. The proposed controllers are also validated on the HIL test platform.

1.3 Thesis Outline

This thesis consists of seven chapters, the detailed outline is shown below.

Chapter 1- Introduction

The basic background of modern light-duty diesel engines and motivations of the study are shown in this chapter. The research objects and approaches are also presented.

Chapter 2- Literature Review

This chapter reviews the publications that are relevant to the thesis. The first section discusses diesel engine's air path. Afterwards, it demonstrates the previous research on diesel engine's transient operations (including engine test cycles). The third section focuses on the review of engine modelling approaches. The last two sections summarize the trend of engine's model-based optimization and control strategies.

Chapter 3- Experimental Setup and Methodology

The experimental setup is formed by the detailed introduction of the test facility, including both hardware and software. It firstly introduces the test engine, the engine test bench and the measurement devices for the engine performance. Then it presents the simulation platform and the HIL test platform. The

methodology of the thesis is followed in the second section, which contains the detailed introduction of the investigation approach and the engine test plans.

Chapter 4- Intelligent Transient Calibration Algorithm

This chapter introduces an intelligent transient calibration method for the engine controller based on chaotic-enhanced particle swarm optimization algorithm (CAPSO). The calibration objects in this case are the engine's MAF, MAP and LPEGR fraction. The accuracy of the simulation platform is validated by the test data at the beginning. The proposed algorithm is compared with the original engine calibration through several case studies.

Chapter 5- Tunable Model Predictive Control

The development of an engine's air-path controller based on tunable model predictive control approach (TMPC) is presented. The systematic design framework of the TMPC controller is also included. The controller performance is evaluated by the comparison between the TMPC controller and the conventional PID controller, which is conducted on the simulation platform. An additional HIL validation process is added to the end of this chapter. The agreement between the offline simulation and the actual ECU response is good.

Chapter 6- Non-linear Model Predictive Control

This chapter proposes a control approach based on neural network model predictive control (NMPC) for the diesel engine's air-path. A neural network model plays the role as the internal prediction model for the controller. To solve the optimization problem of the controller at each time interval, a real-time solver based on the evolutionary algorithm is also built. The controller performance is evaluated by the comparison between the NMPC controller and the conventional PID controller. The HIL tests show that the results of the pure simulation and the actual ECU response are close.

Chapter 7- Conclusions and Future Work

This chapter summarizes the achievements and finds in this thesis. A few ideas and suggestions for the next stage work are provided.

CHAPTER 2 LITERATURE REVIEW

This chapter reviews the publications that are related to the work in this thesis. The components mainly cover the diesel engine's air path, studies on engines' transient behaviors, control-oriented modelling, engine optimization methods and engine control strategies.

2.1 Air Path of the Diesel Engine

The objectives of the thesis are the optimization and control of the diesel engine's air-path. This section reviews the publications that are related to the engine's gas exchange process (including the EGR) and the characteristics of diesel engine's transient emissions.

2.1.1 Exhaust Gas Recirculation

To meet continuously strict emissions' legislation, exhaust gas recirculation (EGR) is applied to modern diesel engines as an *in-situ* approach to NOx reduction (Agarwal et al., 2011; Zhang et al., 2013).

To reduce NOx, the EGR system reduces the oxygen concentration in the engine inlet gas and lowers the in-cylinder flame temperature (Shi et al., 2017). It can be

categorized into thermal (Ladommatos et al., 1997), dilution (Ladommatos et al., 1996) and chemical effects (Ladommatos et al., 1996b; Ladommatos, Abdelhalim and Zhao, 1997). The dilution effect is the main reason for the NOx reduction and the trade-off engine particulates. The EGR gas replaces the inlet fresh air with the CO2 and water vapour, which has higher heat capacity. Therefore, the heat capacity of the inlet gas is increased; but the lower flame temperature reduces the rate of soot oxidation/re-burning and the reduced oxygen lowers the air-fuel ratio. This will bring a negative impact to the engine's HC, CO and soot emissions (Agarwal et al., 2011). Higher soot generated inside the engine also leads to engine deposits, degradation of lubrication oil and enhanced engine wear (Tan and Hu, 2016). The EGR effects on diesel combustion and pollutant formation can be summarized by the figure below:

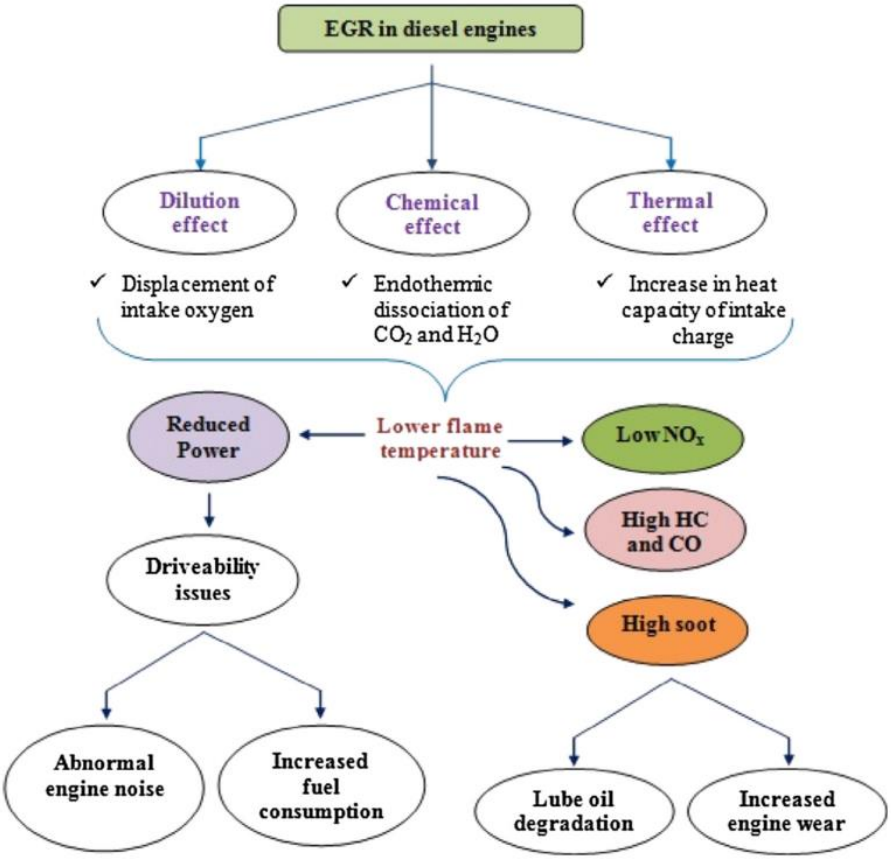

Figure 2-1 EGR Effects on Diesel Engine Combustion and Emissions (Thangaraja and Kannan, 2016)

When the EGR system is installed in diesel engines, the EGR rate should be investigated. The mass measurement defines the EGR rate as the percentage of the EGR mass flow in the total intake mixture. The gas concentration measurement is based on the CO2 or oxygen concentration in the intake and exhaust manifold (Keeler and Shayler, 2008;Maiboom et al., 2009; Desantes et al., 2010). Focusing on the research objectives in this thesis, a properly calibrated and controlled EGR rate is important.

The EGR rate is closely related to the engine's working conditions. At low engine

load conditions, the EGR rate is acceptable in a wider range (up to 50% or more); as the exhaust gas still contains sufficient oxygen and limited CO2 and water vapours. At high load conditions, the oxygen in the exhaust gas becomes insufficient and the inert constituent has a more significant influence, along with the increased exhaust temperature; this restricts the maximum EGR rate (Zheng et al., 2004). This principle should be reflected in the controller's design process. The acceptable EGR rate should be limited by the boundary conditions.

The three commonly used EGR configurations are high-pressure loop EGR (HPEGR), low-pressure loop EGR (LPEGR) and dual-loop EGR (DLEGR) (Zhang et al., 2017). The HPEGR redirects the exhaust gas from the exhaust manifold to the intake manifold with the help of the pressure difference. The LPEGR gas flows from downstream of the aftertreatment device to upstream of the compressor. Normally, the EGR gas in both HPEGR and LPEGR is cooled down by the EGR coolers. However, it should be noticed that even though the cooled EGR is more effective on the engine's NOx reduction (Zheng et al., 2002), the hot EGR gas could achieve a shorter ignition delay and increase the thermal efficiency, due to the increased intake gas temperature (Dishy et al., 1995). The selection between cooled EGR gas and uncooled hot EGR gas should be considered based on the specific engine working conditions. The DLEGR contains both the HPEGR loop and the LPEGR loop. Figure 2-2 demonstrates the structure of a DLEGR system. The advantages of HPEGR are a quick

response in transient conditions and its simple structure. However, HPEGR also suffers coupling effects with the engine's VGT and has difficulties in providing sufficient EGR gas in low-speed high-load conditions (Maiboom et al., 2008;Zhang et al., 2017). When LPEGR is used, the coupling effect between the HPEGR and the VGT is relieved, so the VGT control has less burden during transient conditions (Zhang et al., 2017). The engine pumping loss is then reduced, which is beneficial for the BSFC reduction (Xin and Xin, 2013). Besides that, the engine's DPF reduces the amount of soot and particulates in the EGR gas, which limits the excessive smoke (Shah and Maiboom, 2009). The lower temperature of the intake gas is beneficial for further reducing the engine's NOx (Park and Bae, 2014). The mixture between the EGR gas and the fresh air is enhanced due to the long distance of the gas tube. More homogenous cylinder gas flow can be acquired, which is helpful to reduce engine PM (van Aken et al., 2007). Due to the tiny pressure difference and the long pipeline, LPEGR has a slower dynamic response and more complex control to maintain the desired EGR mass flow, when compared to single HPEGR (Reifarth and Ångström, 2010). Compressor fouling is another problem for LPEGR which is caused by water and particulates in the exhaust gas. The advantages of both HPEGR and LPEGR could be found in DLEGR (Zamboni and Capobianco, 2012). Thus, diesel engine designers have started to adopt this EGR configuration to generate less emissions, achieve a quicker dynamic response and improve fuel economy in

recent years. It provides the flexibility of the EGR split strategy under the same total EGR rate (Park and Choi, 2016). Both HP and LP EGR could be operated efficiently under various working conditions due to their different dynamic responses (Nishio et al., 2013).

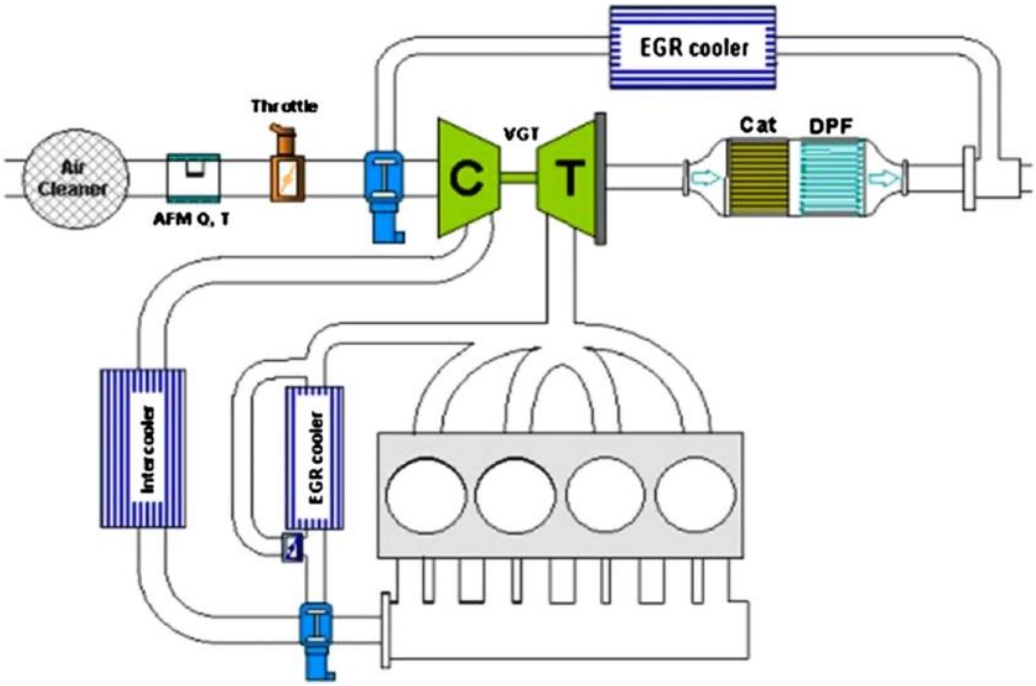

Figure 2-2 Sketch of a Dual-loop EGR System for Light-duty Diesel Engine, Combining both HPEGR and LPEGR (Millo et al., 2012)

2.1.2 Gas Exchange Process

In four-stroke internal combustion engines, the gas exchange process involves both an induction process and an exhaust process. The main function of the engine's air path is to remove the burned gas at the end of the power stroke and prepare the required inlet gas for the next cycle (Heywood, 1988). To promote the performance and efficiency of the air path, new technologies have emerged for

modern light-duty engines. The figure below shows the targets of a diesel engine's air path design. This thesis mainly investigates a diesel engine's air path (dual-loop EGR and VGT system).

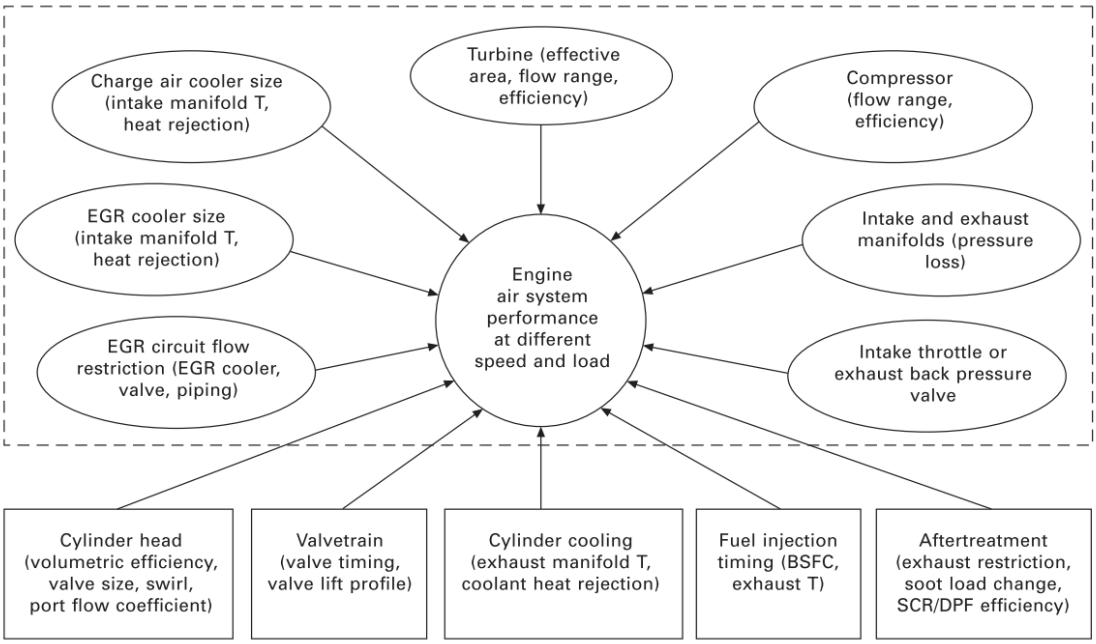

Figure 2-3 Diesel Engine Air Path Design (Xin and Xin, 2013)

Turbocharger is a boosting device in the diesel engine's air-path. It is formed by a compressor, a turbine and a connection shaft. The purpose of adopting this device in modern diesel engines is to increase the engine output by enlarging the mass air flow drawn into the engine (Stone, 1999). The work carried out by researchers at the University of Bath showed that the fuel consumption of diesel engines could be significantly reduced if the intake gas pressure is excessively boosted (Turner et al., 2014). Among the numerous types of turbocharger, the variable-geometry turbocharger (VGT) is now widely used; it regulates the exhaust gas received by the turbine freely via pivoted nozzle vanes (Zamboni

and Capobianco, 2013). Besides, other structures such as a multi-stage turbocharger, supercharger/turbocharger combination and variable geometry compressor (VGC) have also been developed to improve the performance of the boosting system (Dickinson et al., 2015)(Plianos and Stobart, 2008; Dickinson et al., 2015; Zhou et al., 2015). However, the conventional turbocharger powered by the exhaust gas suffers weak boosting capability at low engine loads and a slow transient response (Terdich and Martinez-Botas, 2013). To overcome these drawbacks, electrically assisted turbochargers (EAT) are created. The power assistance for the turbocharger could also contribute to enhance the engine's peak power and lead to a lower pumping loss (Xue and Rutledge, 2017). Although the turbo efficiency is successfully improved, the EAT system requires a special bearing design, solid durability of electrical parts and a higher manufacturing cost, which are all big challenges.

Similar to the variable valve actuation (VVA) on gasoline engines, studies of varying the valve timing or even valve lift have also been carried out on diesel engines (Gelso and Lindberg, 2013). Many of them focus on the timing of the IVC because it has a significant impact on the amount of gas in the cylinders. It is found that late IVC brings lower fuel consumption, as well as fewer emissions (Zhang et al., 2016). In addition, when the diesel VVT combines with LTC combustion mode, an extra reduction on engine is acquired (Murata Y., 2006; Murata et al., 2008). Another highlight of diesel VVA is the reopening of intake or

exhaust valves during the exhaust or intake stroke (defined as 2IVO and 2EVO respectfully). The test results show that the 2IVO strategy could effectively reduce HC emissions and shorten engine warm-up time in cold-start situations (Dittrich et al., 2010). However, this kind of valve actuation is limited due to the sharp increase of the smoke during transient conditions (Fessler and Genova, 2004).

2.1.3 Characteristics of Diesel Engine Transient Emissions

Diesel engines generate higher values of gaseous phase emissions (NOx, THC and CO) and particulate emissions during transient operations, when compared with steady state conditions (Rakopoulos and Giakoumis, 2006). Figure 2-4 shows a typical characteristic of engine NOx and particulates during acceleration conditions.

The research on diesel engines' transient emission characteristics has been speeded up by the progress on real-time emission analysers. With the help of fast-response emission testing equipment, cycle by cycle results can be acquired (Davis and Peckham, 2007). In both speed transient and load transient conditions, the trajectory of EGR valves and the related changes of intake charge composition are the primary responsibility for the emission spikes (Glewen et al., 2011). For the load increment cases, the EGR valves close rapidly to reduce the burden on the VGT system and meet the desired EGR rate; the in-cylinder temperature rises due to the larger amount of fuel injection. These two factors

dominate the overshoot of NOx. The system delay triggers the low air-fuel ratio and extends the duration of diffusion combustion, which enhances the particulates' formation (Kang P. V. Farrell and Kang P. V. Farrell, 2005). Under deceleration conditions, the engine will undergo very lean ignition or even partial burn. A large amount of THC and nucleation particles will still be generated during this period of time (Tian et al., 2014). Different VGT settings have also been tested in transient experiments; the opening of the VGT vane could decrease the engine back pressure effectively, but engine emissions were little improved (Black et al., 2007). The engine-out emission is also affected by the length of the transient periods. When the load ramp time is shorter, the spikes of engine NOx and particulates will become more significant (Hagena et al., 2006).

It should be noticed that the trade-off between NOx and PM still exists, even in transient scenarios. For the control point of view, a properly controlled air-fuel ratio is the key to obtain acceptable emissions during transient conditions (Yokomura et al., 2004).

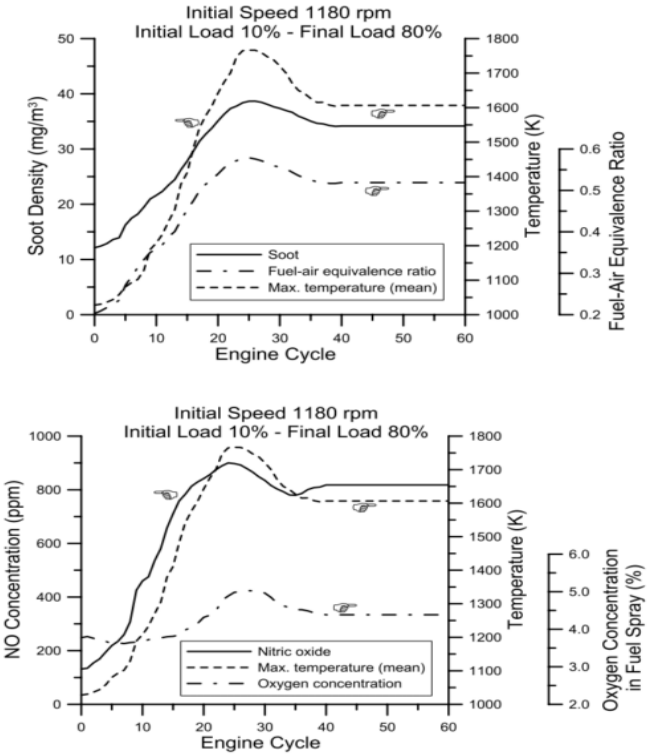

Figure 2-4 Typical NOx and PM Trajectories Measured with Engine Tests during Step-changed Loads (Tian, 2015)

2.2 Diesel Engine Transient Operation

Steady state conditions of diesel engines have been widely investigated and studied in the past decades. However, the major operation patterns of automotive engines in a real-driving condition occur under transient conditions. Engine test results from driving cycles have found that the emissions during transient periods, including acceleration, deceleration and cold start, are the primary source of pollution (Tian et al., 2014). Higher PM, NOx, THC and CO emissions are generated due to the deteriorated performance of engine gas exchange, fuel injection and combustion (Wijetunge et al., 1999). This issue has drawn

researchers' attention in recent years, with the continuous existence of the strict emissions' standards. In this section, the characteristics of diesel engines' transient operations and emissions' behaviours are briefly introduced and analyzed.

2.2.1 System Delay in Transient Operations

The most notable issue of turbocharged diesel engines during transient operations is the mismatch between the gas supply and the fuel injection. The engine fuel injection system could respond to the transaction of the engine's working conditions instantly (Catania et al., 1996); but the diesel engine's air path, including the complex EGR loops and boosting systems, adapts to the transient scenarios slower, which results in a torque deficit and peaks of engine-out emissions.

This topic has been discussed extensively by many researchers and in many studies. There are three main aspects for the system delay in the engine's air path: mechanical, thermal and fluid dynamic phenomena (Rakopoulos and Giakoumis, 2009). Mechanical effect mainly refers to the friction losses and turbo inertia; the thermal factor refers to the heat transfer to the cylinder walls and manifold surfaces. It is claimed by many researchers that the fluid inertia of the gas and the engine's EGR effect account for the primary cause of the air path's system delay (Hu et al., 2014). To minimize the system delay of the diesel

engine's air path, numerous efforts have been made. The majority of the work focuses on the improvement of the fluid dynamics; only limited work mentions the upgrades on the mechanical and thermal aspects (Alberer et al., 2013). The VGT device optimizes the diesel engine's transient response by controlling the vane freely, which accelerates or decelerates the compressor rapidly to overcome the rotation shaft inertia and the flow inertia of the exhaust gas (Filipi et al., 2001). With the help of advanced methodologies on EGR control, the coupling effect between the EGR and VGT could be effectively eliminated. The system delay caused by the EGR effects is minimized (van Nieuwstadt, 2003; Friedrich et al., 2009; Wang et al., 2011; Hong et al., 2015). In summary, the factors that bring the system delay are shown in detail in Figure 2-5.

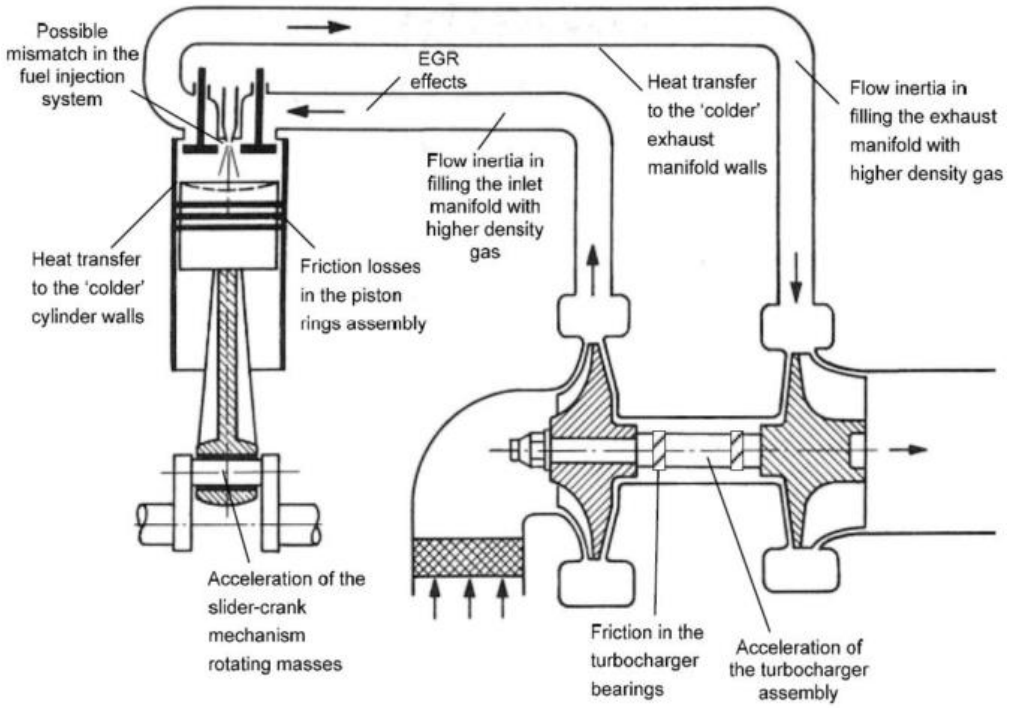

Figure 2-5 Schematic Diagram of a Diesel Engine's Turbo-lag in Transient Operations (Rakopoulos and Giakoumis, 2009)

2.2.2 Engine Test Cycles

The transient performance of internal combustion engines plays an important role in the daily use of modern vehicles. Research has been conducted to investigate the factors that influences the emissions in test cycles since last century (Shayler et al., 1997). The engine test cycles are also continuously changed to get closer to real-world conditions. The evaluation of an engine's fuel consumption and other emissions in Europe and other major markets is originally based on the New European Driving Cycle (NEDC) and its accompanying test protocol (Armas et al., 2013). This procedure is called type-approval (TA). The NEDC contains four equal urban driving segments (UDC), which represents the condition of low vehicle speed and low engine load; and one extra-urban driving segment (EUDC), which accounts for higher vehicle speed and engine load (Sileghem et al., 2014). However, the NEDC cycle has difficulties in reflecting the engine's behaviours under real-driving conditions (Dimaratos et al., 2016). This phenomenon will lead to a mismatch between the real engine emissions and TA emissions (including fuel economy). Besides, the mismatch is reported to be increasing with time (Fontaras et al., 2017a). To control and reverse this increasing gap, the Europe Commission requires a new test procedure to be established to replace the conventional NEDC.

In recent years, the concept of real-life driving conditions has been considered in

the vehicle test procedure and the tail pipe emissions should be measured by on-board portable emission measurement systems (PEMS) (Bishop et al., 2016). From 2017, new vehicles in Europe must undergo the World-wide Harmonized Light Duty Test Cycle (WLTC) and its corresponding test procedure (WLTP) in a TA test. The WLTP cycle is composed of four speed phases: low, medium, high and extra high phases. Based on the present studies, moving from the NEDC to the WLTC has had a more significant impact on diesel engines than on gasoline engines (Pavlovic et al., 2016). The new WLTP brings several improvements to the testing and procedure compared to the current NEDC test. The new WLTP corrects the wrong provisions in the NEDC cycle. Several new provisions are also added to make the WLTP more robust and more representative of fuel consumption and emissions in real driving conditions (RDE) (Bianco-Rodriguez et al., 2016). Focusing on the engine, the WLTP involves more aggressive transient scenarios (more engine acceleration, deceleration and less steady state conditions) and lower engine temperature at the starting period. Besides, the engine needs to be operated in a wider range than the NEDC cycle. Research has been conducted to investigate the differences of engine fuel consumption and emissions under the NEDC cycle and the WLTP cycle (Lee et al., 2013). The results show that the NEDC is far from being a realistic driving cycle. It is reflected in the figure below. The speed of the test vehicle only covers a smaller range when compares the NEDC with the WLTP. The absolute values of vehicle

acceleration and deceleration of the NEDC cycle are also smaller. The numbers of vehicle acceleration and deceleration (vehicle transient conditions) are also increased massively in the WLTP.

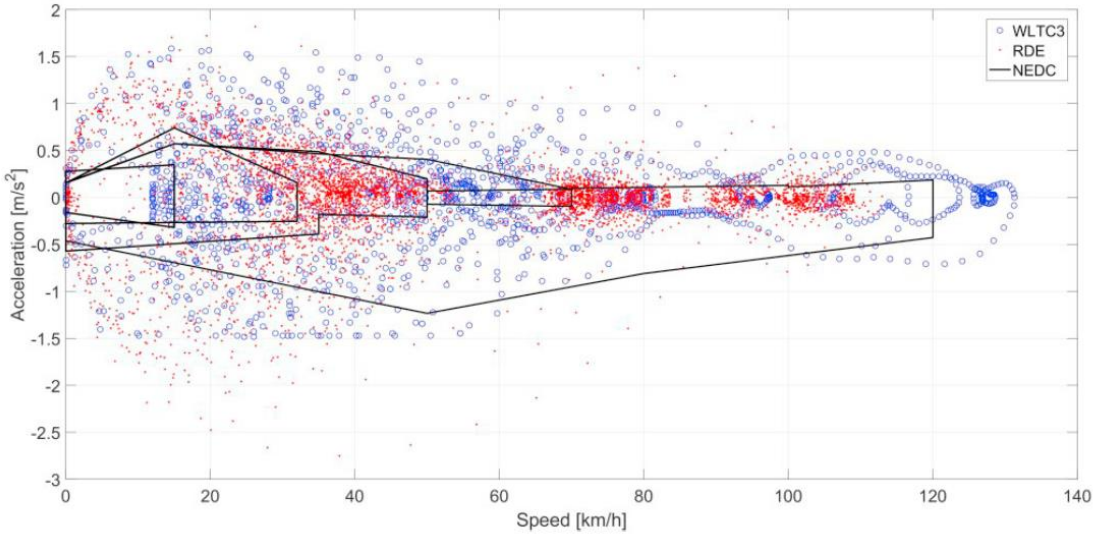

Figure 2-6 Acceleration versus Speed under NEDC, WLTP and RDE Cycles (Donateo and Giovinazzi, 2017)

However, the gap between the laboratory results and the real-world driving results still exists due to the various driving behaviours, engine cold start, weather conditions, vehicle conditions, traffic conditions and the use of on-board devices etc. (Fontaras et al., 2017b). It is also observed that road driving occurs at lower average speeds with higher frequency and magnitudes of accelerations. The frequent acceleration required by road cycles was 100% higher than the WLTC and the relative positive acceleration (RPA) demanded by the road cycles was found to be 60% higher in real-world driving patterns and thereby contributes to higher emissions and fuel consumption (Kumar Pathak et al., 2016). The EU6d

Emission Regulation requires real driving emissions as an additional type approval requirement within the 2017-2020 timeframe, to consider the influence of the road profile, the ambient conditions and the traffic situation, as well as the behaviour of the driver. The new test uses a portable emissions monitoring system (PEMS) to measure on-board, as well as the behaviour of the driver (Donateo and Giovinazzi, 2017).

The new engine test cycles and the consideration of real-world driving conditions make it essential for future diesel engines to be further upgraded and there is a real demand for an intelligent engine management system. Additional work such as mapping the driver's pattern, geographic information, traffic information and advanced thermal management could be considered in engine controller development and calibration processes (Zacharof et al., 2016).

2.3 Control-oriented Model of Modern Diesel Engines

Engine modelling is an indispensable tool in engine optimization and the controller development process. Various modelling approaches have been proposed, but the trade-off between model detail and computational speed is quite significant, as shown in Figure 2-7; it limits their applications for different cases. In this section, the modelling approaches of modern diesel engines are reviewed. They are classified as physical modelling methods, semi-physical

modelling methods and non-physical modelling methods. The current trend of engine modelling is to integrate these techniques together (Millo et al., 2011).

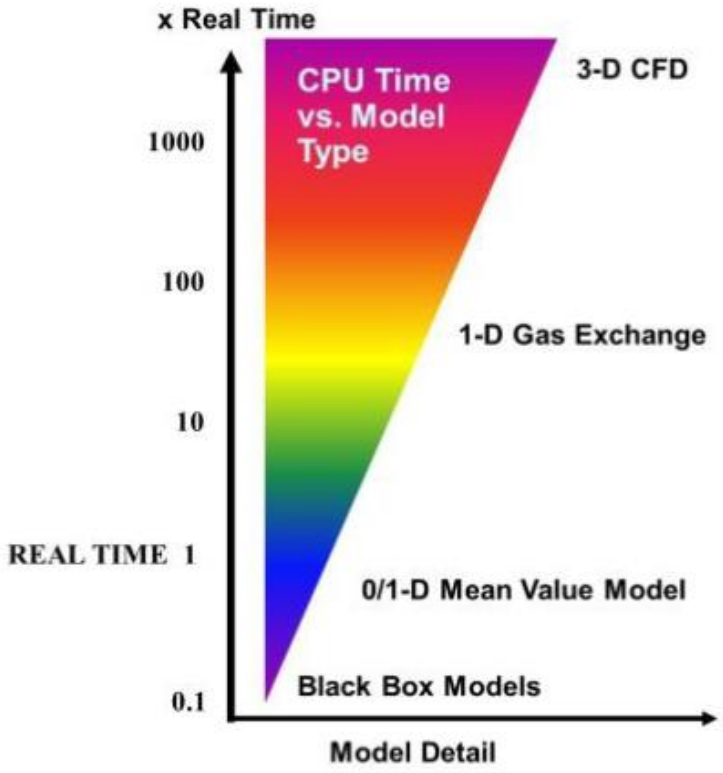

Figure 2-7 Comparison of Different Engine Modelling Methodologies on Model Detail and Computational Speed (Millo et al., 2011)

2.3.1 Physical Modelling Methods

The physical modelling methods are developed based on equations of energy and thermodynamic principles. Heywood classifies the thermodynamic models as the quasi-steady model, the filling and emptying model and multi-zone models (Heywood, 1988). The work in this thesis mainly focuses on engine control strategies, so the modelling approaches reviewed are related to control-oriented

models; the 3D-CFD method is not discussed in this section. Even though they present the most details and highest accuracy, the high computational costs become a burden for the purposes of engine control (Haiyan et al., 2006).

Quasi-steady models are developed based on the assumptions that some engine transient responses are the same as a sequence of steady points. This method presents the engine thermodynamics through the dynamics of a turbocharger and crankshaft and empirical correlations (Grondin et al., 2004). Quasi-steady models are commonly selected to simulate the engine power generation, mass air flow rate and exhaust temperature (Filipi et al., 2001). It is also agreed that combustion signals in each engine cycle could be regarded as a quasi-static condition (Assanis et al., 2000). Besides, quasi-steady models could provide a rough guidance of trends of engine-out emissions according to current engine speed and load (Kirchen et al., 2009). In brief, the quasi-steady model has the advantage of rapid computational speed; but the accuracy and compatibility are unacceptable when a complex system needs to be modelled. A large amount of data is also required for empirical correlation, which makes it difficult to transform one quasi-steady model to another engine platform.

Filling and emptying models, also known as zero-dimensional models, were originally invented to overcome the drawbacks of quasi-steady models (Watson and Marzouk, 1977). The engine components such as pipes, manifolds and

cylinders are regarded as a series of control volumes, which assume the gas mixtures are in uniform states. Some detailed processes (such as fuel spray vaporization) in the engine are then ignored (Kumar et al., 2013). A filling and emptying model successfully simulates the in-cylinder combustion process based on the first law of thermodynamics (Watson and Janota, 1982). Another case in which the filling and emptying methods are frequently seen is in manifolds' modelling (Taraza et al., 2008; Wahlstrom et al., 2011). The manifold volume and surface heat loss are considered. Although the pressure waves inside the manifolds are neglected, an acceptable model fitting rate could still be obtained at common engine operating ranges from the publications mentioned above.

Mean-value models based on the filling and emptying method are capable of capturing most of the characteristics of engine transient operations, especially for the engine's air path (Cieslar et al., 2014). Therefore, this type of model is widely used as the simulation platform for engine controller designs (Nikzadfar and Shamekhi, 2015; Stürzebecher et al., 2015). The mean-value models are developed based on the conservation of mass and energy and the ideal gas law (Haiyan et al., 2006). One significant feature involves a minimum set of differential equations to reduce the computational costs. In mean-value models, the time is an independent variable. It neglects the discrete cycles of the engines (Guzzella and Onder, 2010). Figure 2-8 shows the architecture of a mean-value model of a turbocharged diesel engine with dual-loop EGR. It estimates nine engine states

for pressure, temperature and mass flow rate. The dynamic corrections concerning the temperature, time constant and the fluid transport delay are taken into consideration to improve the model accuracy. However, the number of states in mean-value models may vary among different cases (Tan, 2015). Thus, this technique has been widely used to design the controller of turbocharged diesel engines.

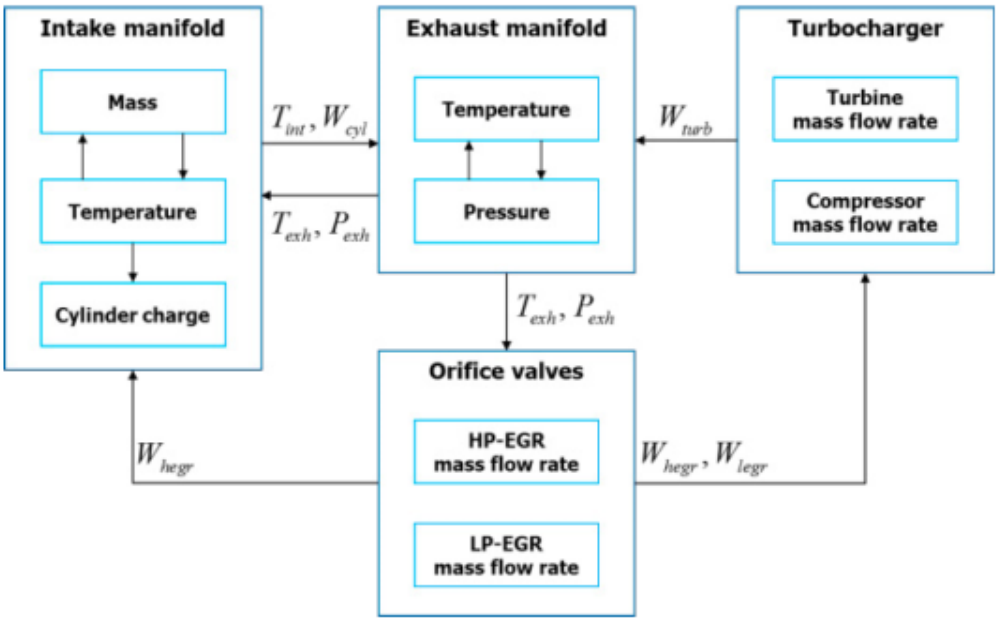

Figure 2-8 The Architecture of a Mean Value Model of a Turbocharged Diesel Engine (Kyunghan et al., 2015)

The multi-zone models are created to simulate the engine combustion process and pollution formation in detail. Compared with other modelling methods, the multi-zone models consider the spatial distribution of products and temperature inside the volume (Xue and Caton, 2012). As a result, it becomes possible to analyses the detailed in-cylinder air-fuel distribution and gas components.

Research work has proved that multi-zone models could simulate combustion signals such as heat release rate, IMEP and heat. They could also contribute to predict the particles and NOx from diesel engines (Midlam-Mohler and Guezennec, 2006). The detailed physical mechanisms behind the multi-zone models enhance the model accuracy, which is beneficial for simulating the engine combustion process or emissions' formation; but rare cases are found for controller design due to the model complexity and defects in real-time performance.

2.3.2 Semi-Physical Modelling Methods

The characteristics of both physical models and non-physical models are contained in semi-physical models. The physical or chemical principles are still embedded inside (Grondin et al., 2004). It has been proved this modelling method is reliable over a wide range. The computational speed is quicker than the pure physical model and the accuracy is better than the pure empirical model (D'Ambrosio et al., 2014). However, the emerging research work has successfully proved that this method is reliable for online estimation of engine-out emissions (Grahn et al., 2012; D'Ambrosio et al., 2014; Karaky et al., 2015). The semi-physical NOx model proposed in 2015 shows a good association between the physical fundamentals of NOx formation and empirical correlation, based on experimental data (Querel et al., 2015). In terms of the diesel particulates, a semi-

physical model is operated as a function of several significant engine parameters (Finesso et al., 2014). Unfortunately, it is found to be difficult to capture the detailed combustion process with the semi-physical models, especially during transient conditions (Rakopoulos and Giakoumis, 2006).

2.3.3 Non-Physical Modelling Methods

Non-physical models, also known as ‘black-box’ models, are suitable for modelling complex systems with little understanding of the principles and fast computational speed. The relationship between model inputs and outputs are established purely based on massive experimental data. The non-physical-based models can be recognized as linear black-box models and non-linear black-box models.

Due to the complexity of physical models, linear black-box models can be deployed as controller internal predictors. These models are identified based on massive experimental data and the model structure is pre-defined (Morari and Lee, 1999). The state space model is a typical type. The rapid computational speed is a major advantage due to the simple model structure. However, these linear black-box models have an acceptable accuracy within the range of the training data. Considering the strong non-linearity of the diesel engine’s air path, the application is limited.

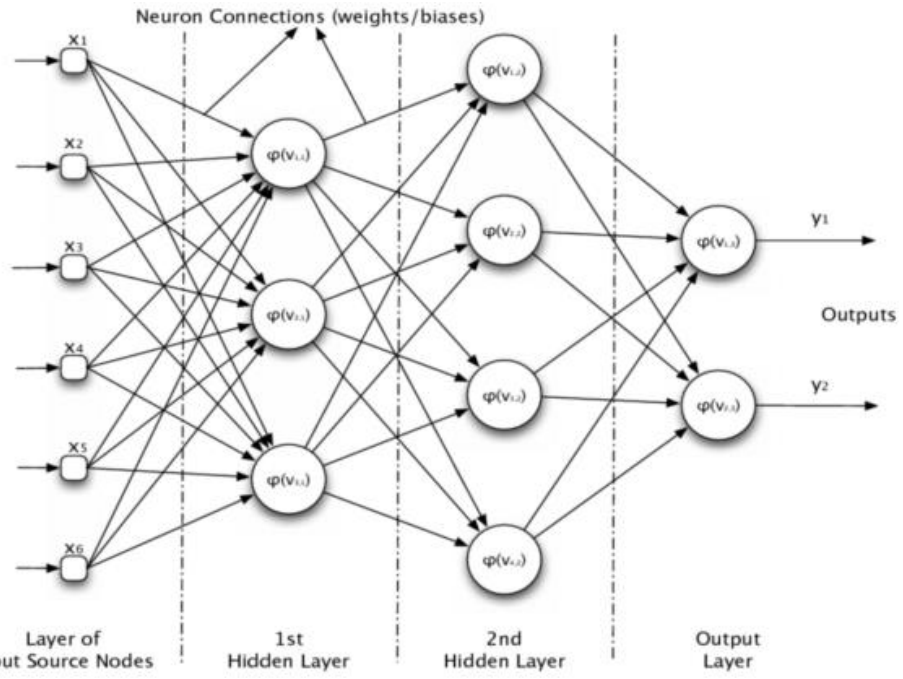

Figure 2-9 Structure of Multilayer Feed-forward Artificial Neural Network (Maass et al., 2011)

In terms of non-linear 'black-box' modes, the artificial neural network (ANN) models are widely used modelling methods for internal combustion engines (Garg et al., 2012). With sufficient experimental data, ANN models are able to capture the selected parameters' highly complex and non-linear characteristics (Atkinson and Mott, 2005; Boruah, 2016). Figure 2-9 shows a general schematic view of a multilayer feed-forward ANN model to predict the in-cylinder pressure. The main training parameters for this type of ANN model are the number of layers, weight values and bias values. The trained NOx model could provide an accurate prediction over the NEDC cycle (Zhang et al., 2015). Research work on the effect of the neurons' number on the model fitting rate indicates that a larger neurons' number is helpful to promote the outputs' accuracy (Alonso et al., 2007). The

recurrent neural network (RNN) model is another type of ANN model commonly used in engine research. The main difference with RNN models is that they take the past input and output values into account for future prediction (Arsie et al., 2010). It has been successfully applied in the case of engine virtue sensing, air path identification and engine air-fuel ratio control (Arsie et al., 2004; Kamat et al., 2006; Kushwaha et al., 2015). A comparison was conducted between RNN and ANN on diesel engine NOx prediction. The simulation and experiment results show that the neural network architecture with historical information is beneficial for the emission prediction during transient scenarios. An accurate prediction (correlation coefficient within the range of 0.987–0.999, mean absolute percentage error in the range of 1.1–4.57%) of the engine NOx is observed in most engine working conditions (De Cesare and Covassin, 2011). The typical structure of an RNN model is shown in Figure 2-10.

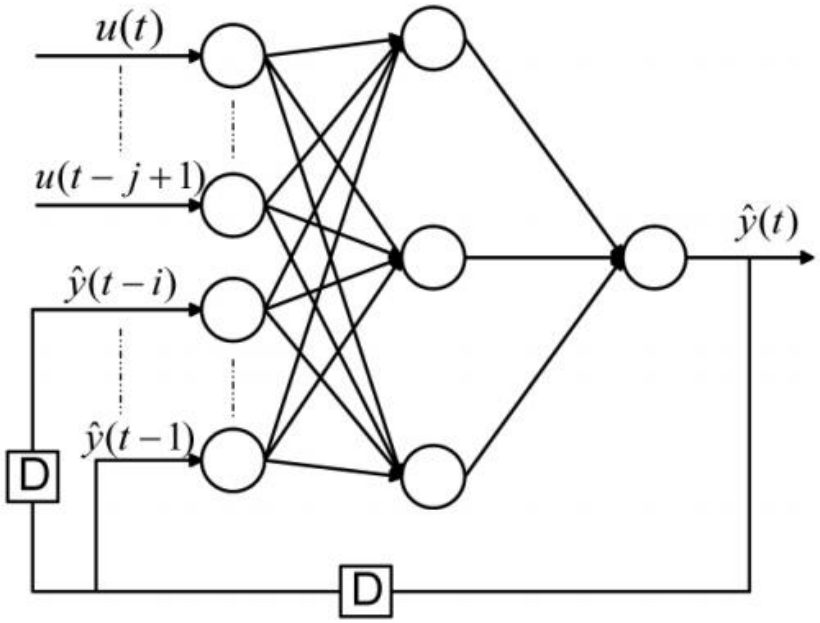

Figure 2-10 General Architecture of Recurrent Neural Network Model (Arsie et al., 2013)

The non-physical models reviewed above, especially the ANN and RNN models, have shown high model accuracy and computational efficiency. However, the non-physical models are not the most optimal solution for control-oriented modelling because the compatibility of non-physical models is poor; which means the model should be rebuilt completely when applied to other cases. Furthermore, these types of models suffer from model over-fitting during the training process (Brahma and Chi, 2012). As a result, the model would show poor prediction ability outside the data range. Even if inside the range of training data, extra data is still needed for a full validation and correlation.

2.4 Engine Calibration Algorithms

To further optimize the engine performance, reduce the engine-out emissions and improve the fuel economy, numerous optimization methods have been applied to internal combustion engines. In recent years, optimization algorithms are used for intelligent calibrations of engines. In this section, the engine calibration methods are reviewed based on commercial software and nature-inspired optimization algorithms.

2.4.1 Engine Calibration Using Model-based Calibration Methods

As the number of actuators associated with the new technologies applied on modern internal combustion engines has increased, it enlarges the time and cost for calibrating such a complex system. It becomes more difficult to achieve the optimum results for all calibration tasks (Turkson et al., 2016). One common way to deal with the engine's degrees of freedom is to use the model-based calibration (MBC) approach, which involves the use of statistic modelling called the design of experiments (DOE) (Guerrier and Cawsey, 2004). Companies such as MATLAB, AVL and ETAS have developed commercial software for the market. However, the statistic modelling approach requires a huge amount of data from engine tests and it is difficult to guarantee the model's accuracy over the whole engine operation range, with data noise during the acquisition process (Atkinson et al., 1998). It should be noticed that the statistical engine model is only suitable

for a specific engine. When the engine that requires calibration is upgraded or replaced, the statistic model needs to be rebuilt completely, even if the updates are not numerous (Ma et al., 2014). The data acquisition process should be repeated. At the current stage, these MBC methods are mainly designed for steady state optimization. They could not be implemented to the case of engine transient calibration, such as controller self-tuning. As introduced in the previous sections, transient calibration plays an increasingly important role for future diesel engines. Furthermore, internal combustion engines with unconventional combustion modes such as HCCI could not be used in the software. Thus, there is a demand for alternative solutions on engine optimization issues.

Many algorithms have also been proposed for optimization purposes in recent decades, such as the frequency domain method and the Ziegler-Nichols (ZN) method (Sanathanan, 1988; Åström and Hägglund, 2001; Pano et al., 2014). However, the major limitation of these methods is the requirement for excessive knowledge of the system's frequency response or controller's transfer functions, which makes them difficult to apply to the case of optimizing internal combustion engines.

2.4.2 Engine Calibration Using Natural-inspired Evolutionary Algorithm

During the engine calibration process, the trade-off between optimization objects is hard to avoid. Therefore, the multiple objective optimization algorithm is

considered to solve this problem by providing a step-by-step procedure of calculations and instructions (Yang, 2014). The nature-inspired evolutionary algorithms have become a popular choice to deal with this problem in recent years. This type of algorithm involves trial-based meta-heuristic search processes, inspired by the evolutions of natural species (Ma, 2012; Tayarani et al., 2015).

The genetic algorithm (GA) is a very popular solution among all nature-inspired evolutionary algorithms. It adopts the natural selection concept among species to locate the optimum on a given response surface (Yang et al., 2013). Each individual agent represents an input for the optimization case. The individuals in each generation are evaluated based on a defined fitness function. Only the fittest individuals can reproduce to form a new generation of citizens. Similar to natural creatures, the individuals also have random ‘mutations’ and ‘mating’ to locate the more optimum results (Thiel et al., 2002). To increase the computational speed of the conventional simple GA, a variation called micro GA (μ GA) was created. The most significant change is a more efficient selection process during the determination of the individuals for the next generation (Srinivasan and Tanner, 2011). The GA-based algorithms have been successfully utilized to optimize engine performance, emissions, or fuel consumption (Finesso et al., 2015). With the development of the CPU capability, the GA algorithms have also been coupled with CFD modelling strategies in the engine design process to optimize the combustion chamber geometries or fuel spray behaviours (Wickman et al.,

2001; Ge et al., 2009; Mattarelli et al., 2009).

The strength Pareto evolutionary algorithm (SPEA) is a very important landmark in the developmental history of nature-inspired evolutionary algorithms. The optimization results are converged to the Pareto optimal fronts (Zitzler and Thiele, 1998). However, the applications of SPEA on engine optimizations are limited by deleting non-dominated individuals accidently and fixed fitness values, which are two significant drawbacks of this algorithm (Abido, 2006). To compensate the shortages mentioned above, the SPEA was upgraded into SPEA2. Unlike SPEA, SPEA2 utilizes a fine-grained fitness assignment method and cooperates with individual density. Moreover, the size of the external archive is fixed. In addition, the clustering technology is replaced by an alternative truncation method, which will not lead to the missing of boundary points (Zitzler et al., 2001). The SPEA2 method has been successfully applied to the optimization of a HCCI engine and GDI engine. Improvements on both fuel consumption and emissions were found by experimental and simulation results (Ma et al., 2014; Ma et al., 2017). Based on this methodology, other algorithms such as SPEA2+, NSGA2 and NSGA3 were also created (Hiroyasu et al., 2005; Deb and Jain, 2013; Jain and Deb, 2014; Niu et al., 2018).

Particle swarm optimization (PSO) is another new type of nature-inspired evolutionary algorithm which can be considered. Compared with other

metaheuristic algorithms, the PSO method has the advantages of easy implementation, less computational effort and fast convergence speed (Ye et al., 2017). Therefore, it is widely used in controller intelligent calibration cases (Rogers and Birge, 2004; Watson et al., 2006; Fang et al., 2011; Reynoso-Meza et al., 2014; Zhang, 2015; Bourouba and Ladaci, 2016). To further improve the convergence speed of the algorithm, the accelerated particle swam optimization (APSO) was created. The fast convergence speed makes the APSO-based controller be of use as the real-time solver for the optimal control issues (Hu et al., 2018). The evidence shows that the APSO algorithm outperforms the PSO algorithm on multiple objective optimization issues (Rahman et al., 2016). However, these APSO-based algorithms may occasionally trap the particles in the local optimal position instead of a global optimal position. Thus, recently an APSO algorithm with chaotic mapping strategies (CAPSO) has emerged to enhance the result's repeatability and get rid of the 'local optimal' trap (Liu et al., 2005; Tan, 2012; Yang et al., 2014; Shen et al., 2016). The chaotic map could create some occasional variety in the particles, which is similar to the mutation process in a GA algorithm and randomly accepts several worse results; but this 'chaos' could help the particles to escape from the trap of local optima (Q. Zhou et al., 2017a). The comparison of the cost function values between CAPSO and APSO is shown in Figure 2-11, which illustrates the effectiveness of the chaos mapping strategy in CAPSO. In that publication, the performance of the CAPSO

algorithm and conventional APSO algorithm are reflected by the cost function values. A smaller cost function value indicates a more optimal result (the hybrid power-train could achieve better fuel economy with smaller powertrain size).

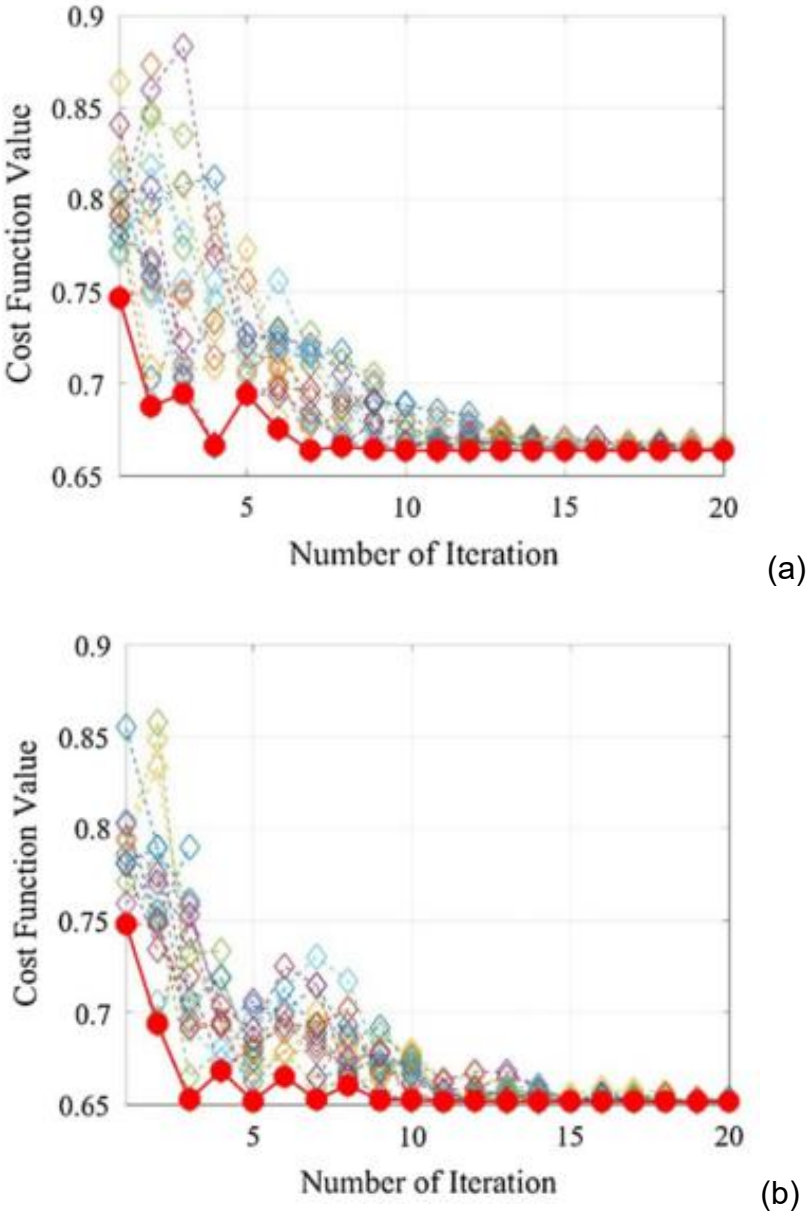

Figure 2-11 Comparison between APSO (a) and CAPSO (b) on Optimization Results (Q. Zhou et al., 2017a)

2.5 Control Strategies of Diesel Engines

The new control strategies for diesel engines have been widely investigated by numerous researchers, to improve these engines' transient performance. The author's work focuses on a diesel engine's air path and the appropriate control of the air path plays an important role in the transient performance. This literature review only discusses innovative control strategies applied on this topic; the publications are categorized into non-model-based control methods and model-based control methods.

2.5.1 Non-model-based Control Methods

Fuzzy logic control is a non-model-based control method based on fuzzy set theory, fuzzy linguistic variables and fuzzy logic-based intelligent computer control (Li, 2015). The fuzzy logic controller imitates mankind, making decisions under different circumstances. It has the advantages of a simple heuristic nature, tolerance to noise and it doesn't require the mathematical deviation related to control theories (Wijetunge et al., 2000). The fuzzy logic control process is formulated through fuzzification, fuzzy inference and de-fuzzification (Montazeri-Gh et al., 2010). The fuzzification transforms the input data into degrees of membership by the membership function. The fuzzy inference deduces the corresponding outputs. Then the resulting fuzzy set is reconverted into control signals that can be sent to the plant (Boiocchi et al., 2016). The design of the

membership function plays a major role in determining the performance of the fuzzy logic controller. With years of developments, fuzzy logic controllers have been successfully applied to the subject of engine control (Ines Abidi et al., 2013; Di et al., 2015). The fuzzy PID controller on a turbocharged gasoline engine is designed to modify the calibration values of a conventional PID controller online, based on the error signals (Li et al., 2015). Simulation results show that the fuzzy PID controller could provide better reference tracking performance on the manifold pressure than a pure PID controller. The structure of a typical fuzzy PID controller for VGT-EGR control is shown in Figure 2-12. The controller's structure is quite simple and the computational requirement is similar to that for the conventional PID controllers.

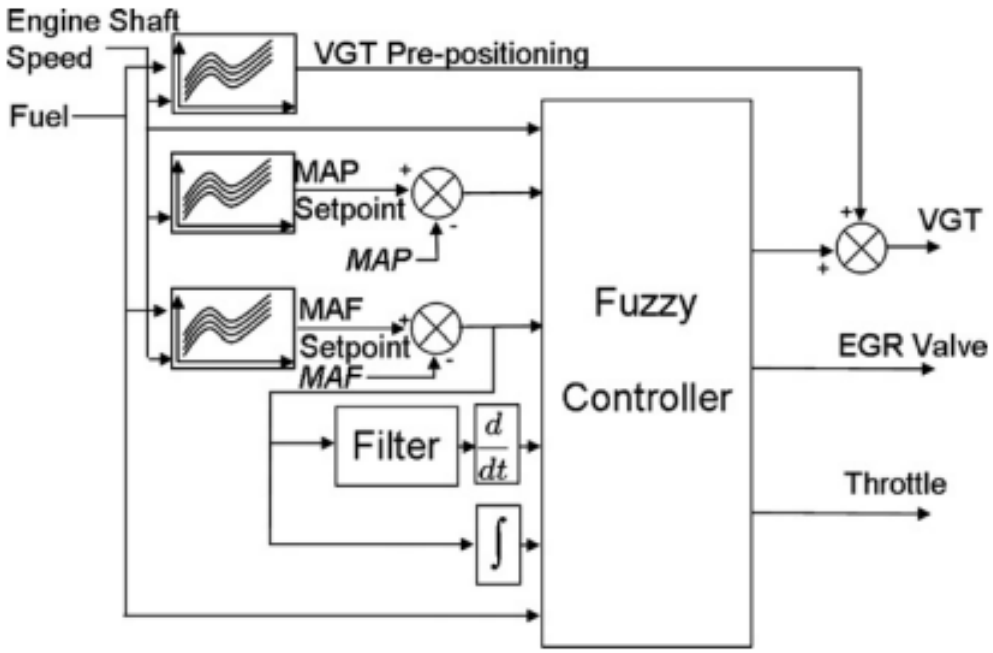

Figure 2-12 Typical Structure of a Fuzzy PID Controller for Engine Control (Arnold et al., 2009)

The development of a fuzzy logic controller depends on the comprehensive understanding of the actuators' behaviour so that the control strategy is pre-determined. This character limits the application on a complex MIMO and coupling system such as the dual-loop EGR. Besides, much calibration work is still needed to obtain optimal control results.

In control theory, robust control is an approach to controller design that could handle system uncertainty. A robust control strategy is static; the controller is designed to work assuming that certain variables will be unknown but bounded (Mercorelli et al., 2011). It should be noticed that the robust control or other classic control methods for internal combustion engines have been investigated extensively (Samokhin and Zenger, 2014). Therefore, the recent robust controllers are now integrated with other control theories.

The sequential robust control is another common type of non-model-based control method that is applied to the air path of a diesel engine. It considers the system's robustness, with both the influence of uncertainties and coupling to a MIMO control system. The advantages of the proposed controller are the easy tuning and simple implementation (Deng et al., 2012). Some robust controllers are associated with the control-Lyapunov function (CLF). A CLF-based robust controller for a turbocharged diesel engine is developed by considering the Jankovich model, which provides additional degrees of freedom and guarantees

to achieve improved controller performance on the EGR-VGT system (Jankovic et al., 1998; Wahlstr, 2008; Kuzmych et al., 2013). Another innovative robust controller is proposed as fuzzy robust tracking control. It also considers the pole placement in linear matrix inequality (LMI) regions and speed variation in the EGR-VGT system. The simulation results (Mercorelli et al., 2011) successfully certificate the effectiveness of the control strategy (I. Abidi et al., 2013). The slide mode control is also combined with the robust control theory for the engine's variable valve control. The control problems such as non-linearities, hysteresis, saturations, and creep were considered. These difficulties were all successfully overcome from the engine tests (Barrero et al., 2011). In terms of the dual-loop EGR system, robust control has also been adopted (Haber, 2010). The robust multivariable feedback controller evaluates the system's uncertainty and robust stability conditions. Coupled-simulation results indicate the controller's ability to reject the disturbances caused by the changes of the engine's working conditions and the optimal performance at the boundaries of the complex air path range.

However, the robust control still suffers from drawbacks: such as the requirement of frequency analysis of the system; the large amount of mathematical processing to develop the controller; and complex offline tuning. Besides that, the controllers built based on this method have a lack of feed-forward control ability.

2.5.2 Model Predictive Control Methods

In recent years, there has been a trend to adopt model-based control methods instead of non-model-based control methods (Ashok et al., 2016). Among these methods, model predictive control (MPC) has been widely adopted because of its capability in dealing with multiple objective control problems (Zheng et al., 2011)(Barrero et al., 2011; Zheng et al., 2011). With the continuously increased complexity of diesel engines, MPC has also been used on this multi-input multi-output (MIMO) platform. The basic idea of MPC is to formulate the control issue into a multiple objective optimization issue and the MPC controller solves the optimization issue at each time interval (Gelso and Dahl, 2016).

The key points of the MPC controller are building internal prediction models and solving the multiple objective optimization issue. Linear MPC controllers have the advantages of simple structure and systematic design approach, but they could not handle the non-linear system directly. The system linearization must be proceeded before implementation on the diesel engine's air path. Internal prediction models are then acquired from the linearization process. To cope with the wide working range of diesel engines, several state-space identified models are trained (Borhan et al., 2015). Each sub identified model would be allocated to an MPC controller. In this way, the single MPC is converted into multiple MPC. The switch between different sub MPC controllers is determined by the engine

working condition (Stewart and Borrelli, 2008). To solve the optimization issue at each time interval, a quadratic programming (QP) method is usually selected as the solver to calculate the optimal sequences of control variables (Bemporad et al., 2014). Experiment results show that the MPC controller achieves a better trajectory tracking performance, which contributes to a better fuel economy (Lu et al., 2016). However, the multiple MPC controller will show a disadvantage when allocating sub-MPC controllers for systems with sudden changes in the operating conditions and non-linearities (Lu et al., 2016).

Recently, a new type of MPC was proposed to reduce the computational costs and adapt to fast-speed systems; it is called explicit MPC (EMPC) (A. Bemporad et al., 2002). In EMPC control, the optimal control laws of the QP problem are pre-computed offline and the piecewise affine results are stored in look-up tables (Dezong Zhao et al., 2013). The main steps to build an EMPC controller are similar to the conventional linear MPC controller; the differences lie in the controller implementation. Figure 2-13 shows the design procedure of an EMPC controller for a diesel engine's air path. This method has also been applied to the air-fuel ratio control, two-stage turbocharger control and fuel path control on several types of engines (Hadef et al., 2013; Deng et al., 2014; Honek et al., 2015; Emekli and Güvenç, 2016). In summary, the EMPC controller can be easily adapted to the constrained multi-objective control issues with real-time capability. This control method provides enormous promise for real-time control in the

applications of internal combustion engines. But the main drawback is the large storage space of the offline look-up tables.

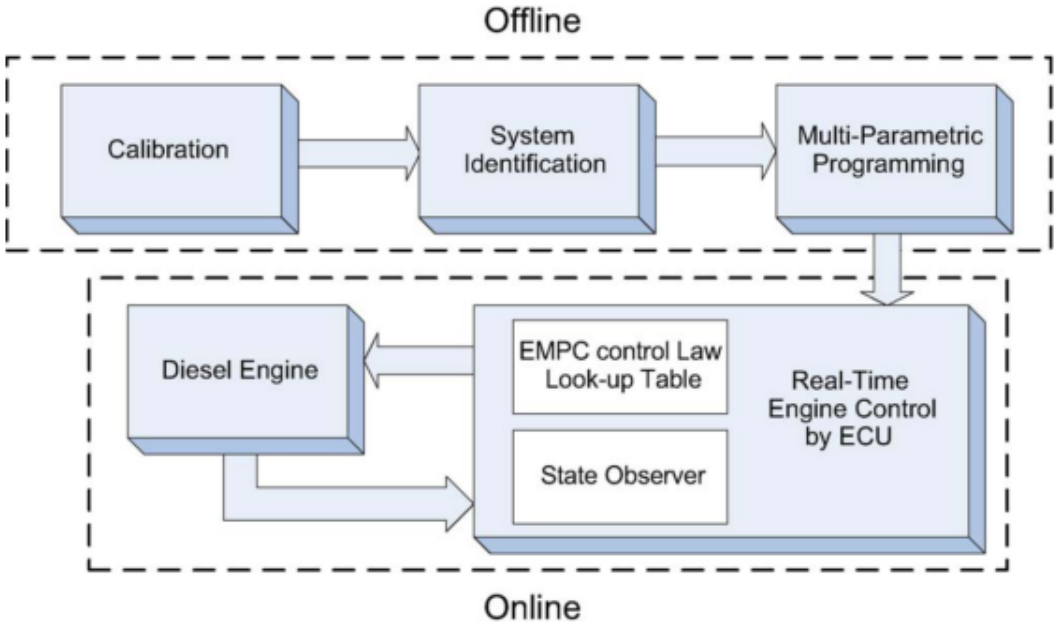

Figure 2-13 Implementation of EMPC Control on a Diesel Engine (Zhao et al., 2014)

Different from the linear MPC controllers, the idea of non-linear MPC was proposed (Garcia-Nieto et al., 2008). The non-linear MPC controllers have also shown a good reference trajectory tracking performance; the biggest challenge is the computational requirement which makes it more complex for engine control applications (Tan, 2015). The key point of non-linear MPC controllers is that they still solve the constrained multiple objective optimization issue. However, the main differences are that the control implementation is based on direct optimal control using an online sequential quadratic programming (SQP) type algorithm and the QP problem has to be condensed at each sampling time (P. et al., 2009;

Albin et al., 2015) The non-linear MPC controller has been successfully applied to the area of diesel engine control (Gorinevsky and Cook, 2003; Garciaa-Nieto et al., 2008). Improved transient behaviours are observed via simulation. Figure 2-14 shows the basic structure of a non-linear MPC controller for a diesel engine with single loop EGR.

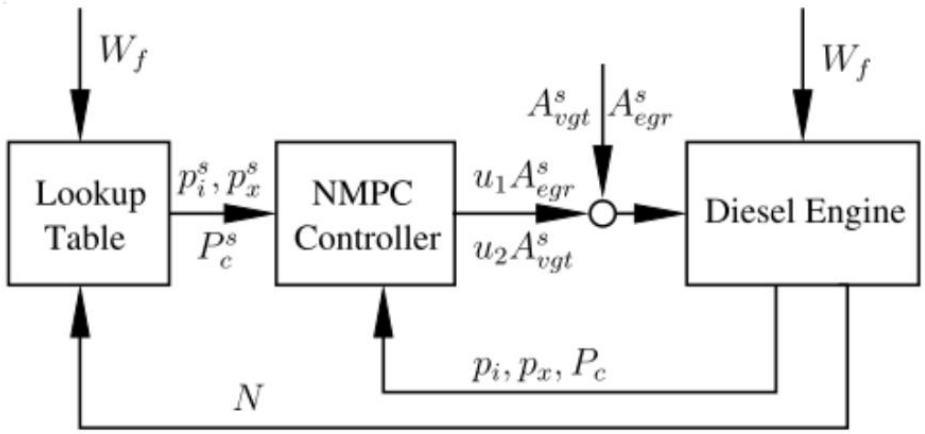

Figure 2-14 Structure of a non-linear MPC Controller for a Diesel Engine (Herceg et al., 2006)

One of the innovations with the non-linear MPC controller is providing alternative solutions to solve the non-linear programming (NLP) issue. The particle swarm optimization (PSO) algorithm is utilized to solve the NLP issue at every time interval for the purpose of idle speed control (Xu et al., 2013). Other methods such as the genetic algorithm (Walker et al., 2016), the bat-inspired algorithm (Elsisi et al., 2016) and the continuation and generalized minimum residual method (C/GMRES) (Kang et al., 2014) have also been considered as the solver for non-linear MPC controllers. The methods mentioned above could calculate

the optimal sequence of control variables within 50 microseconds successfully, which is fast enough for engine control (Huang et al., 2015). Even though the idea of the explicit non-linear MPC controller is used for a turbocharged gasoline engine, the authors point out the explicit non-linear MPC controller has a lack of ability to adapt model changes and does not scale well with even the addition of integral action (Hadef et al., 2013).

Another innovative idea with the non-linear MPC controller is to combine the techniques from an artificial neural network (ANN) with the workflow of model predictive control. Based on the introduction in the section of engine modelling, the neural network model can learn the complex and multi-dimensional relationship between selected variables. It could be used as the internal prediction model (Kittisupakorn et al., 2009). Thus, neural network model predictive control was proposed recently. The controllers using this method have been successfully applied to the air-fuel ratio control of an SI engine (Wang et al., 2006;Sardarmehni et al., 2013) and the combustion control of HCCI engines (Janakiraman et al., 2016). The non-linear MPC controllers were also applied to the air path control of internal combustion engines in recent years, due to the development of the ECU's computational capability (El Hadef et al., 2013;Albin et al., 2015;Li et al., 2016;Albin et al., 2017).

2.6 Summary

This chapter reviews the publications concerning the diesel engine's air path, the characteristics of diesel engines' transient operations, control-oriented modelling, intelligent engine optimization and controller design for diesel engines' air paths. The main findings could be summarized as below:

1. As the dual-loop EGR system is installed, the air path contains more actuators. The coupling effects and system's non-linearity become more severe. This brings more parameters which need to be calibrated and the control strategy should also be able to achieve accurate control of the HPEGR loop and LPEGR loop.

2. Engine transient operations play a major role in the engine-out emissions. In the diesel engine's air path, the coupling effect and system delay of the EGR-VGT system are the main reasons. The future engine test cycle involves real-world driving conditions; the engine will be operated in a wider working range and with more transient scenarios. The conventional controllers based on PI-control strategy and look-up tables will have more and more limitations.

3. Several control-oriented engine modelling approaches are introduced in this section. Each method has its advantages and limitations. To develop

a complete model for a modern diesel engine, a combined modelling approach should be adopted due to the complexity and various features of the sub-systems.

4. To further improve the engine's performance, an optimization process is necessary, especially for transient conditions. Compared with the conventional calibration methods, the evolutionary algorithm is a better solution for the constrained multiple optimization issue. But the optimization results that may trap in a local best result instead of the global best result. Besides, the structure of the algorithm could still be simplified. Among these evolutionary algorithms, the CAPSO algorithm is selected as the candidate for the automatic calibration of the diesel engine's air path during transient conditions.

5. Advanced control strategies for the air path of modern diesel engines are reviewed to obtain optimal transient engine performance. However, there is still a demand for model-based controller that can solve constrained multiple objective control issues and adapt to the real-world driving conditions. To satisfy this demand, the MPC-based controllers could be the solution.

Therefore, after reviewing the above-mentioned publications, it can be concluded that an intelligent calibration method which can solve the constrained multiple

objective optimization issues and locate the global best result, and a controller which can overcome the system's non-linearity, coupling effects and delay within the time interval of engine ECU, are needed for the air path of the diesel engines.

CHAPTER 3 EXPERIMENTAL SET-UP AND METHODOLOGY

This chapter introduces the test facilities involved in the thesis and the methodology of the research activities. The engine specifications, engine test bench, engine performance measurement devices, hardware-in-the-loop (HIL) test platform and the development of a simulation platform are all presented. The methodology introduces the investigation approach of the research objectives and related engine test plans

3.1 Experimental Setup

3.1.1 Engine Specification

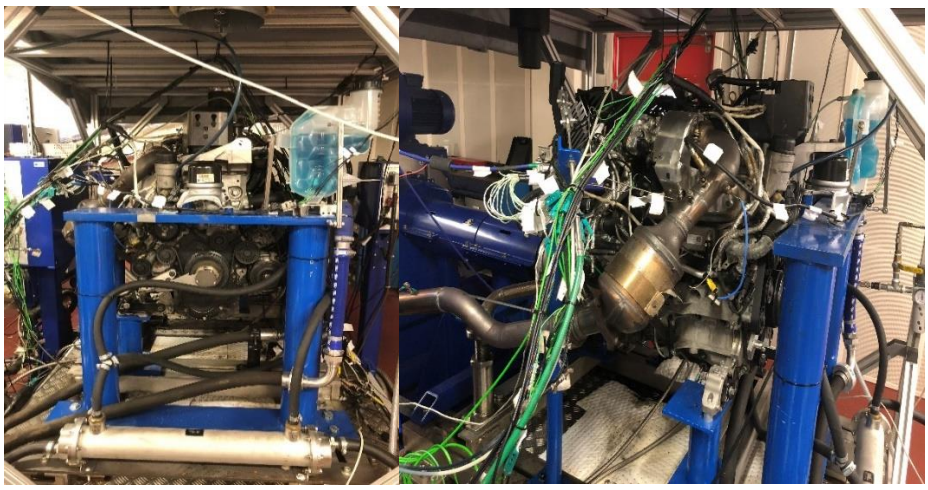

Figure 3-1 Jaguar Turbocharged Diesel Engine

The experiments are conducted on a Jaguar diesel engine which is shown in Figure 3-1 above. It is a modern EURO 6 light-duty diesel engine with a variable geometry turbocharger, a common rail direct injection system and a dual camshaft. This engine also contains a dual-loop EGR system with water cooling system to provide low-temperature recirculated exhaust gas. Furthermore, the multiple injection strategy is included in the engine calibration; this is beneficial to achieve an optimal engine combustion process and high efficiency of the aftertreatment device. Detailed engine technical information is shown in Table 3-1.

Table 3-1 Jaguar Engine Specifications

Engine Type	AJ20D4 Mid Spec
Bore	83 mm
Stroke	92 mm
Displacement Volume	1993 cc
Maximum Torque	430 Nm (1750-2500 rpm)
Maximum Power	132 kW (4000 rpm)
Maximum In-cylinder Pressure	180 bar
Compression Ratio	15.5:1
EGR Type	Cooled EGR
Air-path Actuator	Electrical controlled valves with feedback
Fuel Injection System	Bosch Common Rail Direct Injection System
Maximum Injection Pressure	1800 bar
No. of Injector Holes	6-hole injector
Supplier of VGT	Mitsubishi

In this thesis, the research work mainly focuses on the diesel engine's air path. The architecture of it is shown in Figure 3-2.

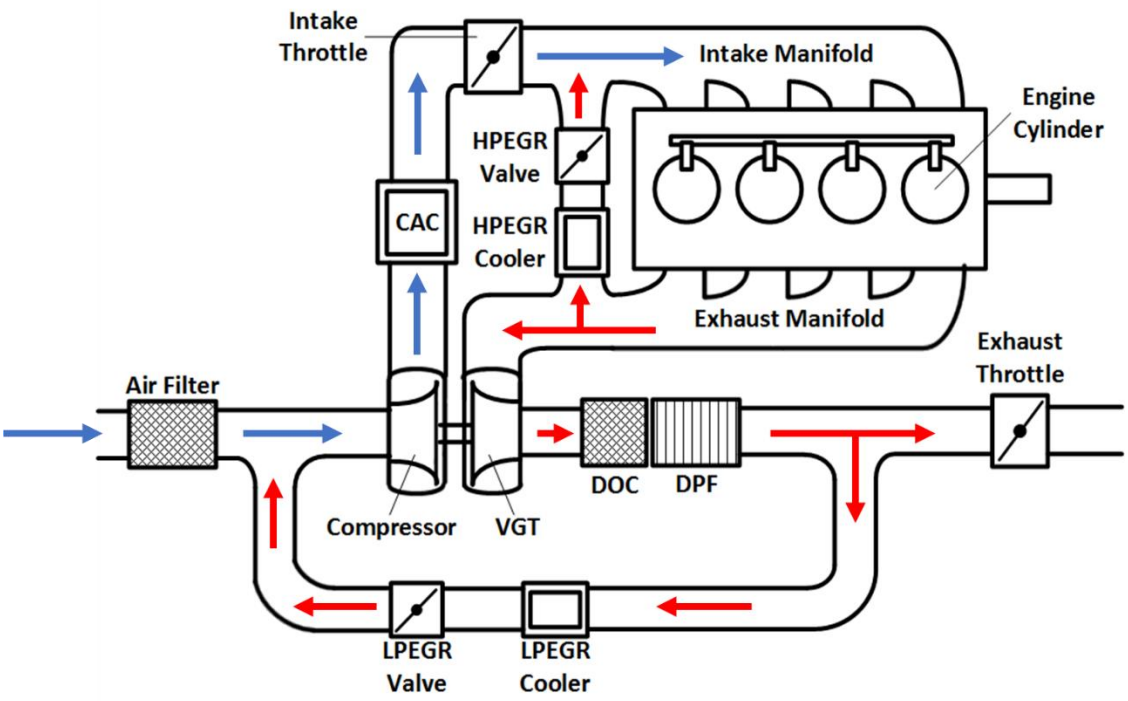

Figure 3-2 Architecture of The Jaguar Diesel Engine's Air Path

The engine's air path consists of a HPEGR loop, a LPEGR loop, a VGT and a charge air cooler (CAC). In this case, the EGR mass flow is controlled by the EGR valve positions. The HPEGR loop is between the intake manifold and the exhaust manifold. As the exhaust gas flows through the engine DOC and DPF, part of it will go into the LPEGR loop. The recirculated gas would then mix with the fresh air in the air inlet tube before reaching the engine compressor. The two EGR loops contain coolers to further reduce the EGR gas temperature. The engine boost pressure is adjusted by the VGT rack position. In this study, both the intake throttle and the exhaust throttle are constantly fully opened (Zhang et al., 2017).

3.1.2 Engine Test Bench

The test bench, known as the cold cell, was originally designed to investigate the behaviours of an engine's cold start. One unique feature of this facility is a complex conditioning system which can control the temperature of the engine coolant, lubrication oil, engine intake air and supplied fuel. The accurate temperature control contributes to the data accuracy and repeatability. The author took over the facility's maintenance work and participated in the engine control project in 2015; which involved test bench reconfiguration for the new engine, open-ECU build-up, engine calibration and system debugging.

The operating and control system of the engine test bench are important for studies of engine transient conditions in this thesis. The test bench could provide full transient engine duty cycles such as the NEDC, WLTC and customized test cycles designed by researchers. The complete schematic view of the cold cell test bench is illustrated in Figure 3-3.

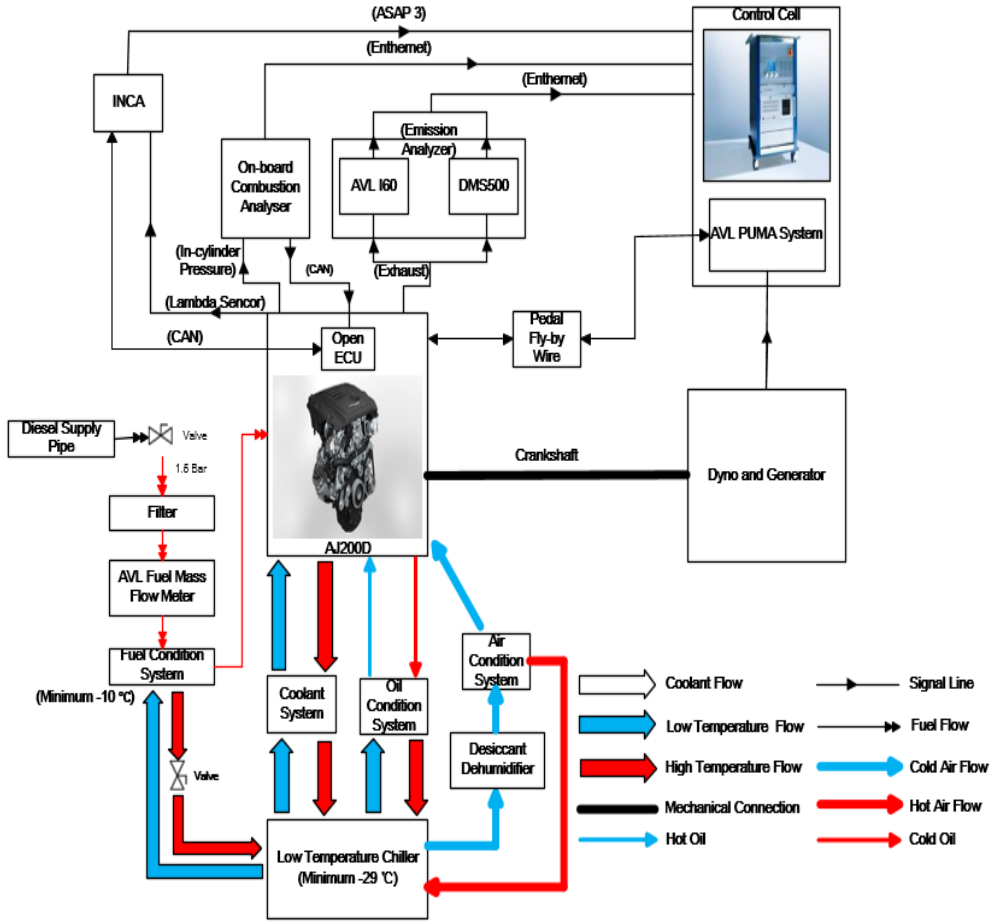

Figure 3-3 Test Bench Subsystem Arrangement

The whole engine test bench (the engine, dynamometer, conditioning system and measurement devices) is controlled by the AVL PUMA system. It takes the role of test bed control, monitoring and data acquisition. The author's main work in the experimental set-up is to reconfigure the test bench to cope with the new engine and open-ECU.

To monitor the test bench signals, the PUMA system contains a fast-front end module (FEM) control unit. So, the PUMA system could monitor the information in real-time during engine tests.

Figure 3-4 shows the data transfer between the test bench and the PUMA system. The PUMA computer calculates the demand values of speed and torque, then sends them to the output modules. The PC board PCI makes these signals communicate between the PUMA computer and the FEM control unit. The digital signals sent from the PUMA computer are converted into analogue signals, which could be used to control actuators. The conditioning system is also controlled through this method and calibrated via tuning the PID parameters (Liu, 2014).

The engine calibration software ETAS INCA is installed on another desktop which connects to the engine's ECU via a USB-CAN bus interface ES581.4. The interface is also a mature product developed by ETAS. The INCA software can obtain and store the required ECU signals; meanwhile, some engine calibration data such as the EGR rate, EGR proportion and boost pressure could be modified or controlled by the researcher. To synchronize the data in INCA and PUMA, an ASAP3 link is established through Ethernet. In this study, the PUMA system is the single source to record the experimental data from different devices.

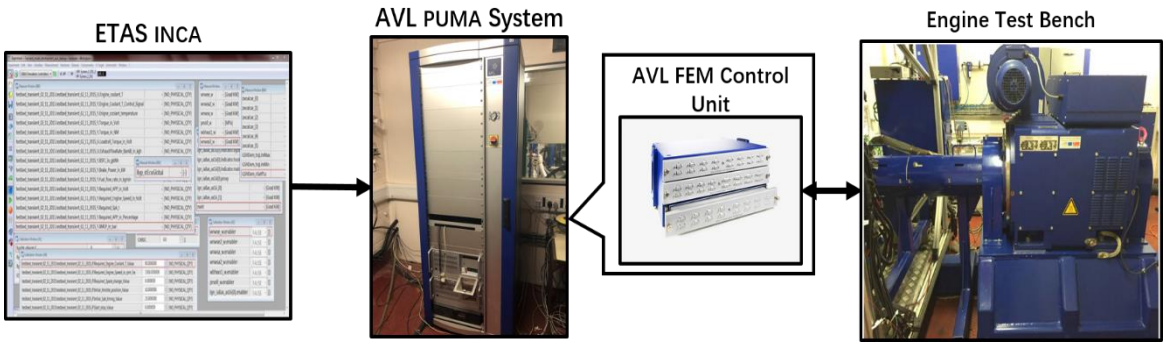

Figure 3-4 Data transfer between the PUMA operation system and the test bench (Tan, 2015)

In terms of the conditioning system, it consists of several subsystems for the engine intake air, fuel, engine coolant and engine oil. In this study, the low temperature conditions are not necessary, but the conditioning system is still needed for the engine tests.

The dynamometer used in the cold cell is shown in Figure 3-5. It is an AC machine with a squirrel cage rotor mounted with a torque flange (Tan, 2015), as shown in Figure 3-5.

Figure 3-5 AVL Transient Dynamometer in the Cold Cell

The demand torque and the speed of the dynamometer are controlled by a control unit which is connected to the AVL PUMA operation system. The dynamometer has two control modes: speed mode and torque mode. Under speed mode, the

engine speed is determined and maintained directly by the dynamometer, the engine adjusts the mass of fuel injection based on the paddle position to achieve the desired torque (Zhang, 2013). Under the torque mode, the torque is regulated by the dynamometer while the engine adapts to the required speed. In this thesis, the speed mode is selected due to its rapid dynamic performance and little fluctuation. The detailed technical information for the dynamometer is shown in Figure 3-6 (“AVL DynoSpirit - Dynamometers for Engine Testing - avl.com,” n.d.).

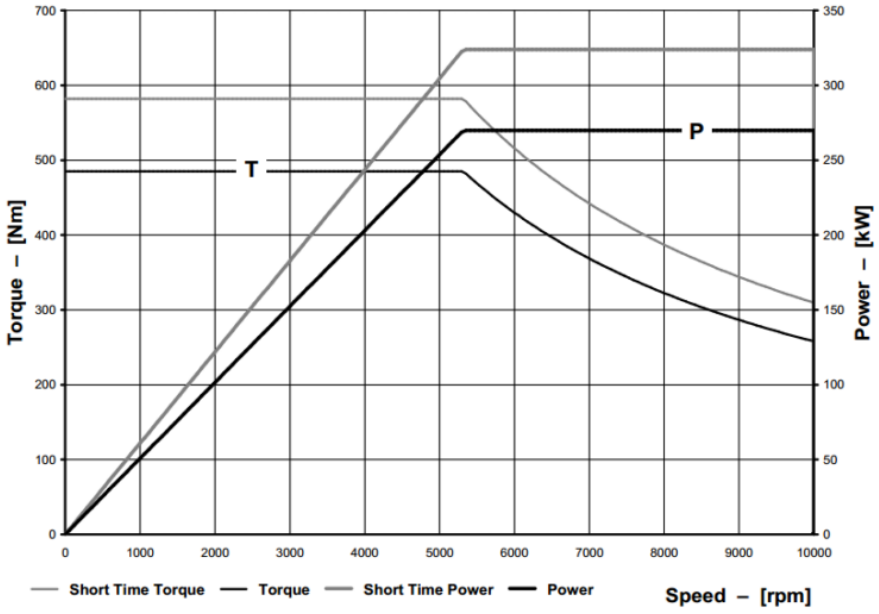

Figure 3-6 Performance Curve of the Dynamometer in the Cold Cell

3.1.3 Engine Performance Measurement

To evaluate the engine performance, several measurement devices are involved in this study. Regular maintenance and calibration are conducted to ensure data accuracy.

Figure 3-7 Pi Innovo M670 Open ECU

The engine parameters such as the MAP, MAF and EGR rate are measured by the engine's ECU. Instead of using standard commercial ECUs such as products from Bosch, a Pi Innovo M670 open-ECU is selected in this case (shown in Figure 3-7). It is a 154-pin high performance engine controller designed to support model-based control for gasoline PFI, GDI, diesel solenoid and alternative fuel application. Engine components including variable valve action, VGT and dual-loop EGR are acceptable for this control platform. Due to the variation between the open-ECU harness and the Bosch ECU harness, a pin adapter is customized by Jaguar Land Rover. This special design is only for academic research activities. The engine control strategy and calibration are duplicated from the commercial ECUs on the same engine and are approved by Jaguar Land Rover for engine tests. The hardware specifications are listed in the table below. Detailed information is shown in reference ("M670 - Pi Innovo Product Overview," n.d.).

Table 3-2 Hardware Specifications of M670 Open-ECU

Processor	MPC5674F	Actuator Supplies	2 x Vbatt@ 10A
Clock Rate	264 MHz	Sensor Supplies	4 x 5 V@ 250 mA
Code Space	3 MB	Communications	4 x CAN 2.0
RAM Space	128 KB	Single-ended	32 x 12 bit
Calibration Space	128 KB	Digital	5
Pin Number	54 (input), 49 (output)	Digital, Frequency, PWM	3
Injection Allowance	8 x software programmable wave form peak and hold	Supply Voltage	12 or 24 v

In this case, the in-cylinder pressure (model 6056A) is measured by a piezoelectric pressure sensor provided Kistler, which is fitted to all four cylinders. The calibration of the in-cylinder pressure transducer is validated by the engine supplier. The pressure transducers generate electric charges at 160 kHz via piezoelectric crystals. This type of material has high sensitivity of pressure variation in the operating temperature range. The measurable cylinder pressure falls between 0 and 300 bars. It is adequate for the engine in this thesis. The AVL shaft encoder is installed to provide accurate crank angle and top dead centre (TDC) measurement. The TDC determination and related calibration work are finished by the engine supplier when the engine is installed to the test bench in Birmingham. The resolution of the engine TDC should fall in the range of $\pm$ 0.2 degrees.

The Miracle2 combustion analyzer designed by Alma Automotive Ltd is used in this case. The pressure transducers, crank angle signal and injection signals can

link to the analyzers via BNC cables. The measured and calculated combustion parameters can also be sent into the engine's ECU through a CAN interface in real time. The combustion parameters (such as IMEP, BMEP) are monitored and recorded instantaneously with other ECU data in the INCA software. Meanwhile, the Miracle2 provides an independent working interface through Ethernet communication which contains the analyzer configuration and data acquisition. In this case, only cycle-based combustion parameters such as IMEP, peak in-cylinder pressure and crank angle of fuel mass fraction burnt (10%, 50%, and 90%) are recorded in INCA due to the limitation of data frequency. The in-cylinder curves are recorded separately when needed.

Figure 3-8 Alma Automotive Miracle2 Combustion Analyser("Real-Time Combustion Analysis System," no date)

To measure the fuel consumption of the engine, the AVL 735S fuel meter is installed right above the fuel conditioning system (AVL 753C). The fuel meter is integrated with the fuel conditioning system for better temperature stability. It is a

Coriolis-flow type meter which guarantees an instantaneous fuel flow measurement. The gas bubbles in the fuel could be separated to further improve result accuracy. Before each test, the PUMA system checks the fuel meter status and calibrates it automatically. The user receives the diagnostic information during the tests and controls the fuel meter remotely. The detailed technical specification of the fuel measurement device is illustrated in the table below ("AVL Fuel Mass Flow Meter and Fuel Temperature Control - Consumption Measurement - avl.com," n.d.).

Table 3-3 Technical Specification of AVL 735S Fuel Meter

Ambient Temperature Range:	5-50 ℃
Fuels:	Gasoline, diesel, winter diesel, up to 6% biodiesel and maximum 20% blending of alcohol
Fuel Circulation Capacity:	240 L/h (standard), 450 L/h (maximum)
Fuel Pressure Range:	0-6 bar (fuel feed in), 0-0.5 bar (turn pressure)
Temperature Stability:	< 0.02 °C
Heating Power:	1.6 kW
Cooling Power:	1.6 kW at 10 °C condition and 0.5 bar cooling water pressure difference
Signal Transmission:	RS232
Energy Consumption:	0.4 kW

3.1.4 HIL Validation

The HIL (hardware-in-the-loop) validation process is a rapid, low-cost, highly flexible and highly repeatable prototyping test method for controllers (Zhang et al., 2017). It is necessary to validate the controller's performance in a real-time

environment before the controller is applied to real engines. As the simulation platform is accurate enough to represent a real application, the controller could be further calibrated in a HIL environment directly. On the HIL test platform, the simulated controller is replaced by a real processor, which co-operates with the rest of the model on a real-time PC.

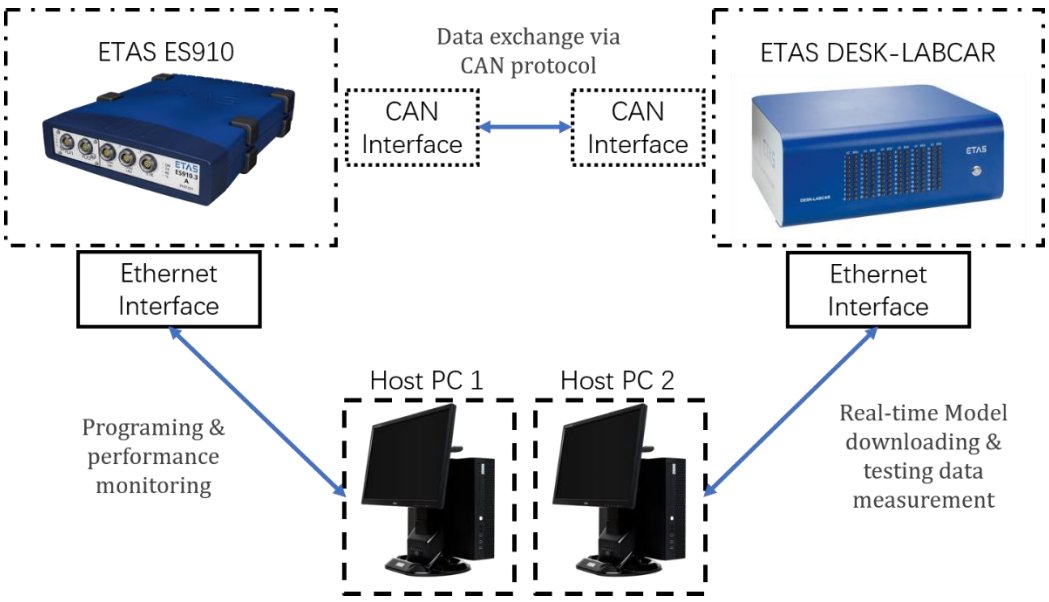

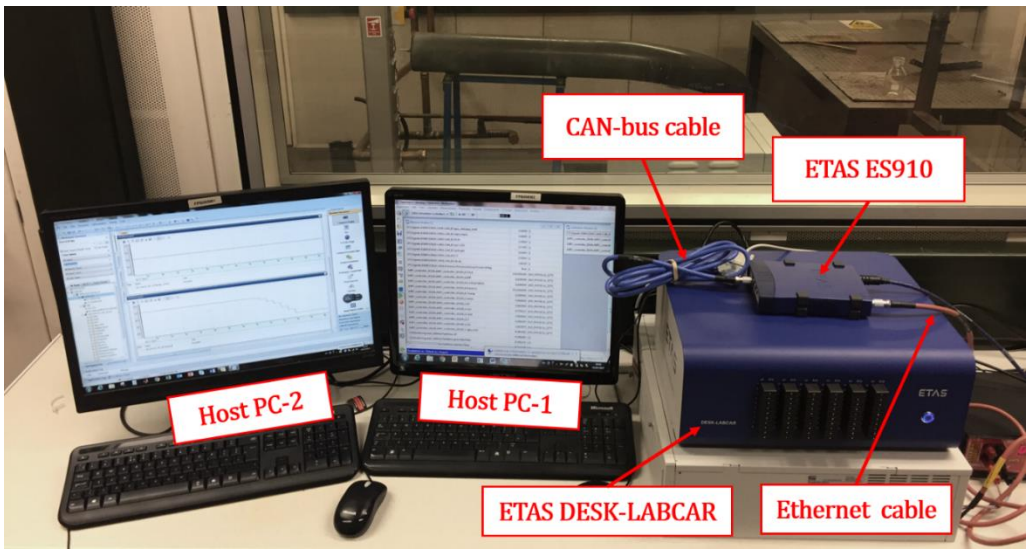

Figure 3-9 Structure of the HIL Test Platform and Photo of the HIL Test Bench

In this thesis, the test equipment is provided by the ETAS Group. The configuration of the HIL test platform is shown in the two figures above. The controllers developed by the author will be compiled from the host-PC 1 in the ETAS ES910. The compiling is finished in the MATLAB environment. It formulates the controller into C codes. The C code is then transmitted into ES910 by the ETAS INTECRIO. This software also establishes the I/O ports of the controller and the model. The real-time model is operated in the ETAS DESK-LABCAR, which is a high-performance Linux-based simulation target. It contains 40 channels multiple I/O, including analogue and digital signals. The communication between the controller and the real-time model is established via the CAN bus. The real-time model is compiled from host-PC 2 into the DESK-LABCAR via the ETAS Experiment Environment (EE), which is based on Ethernet protocol. The real-time model is firstly rebuilt into C code, then it is downloaded into the LABCAR. The outputs from the real-time model are monitored in host-PC 2. The detailed technical data of ETAS 910 are shown in the table below:

Table 3-4 Specification of the HIL Platform (“Technical Data ES910,” 2010)

Make and Model	ETAS ES910
Temperature Range	-40 °C to +70 °C (operation)
Main Processor	NXP PowerQUICC™ III MPC8548 with 800 MHz clock double precision floating point unit
RAM	512 MByte DDR2-RAM (400 MHz clock)
Flash	64 MByte Flash
NVRAM	128 kByte NVRAM
CAN Interface	2 channels, high speed (up to 1 MBaud) or low speed
Ethernet Connection	10/100/1000 Base-T

3.1.5 Data Accuracy and Measurement Uncertainty

The data accuracy is vital for the results obtained from the engine test bench and the measurement uncertainty should be avoided to ensure the data quality.

The measurement device in this study includes the transient dynamometer, fuel meter and in-cylinder pressure sensors. The accuracy of these devices is shown in the following paragraphs.

The table below shows the specification of the dynamometer of the test bench. The torque deviation is less than 0.1%. The dynamometer is maintained by the supplier annually.

Table 3-5 Specification of the Dynamometer in the Cold Cell (“AVL DynoSpirit - Dynamometers for Engine Testing - avl.com,” n.d.)

Model	Dynodur 270	Characteristic Tolerance	< ±0.10%
Nominal Torque	1500 Nm	Linearity Deviation	< ±0.05%
Nominal Power	700 Kw	Temperature Effect per 10 K on the Output Signal	< ±0.05%
Maximum Speed	10000 rpm	Temperature Effect per 10 K on the Zero Signal	< ±0.05%
Mass Inertia	0.31 kgm^2	Relative Standard Deviation of the Reproducibility	< ±0.05%

For the AVL fuel meter, the uncertainty of the fuel flow rate is less than 0.12% and the temperature stability is better than 0.02 °C. The response time of the fuel consumption reading is less than 125 ms. The sample rate of the logged ECU signals is set to 100 ms. So the response of the fuel meter is sufficient to catch up with the engine ECU. Besides, the automatic diagnose and calibration of the fuel meter are conducted by the test bench operation system before the engine tests (“AVL Fuel Mass Flow Meter and Fuel Temperature Control - Consumption Measurement - avl.com,” n.d.).

Measuring range	bar	0 ... 300
Calibrated partial range with RT, 150°C, 250°C, 350°C	bar	0 ... 100, 0 ... 200, 0 ... 250, 0 ... 300
Overload	bar	350
Sensitivity	pC/bar	-30
Natural frequency	kHz	≥65
Linearity, all ranges (at 23°C)	%FSO	≤±0,3
Acceleration sensitivity		
Axial	bar/g	<0,002
Radial	bar/g	<0,0002
Operating temperature range for sensor	°C	-20 ... 350
Temperature min./max.	°C	-40 ... 400
Thermal sensitivity change		
RT ... 350	%	≤±1
250°C ±100°C	%	≤±0,7
Thermal shock error (at 1 500 1/min, IMEP = 9 bar		
Δp (short-term drift)	bar	≤±0,3
ΔIMEP	%	±1,5
Δp_{max}	%	<±1
Insulation resistance at 23°C	MΩ	$\geq 10^{13}$
Tightening torque, greased	N·m	10
Capacitance, without cables	pF	12
Weight (without connector and cables)	g	11,5
Connector		10-32 UNF

Figure 3-10 The Technical Data of the In-cylinder Pressure Sensor (KISTLER, 2018)

Figure 3-10 shows the technical data of the in-cylinder pressure sensor provided by KISTLER. The model is 6056A. The measuring range fits the maximum in-cylinder pressure which is 180 bars. It has Low thermal shock error, long life and good temperature stability of the sensitivity. The resolution of the sensor is sufficient for the research in this case. Besides, this pressure sensor is designed specifically to integrate with the engine glow-plug system. which greatly simplifies the installation process. It is also suggested by the engine supplier.

To minimize the measurement uncertainty and increase the data repeatability, the

temperature control of the engine test bench is vital. It involves the control of the intake air, fuel supply and the engine coolant system.

The temperature of the engine intake air is controlled by an AVL CONSYSAIR 1600 unit. In addition, the test bench contains a dehumidifier to regulate the relative humidity of the intake air based on the test requirements (Tian, 2015). The tests in this thesis are conducted under an ambient condition, the intake air temperature is maintained at 20 ℃. The dehumidifier is activated during these tests. The air humidity is maintained at a constant value for all the tests. The temperature control is necessary for repeatability of the engine test data. The intake temperature would increase along with the testing time if the air conditioning system is turned off, which may lead to mutative engine performance.

The fuel supply to the test engine is monitored and controlled by the AVL 753C control unit. The fuel barrel is kept under ambient temperature and pressure. Before feeding into the fuel conditioning system, the fuel is filtered by a coarse filter and a fine filter. A fuel regulator is set to 2 bars to acquire a stable fuel flow. Then, the mass flow rate of the fuel is measured to ensure accurate fuel consumption readings to the PUMA system. Finally, the fuel enters the conditioning system to reach the desired temperature. The conditioning system could cool down or heat up the fuel within the range of -20 to 80℃. At ambient test mode, the fluctuation of the fuel temperature is ±1 K, which ensures accuracy

and repeatability of the test results.

The engine coolant system is vital in engine tests. The properly controlled coolant makes sure the engine is fully warmed up and could avoid the engine becoming over-heated. The precise coolant temperature also contributes to data repeatability. The control strategy inside the control unit uses a PID controller and the coolant mass flow is verified by a flow control valve. In the ambient test mode, the setpoint of the engine's coolant temperature is set to 90 ℃. To avoid the engine breaking down at an excessively high temperature, the safety alarm would be triggered if the coolant temperature is over 120 ℃ or the cylinder block temperature is over 110 ℃. The engine will be turned into an idling condition automatically. This procedure keeps the circulation of the engine coolant and forces the engine components to cool down, which is effective in protecting the engine. At the beginning, the engine coolant is not circulated in the test bench, only the engine oil absorbs the engine's extra heat and speeds up the engine warm-up. When the engine oil temperature is over 75 ℃, the coolant conditioning system will become involved to cool down the engine with the engine oil synergistically.

3.2 Methodology

3.2.1 Investigation Approach

This section introduces the methodology of this thesis in more detail. The investigation approach for the optimization and control of a dual-loop EGR diesel engine is presented.

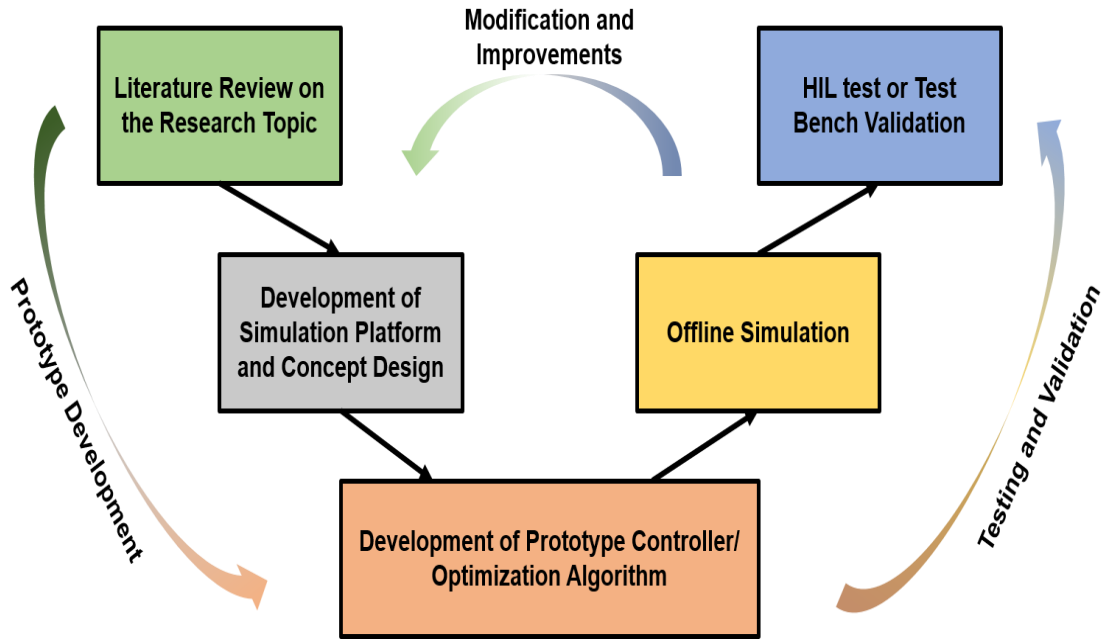

Figure 3-11 Workflow of the Research

As shown in the flowchart above, the research activities can be categorized into five stages. The details of the proposed engine optimization algorithm and advanced engine controllers will be introduced in the following chapters:

- Literature review on the research topic - the compressed ignition engine is a typical engineering product that has existed for a long time. The literature review

on the research topic points out the future trends and the demand for engine optimization and control. It is helpful to inspire innovative ideas for academic research. More importantly, the literature review could provide possible solutions to solve these engineering or scientific problems.

- Development of simulation platform and concept design - for engine control studies, a control-oriented real-time engine model should be developed as a simulation platform. It is used for the first-stage test of the controller or optimization algorithm. This model should capture the characteristics of the air path during transient operations. It should also reflect the engine's torque trajectory with acceptable accuracy to evaluate the engine's fuel economy. The concept design determines the basic structure of the algorithm, the control objects, optimization targets and the control variables.

- Development of prototype controller/algorithm - this stage mainly focuses on building the prototype controller/optimization algorithm. It includes whole algorithm programming, system debugging, and calibration. After this stage, the research continues with testing and validation.

- Offline simulation - the first step in testing and validation. Both the intelligent transient calibration algorithm and the advanced engine controller should be implemented on the simulation platform to show their potential and evaluate their performance. It is necessary to have several case studies to prove the

optimization algorithm, or that the controller could work under various conditions. If the results could not meet the demands, the researcher should go back to the previous stage and conduct modifications.

- Online validation - the last step of the research. The results from the proposed optimization algorithm should be validated on the engine test bench. To reduce the cost and complexity, the proposed engine controller could be tested by the HIL test platform. The main reason is to affirm the controller's real-time capability and robustness. Modification and improvements to the controller or algorithm are still needed if the online validation fails.

3.2.2 Offline Simulation

A control-oriented real-time model for the diesel engine's air path is developed. The engine modelling software 'GT-Power' is used in this study. It is used as the engine model for the research activities in the following chapters. The input and outputs ports are also added to the model so that it could work with the controller or optimization algorithm. The cooperated-simulation is operated in the MATLAB environment (MATLAB 2016a and 2016b). The desktop is equipped with a Windows operating system, Intel I5 2.8 GHz processor and 8 GB ram. The figure below shows the overview of the engine air-path model developed in GT-Power. The development of the model receives the support (providing engine test data and model development guidance) from the engine supplier, Jaguar Land Rover.

A report from JLR is also provided for the modelling of this engine (JLR and València, 2015).

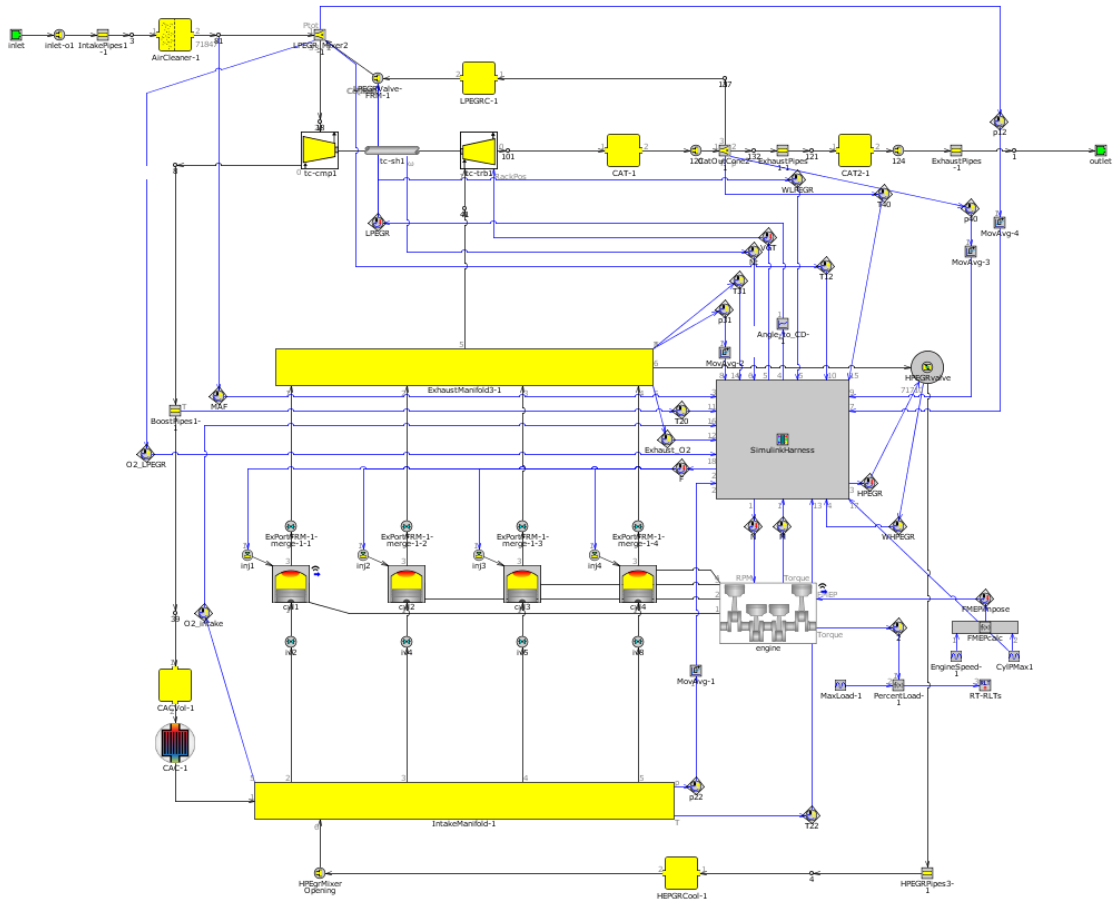

Figure 3-12 Overview of the Engine Air-path's Model in GT-Power

The modelling of the diesel engine's air path combines the method of the mean-value model, system identification and look-up tables. This control-oriented model can be operated in real time and captures the dynamic characters of the diesel air path's behaviours under both steady state and transient conditions (Zhang et al., 2017). As GT-power is a mature engine modelling software, the equations below only show the governing equations for the air-path modelling.

For the research in this thesis, the real-time diesel engine model contains five required inputs (u) and five calculated outputs (y) (Zhang et al., 2017):

$$u = [N_{eng}, Q_{fuel}, A_{VGT}, A_{HP}, A_{LP}]$$

$$y = [MAP, MAF, M_{HPEGR}, M_{LPEGR}, Torque]$$

where N_{eng} is the engine speed (rpm); Q_{fuel} represents the mass of the fuel injection in each cylinder per hub (mg/stroke); A_{vgt}, A_{hp} and A_{lp} are the actuator positions of the VGT, HPEGR valve and LPEGR valve in percentages; the MAP value shows the engine boost pressure in bar; MAF is the engine's mass air flow reading in g/s; and M_{HPEGR} and M_{LPEGR} are the EGR mass flow rate (g/s) in the HPEGR and LPEGR loop respectively. The total EGR rate (R_{EGR}) is defined as the percentage of the total EGR mass flow in the accumulated gas pumped into the engine. In terms of the LPEGR fraction (R_{LP}), it is defined as the part of the LPEGR contribution in the combined EGR mass flow. The percentage is selected as the unit for this parameter. The equations for these two signals are listed below: (Zhang et al., 2017)

$$R_{EGR} = \frac{M_{HPEGR} + M_{LPEGR}}{M_{HPEGR} + M_{LPEGR} + MAF} \times 100\%$$

$$R_{LP} = \frac{M_{LPEGR}}{M_{HPEGR} + M_{LPEGR}} \times 100\%$$

The desired MAP value (MAP_{ref}) and the feed-forward set point of the VGT rack position (VGT_{sp}) are obtained from the engine calibration maps based on the current engine speed and the mass of the fuel injection. The desired values of the EGR mass flow (M_{HPEGR_ref}, M_{LPEGR_ref}) are calculated based on the desired value of MAF (MAF_ref), the total EGR rate set point (R_{EGR_ref}) and the LPEGR portion set point (R_{LP_sp}). The equations to calculate the M_{HPEGR_ref} and M_{LPEGR_ref} are presented below:

$$M_{HPEGR\_ref} = \frac{MAF\_ref \cdot R_{EGR\_ref} \cdot (1 - R_{LP\_ref})}{(1 - R_{EGR\_sp})}$$

$$M_{LPEGR\_ref} = \frac{MAF\_ref \cdot R_{EGR\_ref} \cdot R_{LP\_ref}}{(1 - R_{EGR\_ref})}$$

The modelling of the EGR mass flow is simplified as compressible flow moving through a valve with a variable cross-section area (Heywood, 1988). Furthermore, the temperature of the EGR gas after the EGR cooler is assumed as a constant value because of its minor effect on model accuracy (Guzzella and Onder, 2010). To reduce the complexity of the model, the upstream temperature and pressure of the HPEGR gas are assumed to be identical to those of the exhaust manifold.

The engine M_{HPEGR} and M_{LPEGR} are modelled by the equations below (Wahlstr and Eriksson, 2010):

$$M_{HPEGR} = C_{HP} \cdot A_{HPEGR} \cdot \frac{P_{HP\_us}}{\sqrt{R \cdot T_{HP_{us}}}} \cdot \psi(\frac{P_{HP\_us}}{P_{HP\_ds}})$$

$$M_{LPEGR} = C_{LP} \cdot A_{LPEGR} \cdot \frac{P_{LP\_us}}{\sqrt{R \cdot T_{LP_{us}}}} \cdot \psi(\frac{P_{LP\_ds}}{P_{LP\_us}})$$

where $C_{HP}$and C_{LP} are the discharge coefficient of the EGR valve, the diameters of HPEGR and LPEGR valve are the same, which are 24.3 mm. The EGR valve configuration is the same for both HPEGR and LPEGR. The discharge coefficient of the valve is shown below; A_{HPEGR} and A_{LPEGR} are the effective opening areas of the EGR valve which are the function of the EGR valve position A_{HP_con}, A_{LP_con}; R is the ideal gas constant which is set to 8.314 J / mol·K in this case; P_{HP_us} and P_{HP_ds} represent upstream and downstream of the HPEGR valve. In this case, P_{HP_us} and P_{HP_ds} are assumed to be the same as the pressure of the exhaust and intake manifold; $P_{LP_us}$and P_{LP_ds} are the upstream and downstream of the LPEGR valve; T_{HP_us} and $T_{LP_{us}}$ are the upstream temperature of the HPEGR and LPEGR. The flow function ψ could be defined by the following equations; It is used for both the HPEGR and LPEGR loop (ReB et al., 2015).

$$\psi\left(\frac{p_{EGR\_ds}}{p_{EGR\_us}}\right)$$

$$= \begin{cases} \sqrt{\gamma \cdot (\frac{2}{\gamma})^{\frac{\gamma+1}{\gamma-1}}} & if\ P_{EGR_{ds}} < P_{cr} \\ (\frac{P_{EGR\_ds}}{P_{EGR\_us}})^{\frac{1}{\gamma}} \cdot \sqrt{\frac{2\gamma}{\gamma-1} \cdot [1 - (\frac{P_{EGR\_ds}}{P_{EGR\_us}})]^{\frac{\gamma-1}{\gamma}}} & if\ P_{EGR\_ds} \geq P_{cr} \end{cases}$$

$$P_{cr} = (\frac{2}{\gamma-1})^{\frac{\gamma}{\gamma-1}} \cdot P_{EGR\_us}$$

where $p_{EGR_us}$and p_{EGR_ds} represent the upstream and downstream pressure of the EGR gas; γ is the specific heat ratio which is set to 1.3 and P_{cr} is the critical pressure where the EGR flow achieves a sonic condition. The reverse flow of the EGR gas is neglected in this thesis. When the engine is operated under a low speed, high load and with the VGT fully opened, the p_{EGR_ds} could possibly be larger than the p_{EGR_us}. This phenomenon only happens in a small operating range. Moreover, the reversed flow could also be avoided during engine operations by closing the EGR valves (Zhang et al., 2017).

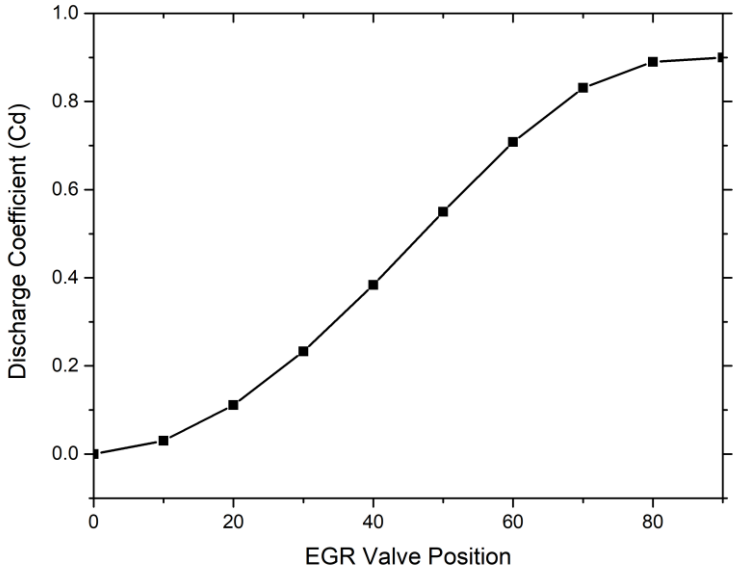

Figure 3-13 Discharge Coefficient of the EGR Valve

As for the engine MAP modelling, due to the strong coupling effect, the MAP model should consider both the engine's VGT rack position and the effects caused by the DLEGR. The equations for the MAP model are listed in the following paragraphs (Wahlström and Eriksson, 2011).

$$\frac{d}{dt}p_{im} = \frac{R \cdot T_{im}}{V_{im}}(W_c + M_{HPEGR} - W_{ei})$$

$$W_c = M_{LPEGR} + \mathrm{MAF}$$

$$[W_c, \eta_{comp}] = f(N_{turb}, T_{comp\_in}, PR_{comp})$$

$$W_{ei} = \frac{N_{eng} \cdot V_{dis} \cdot \eta_{vol}}{120RT_{im}}$$

$$\eta_{vol} = f(N_{eng}, P_{im}, T_{im})$$

where p_{im} is the intake manifold pressure; R is the ideal gas constant; T_{im} represents the intake manifold temperature; V_{im} is the volume of the intake manifold, which is 3.338L; W_c is the compressor mass flow rate; W_{ei} means the amount of gas pumped into the engine cylinders; N_{turb} is the shaft speed of the turbine shaft; η_{comp} is the efficiency of the compressor; T_{comp_in} is the temperature of the gas sucked into the compressor; η_{vol} is the volumetric efficiency of the engine; V_{dis} represents the engine displacement volume, which is 1.996L ; and P_{im} and P_{em} are the pressure of the intake and exhaust manifold (Zhang et al., 2017). Even though the gas temperature after the engine's CAC could be assumed to be a constant value, the involvement of the M_{HPEGR} would significantly affect the T_{im} value. In addition, the change of the A_{HP} and A_{LP} would change the η_{vol} and W_{ei} results (Zhang et al., 2017). The engine MAF and LPEGR mass flow form the mass flow of the compressor. Under the same compressor mass flow, there would be a trade-off between them. As shown in Figure 3-2, the turbine shaft connects the engine compressor and the engine VGT. The kinetic energy received by the VGT results in different N_{turb} values, which determine various W_c and η_{comp} .This process could be modelled by the following equations below (Kocher et al., 2011; Kyunghan et al., 2015;Zhang et al., 2017):

$$\frac{d}{dt}p_{em} = \frac{R \cdot T_{em}}{V_{em}}(W_{ei} + Q_{fuel} - M_{HPEGR} - W_{turb})$$

$$T_{em} = T_{im} + \frac{Q_{LHV} \cdot f(W_{fuel}, N_{eng})}{c_{p,exh} \cdot W_{ei}}$$

$$[W_{turb}, \eta_{turb}] = f(T_{em}, PR_{turb}, N_{turb}, A_{vgt})$$

$$P_t = W_{trub} \cdot c_{p,exh} \cdot \eta_{turb} \cdot T_{em}(1 - \frac{P_{amb}}{P_{em}})^{\frac{\gamma_{exh}-1}{\gamma_{exh}}}$$

$$P_{comp} = \frac{W_c \cdot c_{p,amb} \cdot T_{comp\_in}}{\eta_{comp}}[\left(\frac{P_{cac}}{P_{amb}}\right)^{\frac{\gamma_{amb}-1}{\gamma_{amb}}} - 1]$$

$$\frac{dN_{turb}}{dt} = \frac{\eta_m P_{turb} - P_{comp}}{I_{turb} N_{turb}}$$

where T_{em} is the temperature of the exhaust manifold; V_{em} equals the exhaust manifold volume, which is 1.5L; W_{turb} is the mass flow rate of the VGT; Q_{LHV} means the low heating value of the diesel; P_t and P_{comp} are the power of the VGT and the compressor; η_{turb} is the efficiency of the VGT; PR_{turb} is the pressure ratio of the VGT; $c_{p,exh}$ and $c_{p,amb}$ are the specific heat ratio of the exhaust gas and ambient gas; P_{amb}, P_{cac} represent the gas pressure in the ambient atmosphere and compressed air cooler; γ_{amb} and γ_{exh} are the specific heat ratio for ambient air and exhaust gas; η_m is the mechanical efficiency of the

turbine shaft, which is a constant value; and I_{turb} is the momentum inertia of the turbocharger (including the compressor and the turbine), which is set to 2.5×10^{-5} kg-m^2 (Zhang et al., 2017). $f(W_{fuel}, N_{eng})$ is the correlation factor is determined from an empirical model which uses injected fuel mass and engine speed as model inputs (Kyunghan et al., 2015).

The diesel engine's VGT and compressor are complex devices. To simplify the model and reduce calibration work, the look-up table method is selected in GT-power, the function of $[W_{turb}, \eta_{turb}]$ and $[W_c, \eta_{comp}]$. The performance of the VGT and compressor (rotation speed, efficiency) are modelled into several look-up tables. The VGT maps can be summarized as a series of performance data points, each map describes the operating condition by speed, pressure ratio, mass flow rate and thermodynamic efficiency. The VGT data used in this work is provided by the engine supplier. The figure below shows the maps of the engine compressor from the compressor supplier Mitsubishi.

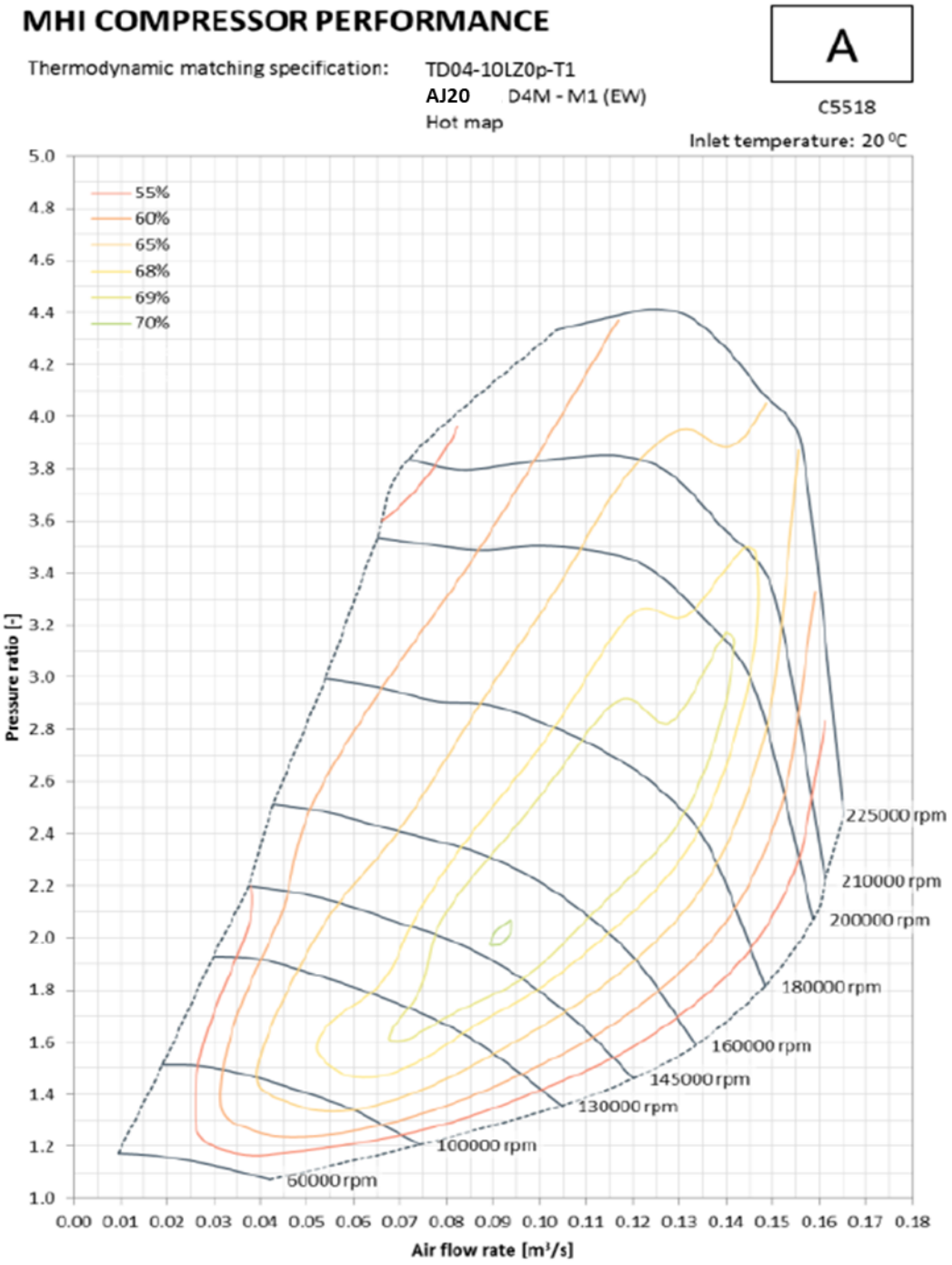

Figure 3-14 Compressor Map from the Supplier

The figure below shows the VGT mapping data in GT-Power. Due to the huge amount of the data, the figure only shows one set of the VGT mapping data as an example.

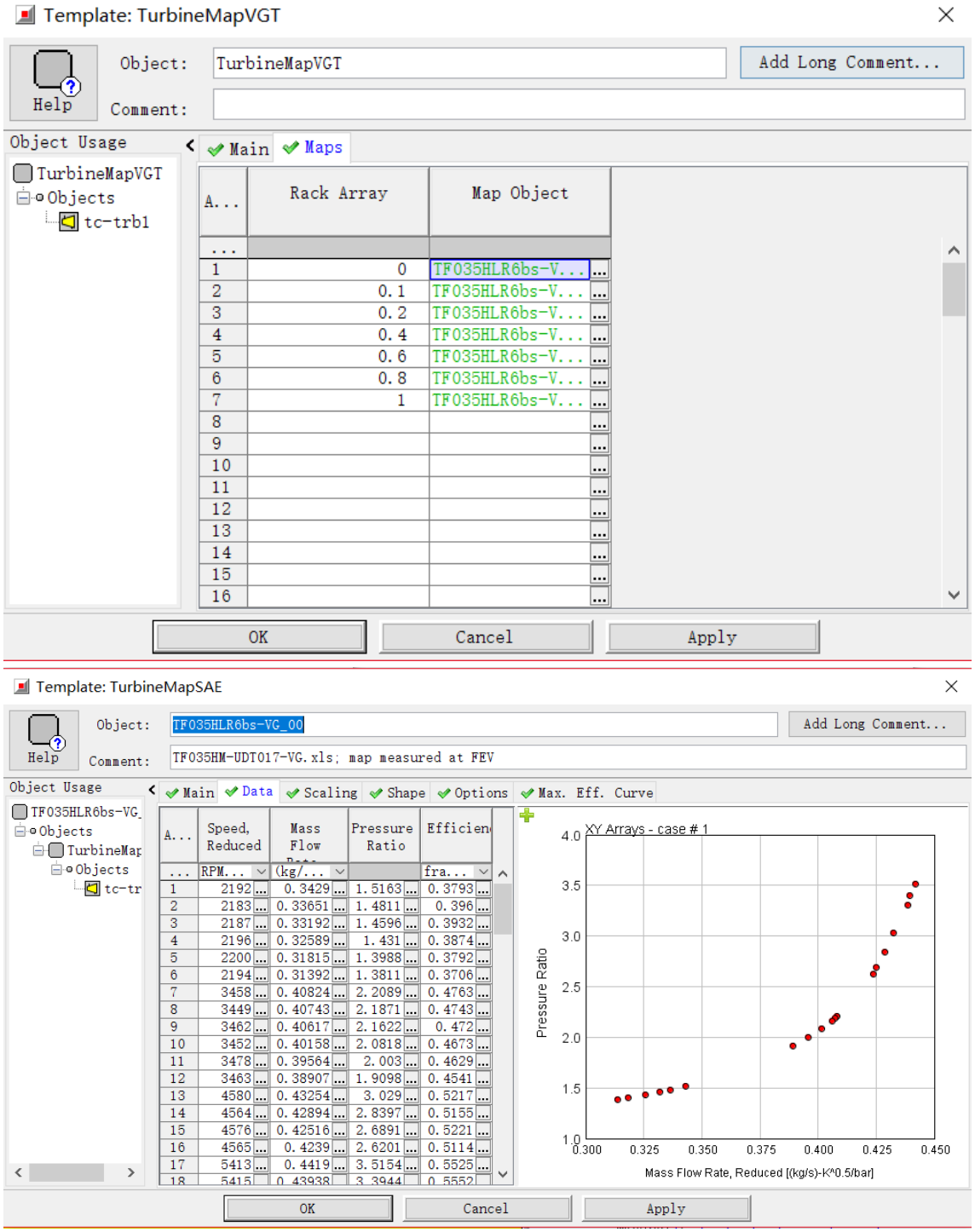

Figure 3-15 VGT Mapping Data in GT-Power

The simulation platform is designed for developing real-time controllers, a detailed thermodynamic method is not considered in the engine combustion modelling process. The engine fuel injection strategies are simplified into one pilot

injection and one main injection. In GT-Power, the following equations are used to model the engine IMEP

$$IMEP = \eta_e \cdot \frac{Q_{LHV} \cdot Q_{fuel}}{V_d}$$

$$\eta_e = f(N_{eng}, Q_{fuel}, R_{EGR})$$

where η_e is the correlation factor determined by a 3D look-up table (the three inputs are engine speed, mass of fuel injection and total EGR rate), the raw data to formulate the look-up table is supplied by the engine supplier; Q_{LHV} is the low heat value of diesel which is 42.6 MJ/kg. Several engine parameters such as air-fuel ratio and injection timing etc. could affect the efficiency of the engine's combustion process. Considering the available model parameters and the computational time, only the total EGR rate is selected to avoid increasing the model complexity unnecessarily (Zhang et al., 2017). The table blow shows the correlation map.

In the FMEP model, the mechanical inertias of the engine crankcase integrate with other friction losses. It is an empirical model which considers the engine speed and maximum cylinder pressure (Zhang et al., 2017). The governing equation is defined as (JLR and València, 2015):

$$FMEP = a_1 + a_2 \cdot N_{eng} + a_3 \cdot P_{cyl\_max} + a_4 \cdot {N_{eng}}^2 + a_5 \cdot {P_{cyl\_max}}^2 + a_6 \cdot N_{eng} \cdot P_{cyl\_max}$$

where P_{cyl_max} is the maximum cylinder pressure in bar; $a_1, \cdots, a_5$ are constant numbers which are identified via curve fitting with experiment data. Based on the test data from the engine supplier, the values for $a_1, \cdots, a_5$ are determined as 0.614, 7.16×10^{-5}, 3.24×10^{-4}, $0.93 \times 10^{-7}$and 2.34×10^{-5}.

As for the pumping mean effective pressure (PMEP), the equations are defined as (Heywood, 1988):

$$PMEP = P_{em} - P_{im} \quad if\ P_{em} > P_{im}$$

$$PMEP = -(P_{em} - P_{im}) \quad if\ P_{im} > P_{em}$$

Normally, the engine PMEP would be a positive value. But when the engine operated at low-speed full load with sudden-opened EGR valves, the PMEP value would be a negative value. But the full-load condition is not investigated in this thesis. Besides, the EGR values shouldn't be opened in such conditions as the engine will no longer maintain the boost pressure and the engine EGR rate is also not achievable as the EGR flow couldn't flow into the intake manifold. So the

equation above could be used in this case.

So, the engine brake mean effective pressure (BMEP) is calculated based on IMEP, FMEP and PMEP.

$$BMEP = IMEP - FMEP - PMEP$$

The detailed validation of the simulation platform is shown in Chapter 4, in the section of results and discussions.

3.2.3 Engine Test Plan

To evaluate the performance of the proposed optimization algorithm and advanced engine controller, engine transient scenarios should be designed. The designed engine test sequences on the test bench are different from those on vehicles. As introduced in section 3.1, the dynamometer is operated in the speed mode. To cope with the operation mode and guarantee the results' accuracy, the test sequences are designed as step-changed engine loads under constant engine speed. They are suitable for the engine transient study on the test bed. The dynamometer has the advantage of the maintaining stable engine speed. The engine is only in charge of the torque generation. This kind of test sequence is to avoid uncontrolled fluctuation of engine speed, which decreases the complexity of data processing and improves the repeatability of the results. The

engine speed is set as 1500 and 2000 rpm, which are the typical working range for modern light-duty diesel engines. The engine load is adjusted by the mass of fuel injection, which falls between 10 and 50 mg/stroke. It helps to get rid of the affection of the paddle fluctuation, which helps to improve the data quality. Besides, the engine torque could be used directly to evaluate the performance the fuel economy. Under the same fuel injection trajectory, a larger torque means higher engine efficiency and more optimal fuel economy. The study in this case mainly focuses on the light and medium load.

To test the capability of the proposed CAPSO algorithm, several case studies are presented. The designed test sequences are shown below:

Table 3-6 Design of Test Sequences

Engine Speed	Mass of Fuel Injection	Transient Period
1500 rpm	15-20 mg/stroke	0.1s
	15-40 mg/stroke	0.1s
	15-30 mg/stroke	0.1s
2000 rpm	15-20 mg/stroke	0.1s
	15-40 mg/stroke	0.1s

In terms of the test sequence for advanced engine controllers, the engine's speed is maintained at 2000 rpm and the mass of the fuel injection changes based on the trajectory shown in Figure 3-12. The mass of fuel injection remains stable for

50 s to stabilize the model's outputs. This kind of sequence is used to cope with the speed operation mode introduced in section 3.1. The transient period is a setting of experiment design, which determines the time for the mass of fuel injection to change from one value to another. It is could be controlled by the test bed controller. Even though only the mass of fuel injection changes in this case, it is still capable of evaluating the controllers' performance. The design of the proposed controllers has considered both engine speed change and mass of fuel injection change.

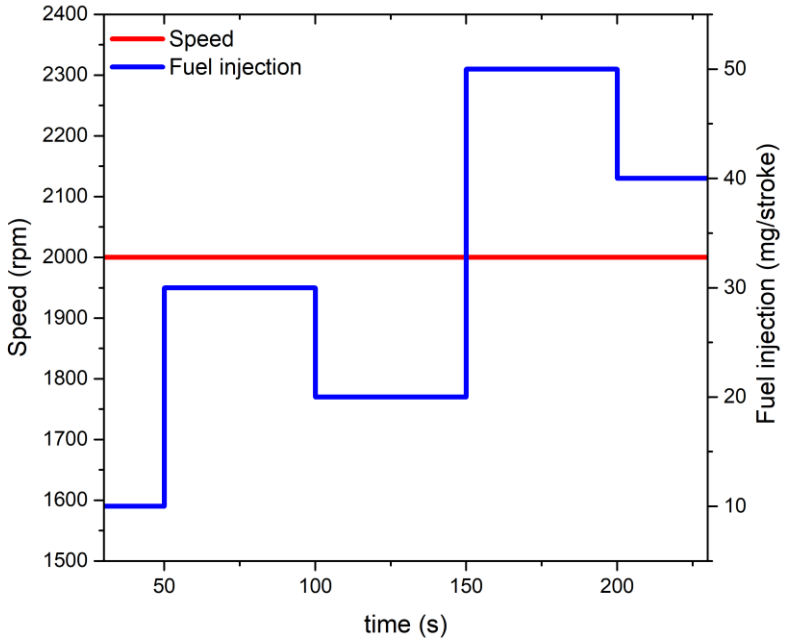

Figure 3-16 Trajectory of Engine Speed and Mass of Fuel Injection

As for the HIL test, the test sequence is still formed by a step-changed mass of fuel injection under a constant engine speed. The engine speed is still designed as 2000 rpm while the mass of the fuel injection increases from 15 mg/hub to 20 mg/hub and then decreases back to 15 mg/hub (Zhang et al., 2017).

3.3 Summary

This chapter introduces the experiment set-up and the methodology for the study. The experimental system consists of the engine specification, engine test bench, and HIL test platform. The test bench can conduct transient manoeuvres with the help of a powerful dynamometer; while the conditioning system maintains accurate temperature control during the experiments. The AVL PUMA system and the engine's ECU play the role of monitoring and recording the test data. The HIL platform is used as a flexible, low-cost testing method to validate the real-time capability of the controller.

The methodology involves the investigation approach, the real-time engine model and the engine test plans. The investigation approach can be categorized into the stages of prototype design, offline simulation and online validation. The real-time model provides the software environment to conduct the simulation. The engine test plan provides the same evaluation standard for the results.

CHAPTER 4 INTELLIGENT TRANSIENT CALIBRATION

The author has published the work presented in this chapter in the journal of 'Proceeding of IMechE, Part D: Journal of Automobile Engineering' as the first author (Zhang et al., 2018). In this chapter, an CAPSO-based intelligent transient calibration method is presented for the air path controller of a light-duty diesel engine. The target of this method is reducing the fuel consumption of the engine during transient scenarios through the optimization of the controller parameters (Zhang et al., 2018). The optimization results of the proposed CAPSO-based method are compared with the results of using the baseline calibration. Finally, engine tests are conducted to validate the performance with the calibrated controller (Zhang et al., 2018).

4.1 Introduction

The air path of the diesel engine which includes the dual-loop EGR can be regarded as a multiple-input, multiple-output (MIMO) system, which has the characteristics of coupling effect, strong non-linearity and delay. As a result, the engine calibration, especially the transient calibration process, has been made more complex and will consume more time. To overcome these difficulties, commercial software, including the AVL CAMEO and Matlab Model-based

Calibration toolbox, have been developed for automotive industries. However, the above-mentioned software mainly focuses on the calibration of static conditions. Moreover, they require a large amount of data to build the empirical model (Ma et al., 2014;Zhang et al., 2018). The swarm intelligence algorithms have the advantages of less computational effort and easy implementation, compared with other metaheuristic algorithms (Guzzella and Onder, 2010; Tayarani et al., 2015). Thus they are applied in the area of controller intelligent calibration (Rogers and Birge, 2004;Watson et al., 2006;Fang et al., 2011;Reynoso-Meza et al., 2014;Bourouba and Ladaci, 2016;Zhang et al., 2018). Researchers have found that the accelerated particle swarm optimization (APSO) algorithm has a better performance than the conventional PSO algorithm in dealing with multiple objective optimization issues (Rahman et al., 2016;Zhang et al., 2018). However, the results of both PSO and APSO algorithm may occasionally trap in a local optimal position, rather than a global optimal position. To solve that problem, chaotic mapping strategies are combined with the APSO algorithm to develop a novel CAPSO algorithm. The CAPSO algorithm not only jumps out of the ‘local optimal’ trap, but also enhances the result’s repeatability (Liu et al., 2005;Tan, 2012;Yang et al., 2014; Shen et al., 2016;Zhang et al., 2018).

In this chapter, an intelligent transient calibration method is developed for the air path controller of a diesel engine. This work is organized as follows: in section 4.2, the structure of the air path controller is introduced. Section 4.3 firstly

demonstrates and explains the proposed CAPSO-based calibration algorithm. Then follows the experimental apparatus and procedure. Section 4.4 validates the proposed transient calibration method via several case studies and proceeds a Monte Carlo analysis and a repeatability test to compare the CAPSO algorithm and conventional APSO algorithm. The simulation platform is also validated in this chapter. Eventually, the conclusions are summarised in section 4.5.

4.2 Controller Structure

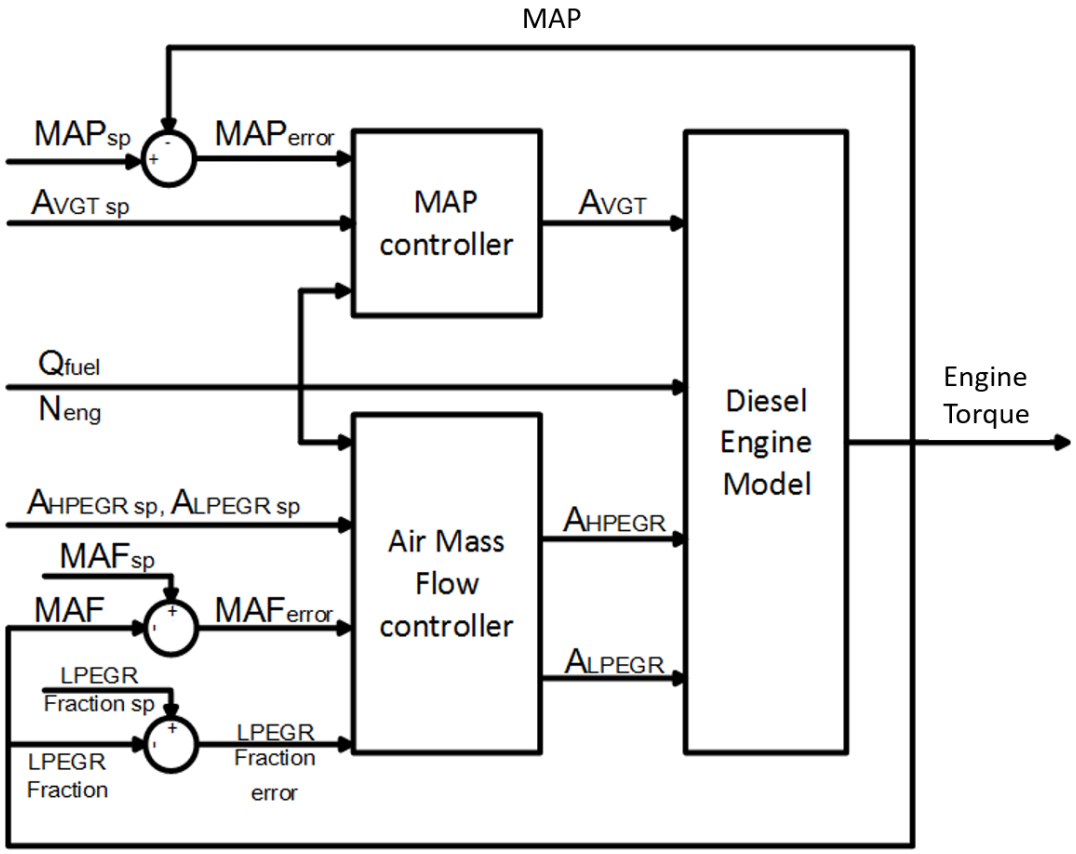

Figure 4-1 Structure of the embedded engine model

As shown in Figure 4-1, the embedded model consists of a diesel engine model

and an air path controller (Zhang et al., 2018). The detailed introduction of the engine model has been shown in the chapter 3, section 3.1.5. In terms of the air path controller, the conventional PI control strategy is adopted. The control strategy for the model is same with the one used in the engine ECU. The air path controller could be divided into two parts: the boost pressure control and the air mass flow control. For the boost pressure controller, the inputs are the VGT rack position set point, MAP error, mass of fuel injection and engine speed. In particular, the MAP error represents the difference between the actual MAP and MAP setpoint (Zhang et al., 2018):

$$e_{MAP\,(t)} = MAP_{sp} - MAP_{actual}$$

The MAP controller is applied to control the VGT rack position based on this error signal. The final outputs of the MAP controller include not only the feedback PI strategy, but also the feed-forward setpoint of the VGT rack position (Zhang et al., 2018).

$$VGT_{(t)} = K_p \cdot e_{MAP\,(t)} + K_i \cdot \int_0^t e_{MAP\,(t)} \cdot dt + A_{VGT_{sp}\,(t)}$$

The air mass flow control is achieved through the combination of two PI controllers. One PI controller focuses on the MAF trajectory tracking, the other

takes charge of the LPEGR fraction. The required inputs are the MAF error, LPEGR fraction error, HPEGR valve position set point, LPEGR valve position set point, engine speed and mass of fuel injection (Zhang et al., 2018), while the actual HPEGR and LPEGR valve positions are the outputs of the controller. The detailed structure, the LPEGR fraction error and the MAF error are introduced by the following equations (Zhang et al., 2018):

$$e_{MAF\ (t)} = MAF_{sp} - MAF_{actual}$$

$$e_{LPEGR\ fraction\ (t)} = LPEGR\ fraction_{sp} - LPEGR\ fraction_{actual}$$

Based on the report about the air path controller (JLR and València, 2015), the MAF value is monitored by the MAF controller via a 'virtual EGR valve' ($EGR_{(t)}$) in this case. The virtual EGR valve signal is divided into two different signals for both HPEGR and LPEGR valves by a splitting factor (κ). Through actuating over the splitting factor (κ), the LPEGR fraction controller could keep the desired LPEGR fraction following the desired value. The equations are shown as following (Zhang et al., 2018):

$$EGR_{(t)} = K_p \cdot e_{MAF\ (t)} + K_i \cdot \int_0^t e_{MAF\ (t)} \cdot dt + EGR_{sp\ (t)}$$

$$\kappa_{(t)} = K_p \cdot e_{LPEGR\ fraction\ (t)} + K_i \cdot \int_0^t e_{LPEGR\ fraction\ (t)} \cdot dt + LPEGR_{sp\ (t)}$$

$$EGR_{sp\ (t)} = HPEGR_{sp\ (t)} + LPEGR_{sp\ (t)}$$

$$HPEGR_{(t)} = EGR_{(t)} \cdot \kappa_{(t)}$$

$$LPEGR_{(t)} = EGR_{(t)} \cdot (1 - \kappa_{(t)})$$

The control strategy of the diesel engine's air path is developed in an Open-ECU, it cannot be compared with strategy in the commercial ECU. But the feed-forward control still exists in the controller (Zhang et al., 2018). The feed-forward values of the actuator positions are included in the controller design. In this case, the feed-forward setpoints are acquired by the engine working conditions (engine speeds and mass of fuel consumptions). They are set to the same values of the actuator positions under steady state conditions to reduce the complexity of the controller (Zhang et al., 2018). To solve this specific problem, the proposed CAPSO-based calibration algorithm mainly focuses on the optimization of the PI values.

4.3 Methodology of Model Based Optimization

4.3.1 Multiple-Objective Optimization Issue

Three control objects: the engine MAP, MAF and LPEGR fraction, are contained in the controller. Therefore, the calibration process can be regarded as a multiple objective optimization problem with constraints, which can be processed by the proposed CAPSO algorithm.

In this work, Kp and Ki values ($K_{p\_MAP}, K_{i\_MAP}, K_{p\_MAF}, K_{i\_MAF}, K_{p\_LPF}\ and\ K_{i\_LPF}$) are selected as the calibration parameters. The boundaries of these calibration parameters are restricted by the search area. A wider search area could help to get more optimal results; however, it will also consume more computational time.

The cost function is the criterion for the optimization algorithm. The integrals of square error (ISE) are selected as the cost function of the parameter tuning (Zhu Wang et al., 2016;Zhang et al., 2018).

$$ISE_i = \int_0^{t_s} e_i^2(t)\, dt$$

where ei(t) = ri(t) - y(t), it is the error value of each controller object. The ISE values for each target are named as ISEMAP, ISEMAP and ISELPF respectively (Zhang et al., 2018).

Therefore, the overall ISE value of the three control targets using the weighted sum method (Fonseca and Fleming, 1993) is designed as the cost function of the controller behaviour, as shown in the following equations::

$$J_1 = W_1 \cdot \frac{ISE_{MAP}}{CF_1^*} + W_2 \cdot \frac{ISE_{MAF}}{CF_2^*} + W_3 \cdot \frac{ISE_{LPEGR\ fraction}}{CF_3^*}$$

$$W_1 + W_2 + W_3 = 1 \quad W_1, W_2, W_3 \in (0,1)$$

where W_1, W_2 and W_3 are the weighting factors allocated to the optimization objects. A lower weight value means it has a lower impact to the total cost function. Due to coupling effects, the MAP, MAF and LPEGR fraction will affect each other. Since the MAP value regulates the total amount of the gas pumped into cylinders, the MAP weight should be relatively higher. CF_1, CF_2 and CF_3 are correlation factors to assure the ISE value for each control object could be in the same scale (Zhang et al., 2018).

The stability of the optimal controller is also considered when designing the optimization cost function. In this work, the cost function is designed in the format of integrals of square error (ISE) based on the literature review focusing on this problem. The ISE calculates the integral of the squared output error. Therefore, when the system outputs are unstable, the value of the cost-function could reflect the instability. Besides, different engine speeds and loads are involved in the test

sequences. In this way, the stability of the optimal controller under various working conditions can be tested.

4.3.2 Structure of the Intelligent Transient Calibration Algorithm

The chaos-enhanced accelerated particle swarm optimization (CAPSO) algorithm (Q. Zhou et al., 2017a;Zhang et al., 2018) is modified based on the conventional APSO algorithm. Figure 4-2 shows the calibration process of the CAPSO-based algorithm for a diesel engine's air path controller (Zhang et al., 2018). The CAPSO-based algorithm, as shown in Figure 4-2, is formed by three parts. The first part is the setting of the initial conditions, including the number of iterations, number of particles in each swarm and the boundaries of the search area. The initial particles are generated randomly from the information provided in this part (Zhang et al., 2018). Then the iteration process begins after the initial particles are generated. The cost function value of each particle will be obtained through the co-simulation with the engine model. They will be compared to find the current local optimum result. Next, in each iteration, the particles will be updated based on their current positions, the local best position in the swarm and a random factor. The process is repeated based on iterations. When the boundaries are achieved or the iteration stops, the solution of the last iteration is the final optimal result.

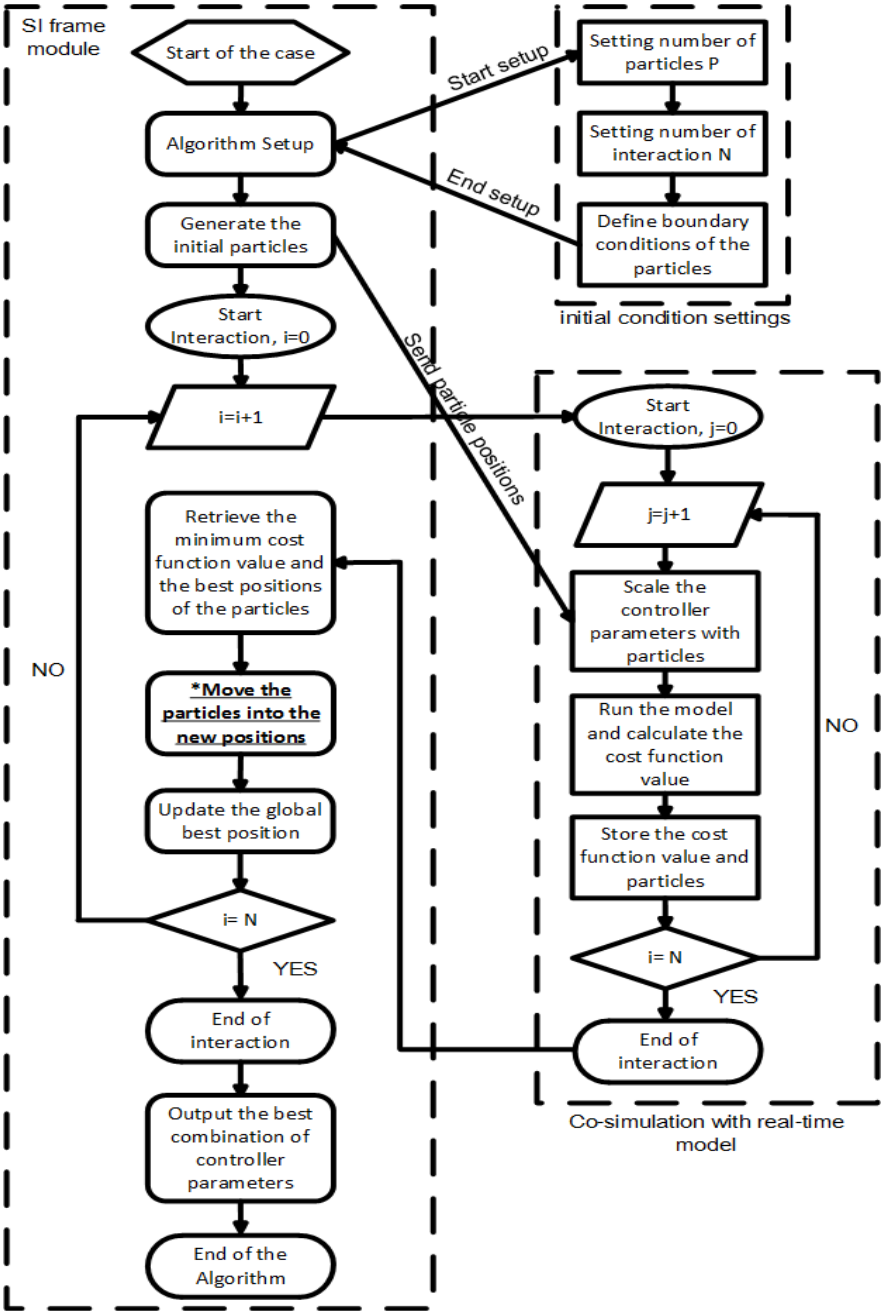

Figure 4-2 Workflow of the CAPSO Algorithm in the calibration of a Diesel Engine's Air Path Controller

It is shown in section 4.3.1, the particles in the swarm are defined as (Zhang et al., 2018):

$$x^{(i,j)} = [Kp_{map}{}^{(i,j)}, Ki_{map}{}^{(i,j)}, Kp_{maf}{}^{(i,j)}, Ki_{maf}{}^{(i,j)}, Kp_{LPEGR\ fraction}{}^{(i,j)}, Ki_{LPEGR\ fraction}{}^{(i,j)}]$$

where i (1, 2, 3…N) is the index of the interactions, for a CAPSO algorithm that has N iterations; j (1, 2, 3…P) is the index of the particles in each swarm (Zhang et al., 2018).

The evolution of the particles is the key part in the CAPSO algorithm. The governing equations are shown below (Zhang et al., 2018):

$$x^{(i+1,j)} = x^{(i,j)} + \beta\left(g^{(i,*)} - x^{(i,j)}\right) + \alpha^{(i)} \cdot r^{(i,j)}$$

$$\alpha^{(i)} = \alpha^{(0)} \cdot \rho^{i}$$

where β is the attraction parameter of the CAPSO algorithm; $r^{(i,j)}$ is a random movement of the particle inside its searching area; $g^{(i,*)}$ is the best position at ith interaction; α is the convergence parameter which will be updated during each

iteration. The setting range of $\alpha^{(0)}$ is suggested to fall between 0.5 and 1, while the setting range of ρ is suggested to fall between 0 and 1 by Bourouba and Ladaci (Bourouba and Ladaci, 2016). In this work, $\alpha^{(0)}$ is determined as 0.9, and ρ is determined as 0.8. The value of β normally falls between 0 and 1, and it has strong relation with the convergence speed of the CAPSO algorithm. In the conventional APSO algorithm, β is a fixed value of 0.5 (Q. Zhou et al., 2017a). This setting could work effectively, however, the optimization results still change slightly. To overcome the problem, chaotic mapping strategies are adopted in CAPSO algorithm to form a variable setting of β value. Through this way, the particles could escape from a local best result. In this work, logistic mapping strategy is used as the chaotic mapping strategy considering its high dispersion of the randomly generated number (Gandomi et al., 2013; Q. Zhou et al., 2017a;Zhang et al., 2018) , which can be described by the following equation:

$$\beta^{(i+1)} = a \cdot \beta^{(i)} \cdot (1 - \beta^{(i)})$$

where a is set to 0.4 and the initial value of β is set to 0.7 for this case. Both alpha and beta values are the parameters to update the particle's position. It should be noticed that the value of alpha and beta will only affect the performance of the algorithm and they have no relation with the engine load conditions (Zhang et al., 2018).

4.3.3 Transient Calibration System

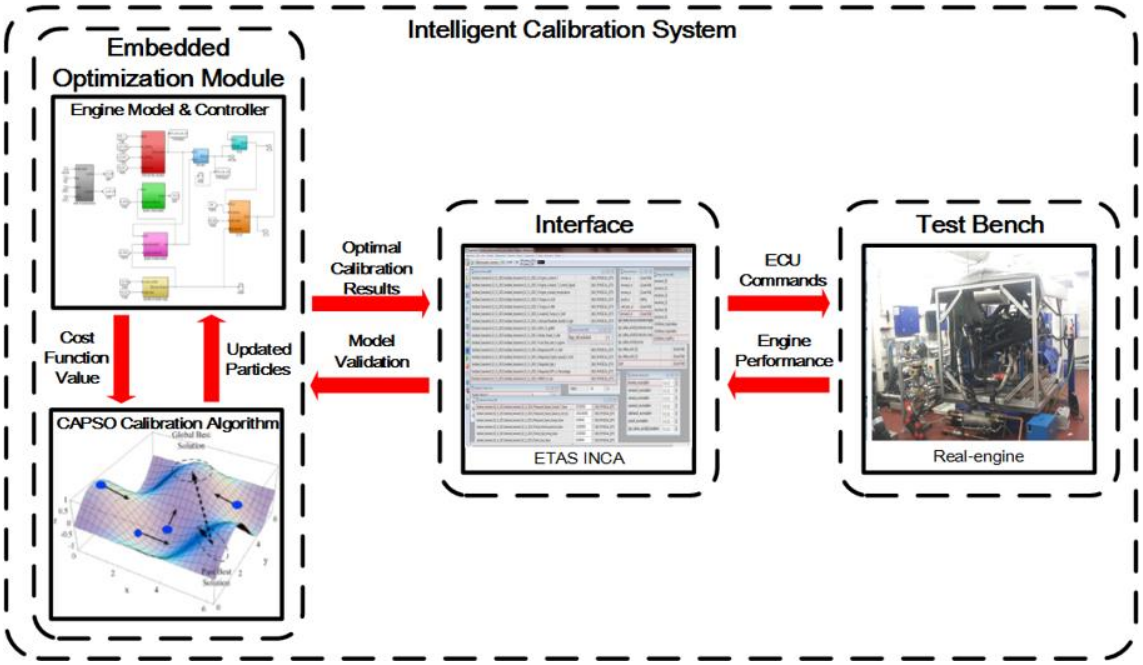

Figure 4-3 Interface of the real-time model and the CAPSO calibration algorithm

The structure of the transient calibration system is shown in Figure 4-3. This system is formed by the ECU interface, the embedded optimization module and the engine test bench. The embedded optimization module includes the transient calibration algorithm and the engine. After the model-based optimization process, the calculated results will be sent into the ECU interface, which could use the results from the embedded optimization module to replace the ECU calibration. The model-based optimization results could be validated through the real engine tests (which have been introduced in chapter 3), while the test bench data are beneficial for the further improvement of the engine model's accuracy (Zhang et al., 2018).

4.4 Result and Discussion

4.4.1 Validation of the Simulation Platform

The simulation platform is validated by WLTP cycle. The trajectories of mass of fuel injection, the engine speed, VGT rack position and LPEGR valve position are recorded from the real engine, and then they are taken as the model inputs which will be sent into the simulation platform. The validation process mainly focuses on the trajectories engine MAF, MAP, LPEGR fraction and the engine torque, as shown in Figure 4-4 (Zhang et al., 2018). The model accuracy is evaluated by calculating the fitting rate and the dynamic error. Their equations are listed (Tan, 2015;Zhang et al., 2018):

$$fit(i) = \left[1 - \frac{\|y_{meas} - y_{model}\|}{\|y_{meas} - \bar{y}_{meas}\|}\right] \times 100\%$$

$$y_{error}(i) = \frac{y_{meas}(i) - y_{model}(i)}{1/N \sum_{i=1}^{i=n} y_{meas}(i)} \times 100\%$$

where y_{meas} and y_{model} are the measured output of the engine and the simulated output from the model, respectively; $\bar{y}_{meas}$ is the mean value of the data sequences of the engine; '|| ||' means the Euclidean distance.

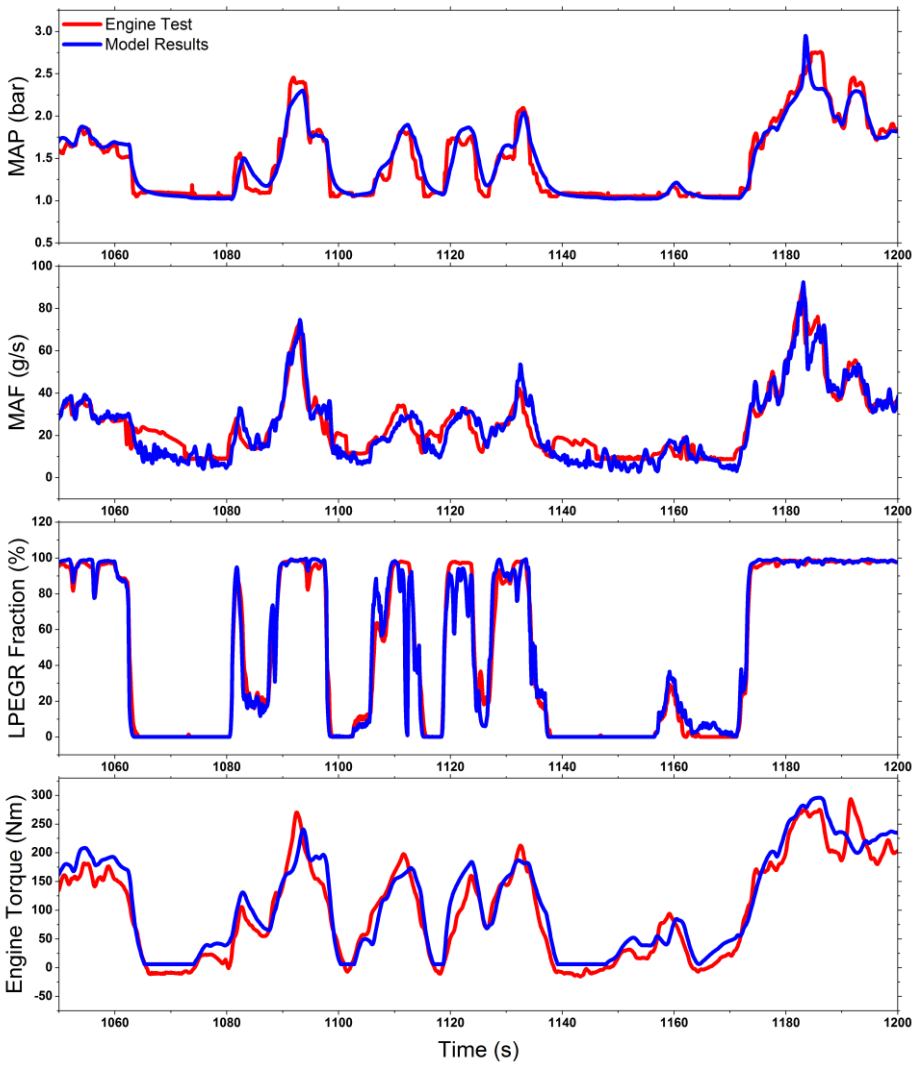

Figure 4-4 Comparison between the Simulation Results and Engine Test Results of WLTP (1070s-1200s); MAP; MAF; LPEGR Fraction and torque

Even though the presented figure includes only part of the test cycle, the model fitting rate and the dynamic error are calculated based on the whole test cycle (Zhang et al., 2018). . The simulation results agree well with the experimental data. The engine MAP, MAF, LPEGR fraction and engine torque show a fitting rate of 83.74%, 85.41%, 80.86% and 82.53%, respectively (as listed in Table 3-6). The dynamic errors of them are all less than 10%. Based on engine modelling work in the research team's previous thesis (Ma, 2012; Tan, 2015), the dynamic

error and fitting rate of the engine model in this work are still within the acceptable range. Besides, during transient operations, most peaks and troughs of the engine parameters could be successfully captured by the simulation platform. The characteristics of the diesel engine's air path are reflected properly. Therefore, it could be concluded that this platform is qualified of presenting the results for the research activities in the thesis.

Table 4-1 Model Fitting Rate and Dynamic Error

Specification	Fitting Rate	Dynamic Error
MAP	83.74%	5.57%
MAF	85.41%	9.49%
LPEGR Fraction	80.86%	8.22%
Torque	82.53%	7.84%

4.4.2 Comparison between CAPSO and Conventional APSO Algorithm

In this thesis, the proposed CAPSO calibration algorithm is modified from conventional APSO algorithm. The evaluation in this study should consider both the algorithm itself and case studies of the engine transient scenarios. Therefore, the comparison between the APSO and CAPSO, including the convergence speed, Monte Carlo analysis and the reputation evaluation, is conducted based on one case study in the following paragraphs.

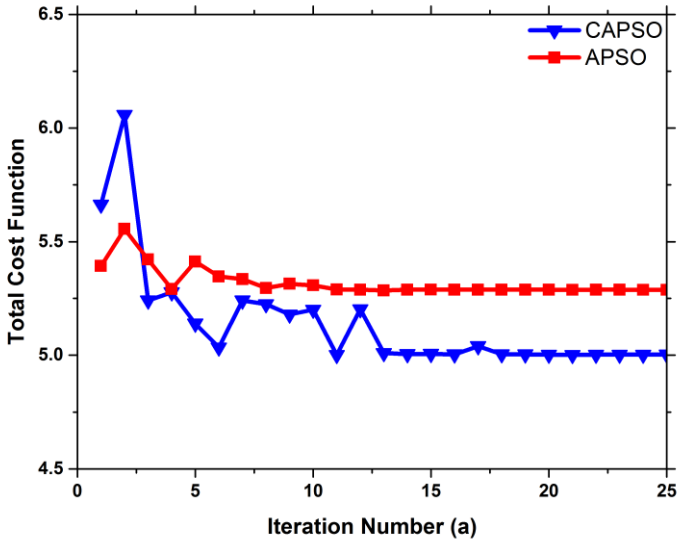
CAPSO
APSO
Total Cost Function
Iteration Number (a)
6.5
6.0
5.5
5.0
4.5
0
5
10
15
20
25

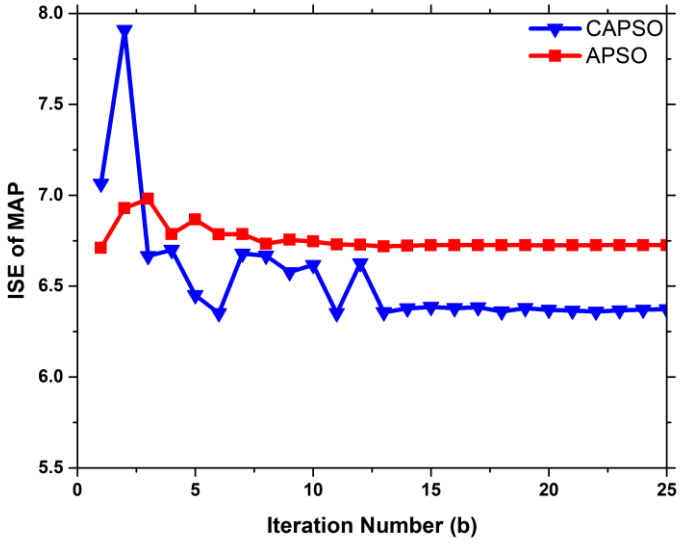
CAPSO
APSO
ISE of MAP
Iteration Number (b)
8.0
7.5
7.0
6.5
6.0
5.5
0
5
10
15
20
25

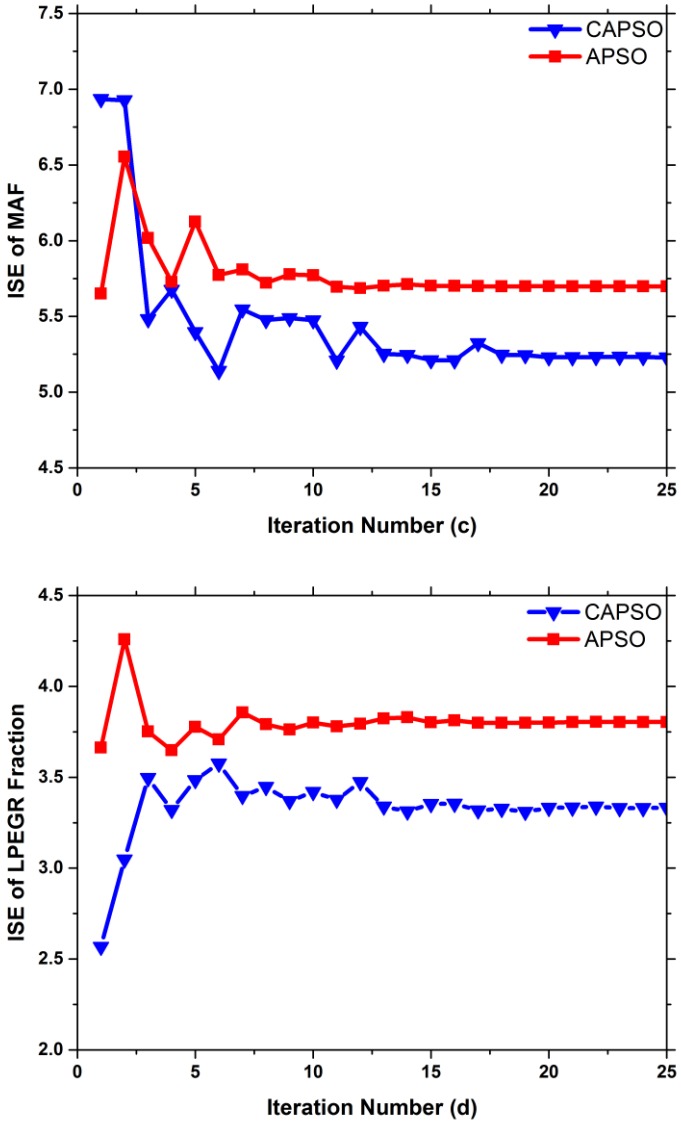

Figure 4-5 Trajectory of the Total Cost Function Value (a); ISE of MAP (b); ISE of MAF (c); ISE of LPEGR Fraction (d); Using the CAPSO Algorithm and conventional APSO Algorithm

Figure 4-5 presents the intelligent calibration results of APSO and CAPSO algorithm, respectively. From Figure 4-5, both the two algorithms could get converged within 25 iterations. Also, it can be found that the CAPSO algorithm could always achieve smaller values of the sub cost function and the total cost function. However, it should also be noticed that the trajectories of CAPSO show greater randomness compared with the standard APSO algorithm, which means

the CAPSO could achieve a wider search area and thus achieves the global optimal result, instead of a local optimal result. However, the performance of the APSO and the CAPSO algorithm could not be judged through single attempt, since both these two algorithms involve random number generation. To compare the results reliably, a repeatability test and a statistical analysis are conducted in this work.

As mentioned above, to evaluate the APSO and CAPSO algorithms, a Monte Carlo analysis and a repeatability test are performed in this work. In the Monte Carlo analysis, with uniformly distributed random initial values, both APSO and CAPSO algorithms are operated 20 times. The mean value as well as the cost function's standard deviation of the two algorithms are listed in Table 4-2 (Zhang et al., 2018).

Table 4-2 Mean Value and Standard Deviation of the Cost Function Values using CAPSO and Conventional APSO

Mean Value	CAPSO	APSO
Total Cost Function	5.163	5.387
MAP	6.479	6.813
MAF	5.753	5.748
LPEGR Fraction	3.173	3.481

Standard Deviation	CAPSO	APSO
Total Cost Function	0.139	0.213
MAP	0.128	0.241
MAF	0.554	0.568
LPEGR Fraction	0.296	0.341

As it is evident from Table 4-2, for the cost function's standard deviation, CAPSO algorithm could always get a smaller value than the APSO algorithm: in terms of the mean total cost function, the CAPSO algorithm gets a value which is 4.1% less than that of the APSO algorithm; focusing on the average cost function value of the engine MAP and LPEGR fraction, the CAPSO algorithm gets a value which is 4.9% and 8.8% less than that of APSO algorithm, respectively. Considering that both the two algorithms have random factors, it is necessary to take the deviation of the optimization results into account. A higher standard deviation value means

a lower possibility of achieving the global optimal result in one attempt. The value of standard deviation of the APSO algorithm is 0.213, while it is reduced to only 0.139 when using CAPSO algorithm.

4.4.3 Investigation of Weight Tuning on the Calibration Results

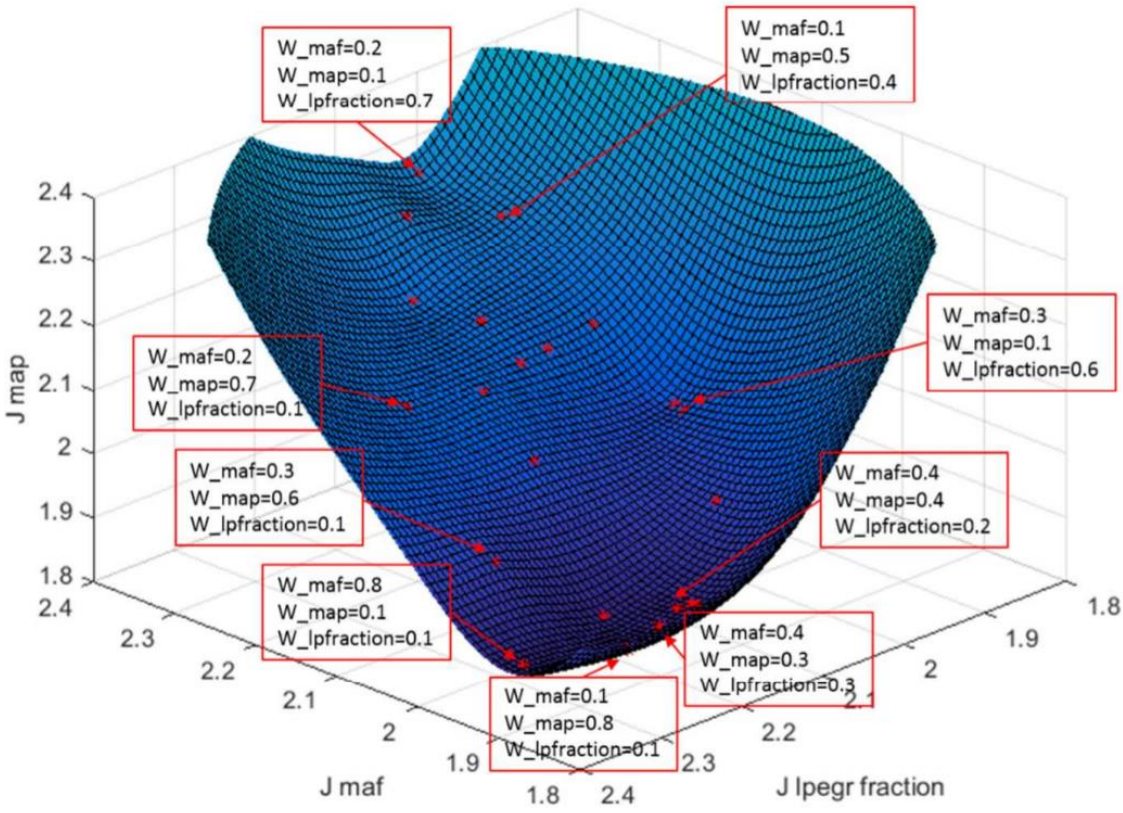

Figure 4-6 Pareto Frontier for Different Weight Value Settings

Figure 4-6 shows the Pareto front of the optimization results as the weighting is adjusted in a specific range. The red dots in the figure are the collected test data and the blue part shows the generated surface (Zhang et al., 2018). One phenomenon is that if one weight value is set to some extreme conditions (extremely large or extreme small values), the cost function values for the other

two optimization objects also get larger as they compare with other weight settings (Zhang et al., 2018). For example, when the MAP and MAF trajectories are deteriorated, the cost function value and trajectory tracking performance are worse. Another phenomenon is the coupling effect inside the diesel engine's air path, there is a trade-off between three optimization objects. The characteristic of the slow dynamic response in the LPEGR loop is also reflected in the figure (Zhang et al., 2018). Regardless of the weight settings, the cost function value of the LPEGR fraction falls in a smaller range when compares with other optimization objects. The figure indicates the diesel engine's air path is more sensitive to the MAF and MAP weight settings. In this case, when the MAF and MAP weights are set between 0.3 and 0.4, the total cost function value achieves its minimum level (Zhang et al., 2018).

4.4.4 Test Bench Validation

Using a transient sequence, the proposed CAPSO algorithm is verified on the test bench. The mass of fuel injection is set to follow stepped changes, while the engine speed is kept at constant value. This kind of scenario could also be seen in many other studies on the transient behaviours of engines. In this case, the engine working condition is 1500 rpm with a stepped change of fuel injection from 15 to 30 mg/stroke. The baseline calibration of the engine is provided by the engine supplier. As it is introduced in section 4.2, the calibration is copied from

the Bosch commercial ECU used for the same type of engine (AJ20D4). Additional modifications are added to convert the vehicle ECU settings to the test bed ECU settings for Cold Cell.

Before presenting the results, the definitions of the overshoot and the settling time are shown by the figure below. These definitions are used for the all work presented in this thesis.

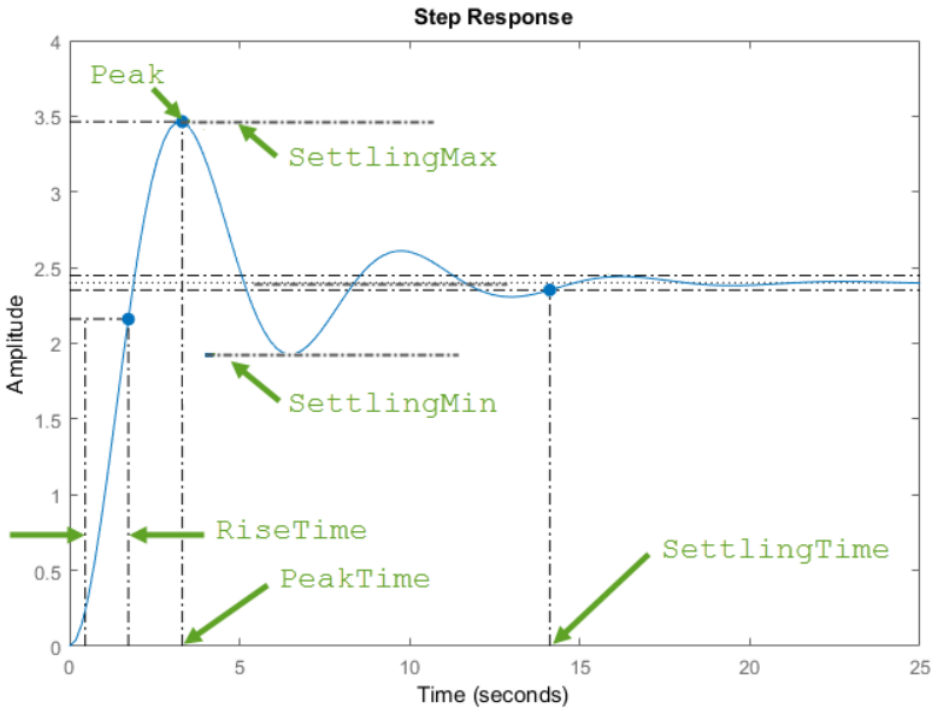

Figure 4-7 Diagram that Defines the System Overshoot and Settling Time (MathWorks, n.d.)

The rise time is defined as the time the signal takes for the signal to rise from 10% to 90% of the steady-state setpoint. The settling time is defined as the error of signal ($|y_t - y_{set}|$) falls within 2% of the setpoint value. The overshoot (%) is defined by the following equation:

$$overshoot = \frac{y_{peak} - y_{set}}{y_{set}} * 100\%$$

Where y_{peak} is the peak absolute value of y_t and y_{set} is the steady-state setpoint of the signal.

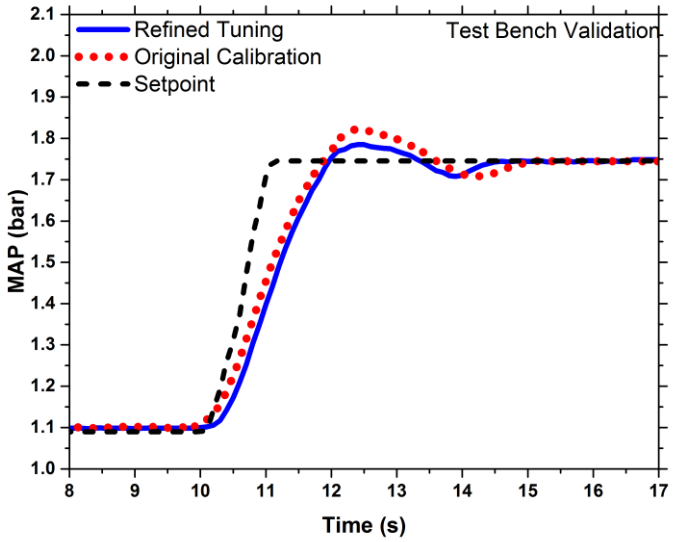

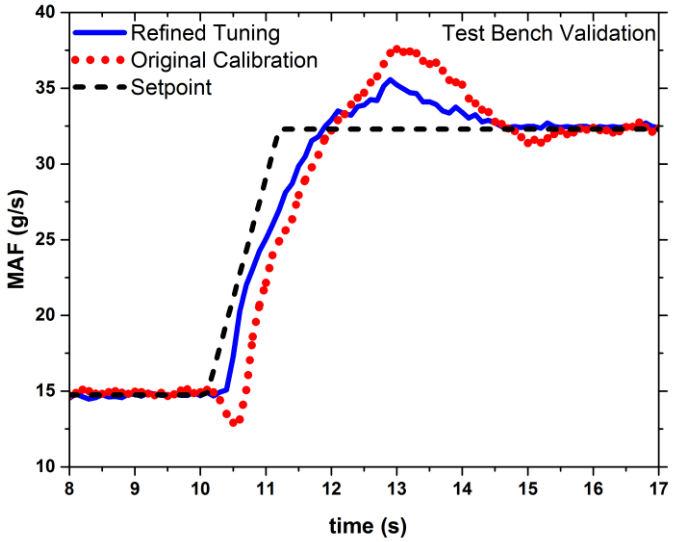

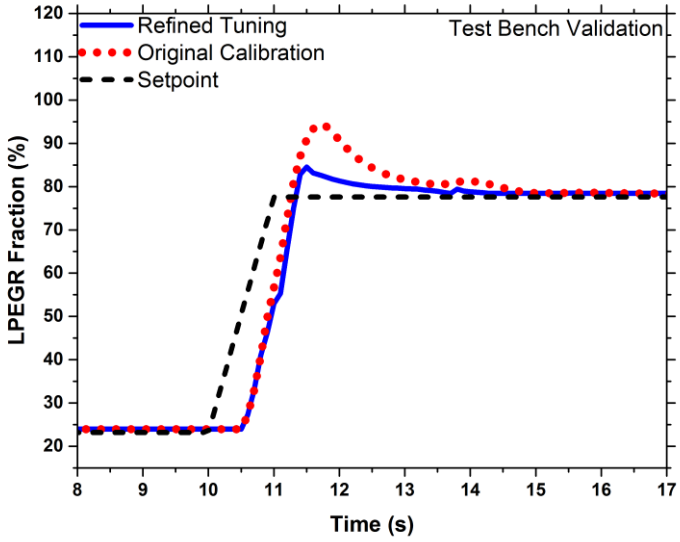
Refined Tuning
Original Calibration
Setpoint
Test Bench Validation
LPEGR Fraction (%)
Time (s)

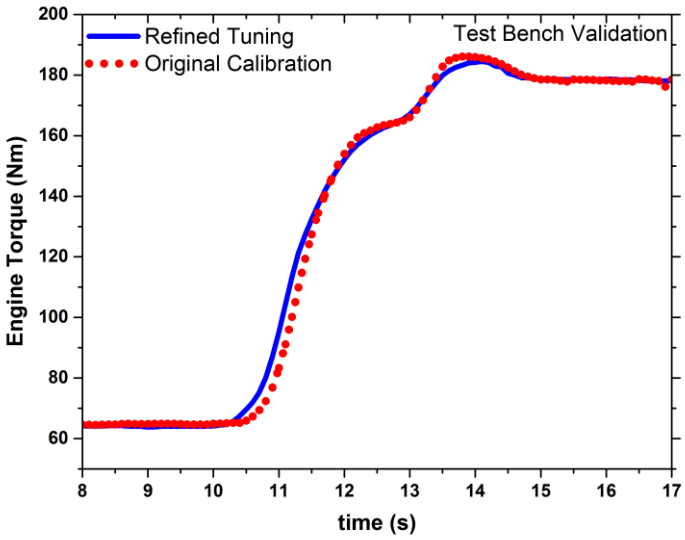
Refined Tuning
Original Calibration
Test Bench Validation
Engine Torque (Nm)
time (s)

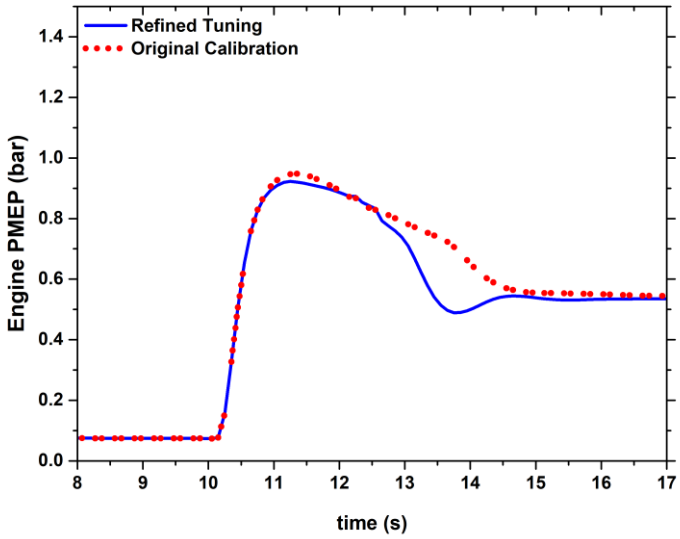

Figure 4-8 Trajectories of Engine Parameters using CAPSO Calibration Algorithm by Engine Tests

Figure 4-8 shows the test results of engine MAP, MAF, LPEGR fraction and the engine torque obtained through the test bench. From the first three figures, it can be seen that both the overshoot and settling time of the engine MAP, MAF, LPEGR fraction are significantly reduced. The high combustion temperature and the excessive amount of air are two key factors that affect the engine NOx generation (Tian et al., 2014;Zhang et al., 2018). The temperature inside the cylinder would be raised by the increased mass of fuel injection at 10s. At this time, the higher overshoot of the engine MAF, which is caused by the original calibration, provides an overdosed amount of air for NOx formation. In addition, through the validation of the test bench, the accumulated BSFC is also found to have a reduction of 0.78%. As it is verified in previous work of Lu et al and Zhang et al, HPEGR and proper controlled VGT act as a dominating role (Lu et al., 2016;Zhang et al., 2018). Since the engine PMEP turns back to the steady state

value more rapidly by the refined tuning of the engine controller, the brake torque generation of the engine could thus be increased.

Figure 4-9 shows the trajectories of the actuators. As it is evident from Figure 4-8, by using the CAPSO calibration algorithm, the trajectories of the HPEGR valve, LPEGR valve and VGT are all stabilized(Zhang et al., 2018).

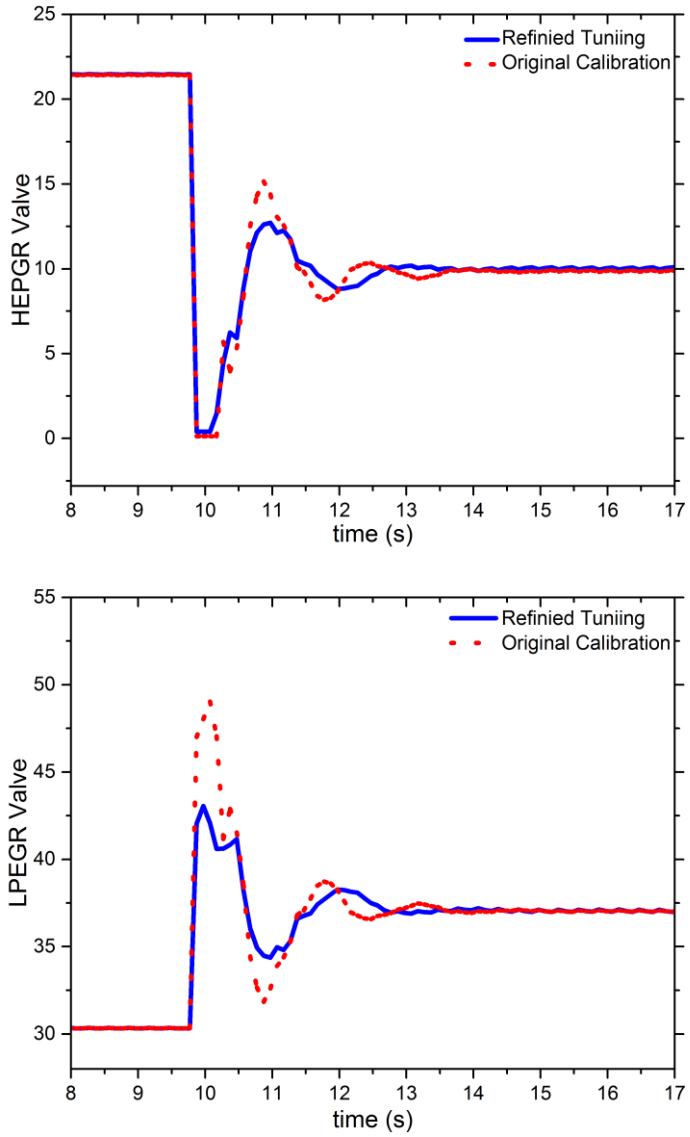

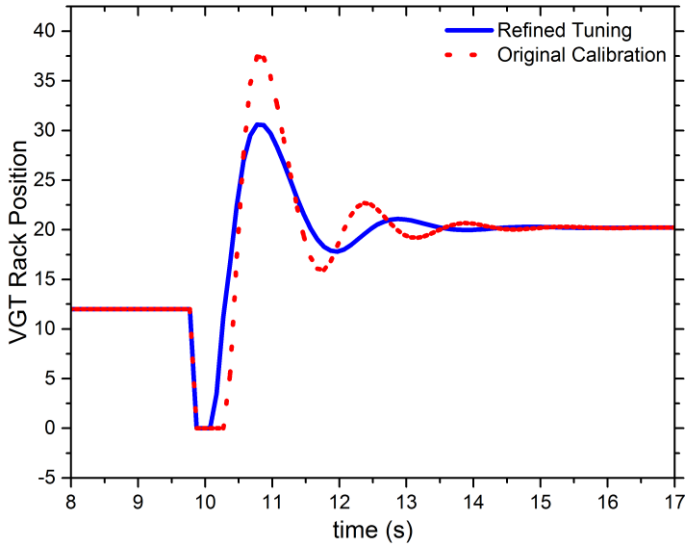

Figure 4-9 Trajectories of engine parameters using CAPSO calibration algorithm

4.4.5 Case Study of Engine Transient Calibration

In previous paragraphs, the capability of the CAPSO-based calibration algorithm has been verified. However, many other factors, i.e. the delay of the actuators, may also have an affection to the calibration results. Therefore, one single test sequence is not enough to evaluate the algorithm. To solve this problem, several other transient scenarios, which involve various mass of fuel injection and engine speed, are also demonstrated. The details of the designed test sequences have been introduced in chapter 3.2.2.

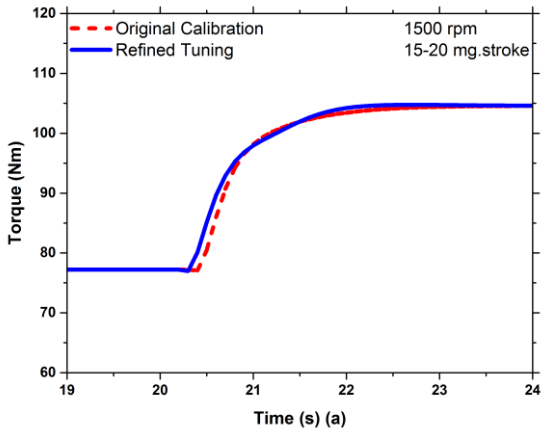
Original Calibration
Refined Tuning
1500 rpm
15-20 mg.stroke
Torque (Nm)
Time (s) (a)

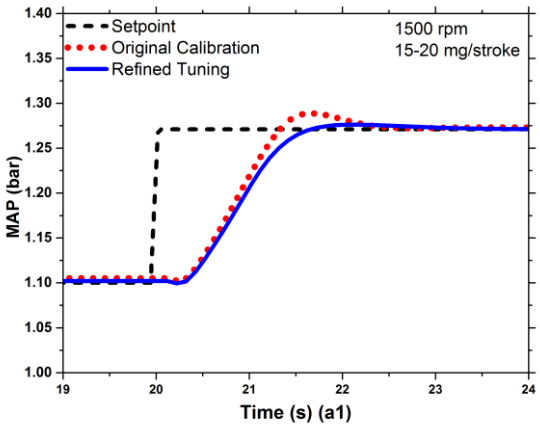
Setpoint
Original Calibration
Refined Tuning
1500 rpm
15-20 mg/stroke
MAP (bar)
Time (s) (a1)

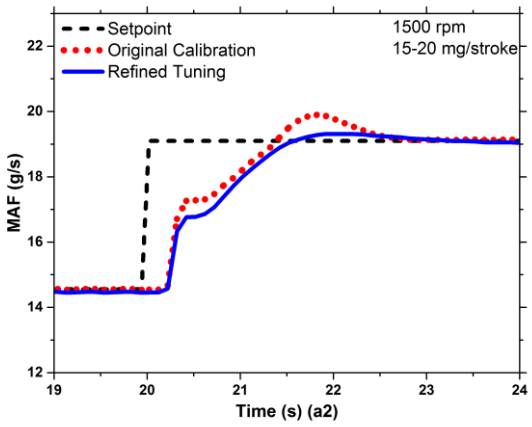
Setpoint
Original Calibration
Refined Tuning
1500 rpm
15-20 mg/stroke
MAF (g/s)
Time (s) (a2)

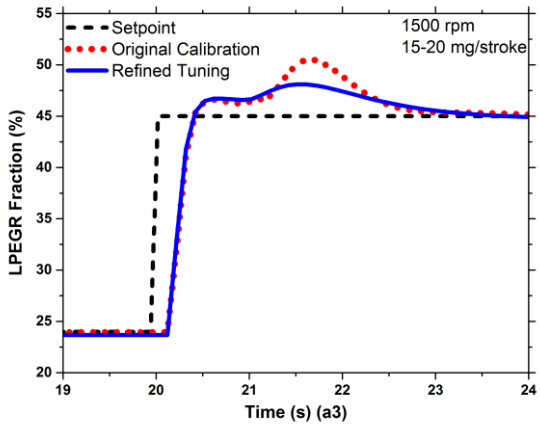
Setpoint
Original Calibration
Refined Tuning
1500 rpm
15-20 mg/stroke
LPEGR Fraction (%)
Time (s) (a3)

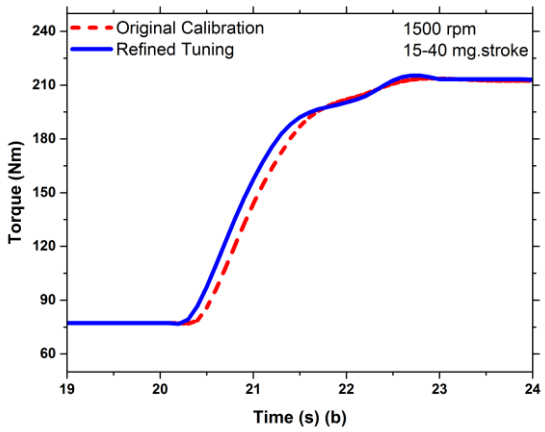
Original Calibration
Refined Tuning
1500 rpm
15-40 mg.stroke
Torque (Nm)
Time (s) (b)

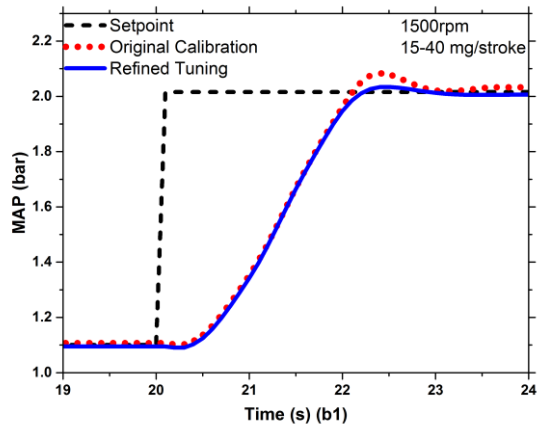
Setpoint
Original Calibration
Refined Tuning
1500rpm
15-40 mg/stroke
MAP (bar)
Time (s) (b1)

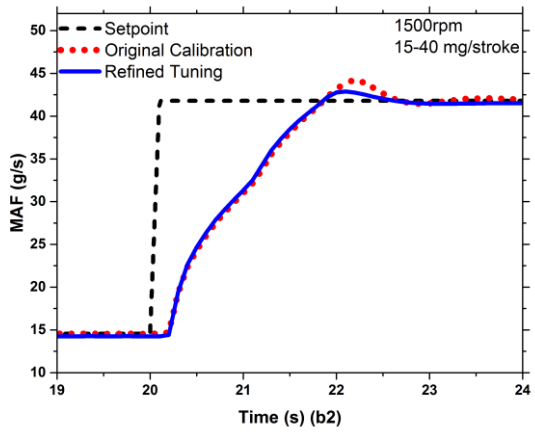
Setpoint
Original Calibration
Refined Tuning
1500rpm
15-40 mg/stroke
MAF (g/s)
Time (s) (b2)

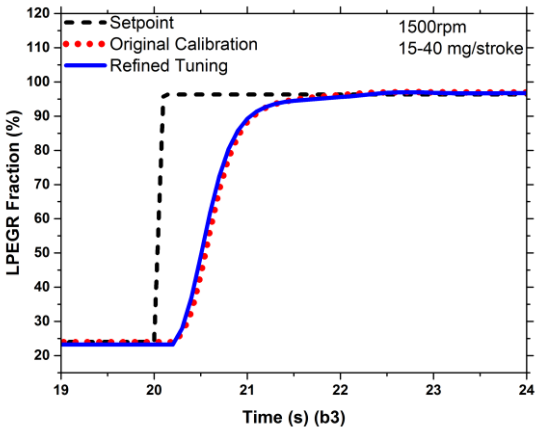
Setpoint
Original Calibration
Refined Tuning
1500rpm
15-40 mg/stroke
LPEGR Fraction (%)
Time (s) (b3)

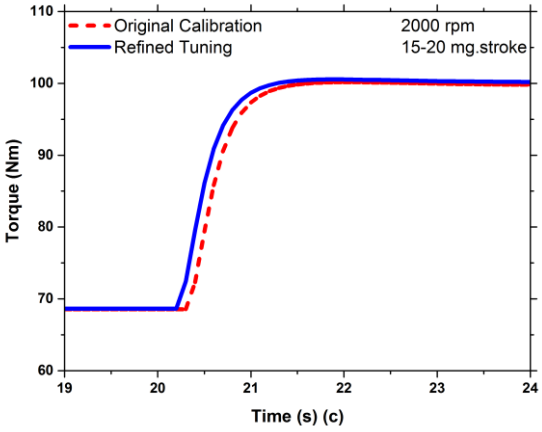
Original Calibration
Refined Tuning
2000 rpm
15-20 mg.stroke
Torque (Nm)
Time (s) (c)

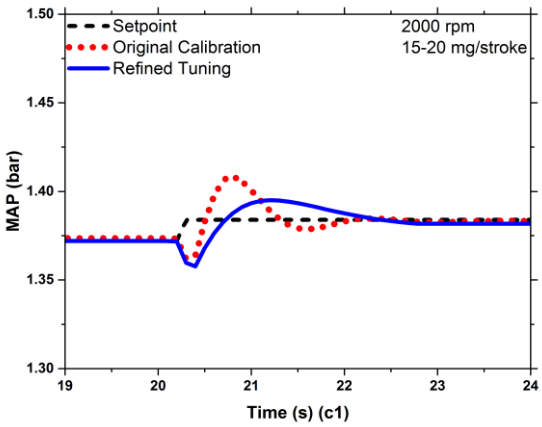
Setpoint
Original Calibration
Refined Tuning
2000 rpm
15-20 mg/stroke
MAP (bar)
Time (s) (c1)

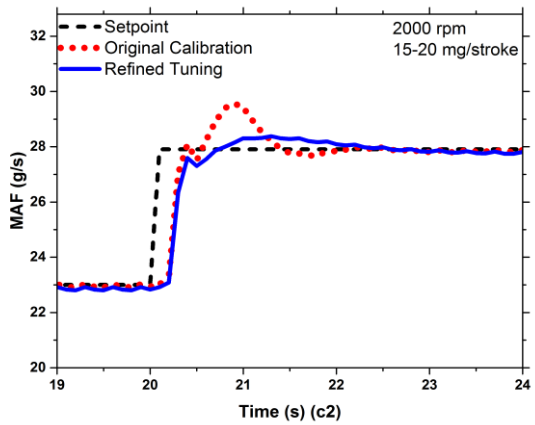
Setpoint
Original Calibration
Refined Tuning
2000 rpm
15-20 mg/stroke
MAF (g/s)
Time (s) (c2)

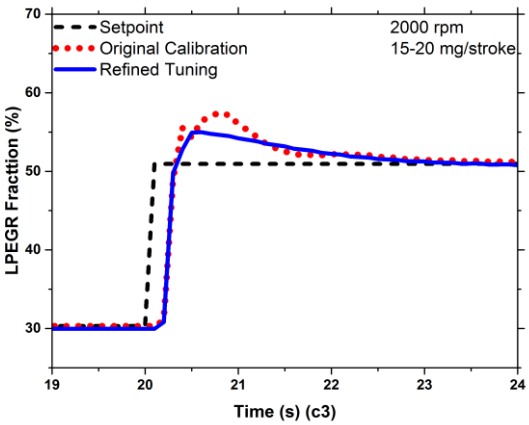
Setpoint
Original Calibration
Refined Tuning
2000 rpm
15-20 mg/stroke
LPEGR Fracttion (%)
Time (s) (c3)

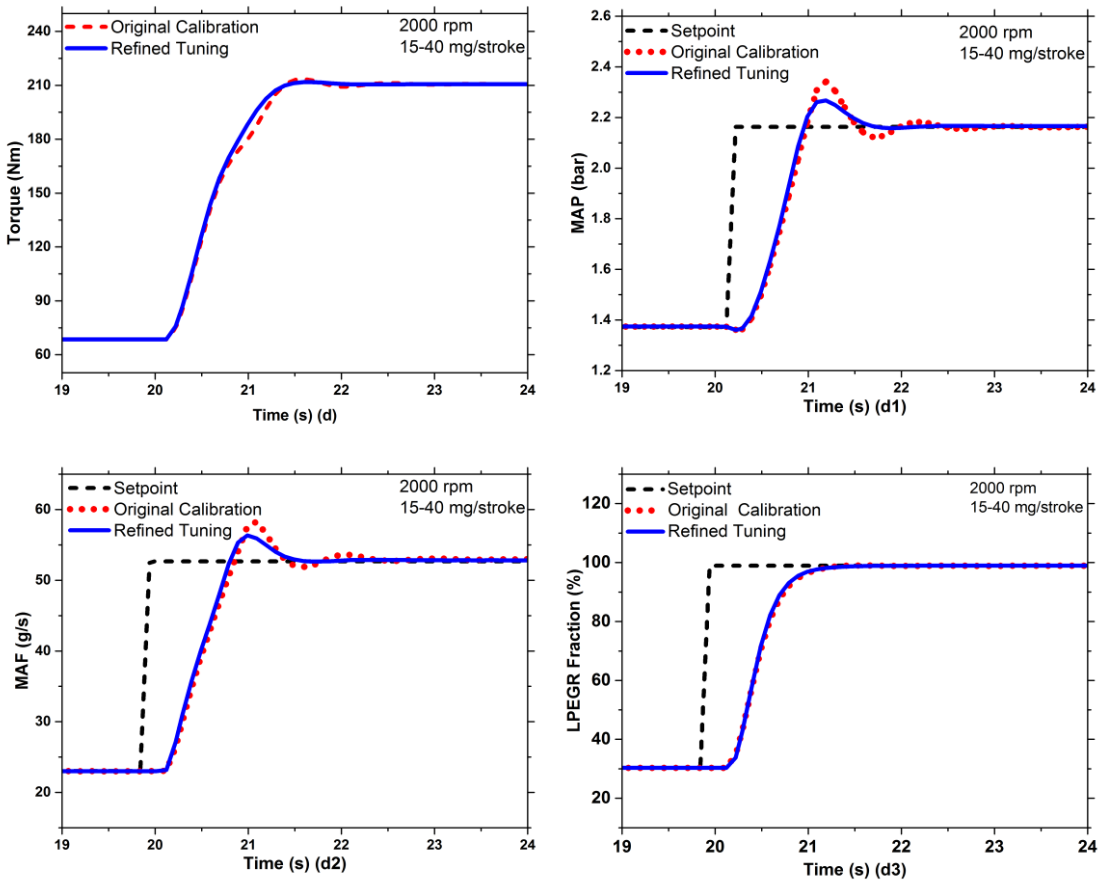

Figure 4-10 Trajectories of Engine Parameters under Various Transient Scenarios using CAPSO Calibration Algorithm and Original Calibration: (a) 1500rpm 15-20 mg/stroke; (b) 1500rpm 15-40 mg/stroke; (c) 2000rpm 15-20 mg/stroke; (d) 2000rpm 15-40 mg/stroke

Figure 4-10, it can be concluded that by using the CAPSO-based calibration algorithm, the refined tuning can reduce the overshoot, system response time and settling time. In terms of the system overshoot, a reduction of 59.9% has been observed, while for the settling time, a reduction of 35.4% is achieved. Therefore, the dynamic performance of the diesel air path has been improved in the control point of view. More optimal fuel economy is also achieved thanks to proper controlled engine's air path. A reduction of 0.91% is achieved in terms of the fuel consumption.

4.5 Summary

In this work, a novel CAPSO-based engine transient calibration method has been proposed. The unique part of the algorithm is the chaotic mapping strategy, which contributes to finding the global optimum controller parameters. Case studies have been performed to obtain the engine performance with different tuning results. To evaluate the CAPSO-based algorithm, a repeatability test and a Monte Carlo analysis are also performed. The conclusions are listed as follows:

1. Under various working conditions, the transient behaviour of the air path of the engine could be optimized by the proposed CAPSO-based calibration algorithm. Compared with the baseline engine calibration, reduction of 41.5% and 22.3% have been achieved in terms of the overshoot and the settling time of the engine MAP. In terms of the engine MAF, the reduction of overshoot and settling time is 60.3% and 12.9% respectively. The reduction on LPEGR fraction's overshoot and settling time is 51.8% and 21.7%.

2. An improved engine fuel economy is achieved with the help of the more optimal calibration. Through several case studies, it is proved that the accumulated fuel consumption can be reduced by 0.91% (on average) through the proposed transient calibration method.

3. Through the Monte Carlo analysis, it can be found that the CAPSO-based

algorithm achieves a 4.1 % lower value of the optimization objects than the APSO algorithm. Through the repeatability test, it can also be found that the standard deviation of the optimization object using CAPSO-based algorithm is 65.2% less than that of APSO-based algorithm.

Therefore, based on the above analysis, the proposed CAPSO-based algorithm is a good solution for the engine transient calibration as it has a simple structure and shows a strong capability for locating the global best result instead of a local best result. Besides, it could be applied to both offline and real-time optimization.

CHAPTER 5 TUNABLE MODEL PREDICTIVE CONTROL

The author has published the work presented in this chapter in the journal of 'Proceeding of IMechE, Part D: Journal of Automobile Engineering' as the first author (Zhang et al., 2017). This chapter presents a tunable model predictive control (TMPC) controller for the air path of a diesel engine. The objective is to control the variable geometry turbocharger (VGT) and EGR valves to meet the time-various set points of the intake manifold pressure and EGR mass flow in each loop. The design framework of the proposed controller is based on the multiple linear MPC controller, it also contains a map based switching scheme of the local controller and the controller's weight (Zhang et al., 2017). The TMPC controller and the conventional PID controller are firstly compared. The HIL validation process is followed.

5.1 Introduction

At the current stage, most commercial ECUs use the separate SISO PID controller (Zhao et al., 2014). The major obstacles for the control of the air path of the diesel engine are the system nonlinearity and coupling effects (Haber,

2010). It is difficult to acquire accurate control of the EGR mass flow in a dual-loop EGR system. The conventional PID controllers with look-up tables and logic switches may cause obvious delay or overshoot in the EGR mass flow, which eventually result in engine emissions (Maruyama et al., 2011;Dezong Zhao et al., 2013;Kim et al., 2014;Zhang et al., 2017). When there is an overshoot of EGR mass flow, the concentration of the intake oxygen may get far below the desire valued. The incomplete combustion will occur, the combustion efficiency would be lower, which leads to lower engine efficiency and worse fuel economy. During transient scenarios, NOx and PM spikes will be induced by the turbo lag and the large overshoot of the engine boost pressure (Rakopoulos et al., 2010;Zhang et al., 2017). Besides, the engine drivability gets worse when the VGT rack position fluctuates with opened EGR valves, which is due to the unstable EGR mass flow (R.S.Wijetunge et al., 2000;Zhang et al., 2017). Recently, model predictive control (MPC) has been applied to the field of engine control due to its capability in dealing with above-mentioned obstacles (Zheng et al., 2011;Barrero et al., 2011;Zhang et al., 2017). It formulates the control problem to an optimization problem, and achieves accurate reference trajectory tracking while complying with the constraints (Darby and Nikolaou, 2012;Zhang et al., 2017). MPC controllers for diesel engines with single loop EGR and VGT has been extensively explained (Stewart and Borrelli, 2008;Ortner and Re, 2007;Zhou et al., 2014;Hrovat et al., 2012); a clear scale of MPC controllers' design process and

its measurable improvements on an engine's BSFC and emissions are provided in these studies. However, when designing local controllers for a system which has the characteristics of strong nonlinearities and sudden changes in operating conditions, the above-mentioned MPC controllers are challenged (Zhang et al., 2017).

This chapter presents a TMPC controller based on a 2-D map switching scheme of controller parameters for the air path of a diesel engine. The remaining sections of this chapter are organized as follows (Zhang et al., 2017): in section 5.2, the controller structure is introduced. Section 5.3 presents the algorithm and the design framework of the proposed controller. The performances of the PID controller and the TMPC controller are compared in section 5.4. The introduction of the PID controller is also added. The TMPC controller' real-time capability is also evaluated on a HIL platform. Finally, conclusions are summarized and listed in section 5.5.

5.2 Controller Structure

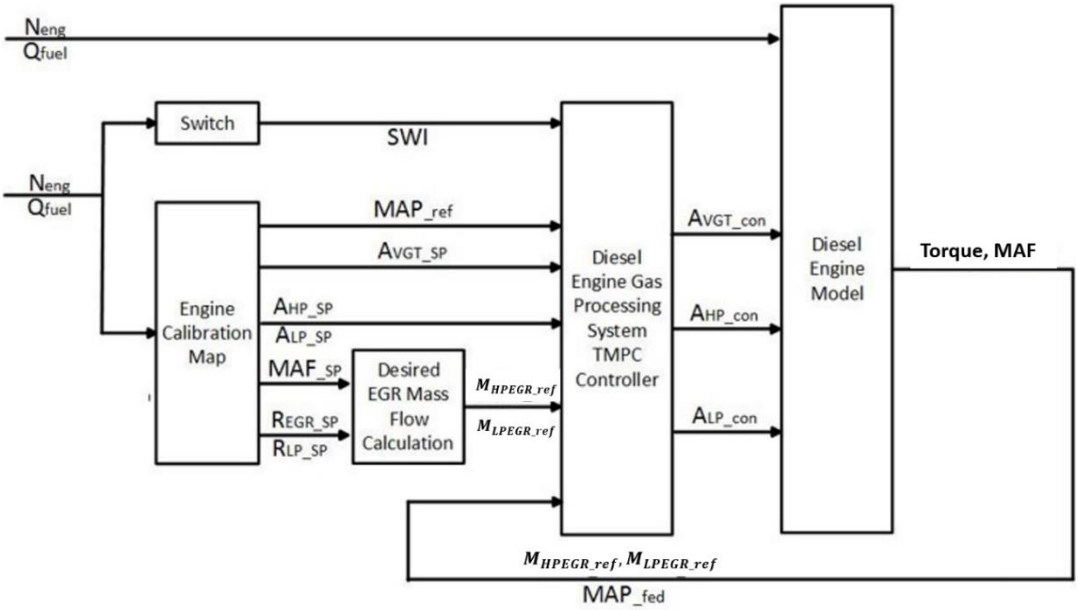

Figure 5-1 Tuneable Model Predictive Control System for a Diesel Engine's Air path

The HPEGR mass flow (M_{HPEGR}), MAP and LPEGR mass flow (M_{LPEGR}) are selected as the control objectives. The control variables are the offset on the VGT rack position (A_{VGT}), LPEGR valve position (A_{LP}) and HPEGR valve position (A_{HP}) (Zhang et al., 2017). The proposed TMPC controller also requires the engine speed, mass of fuel injection, the desired values of the control objects, feedback values of the control objects and the setpoint of the actuators to calculate the optimal control sequence(Zhang et al., 2017).

The engine calibration maps determine the desired value of MAP ($MAP_{\_ref}$) and the feed-forward set point of the VGT rack position ($VGT_{\_sp}$) based on current engine working conditions. The desired values of the EGR mass flow (M_{HPEGR_ref}, M_{LPEGR_ref}) are calculated based on setpoints of the engine total EGR rate

(R_{EGR_ref}), MAF (MAF_ref) and the LPEGR fraction (R_{LP_sp}) (Zhang et al., 2017). The equations are presented below:

$$M_{HPEGR\_ref} = \frac{MAF\_ref \cdot R_{EGR\_ref} \cdot (1 - R_{LP\_ref})}{(1 - R_{EGR\_sp})}$$

$$M_{LPEGR\_ref} = \frac{MAF\_ref \cdot R_{EGR\_ref} \cdot R_{LP\_ref}}{(1 - R_{EGR\_ref})}$$

In this work, the total EGR rate (R_{EGR}) is determined by the percentage of total EGR mass flow in the total inducted gas. In terms of the LPEGR fraction (R_{LP}), it is defined as the part of the LPEGR contribution in the combined EGR mass flow. The percentage is selected as the unit for this parameter. The equations are shown below (Zhang et al., 2017):

$$R_{EGR} = \frac{M_{HPEGR} + M_{LPEGR}}{M_{HPEGR} + M_{LPEGR} + MAF} \times 100\%$$

$$R_{LP} = \frac{M_{LPEGR}}{M_{HPEGR} + M_{LPEGR}} \times 100\%$$

In terms of the diesel engine model, the detailed introduction has been shown in the chapter 3, section 3.1.5.

5.3 Controller Algorithm and Design Framework

5.3.1 TMPC Controller Algorithm

To achieve optimal air path control, the algorithm of the linear MPC and the function of multiple MPC are adopted in this work (Zhang et al., 2017). Figure 5-2 shows the basic principle of model predictive control. The target is to calculate the optimal sequence of the control variables $[u|k, u|k+1, \dots, u|k+M-1]$ at each time interval (k), which achieves the minimum error between the matrix of predicted control object $[y_{m(k+1|k)}, y_{m(k+2|k)} \cdots, y_{m(k+p|k)}]$ and the matrix of reference value $[y_{ref(k+1)}, y_{ref(k+2)}, \dots, y_{ref(k+P)}]$; where M means the control horizon; and P represents the prediction horizon (Zhang et al., 2017). The algorithm should be operated within the boundaries of the control objects, control variables and the control variables' rate of change (Zhang et al., 2017). However, only the first move of the optimal control sequence would be used. The calculation is repeated at the next time interval, and a new sequence of control signals will be generated.

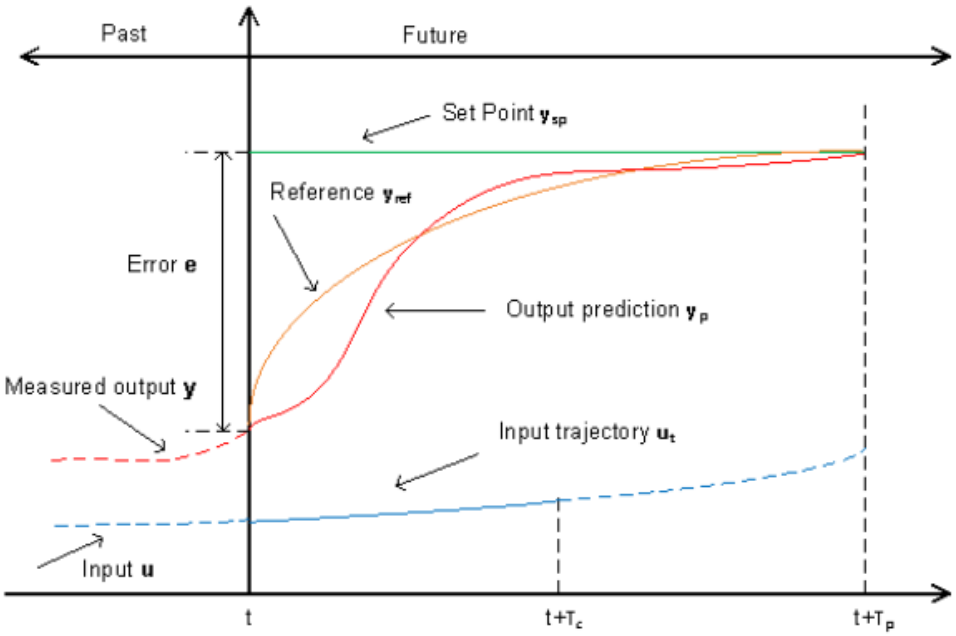

Figure 5-2 Principle of Model Predictive Control (Tan, 2015)

The calculation is carried out through the optimization of a cost function – specifically, a quadratic program (QP) while considering system dynamics and constraints (Rawlings, 1999;Tan, 2015;Emekli and Güvenç, 2016;Zhang et al., 2017). The cost function is designed as following (Zhang et al., 2017):

$$J(z_k) = J_y(z_k) + J_u(z_k) + J_{\Delta u}(z_k)$$

Where z_k is the QP decision; $J_y(z_k)$ is the tracking performance of control objects; $J_u(z_k)$ means the deviation of the control variables; $J_{\Delta u}(z_k)$ indicates the control variables' rate of change (Zhang et al., 2017). For the control problem in this work, the above cost function could be presented by the following equation:

$$J = \min\{W_y \cdot [(y_{(k)} - y_{ref(k)})^2 + \left(y_{m(k+1|k)} - y_{ref(k+1)}\right)^2 + \left(y_{m(k+2|k)} - y_{ref(k+2)}\right)^2 + \cdots + \left(y_{m(k+p|k)} - y_{ref(k+p)}\right)^2]$$

$$+W_u \cdot [(u_{(k)} - u_{sp(k)})^2 + \left(u_{(k+1|k)} - u_{sp(k+1)}\right)^2 + \left(u_{(k+2|k)} - y_{sp(k+2)}\right)^2 + \cdots + \left(u_{(k+m-1|k)} - u_{sp(k+m-1)}\right)^2$$

$$+W_{\Delta u} \cdot [(u_{(k+1)} - u_{(k)})^2 + \left(u_{(k+2|k)} - u_{(k+1|k)}\right)^2 + \left(u_{(k+3|k)} - u_{(k+2|k)}\right)^2 + \cdots + \left(u_{(k+m-1|k)} - u_{(k+m-2|k)}\right)^2\}$$

$$y(n)_{min} \leq y(n) \leq y(n)_{max}\ n = 1,2,\dots,p$$

$$u(n)_{min} \leq u(n) \leq u(n)_{max}\ n = 1,2,\dots,m-1$$

$$\Delta u(n)_{min} \leq \Delta u(n) \leq \Delta u(n)_{max}\ n = 1,2,\dots,m-1$$

Where W_u, W_y and $W_{\Delta u}$ are the weight matrix of the input trajectory, output trajectory and input rate of change; $y_{ref|k}$ represents the desired values of the control objects at moment k; $y_m(k+i|k)$ represents the predicted control objects in the span of the prediction horizon generated by the TMPC controller; $y_{(k)}$ represents the output of the model plant at moment k; $u_{k+l|k}$ is the series of the control variables in the span of the control horizon calculated by controller; $u_{sp|k}$ is the feed forward set point of the control variables (Zhang et al., 2017). For the boundary conditions, $y(n)_{min}$ and $y(n)_{max}$ are the lower and

upper limit of the HPEGR mass flow, LPEGR mass flow and engine boost pressure. The $u(n)_{min}$ and $u(n)_{max}$ limit the range of the offset on the HPEGR valve position, LPEGR valve position and VGT rack position. The $\Delta u(n)_{min}$ and $\Delta u(n)_{max}$ limit the minimum and maximum rate of the change on those actuators (Zhang et al., 2017).

The output weight is capable in scaling the control objects and concentrating more efforts towards the selected targets. With a larger output weight, rapid trajectory tracking can be achieved. However, when the output weight is too large, fluctuation on the control objects and large overshoot of the system cannot be avoided (a. Bemporad et al., 2002;Zhang et al., 2017). When input weights are increased, the controller would be more conservative by suppressing the magnitudes of the input moves. Therefore, the inputs become smoother, but the output responses will suffer from slower response and longer settling times (Zhang et al., 2017). Penalizing the inputs' rate of change causes a more robust controller, but the controller would be more sluggish as a result (Garriga and Soroush, 2010;Zhang et al., 2017).

In this work, in the TMPC controller, the W_y, W_u and $W_{\Delta u}$ are no longer one fixed value. In different working conditions of engine, the controller weights are set as different values. Eventually, these values form several look-up tables (Zhang et al., 2017). In addition, the weight values of these tables could also be

adjusted online during operations (Bemporad et al., 2014). For the 2-D switch scheme, the mass of fuel injection (Q_{fuel}) and engine speed (N_{eng}) are selected as the triggers. (Zhang et al., 2017).

The control objects' future behavior inside the TMPC controller is predicted by the local discrete-time identified state-space models (Bemporad et al., 2014;Zhang et al., 2017). The equations are presented below:

$$X_{(k+1)} = A \cdot X_{(k)} + B \cdot u_{(k)}$$

$$Y_{(k)} = C \cdot X_{(k)}$$

where A, B and C are the state matrixes obtained during the identification process (Zhang et al., 2017). The input matrix $u_{(k)}$ [Δu_{HPEGR} Δu_{LPEGR} Δu_{VGT}] involves the adjustments of the LPEGR position, the VGT rack position and the HPEGR valve position; the output matrix $Y_{(k)}$ [m_{hpegr} m_{lpegr} MAP] involves the EGR mass flow in each loop and intake manifold pressure (Zhang et al., 2017).

However, modern light-duty diesel engines are operated in wide working conditions, therefore, one MPC controller is inadequate to achieve the optimum control of the air path. To solve the problem, multiple model predictive control (MMPC) with gain scheduled switch logic is considered (Zhang et al., 2017). The

figure 5-3 shows the structure of the TMPC controller in this work (Zhang et al., 2017).

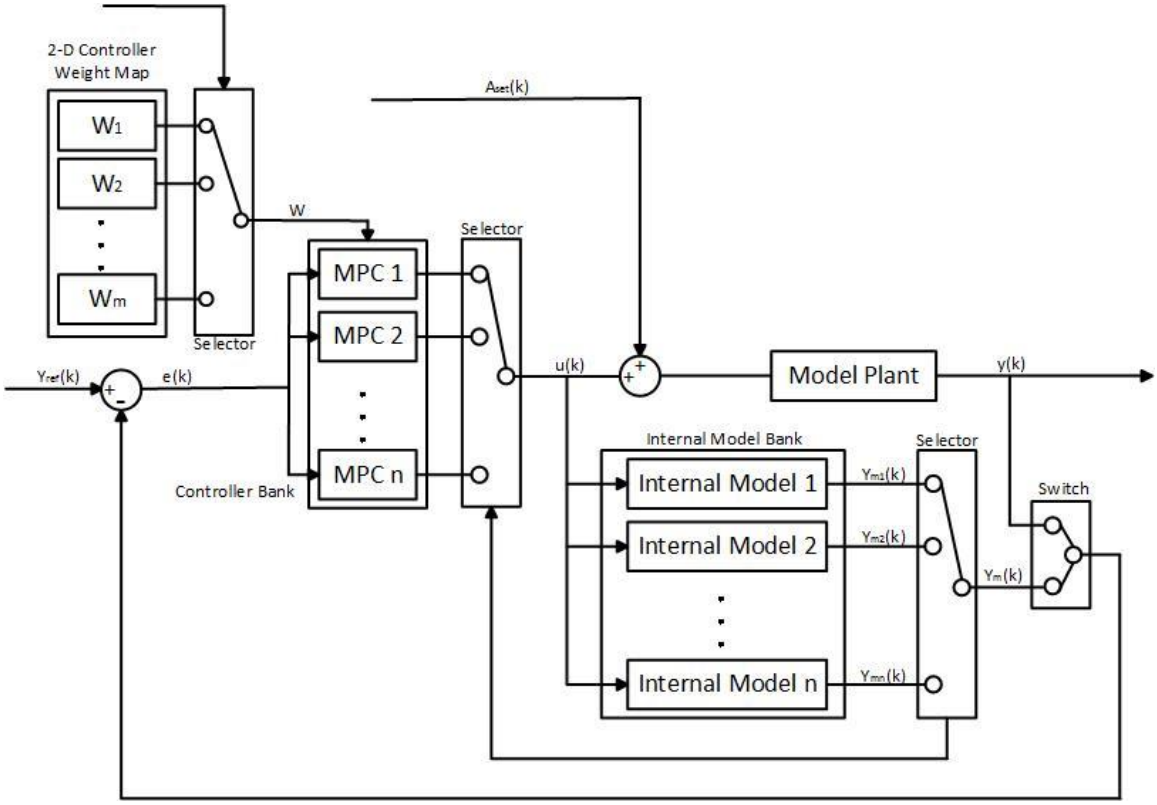

Figure 5-3 Map Based Switching Scheme of the TMPC Controller

In Figure 5-3, the sub MPC controllers (MPC1, MPC2…MPC n) are stored in the controller bank, while the internal prediction models (internal model 1, internal model 2… internal model n) are contained in the internal model bank. All of them are arranged in parallel (Zhang et al., 2017). The whole assignments for the input weight, input rate weight and output weight are contained in controller weight bank ($w_1, w_2, \cdots, w_m$). Different with the conventional offline-tuned MPC controllers, the number of the weight values is not necessarily identical to the number of the sub MPC controller ($m \neq n$). Each sub MPC controller could

operate with different weight settings. The controller weight w is determined based on the current engine working condition (Zhang et al., 2017). At each time interval k, only one sub MPC controller, one internal model and one set of the controller weights are activated to progress the optimization calculation based on the engine working condition (N_{eng} & Q_{fuel}) (Zhang et al., 2017). However, these sub MPC controllers will still update their state estimation. The switch scheme is presented below (Zhang et al., 2017):

$$if\ N_{eng} \in [A_i, B_i]\ and\ Q_{fuel} \in [C_i, D_i]$$
$$then\ W_y = W_{y_i}; W_u = W_{u_i}; W_{\Delta u} = W_{\Delta u_i}$$

$$then\ swi\ is\ N\ (i.e\ MPC\ N\ and\ internal\ model\ N\ is\ active)$$

The engine calibration maps are used to obtain the desired values of the control objects $y_{ref}(k)$ (Zhang et al., 2017). The identified internal models in the internal model bank run with the model plant simultaneously. The plant model provides the feedback values of $y_{(k)}$ at each time interval, while the internal model forecasts the trajectory of the $y_{m(k)}$in the span of the prediction horizon p (Zhang et al., 2017). The signal of $e(k)$ have two functions. The first one is calculating the error between the desired value $y_{ref}(k)$ and the plant output $y(k)$ to update the state of the current controller. The second one is calculating the error between $y_{m(k)}$ and $y_{(k)}$ which would be used in the QP decision (Zhang et al., 2017). At each time interval, the switch between these two functions

will be accomplished automatically by the controller (Zhang et al., 2017). The final inputs of the simulation platform $A_{con}(k)$ are equal to the product of the adjustment value and the set point $A_{ref}(k)$: (Zhang et al., 2017)

$$A_{con}(k) = A_{ref}(k) \times (1 + u(k))$$

The selector between each controller and the internal model is triggered by the working condition of the engine which adopts the same parameters as the controller weight assignment (Zhang et al., 2017). Each sub controller and internal model covers a small area of the working conditions of the engine. Only one specific sub controller is activated by the selector and progresses the calculation at each moment. Other sub MPC controllers continue updating their internal state estimation (Zhang et al., 2017). Based on the boundaries of each region, the switch logic determines the sub MPC controller to continue the control of the HPEGR, VGT and LPEGR of the engine when the working condition of engine changed (Zhang et al., 2017).

5.3.2 TMPC Controller Design Framework

Based on the demand of MPC-based controllers, it is important to convert the complex air path of the engine into a simplified data-driven model which could accurately capture the nonlinear relationship between the control variables and

control objects (Henningsson et al., 2012;Zhang et al., 2017). This process is called system linearization. Figure 5-4 demonstrates the system linearization process on the simulation platform (Zhang et al., 2017).

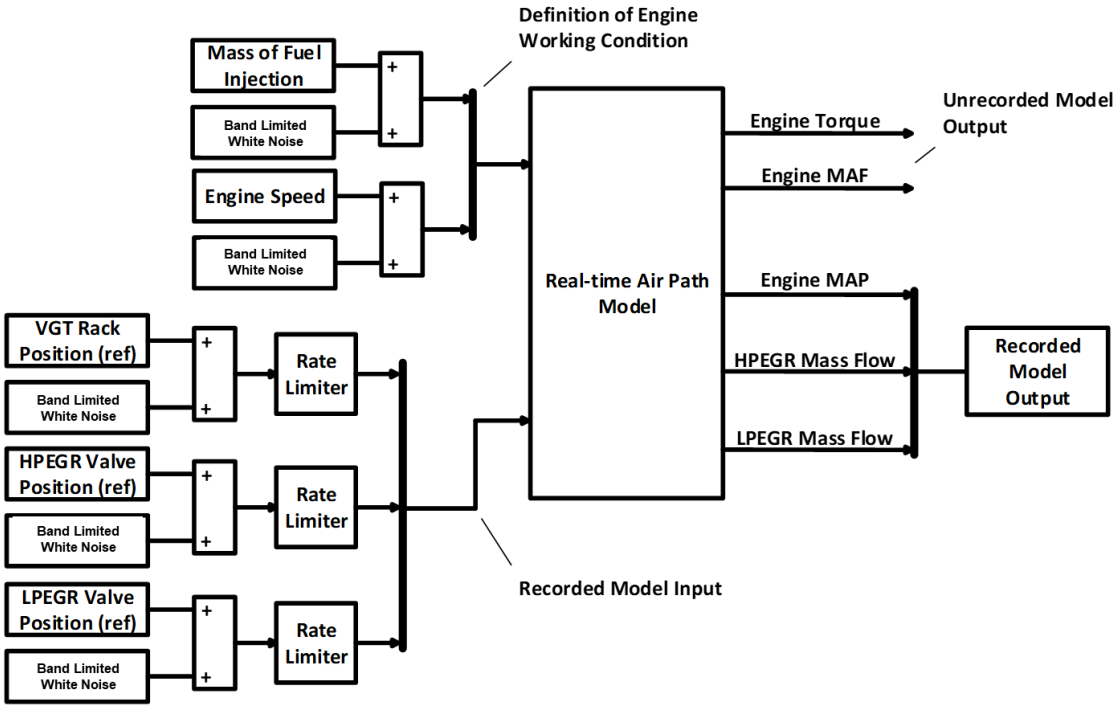

Figure 5-4 Structure of the System Identification Process on the Simulation Platform

The internal prediction model is developed in the form of state-space model. The governing equations of this state-space model are listed in the previous section (Zhang et al., 2017). This model's basic function is predicting the future behaviour of the control objects. The obtained prediction results could help the algorithm inside the controller to calculate the optimal sequences of the control, and thus the minimum cost function can be acquired. This prediction model contains the dynamic of the system. Therefore, this model is suitable in predicting both steady states and dynamic conditions (Zhang et al., 2017). The identification process is

to apply random deviation signals, which are limited under a certain range, onto the control variables and record the corresponding control objects (Zhang et al., 2017). The White noise generator is used to achieve this function. In this case, rate limiters are also added to the actuators on the model to regulate the rate of change, which is closer to the physical characteristics of the actuators on real engines. Other engine parameters, including the mass of the engine fuel injection and engine speed, are remained constant (Zhang et al., 2017). The maximum prediction horizon, model order, past outputs and past inputs used in the predictor consisted the main tuning parameters. To take an example, one identification process is shown below (Zhang et al., 2017).

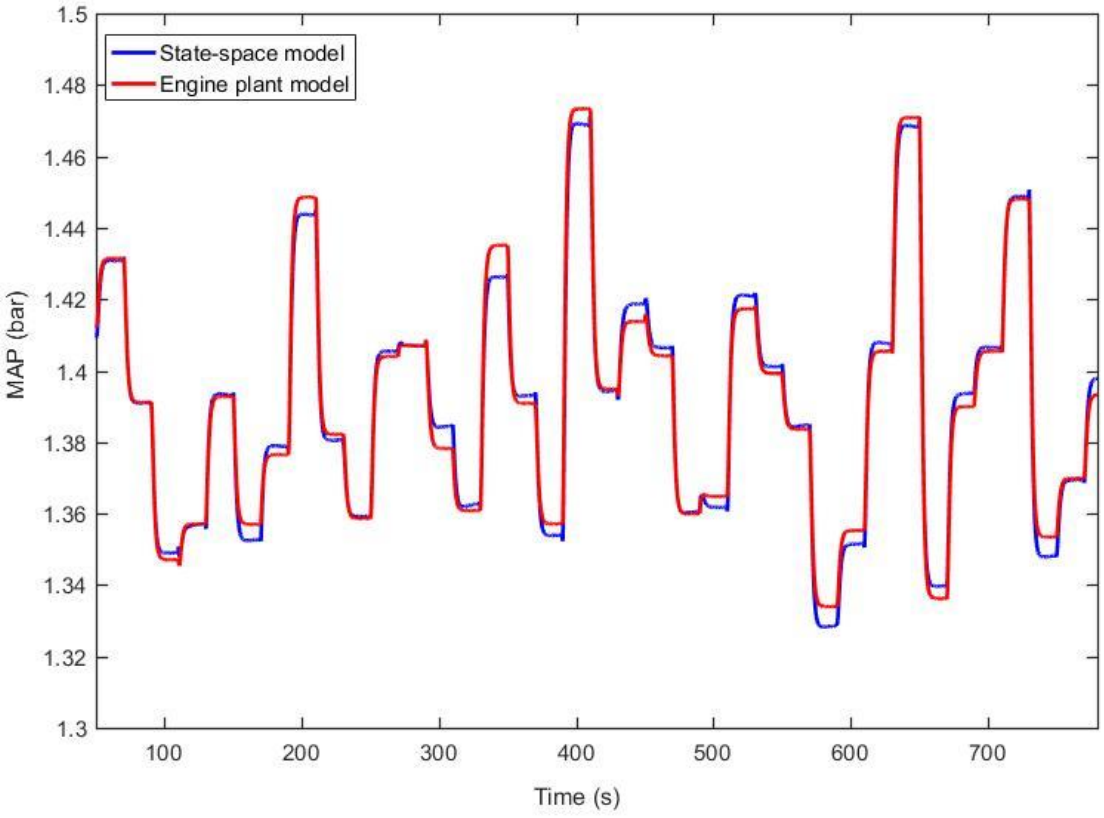

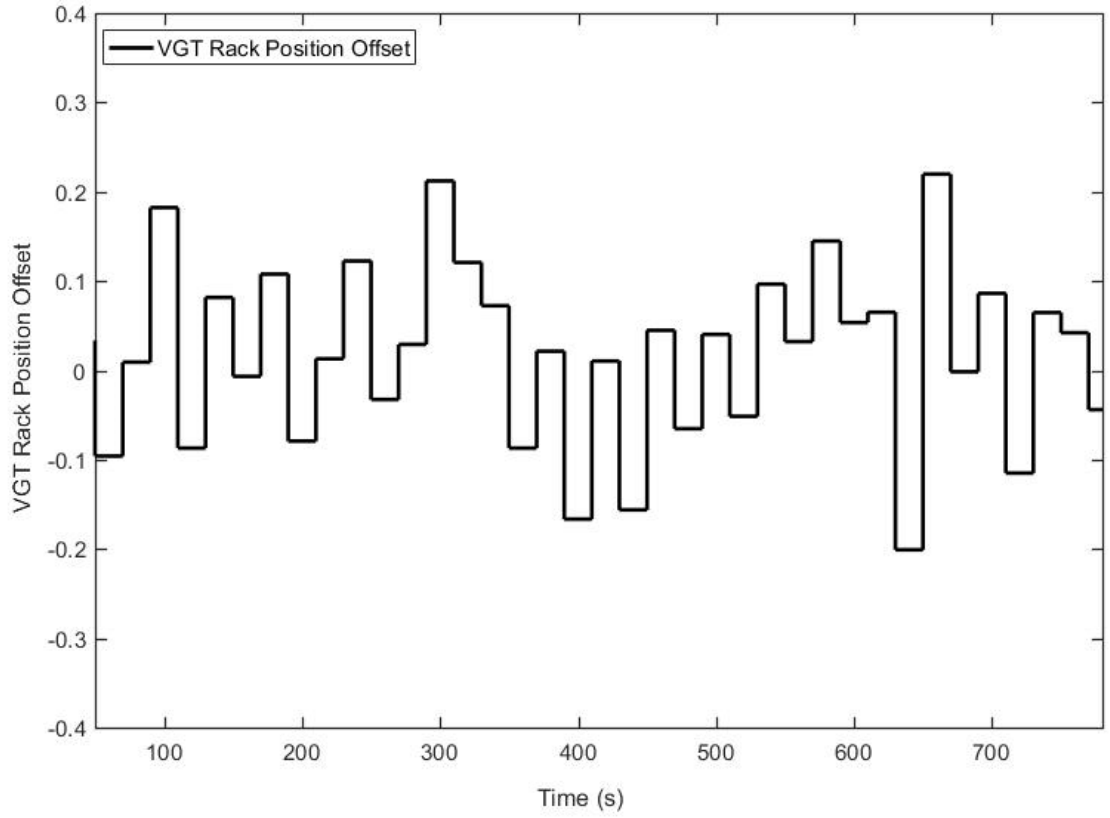
VGT Rack Position Offset
VGT Rack Position Offset
Time (s)
0.4
0.3
0.2
0.1
0
-0.1
-0.2
-0.3
-0.4
100
200
300
400
500
600
700

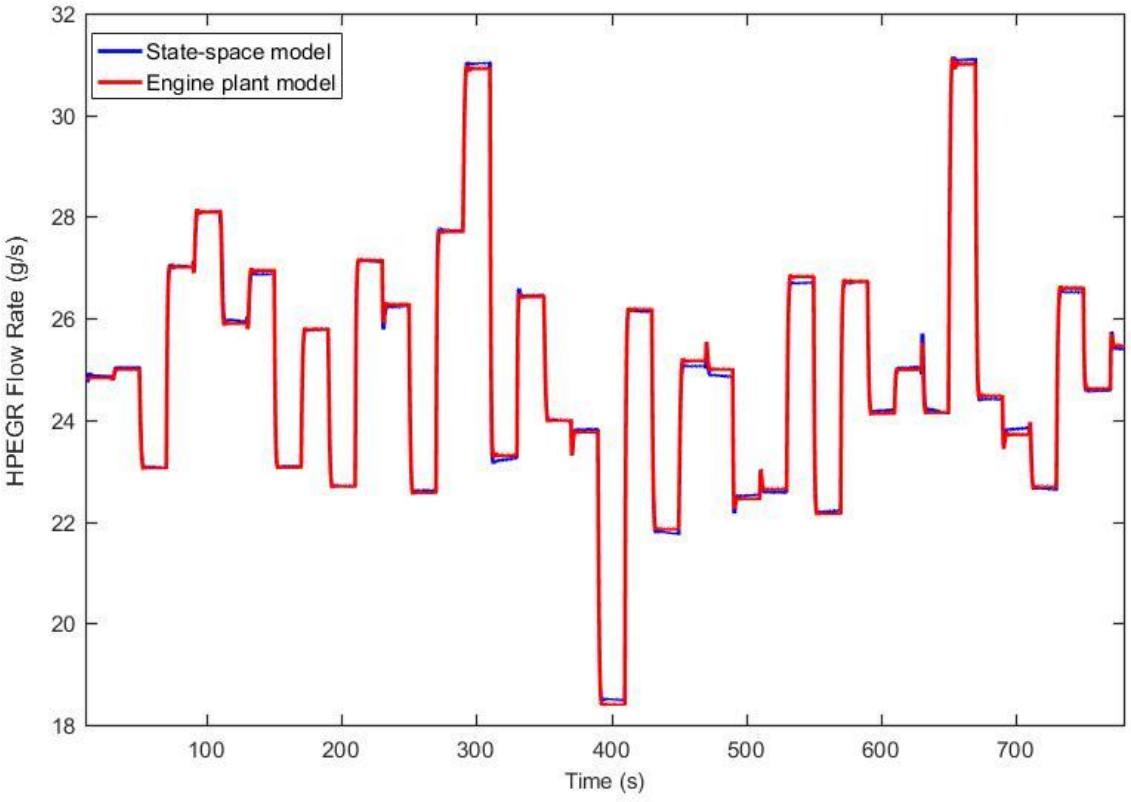
State-space model
Engine plant model
HPEGR Flow Rate (g/s)
Time (s)
32
30
28
26
24
22
20
18
100
200
300
400
500
600
700

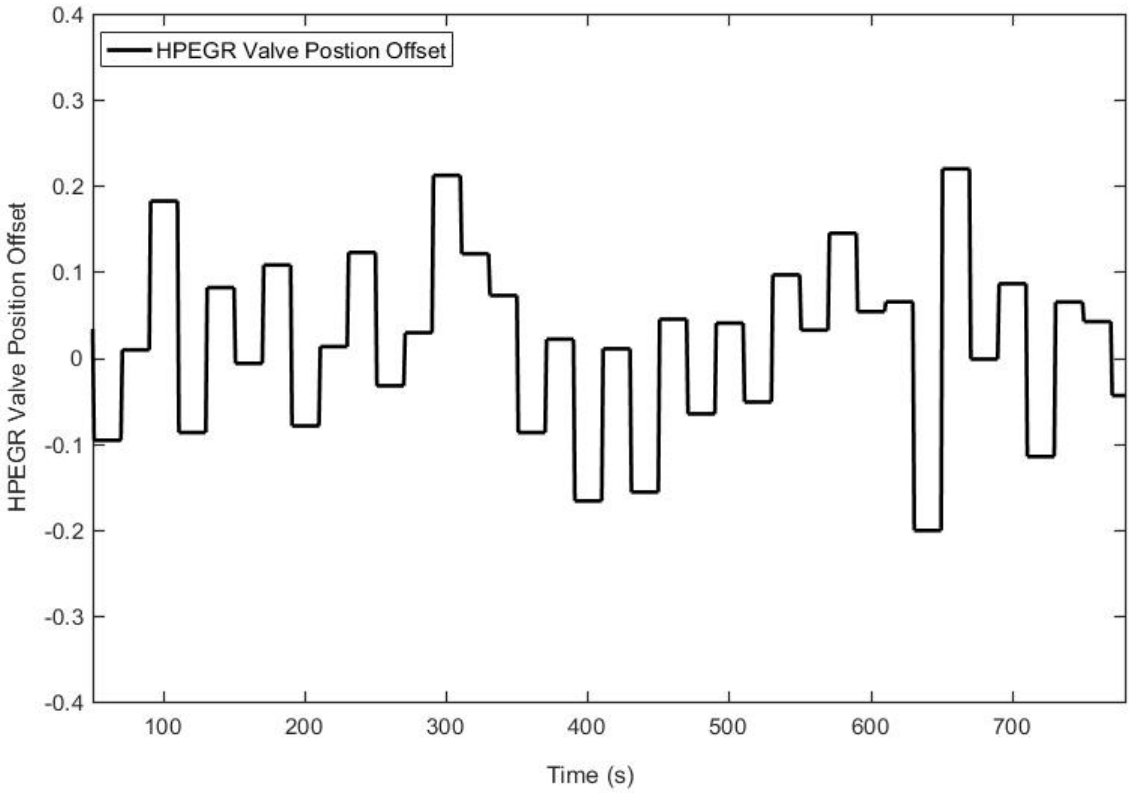
HPEGR Valve Postion Offset
HPEGR Valve Position Offset
0.4
0.3
0.2
0.1
0
-0.1
-0.2
-0.3
-0.4
100
200
300
400
500
600
700
Time (s)

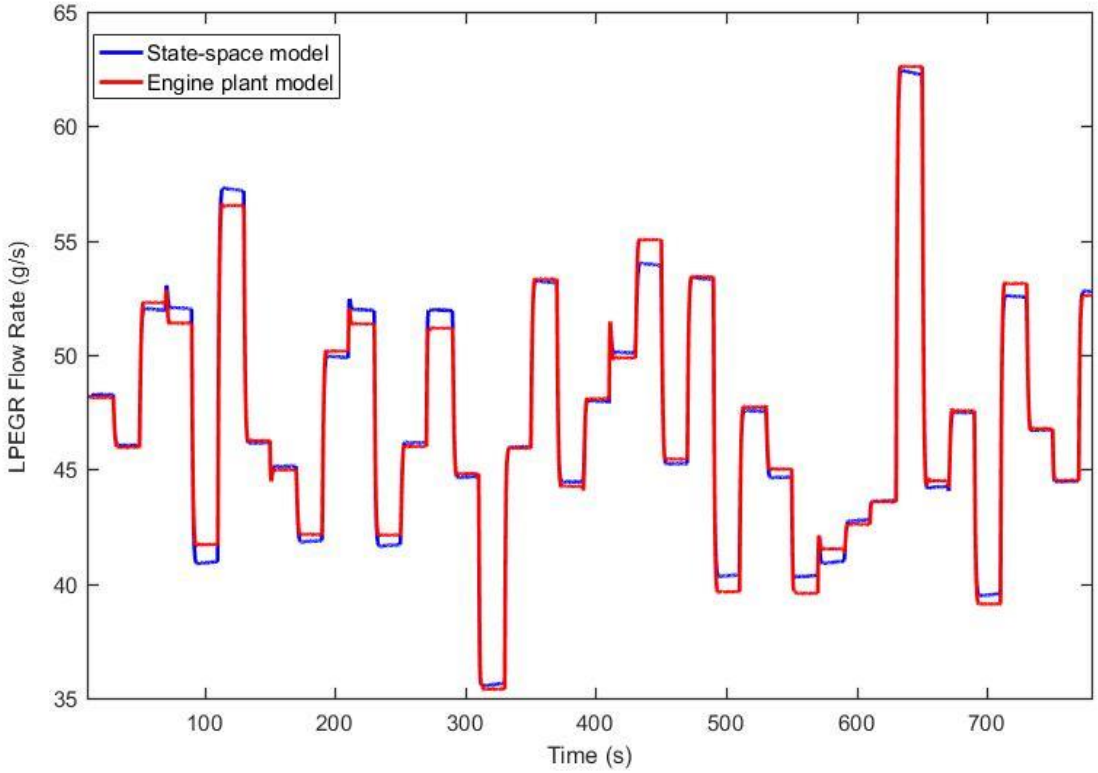
State-space model
Engine plant model
LPEGR Flow Rate (g/s)
65
60
55
50
45
40
35
100
200
300
400
500
600
700
Time (s)

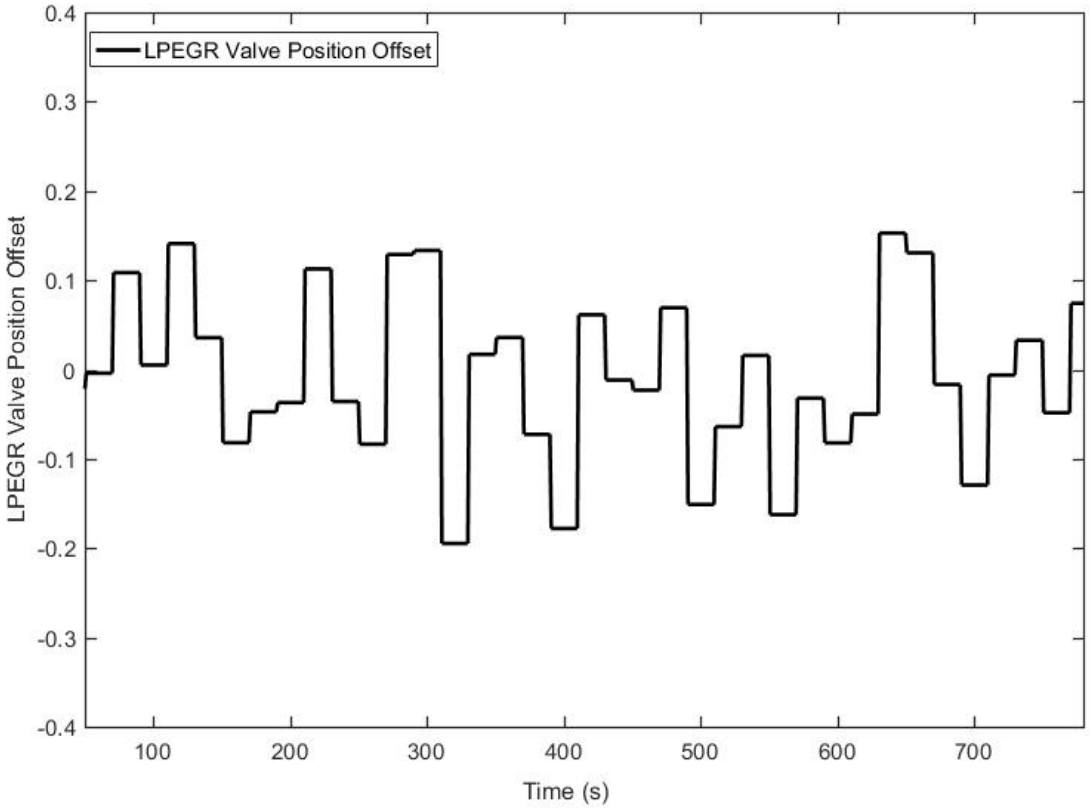

Figure 5-5 Validation of the Internal Prediction Model

The sampling time of both the internal prediction models and the TMPC controller are 0.1s, which are identical to the real-time model. The order of each state-space model falls into the range between 1 and 20. The main tuning parameters, which consist of the past inputs, past outputs maximum and prediction horizon used in the predictor, are defined as 'N4HORIZON' (Zhang et al., 2017). From figure 5-5, it can be concluded that after stepped changes on the EGR valve position, the identified state-space model could reflect the trend of the EGR flow rate variation accurately. For HPEGR, LPEGR loop and MAP, the error reaches $\pm$2.5%, $\pm$4% and $\pm$6.12% respectively. Therefore, it can be proved that the above identified model is as reliable as the predictor model for the MPC controller (Zhang et al.,

2017). Even though the error always exists due to the nature of identified model, it could be minimized by the proper designed close-loop control strategy (Zhang et al., 2017).

The next stage is the controller calibration process. In this work, the prediction horizon, control horizon, input weight, output weight, constraints and input rate weight are the main tuning parameters (Zhang et al., 2017). The selection of the control horizon is vital for the MPC-based controllers. It should be balanced between computational speed and control accuracy. A longer control horizon would lead to more accurate control of the control objects as it increases the span of the control variables that needs to calculate, but it will sacrifice the computational speed. Both the control horizon the prediction are parameters without units. The time span of the model prediction and the control variables are listed below:

$$\text{Time span of prediction model} = \text{time interval} * \text{pridiction horizon}$$

$$\text{Time span of calculated control variables} = \text{time interval} * \text{pridiction horizon}$$

In this work, the control horizon is taken as 2, while the prediction horizon is taken as 10. For the controller and the engine model, the time interval are taken as 0.1s to deal with rapid transient conditions (Zhang et al., 2017). The optimum tuning

of the TMPC parameters could help to achieve a quick response with smaller overshoot and shorter settling time (Zhang et al., 2017)

The system identification process is conducted under a constant fuel injection rate and engine speed (Ortner et al., 2006;Zhang et al., 2017). Since it is not only impractical but also inaccurate to cover the full engine working range with only one model, different regimes of the engine operating conditions are defined based on the mass of fuel injection and engine speed. Then, to select the corresponding sub-controller, a switch logic is established. The table below shows the representative engine working conditions to define the boundaries of sub-TMPC controllers (Zhang et al., 2017).

Table 5-1 Engine Working Conditions to Allocate the Sub-TMPC controller

No. of Sub-TMPC Controller	Range of Engine Speed (rpm)	Mass of Fuel Injection (mg/hub)
1	Engine Speed ≤1250	Mass of Fuel Injection ≤15
2	Engine Speed ≤1250	Mass of Fuel Injection >15
3	1250 < Engine Speed≤1750	Mass of Fuel Injection ≤20
4	1250 < Engine Speed≤1750	20 < Mass of Fuel Injection≤40
5	1250 < Engine Speed≤1750	Mass of Fuel Injection >40
6	1750 < Engine Speed≤2250	Mass of Fuel Injection ≤20
7	1750 < Engine Speed≤2250	20 < Mass of Fuel Injection≤40
8	1750 < Engine Speed≤2250	Mass of Fuel Injection >40
9	2250 < Engine Speed	Mass of Fuel Injection ≤20
10	2250 < Engine Speed	20 < Mass of Fuel Injection≤40
11	2250 < Engine Speed	Mass of Fuel Injection >40

5.4 Results and Discussion

5.4.1 Comparison between TMPC Controller and Conventional PID Controller

To evaluate the performance of the conventional PID controller and the TMPC controller, the results obtained from the simulation platform are listed below (Zhang et al., 2017). To achieve fair comparison with the proposed TMPC

controller, the PID controller is also calibrated by the author. The intelligent transient calibration method shown in chapter 4 is used to calibrate the PID controller. Similar to the control logic on production ECUs, each actuator of the air path is applied to a PID controller including the anti-windup section. (Zhang et al., 2017).

The test sequence in this case is designed as a constant engine speed with step changes of fuel injection quantity. The profile is shown in the chapter 3, section of experiment design. So, it is not shown in this chapter. In this work, the evaluation of the TMPC and PID controller mainly focuses on the overshoot time, average response time and settling time. These parameters are mutually recognized aspects to evaluate the controllers' performances (Zhang et al., 2017). Other parameters which are strongly related to the performance, fuel economy and emissions of the engine, including the engine MAF, MAP, LPEGR portion, total EGR rate, actuator positions and EGR mass flow, are also evaluated (Zhang et al., 2017). The designed test sequence has been shown in chapter 3, section of design of experiments. The detailed comparison will be introduced through the following figures(Zhang et al., 2017).

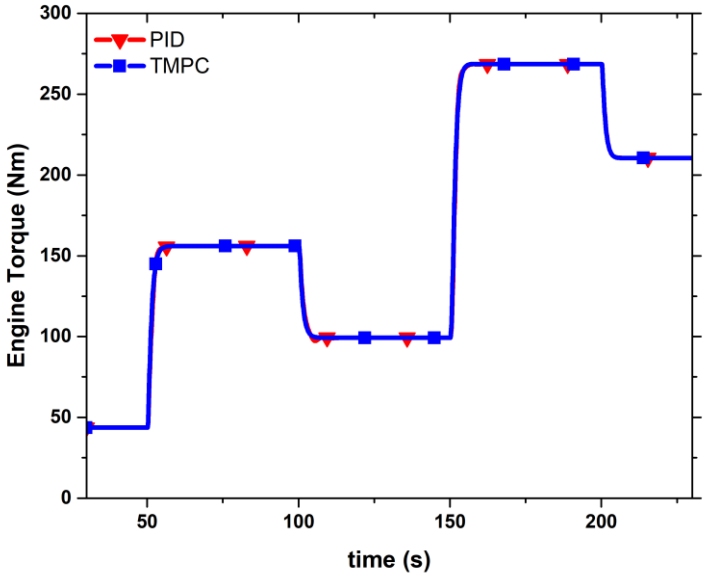

Figure 5-6 Trajectory of engine torque using TMPC controller and PID controller

Figure 5-6 is the torque response of the engine in the test scenario. Under steady state conditions, the trajectories of the torque of the engine with the PID controller and the TMPC controller are identical; however, under transient scenarios, the torque curves differ slightly. The torque trajectories with both step decreased and step increased fuel injection are compared in the following figures (Zhang et al., 2017).

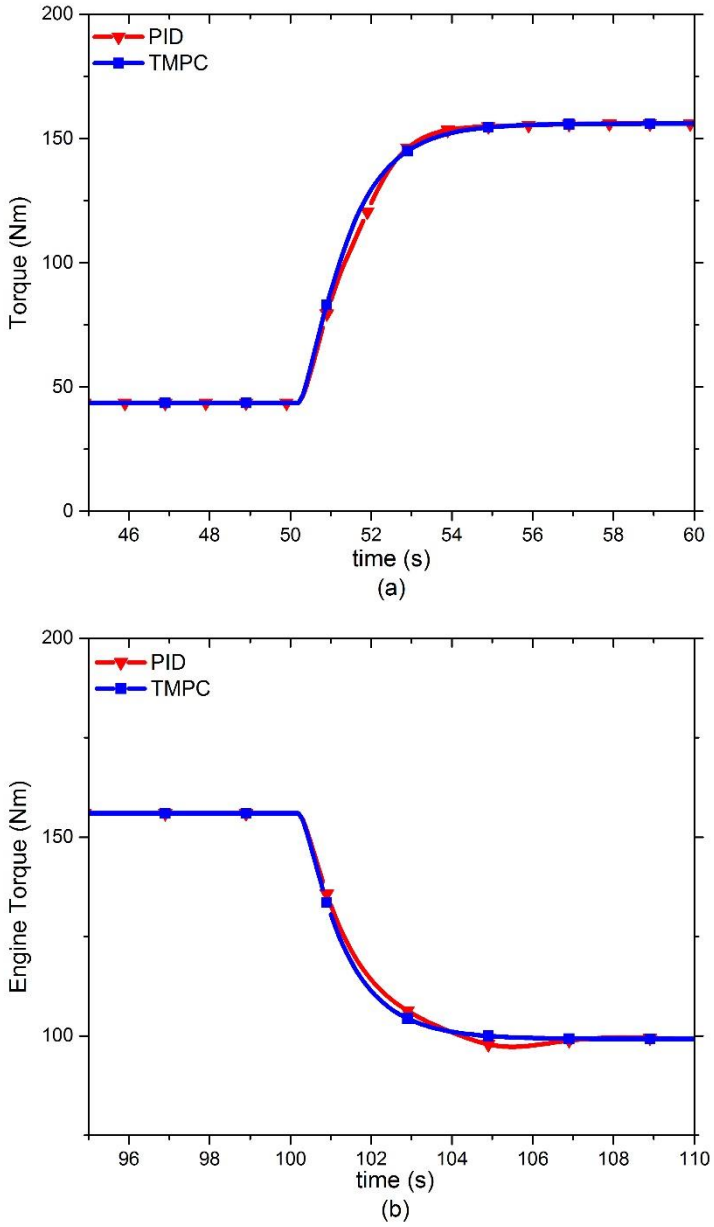

Figure 5-7 Detailed Engine Torque Comparison under Step Increased and Step Decreased Fuel Injection

When the mass of the fuel injection increases, from 50 s to 52.6 s, the TMPC controller could achieve a faster torque response than the PID controller. Even though from 152.3 s to 154.4 s, the PID controller could help the engine generating a higher torque of 1.9 Nm than that of the TMPC controller. The larger overshoot on engine MAF and MAP is the main reason for this. In terms of the

BSFC result, the TMPC controller could get a value which is 1.3% less than that of the PID controller due to the torque deviation (Zhang et al., 2017). Because of the strong non-linearity and coupling effect of the control objects, for the step decreased fuel injection, a 3% drop of the engine torque is appeared for the PID controller at 105.4 s. Moreover, between 100 s and 103.8 s, the torque rate of change under the TMPC controller is quicker than under the PID controller (Zhang et al., 2017).

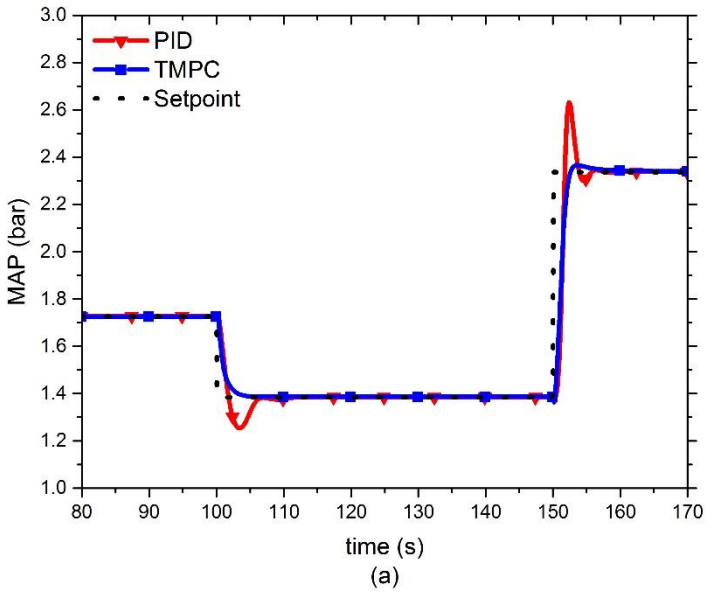

(a)

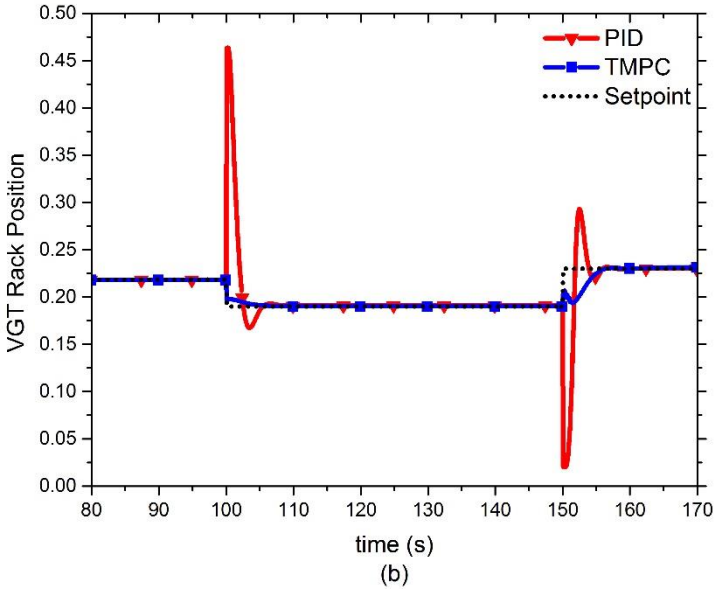
PID
TMPC
Setpoint
VGT Rack Position
0.50
0.45
0.40
0.35
0.30
0.25
0.20
0.15
0.10
0.05
0.00
80
90
100
110
120
130
140
150
160
170
time (s)

(b)

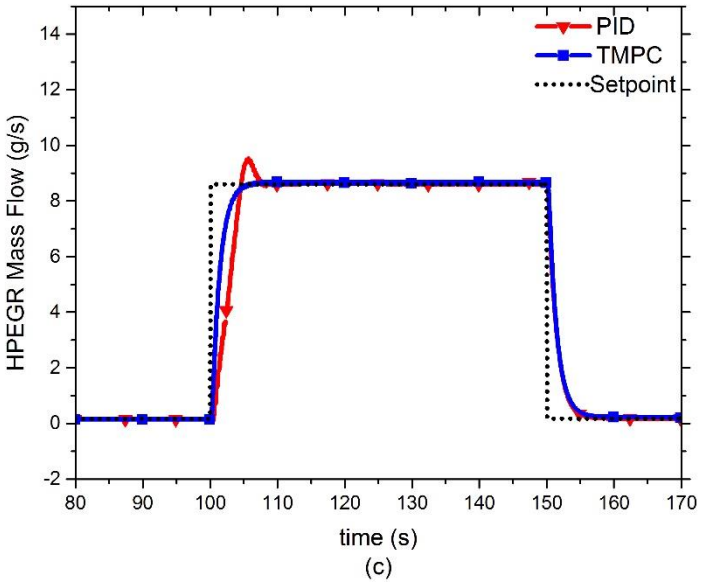
PID
TMPC
Setpoint
HPEGR Mass Flow (g/s)
14
12
10
8
6
4
2
0
-2
80
90
100
110
120
130
140
150
160
170
time (s)

(c)

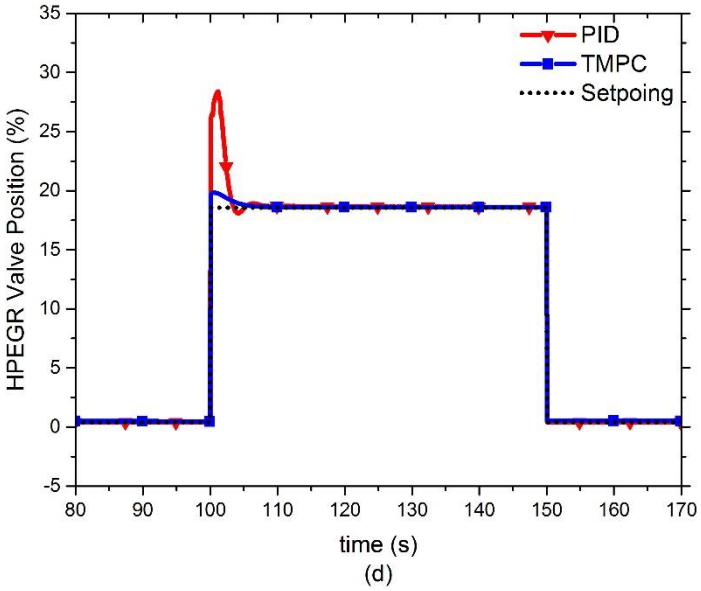
PID
TMPC
Setpoing
HPEGR Valve Position (%)
time (s)

(d)

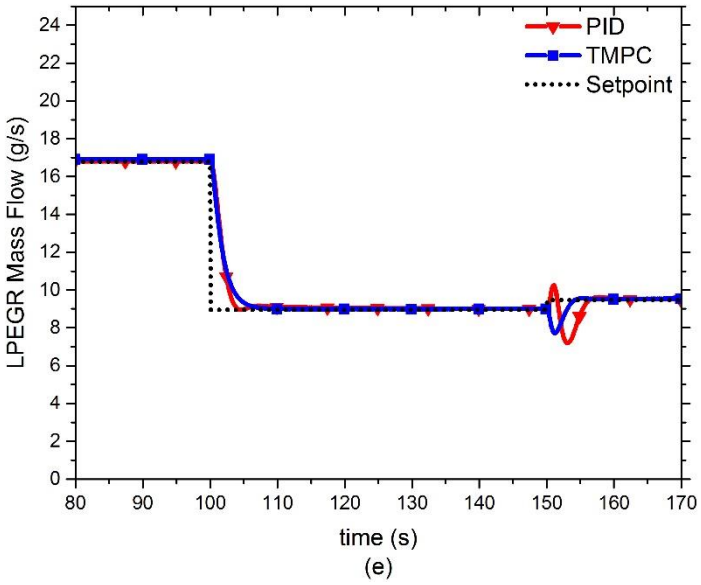
PID
TMPC
Setpoint
LPEGR Mass Flow (g/s)
time (s)

(e)

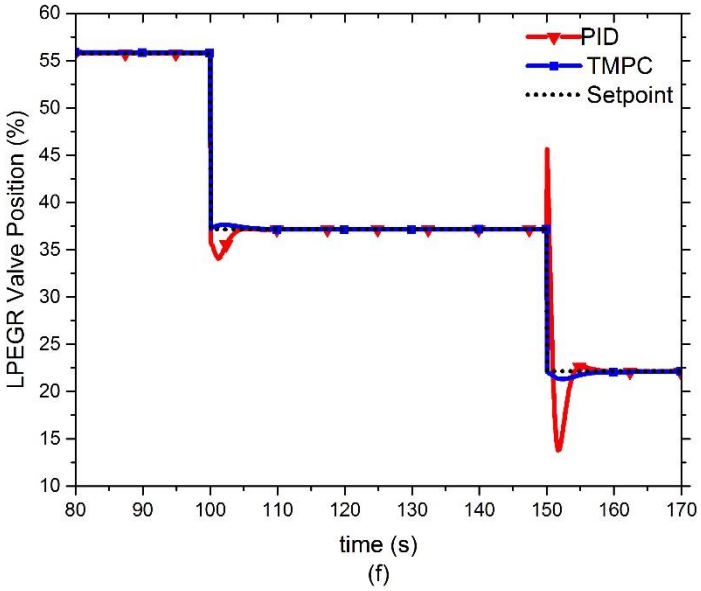

Figure 5-8 Trajectories of Engine MAP (a), VGT Rack Position (b), HPEGR Mass flow (c), HPEGR Valve Position (d), LPEGR Mass Flow (e), LPEGR Valve Position (f)

Figure 5-8 (a) and (b) compare the trajectories of the MAP and VGT's rack position. For turbocharged diesel engines, the MAP value is the key parameter to regulate the accumulated amount of the gas pumped into the engine (Heywood, 1988;Zhang et al., 2017). The average overshoot under the TMPC controller during this period drops to 1.7%; while the average overshoot of the PID controller reaches 9.1%. The average settling time of the TMPC controller is also shorter than that of the PID controller. The settling time for the TMPC controller is 5.7 s; while for the PID controller it is 7.3 s (Zhang et al., 2017). As shown in Figure 5-8(b), when the mass of the fuel injection changes at 100 s and 150 s under the PID mode, either the extra-large or extra small VGT's rack position would affect the kinetic energy of the exhaust gas received by the VGT; which eventually leads to a worse performance of the compressor and a larger overshoot on the MAP

(Zhang et al., 2017). However, when the TMPC controller is applied to the diesel air path, the VGT's rack position constraint is helpful to avoid aggressive movements of the actuators (Zhang et al., 2017). The various trajectories of the VGT rack position using the PID controller and TMPC controller are caused by the differences between these two control methods. The PID controller can only adjust the control variables based on the feedback error of the control object. While the TMPC controller aims to calculate the optimal sequence of the control variable based on both feedback and prediction of the control object's behaviour.

In this work, the control objects include the engine MAP value, engine HPEGR mass flow and the LPEGR mass flow. As it is shown in Figure 5-8(c), under the same pace with both the PID and TMPC controllers, the HPEGR mass flow decreases quickly at 150 s. According to the calibration, during these periods, the HPEGR mass flow set point is less than 1 g/s. The differences between the settling time and overshoot have little impact on the air path (Zhang et al., 2017). Under the PID controller, the settling time and overshoot of the HPEGR mass flow are 7.9 s and 8.6% when the mass of fuel injection changes from 30 mg/stroke to 20 mg/stroke at 100 s. The TMPC controller is capable to reduce these two parameters to 6.4 s and 0% (Zhang et al., 2017). Under the PID controller, the over flow of the HPEGR mass flow is caused by the large EGR valve opening shown in Figure 5-8(d), which will reduce the efficiency of the compressor. Also, as shown in Figure 5-8 (a) and Figure 5-9 (b), this coupling

effect would eventually results in a drop in terms of MAP and an increase in the total EGR rate (Zhang et al., 2017). Because of the high non-linearity and the large transport delay, the control on the LPEGR mass flow through the PID controller might have a longer settling time and a larger overshoot (Zhang et al., 2017). From Figure 5-9(c), the PID controller could obtain a trajectory with a settling time of 6.9 s and average overshoot of -16.3%. In comparison, the TMPC controller shows a better performance by achieving a settling time of 6.1s and a smooth trajectory with zero overshoot (Zhang et al., 2017).

The section of results and discussion also includes the trajectories of engine actuators (VGT and EGR valves). At steady state conditions, the baseline for the control variables is provided by the VGT rack position, the HPEGR and LPEGR valve position set points, and the optimal adjustment on the above three variables is determined by the TMPC controller to meet the control objectives during transient scenarios (Zhang et al., 2017).

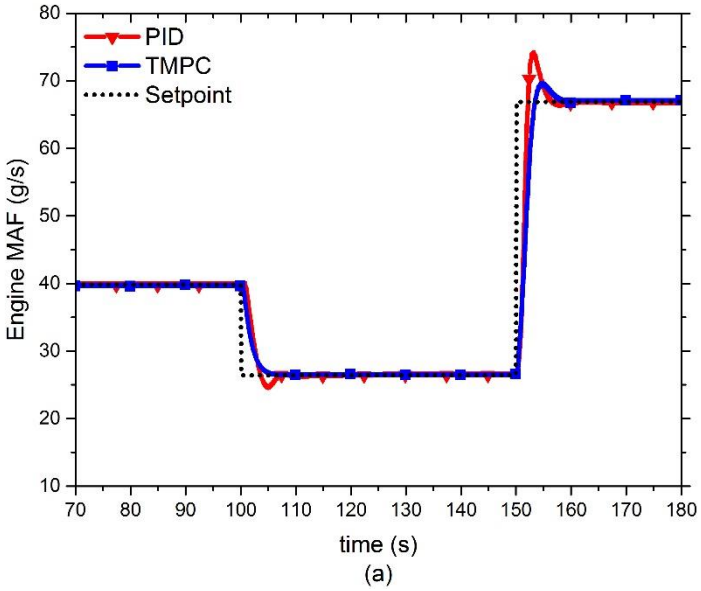
PID
TMPC
Setpoint
Engine MAF (g/s)
time (s)

(a)

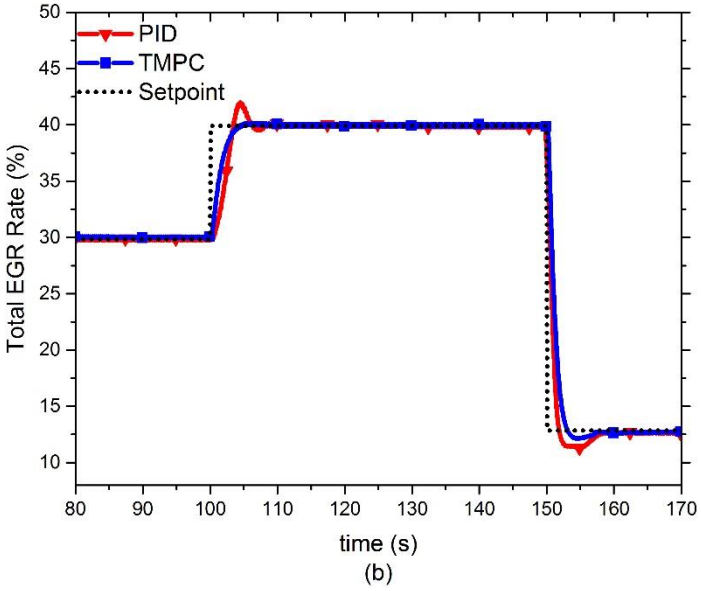
PID
TMPC
Setpoint
Total EGR Rate (%)
time (s)

(b)

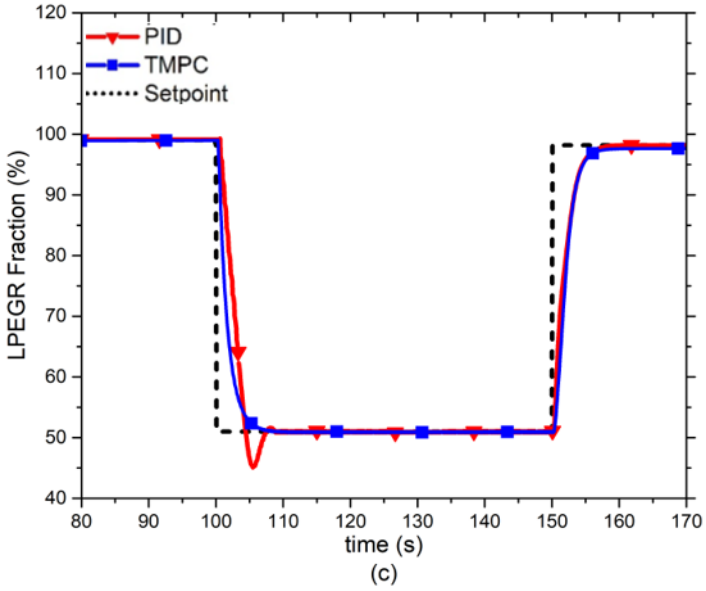

Figure 5-9 Trajectories of Engine MAF (a), total EGR rate (b) and LPEGR Fraction (c)

Based on the equations shown in section 5.3, the EGR mass flow affects the engine MAF, the LPEGR fraction and total EGR rate significantly. Therefore, the precisely controlled EGR mass flow, which is shown in Figure 5-8, could contribute to these signals (Zhang et al., 2017). In terms of the MAF control, the PID controller contains an average overshoot of 10.09%. However, the TMPC controller could minimize it to as less as 4.2%. Besides, in terms of the settling time, it is also being reduced from 8.2 s to 7.4 s. The overdosed amount of air and the high combustion temperature are widely regarded as the key elements for NOx formation (Tian et al., 2014;Zhang et al., 2017). However, the temperature inside the cylinder would be obviously raised by the sudden increased fuel injection at 150 s. In addition, at this moment, an excessive amount of air for NOx formation is also be provided by the higher overshoot of the MAF trajectory under the PID controller. Therefore, it is foreseeable that at these

moments, the NOx spike would be larger than that using the TMPC controller (Zhang et al., 2017). The MAF also has strong relation with the particulate emissions of diesel engines (Johnson, 2001;Zhang et al., 2017). In Figure 5-9(a), a low level of MAF value is provided by the larger negative overshoot of the MAF trajectory at 100 s, which contributes to the PM increment (Zhang et al., 2017).

In the in DLEGR control, the LPEGR portion and the total EGR rate are critical parameters. The trajectories of the LPGR portion and the total EGR rate are shown in Figure 5-9(b). Under the PID controller, the settling time and the overshoot of the total EGR rate are 7.5 s and -8.6% when the mass of the fuel injection is decreased from 30 mg/stroke to 20 mg/stroke at 100 s. As comparison, they have been reduced to 5.9s and 0% by the TMPS controller (Zhang et al., 2017). The settling time and overshoot of the PID controller are 8.4 s and -11.59% under the condition of a step-increased mass of fuel injection from 20 to 50 mg/stoke at 150 s. However, they can be reduced to 7.6 s and –6.15% by the TMPC controller (Zhang et al., 2017).

The EGR flow allocation is the biggest difference between the DLEGR control and the traditional single loop EGR control (Zhang et al., 2017). It is mentioned in literature review that when the LPEGR portion value becomes too low, the smoke opacity would be increased (Gihun Lim, 2011). It can be seen from Figure 5-9 (c) that under both the TMPC and PID controllers, the LPEGR portion could

reach the desired value with neglected overshoot at 150 s (Zhang et al., 2017). However, the overshoot of the PID controller is -11.8% when the mass of the fuel injection decreases at 100 s, while a smooth transaction of LPEGR proportion could be achieved by the TMPC controller. It can be concluded from previous discussions that at this moment, a larger overshoot means that more PM emissions would be produced. (Zhang et al., 2017)

5.4.2 Validation on the HIL Test Platform

Both the PID controller and the TMPC controller are validated on a HIL test platform. The structure of the HIL test platform and the designed test sequence have been introduced in chapter 3. The comparisons between the simulation and the actual ECU response are shown in figure 5-10 (Zhang et al., 2017).

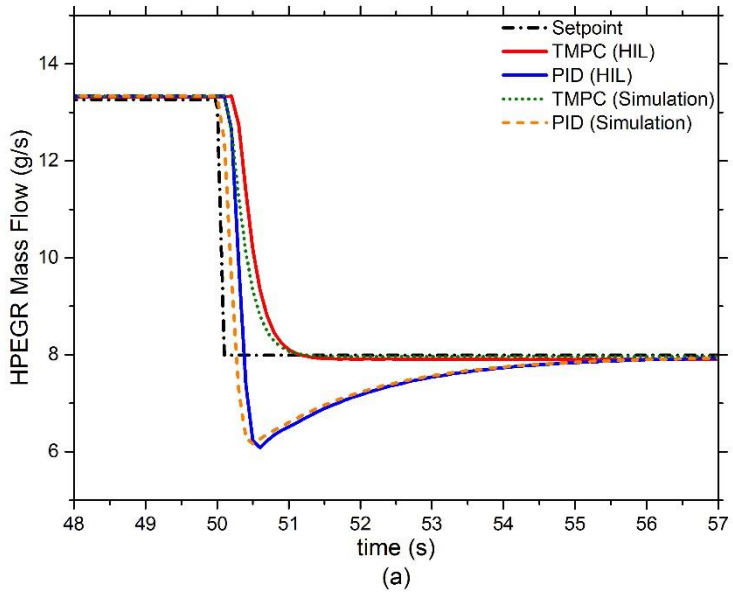

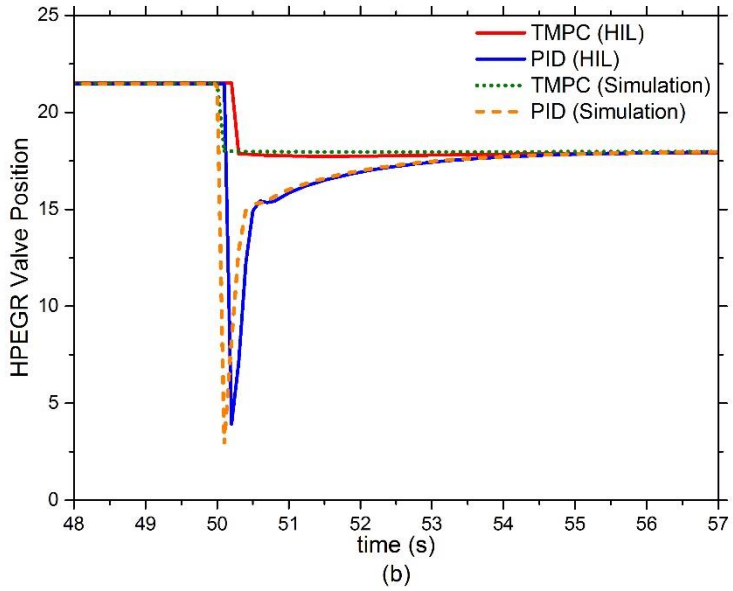
TMPC (HIL)
PID (HIL)
TMPC (Simulation)
PID (Simulation)
HPEGR Valve Position
time (s)

(b)

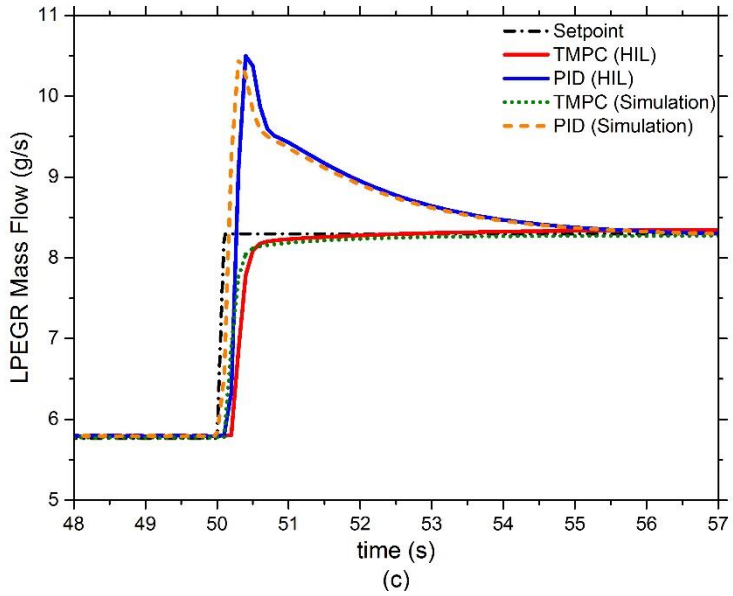
Setpoint
TMPC (HIL)
PID (HIL)
TMPC (Simulation)
PID (Simulation)
LPEGR Mass Flow (g/s)
time (s)

(c)

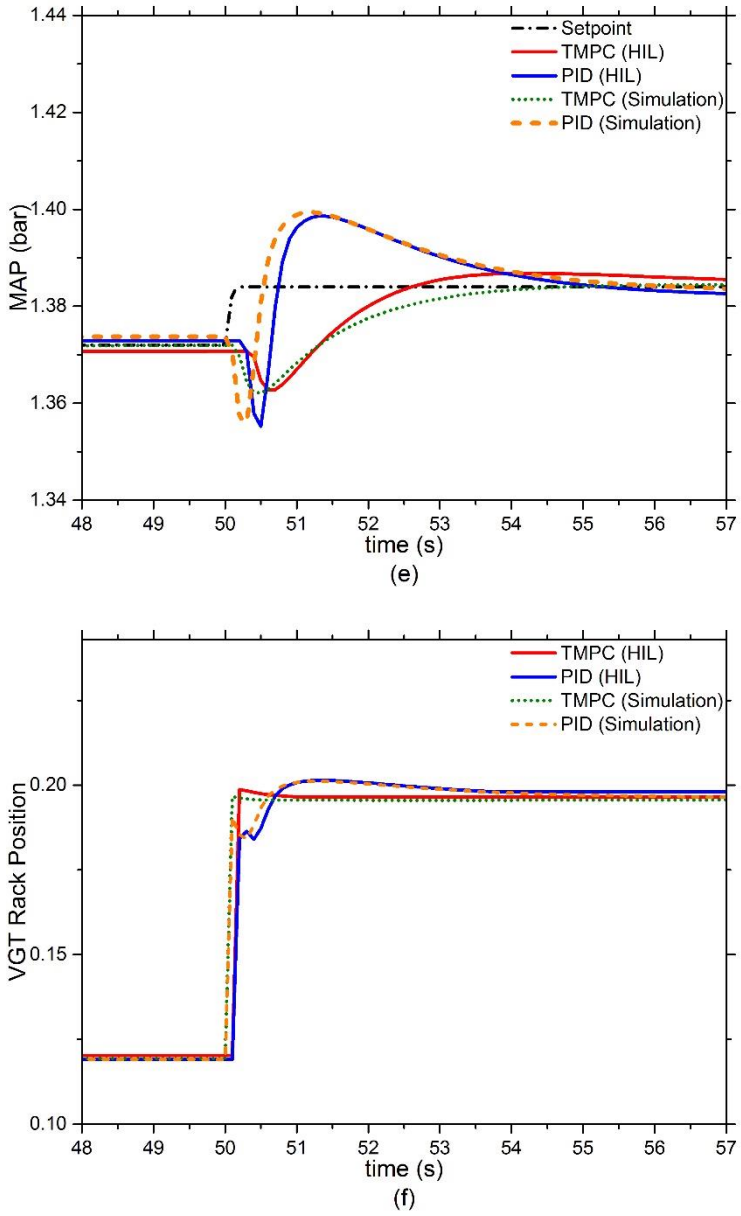

Figure 5-10 Comparison Between the Simulation Results and HIL results; HPEGR mass flow (a); HPEGR Valve Position (b); LPEGR Mass Flow (c); LPEGR Valve Position (d); MAP (e); VGT Rack Position (f)

Figure 5-10 shows that the overshoot and settling time of the control objects using the TMPC controller are still smaller than those using the PID controller; which follows the same trend as results from the simulation. However, for both the TMPC controller and the conventional PID controller, tiny lags of signals still exist.

This phenomenon could be explained from two aspects: firstly, it is the signal transmission between the processor and the real-time target PC, which makes the processor receive the signals from the real-time PC with a delay of one sample time. Although the sample time is set to 0.1 s in this case, the trajectories of control objects are still affected. The second aspect is the computational requirements of the TMPC controller. Because of the mechanism of MPC-based controller, the prediction of control objects and the calculation of the optimal control sequence must be finished online. The difference of computational capability between the processor and the desktop PC processor is non-negligible.

5.5 Summary

In this chapter, a TMPC controller for the air path of a diesel engine is presented. Case studies and HIL validation are conducted to evaluate the performance of the proposed controller. The obtained results are also compared with the results of conventional PID controller. The conclusions are listed as follows (Zhang et al., 2017):

1. The settling time and average overshoot of the engine MAP using PID controller are 7.3 s and 9.1%, respectively. The TMPC controller could reduce them to 5.7 s and 1.2%, respectively (Zhang et al., 2017).

2. The PID controller could achieve a settling time of 7.1 s and an 8.6%

overshoot for the HPEGR mass flow, while the TMPC controller could reduce them to 6.4s and 0.5%.

3. The settling time and the average overshoot of the LPEGR mass flow using the PID controller are 6.9 s and -26.3%, while the TMPC controller can reduce them to 4.3 s and-18.7% (Zhang et al., 2017).

4. A 1.2% drop of the BSFC result is achieved during transient scenarios by adopting the TMPC controller.

5. The HIL test validate the real-time capability of the proposed controller. The agreement between the actual ECU response and the simulation results is good (Zhang et al., 2017).

Therefore, it can be concluded that the proposed TMPC controller achieves better performance than the conventional PID controller in reducing the overshoot and settling time of the engine's air path during transient scenarios. An improved fuel economy is also achieved by the TMPC controller since it can overcome the nonlinearity, coupling effects and delay of the engine's air path.

CHAPTER 6 NEURAL NETWORK MODEL PREDICTIVE CONTROL

After introducing the TMPC controller in chapter 5, another control approach for the diesel engine's air path is introduced in this chapter; in which a neural network MPC (NMPC) controller is developed. Due to the more complex control mechanism, a neural network model is built based on engine data and it acts as the internal predictor for the controller. To solve the optimization problem inside the controller at each time interval, a real-time solver based on an evolutionary algorithm is also built. The proposed NMPC controller is firstly compared with the conventional PID control. To test the capability of real-time processing, the controller is also validated on the HIL test platform. Then the comparison between the NMPC controller and the TMPC controller is conducted.

6.1 Introduction

In order to investigate the MPC control of the diesel engine's air path more extensively, it is necessary to develop various types of MPC-based controllers. Compared with the proposed TMPC controller in chapter 5, the NMPC controller is a more recently created MPC-based control method, which expands the MPC

control theory. The NMPC is in the category of non-linear MPC control methods. It provides an alternative solution for the constraint multiple-objective control problems.

The real-time applicability on standard ECU with sampling time in millisecond range is still a challenge due to complex algorithm of non-linear MPC controllers. Generally, the optimal control problem in the non-linear MPC controller is solved by gradient-descent Newton's method. One commonly used method is to use sequential quadratic programming (SQP) (Zhu et al., 2017a). Previous work has proved the possibility of applying SQP to non-linear MPC (Study et al., 2016;Harder et al., 2017). The advantage of SQP is transforming a complex non-linear programming (NLP) problem into a sequence of sublevel QP problems (to compute the Hessian and Jacobi matrixes of the NLP problem) (Zhu et al., 2017b). The MATLAB function could also be used to solve this kind of optimization problem (Jain and Deb, 2014). However, the MATLAB function has a shortage of high computational requirements and thus, which is not suitable for engine control applications with the need for real-time calculation. Other methods such as the Laguerre function (El Hadef et al., 2013), NAG toolbox (X. Zhou et al., 2015; Li et al., 2016) and dynamic programming (Tan et al., 2015) have also been used as non-linear MPC solvers. As the neural network models have the advantage of capturing the characteristics of complex systems, they have attracted the attentions of the researchers in recent years. Techniques including a recurrent

neural network (RNN), or an extreme learning machine (ELM) have been successfully used for non-linear MPC controllers (Chen et al., 2017; Janakiraman et al., 2016).

In recent years, it has been found that an evolutionary algorithm can be a potential candidate as a global NLP solver for non-linear MPC controllers. The genetic algorithm (Chen et al., 2009), NSGA-II (Wei et al., 2017), nested-partition algorithm (Chauhdry and Luh, 2012) and particle swarm optimization (PSO) algorithm (Xu et al., 2013) are all proposed to solve the non-linear optimization problem. Among these methods, the PSO-based algorithm is a population-based stochastic method with the advantages of not needing to calculate the gradient, a quick convergence speed, global search capability, simple structure and easy implementation (Thomas, 2014). Besides, the performance can be further improved by upgrading the conventional PSO algorithm into a chaos-enhanced accelerated particle swarm optimization (CAPSO) algorithm (Gandomi et al., 2013). Publication that author participated has proved that the CAPSO algorithm is a feasible solution for energy management; the controller's stability and tracking performance are fully presented (Q. Zhou et al., 2017b). Therefore, the idea of adopting a CAPSO algorithm to solve the NMPC problem in the diesel engine's air path is promising.

This chapter presents a NMPC controller for a diesel engine's air path, which

adopts the recurrent neural network model as the internal predictor and the CAPSO algorithm as the real-time solver. The outline is organized as follows: section 6.2 introduces the controller's structure (control objectives and control variables); section 6.3 presents the algorithm and the design workflow of the NMPC controller; section 6.4 firstly shows the comparison between the NMPC controller and the PID controller, which is conducted on the real-time engine model. The optimization performance of the NMPC controller is further discussed afterwards. The NMPC controller is also validated on a HIL platform. Finally, the conclusions of this work are summarized and listed.

6.2 Controller Structure

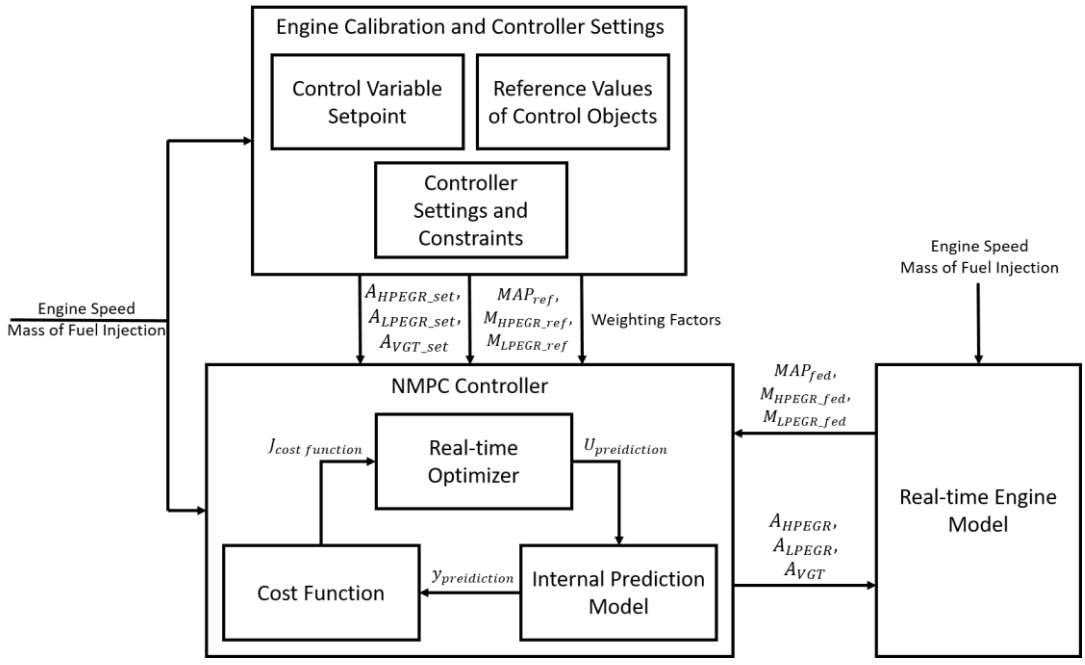

Figure 6-1 Structure of the NMPC Controller

The structure of the NMPC controller is shown in Figure 6-1. In this case, the

control objects are the engine boost pressure (MAP), HPEGR mass flow (M_{HPEGR}) and LPEGR mass flow (M_{LPEGR}). The control variables are the HPEGR valve position, LPEGR valve position and VGT rack position ($A_{HPEGR}, A_{LPEGR}\ and\ A_{VGT}$). To achieve the function of the engine air path control, the NMPC controller also requires the engine speed, mass of fuel injection, setpoint of the control variables ($A_{HPEGR\_set}, A_{LPEGR\_set}\ and\ A_{VGT\_set}$), the reference values of the control objects ($M_{HPEGR\_ref}, M_{LPEGR\_ref}\ and\ MAP_{ref}$), feedback values of the control objects ($M_{HPEGR\_fed}, M_{LPEGR\_fed}\ and\ MAP_{fed}$) and controller weighting factors to calculate the optimal control sequence. The setpoint of control variables, the desired values of control objects, weighting factors and controller constraints are obtained from the pre-stored calibration maps. The desired values of the HPEGR and LPEGR mass flow are calculated by engine MAF, total EGR rate and LPEGR fraction. The equations to define the total EGR rate and LPEGR fraction are shown below:

$$EGR\ Rate_{ref} = \frac{M_{HPEGR\_set} + M_{LPEGR\_set}}{MAF_{set} + M_{HPEGR\_set} + M_{LPEGR\_set}}$$

$$LPEGR\ fraction_{set} = \frac{M_{LPEGR\_set}}{M_{HPEGR\_set} + M_{LPEGR\_set}}$$

The equations to calculate the M_{HPEGR_ref} and M_{LPEGR_ref} are:

$$M_{HPEGR\_ref} = \frac{MAF_{ref} \cdot R_{EGR\_ref} \cdot (1 - R_{LP\_ref})}{(1 - R_{EGR\_ref})}$$

$$M_{LPEGR\_ref} = \frac{MAF_{ref} \cdot R_{EGR\_ref} \cdot R_{LP\_ref}}{(1 - R_{EGR\_ref})}$$

Inside the NMPC controller, it consists of three parts: the cost function, the real-time optimizer and the internal prediction model. The detailed introduction of each part is shown in the next section. The real-time optimizer calculates the optimal sequence of the control variables. The internal prediction model predicts the future trajectory of the control objects. The cost function module formulates the control problem into an optimization problem and provides an evaluation standard for the results from the internal prediction model. Eventually, the optimal results of the control variables are generated by the NMPC controller and sent to the real-time engine model at each time interval.

In terms of the real-time diesel engine model, it is the same model used for the simulation work in chapter 4 and 5. The detailed introduction has been shown in chapter 3, section 3.1.5.

6.3 Nonlinear Model Predictive Control Approach

6.3.1 Cost Function Design

In general, an MPC-based controller formulates the control problem into calculating the optimal sequence of the control variables. The goal of the NMPC controller is to assure that the control objects track the given reference while penalizing any large excursion in the control variables.

The author adopts the cost-function design of conventional linear MPC controller in chapter 5 and formulates the cost function as:

$$J\left(x_{(k)}, u_k\right) = \sum_{i=1}^{N_p} \|\bar{y}_c(k+i) - r(k+i)\|_Q^2 + \sum_{i=0}^{N_c-1} \|\bar{u}_c(k+i) - r_u(k+i)\|_R^2$$

$$u_c(n)_{min} \le u_c(n) \le u_c(n)_{max} \quad n = 1,2,3 \ldots N_c - 1$$

$$\Delta u_c(n)_{min} \le \Delta u_c(n) \le \Delta u_c(n)_{max} \quad n = 1,2,3 \ldots N_c - 1$$

$$y_c(n)_{min} \le y_c(n) \le y_c(n)_{max} \quad n = 1,2,3 \ldots N_p - 1$$

where N_p and N_c are the prediction horizon and control horizon, with the condition $N_c \le N_p$; Q and R are the weighting matrix of the control objects and

control variables respectively; $\bar{y}_c(k+i)$ is the predicted control objects in the span of the prediction horizon from the internal prediction model; $\bar{u}_c(k+i)$ is the calculated sequence of the control variables in the span of the control horizon from the real-time solver; $r(k+i)$ represents the desired values of the control objects and $r_u(k+i)$ means the setpoint of control variables. Meanwhile, the cost function is limited by the boundary conditions, which define the upper and lower limit of control objects and control variables. To limit the control variables' rate of change, an extra limitation module is added to the proposed NMPC controller. The limitation of the rate of change reflects the physical characteristics of the HPEGR valve, LPEGR valve and VGT.

As with the conventional linear MPC, only the first value of the optimal control sequence is applied to the engine plant at each time interval. The optimization process is conducted again for the next time instant. It is helpful to handle the model inaccuracies and external disturbances such as the change of engine working conditions (Janakiraman et al., 2015).

6.3.2 CAPSO-based Solver for the Optimization Problem

In this case, the optimization problem is solved using the chaos-enhanced accelerated particle swarm optimization (CAPSO) algorithm. Compared with other nature-inspired evolutionary algorithms, the CAPSO algorithm has the advantages of requiring fewer tuning parameters and computational resources to

solve the multiple-objective optimization issues (Q. Zhou et al., 2017a). It should be noticed that the choices of the parameters in the CAPSO-based solver are very important to balance the convergence speed and results accuracy.

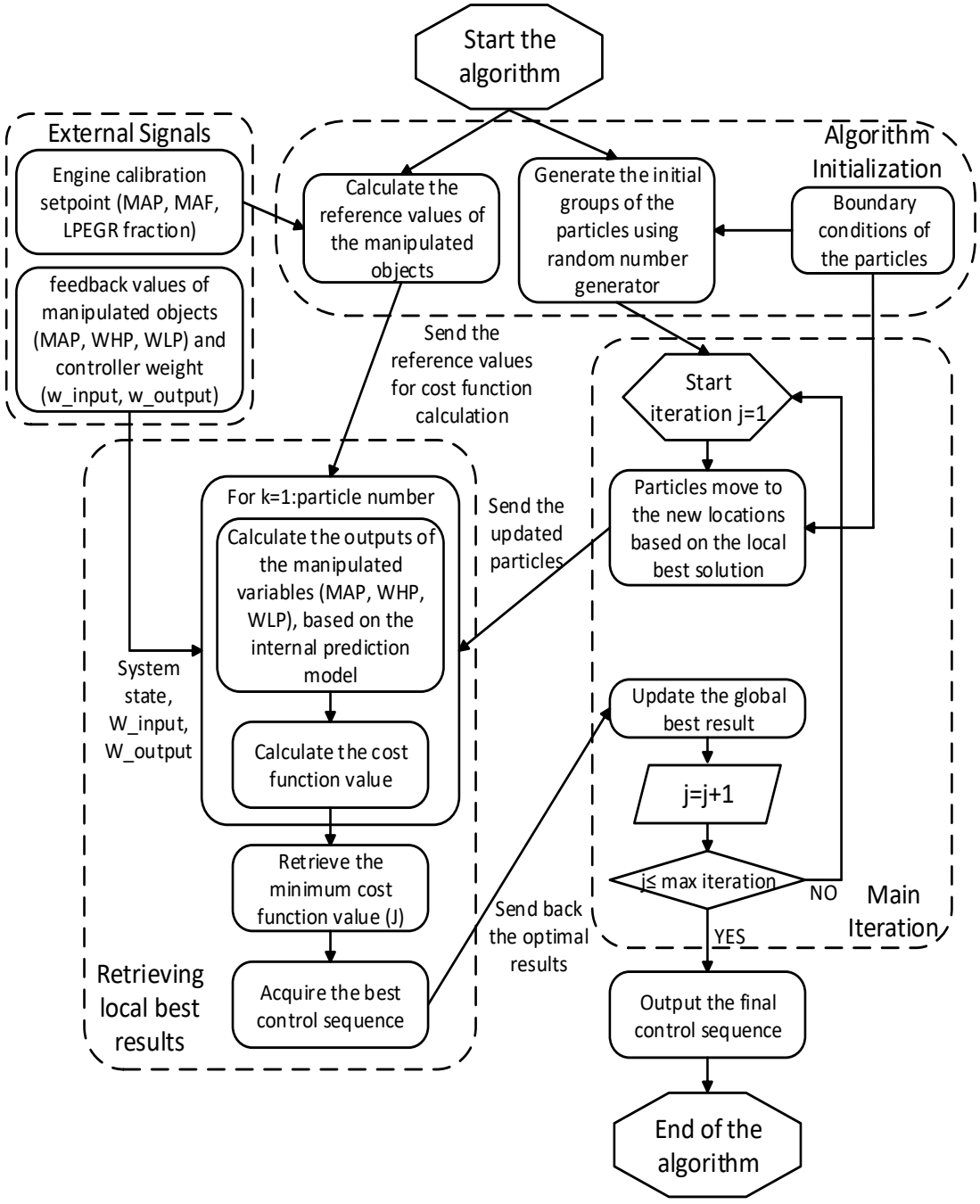

Figure 6-2 Flowchart of the CAPSO-based Solver for the NMPC Controller at Each Time Interval

The figure above shows the flowchart of the CAPSO solver, which is formed by four modules: algorithm initialization, retrieving local best results, main iteration and external signals. To solve the optimization problem in the previous section online, the algorithm is modified in the following aspects.

At the beginning of the algorithm, the initial particles in the swarm are generated inside the defined particle ranges. This module also formulates the reference values of the control objects and control variables into the format that could be used by the other functions such as the cost function calculation. Furthermore, the algorithm initialization module also determines the prediction horizon and control horizon. As discussed in the previous chapter, the control horizon is very important for the MPC-based controller.

All the particles in each generation would be used to calculate the outputs (predicted values of control objects) based on the internal prediction model (shown in the module of retrieving the local best results). These outputs are needed for calculating the cost function value. This process also requires the controller's weights (received from the module of external signals) and reference values of the control objects (received from the module of algorithm initialization). Then it retrieves the minimum cost function and the local best particle.

The proposed real-time solver is developed based on an iterative algorithm. The main iteration module plays a dominating role in the whole algorithm as it involves

updating the local best result in each generation and particle positions in the swarm. As introduced in Chapter 4, the CAPSO algorithm brings the chaotic mapping strategy to the convergence process of the particles. The governing equations are shown in the following (Q. Zhou et al., 2017a):

$$P_{(k,j+1)} = P_{(k,j)} + \beta_j \cdot \left(P^*_{(k,j)} - P_{(k,j)}\right) + \alpha_j \cdot RNG(particle\_range)_{(k)}$$

$$\alpha_j = \alpha_{j-1} \cdot \rho^{j-1}$$

where $P_{(k+1,j)}$ is the updated particle at the next iteration (j+1); $P_{(k,j)}$ is the particle's current position (k); $P^*_{(k,j)}$ is the local best particle position at the current iteration (j); j is the iteration number; and k is the specific particle index; ρ is a reducing factor to make α_j decrease gradually to ensure the convergence of the results. The RNG is the random-number generator, which is extremely necessary for PSO-based algorithm. The $particle\_range$ is the searching area of the particles, which is defined by the boundary conditions. Both $\alpha_0$and γ are tuning parameters in this algorithm. After calibration, they are set to 0.7 and 0.7 respectively in this case. β is the unique part of the proposed CAPSO algorithm. It is called the attraction parameter and the detailed introduction of this part has been presented in the previous chapter (Chapter 4). Based on the publication that author contribute to (Q. Zhou et al., 2017b), the logistic map achieves better

performance on generating the array of the attraction parameter. The equation is shown below:

$$\beta_j = \rho \cdot \beta_{j-1} \cdot (1 - \beta_{j-1})$$

According to the reference listed in the previous paragraph, the initial value (β_0) is set to 0.7 and the ρ is chosen as 4.

In this algorithm, the particle position updating is formed by the particle move towards the local best result with the chaotic mapping strategy and the random move inside the particle range. The equations of the random particle move are developed based on the linear congenital generator (LCG) (Xu et al., 2016). This method has the advantages of easy understanding and fast implementation. Due to the physical limitation of the actuators in the diesel engine's air path, the random numbers need to have the resolution of 0.01. Because the operation range of the EGR valves and VGT rack position in this thesis is between 0 and 100, the minimum resolution of the actuator is 0.1. The offset of the actuator position caused by the LCG should match with the minimum resolution of the actuators. So, the solution of the random number generator matches with the characteristic of the actuators. Based on the design of the controller, the randomly generated numbers should fall in the range between -0.5 and 0.5.

$$R_{(k)} = (a \cdot R_{(k-1)} + c)(mod\ M)$$

$$RNG_{(k)} = round\left(\frac{R_{(k)}}{M}, 3\right)$$

$$RNG\left(particle_{range}\right)_{(k)} = RNG_{(k)} - 0.5$$

The equations above define the sequence of randomly generated numbers ($RNG_{(k)}$) with the initial seed R_0. These numbers are limited in the range between 0 and 1; a, c, M are the multiplier, additive value and modulus, which are the calibrated variables. To meet the most optimal pseudo-random number performance, these parameters are selected as R_0=9, a=27, c=0 and M=2^{20}. The effect of these calibrated variables on the LCG performance and more detailed principles of the LCG can be found in the work carried out by Tan and Hui (Tang, 2007).

The random numbers generated by the LCG are shown in the figure below (Figure 6-3). The random numbers achieve a uniform distribution and satisfy the boundary conditions required by the CAPSO-based solver after 2000 iterations.

The main reason to use the RNG introduced in the previous paragraphs is to make sure the whole NMPC controller could be validated by the HIL test; as there is no direct substitute for this MATLAB function in the HIL platform.

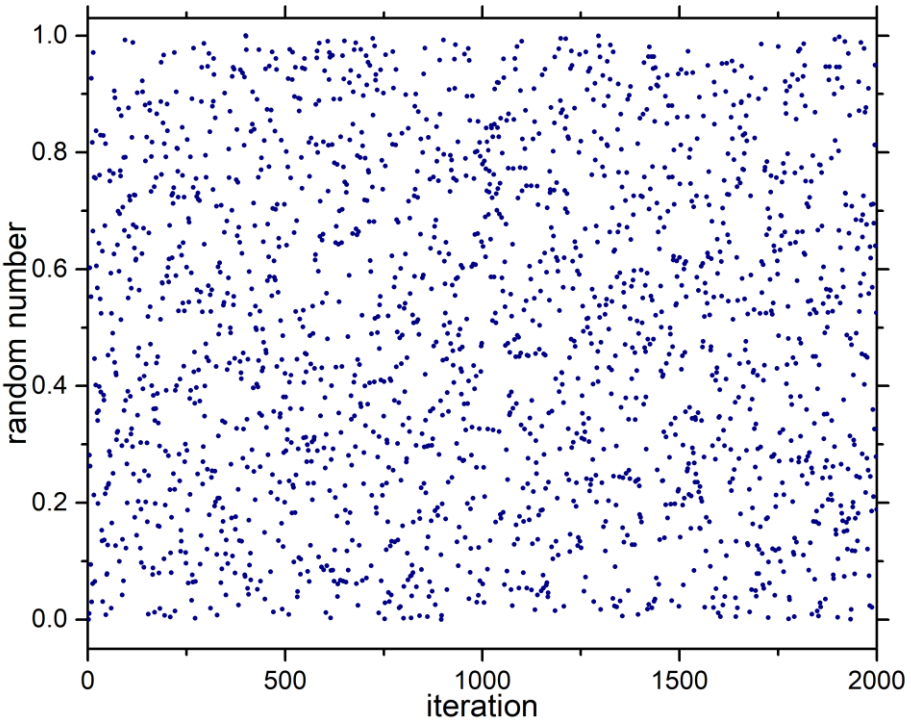

Figure 6-3 Random Number Distribution by LCG

At the end of the iteration process, the algorithm results are successfully converged. The optimal control sequence is generated. Then the first column of the matrix$\bar{u}_c(k) = [\bar{u}_{HPEGR}(k); \bar{u}_{LPEGR}(k); \bar{u}_{VGT}(k)]$ would be final output of the NMPC controller and sent into the real-time engine model.

6.3.3 Internal Prediction Model

To acquire the predicted trajectories of the control objects, the internal prediction model is compulsory for the proposed NMPC controller. The internal prediction model in this case is a non-linear ARX model (NARX) which has the advantage of anticipating time-series data. Moreover, it is also able to cope with the strong non-linearity and coupling effects of the diesel engine's air path. The training of

the internal prediction model of the NMPC controller no longer needs the system linearization procedure. It is helpful to further increase the prediction accuracy (Bc. Ondrej Mikulas, 2016). The third reason to select this model is its easy implementation. The MATLAB code of the model can be directly generated, which makes it compatible in the Simulink environment. The details of this model are shown in the following paragraphs.

The governing equations for the NARX model are shown below (F. Zhou et al., 2017):

$$y_{(k)} = f(y_{(k-1)}, y_{(k-2)}, \dots, y_{(k-n)}, u_{(k)}, u_{(k-1)}, u_{(k-2)}, \dots, u_{(k-m)})$$

While the model inputs and outputs are constrained in the form of:

$$u_{(k)} \in U, \forall\, k \geq 0$$

$$y_{(k)} \in Y, \forall\, k \geq 0$$

$$U = \{u \in \mathbb{R}^{n_u} \mid u_{min} \leq u_{(k)} \leq u_{max}\}$$

$$Y = \{y \in \mathbb{R}^{n_y} \mid y_{min} \leq y_{(k)} \leq y_{max}\}$$

where $f(\cdot)$ is a non-linear function which involves the current model's inputs and the previous model's inputs and outputs. The main tuning parameters are the number of hidden layers and the orders of the past input and output delays that will be fed into the network. They are determined by the training data acquired by the experiments. The training algorithm should also be chosen to balance the training speed and the results' accuracy. The NARX model also requires the initial delay states of the inputs and outputs for simulation (TDL). The detailed structure of the NARX prediction model is shown in Figure 6-4.

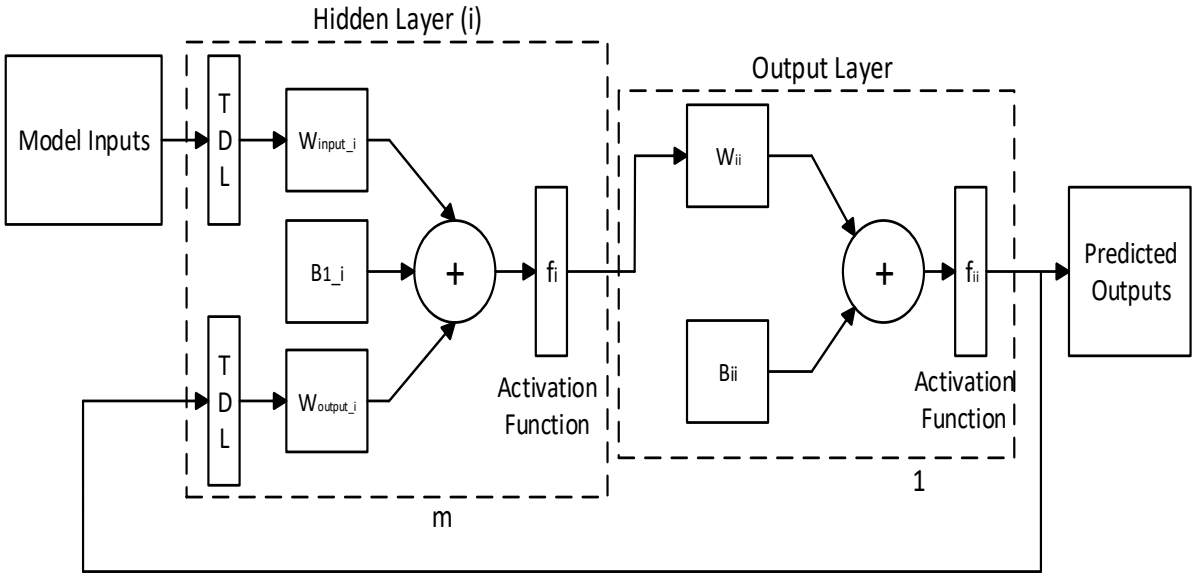

Figure 6-4 Structure of the Internal Prediction Model Based on NARX ("Design Time Series NARX Feedback Neural Networks - MATLAB & Simulink - MathWorks United Kingdom," n.d.)

The NARX model can be designed in the form of open-loop and closed-loop. Compared with the open-loop form, the closed-loop form is more suitable for multi-step prediction as it continues to work when the external feedback is

unavailable, by using the internal feedback values. This kind of structure is also known as a parallel structure.

In this case, the inputs of the model are selected as: the engine speed, mass of fuel injection per stroke, HPEGR valve position, LPEGR valve position and VGT rack position. The model's outputs are the control objects; which are the engine MAP, HPEGR mass flow and LPEGR mass flow. The training process is to apply randomly generated offset to the five parameters that would be used as the model inputs, then recording the trajectories of the control objects. Before sending all the data into the neural network training process, data processing is needed. A median and a low-pass filter are added to minimize the noise in the raw data. In addition, correlation factors are added to make sure the input data and output data are in the scale. Eventually, a multi-layer multi-step prediction neural network structure with one input and output delay is deployed after calibration. The Levenberg-Marquardt back propagation algorithm is selected as the training algorithm. The fluctuation and the noise of the air path are noticed. Filters (low-pass filter and median filter) are added in the data acquisition process. To reflect the physical characteristics, the actuators' transport delay is also considered (Kyunghan et al., 2015).

The performance of the NMPC controller is significantly affected by the accuracy of the internal prediction model. The test data provided by the engine supplier

and the data acquired by internal prediction model are compared. The whole test sequence continues for over 1500 s. The figure below only shows a selected period of it as a demonstration.

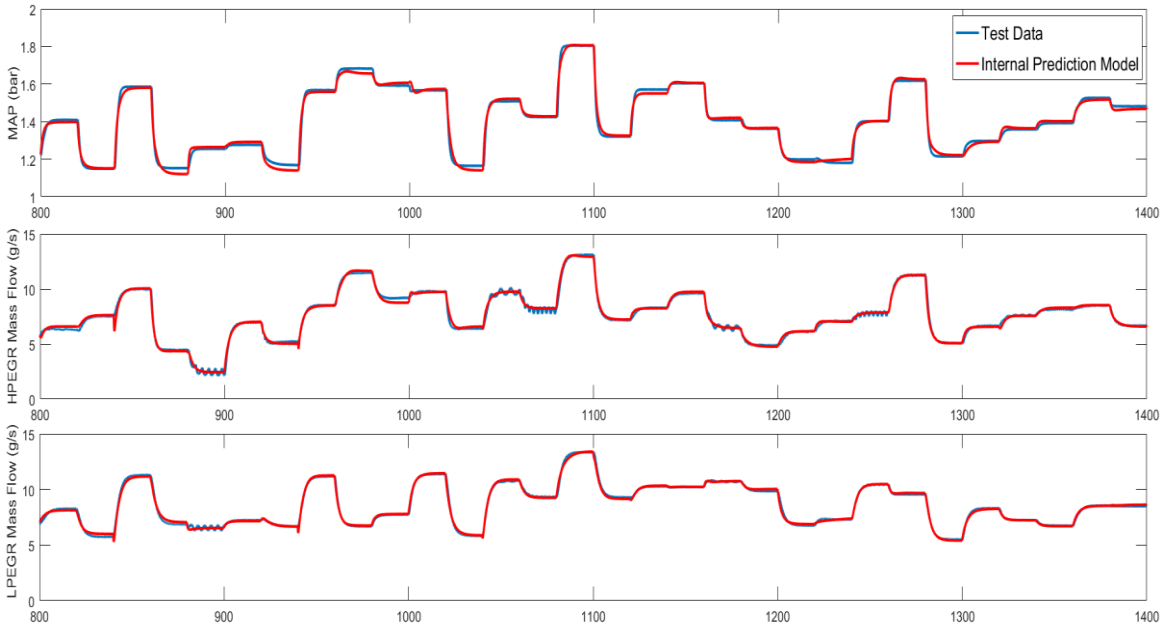

Figure 6-5 Validation of the Internal Prediction Model

To analyse the statistical performance of the prediction model in quantity, different evaluation approaches are carried out. These statistical approaches are often selected for comparisons. The values are determined by the following equations (Boruah, 2016):

$$RMSE = \left(\left(\frac{1}{N}\right)\sum_i |T_i - P_i|^2\right)^{\frac{1}{2}}$$

$$R^2 = 1 - \left(\frac{\sum_i |T_i - P_i|^2}{\sum_i (P_i)^2}\right)$$

$$MEP = \frac{\sum_i \left(\frac{T_i - P_i}{T_i}\right) \times 100}{p}$$

$$SSE = \sum_{i=1}^{N} (T_i - P_i)^2$$

where RSME denotes the standard deviation of the difference between the model outputs and the experimental data. The R^2 indicates how well the data fit in a mathematical model; MEP is a measure of the dynamic error of the predicted outputs; SSE shows the discrepancy between predicted values and target values; i is the sample index; N is the total sample number; P_i is the predicted output from the model; T_i is the actual value from the experiments.

Table 6-1 Statistical Analysis of the Internal Prediction Model

Model Outputs	MAP (bar)	HPEGR Mass Flow (g/s)	LPEGR Mass Flow (g/s)
RMSE	0.017	0.217	0.1299
R^2	99.985	99.924	99.976
MEP (%)	0.861	2.061	1.237
SSE	0.012	0.144	0.094

The results in Table 6-1 show that the outputs from the internal prediction model have a close trajectory tracking with the experiment data. Even though the error still exists due

to the nature of the data-driven model, the results indicate the NARX model is solid enough as the predictor for the NMPC controller.

6.4 Results and Discussion

6.4.1 Comparison between NMPC Controller and PID Controller

To evaluate the performance of the NMPC controller, the results obtained from the simulation platform are shown below. It is compared with the conventional PID controller. The structure and calibration of the PID controller are identical to the controller used in Chapter 5. The comparison still mainly focuses on the air path's overshoot, settling time and rise time, which are mutually recognized aspects to evaluate the performance of controllers. Other than the control objects (MAP, HPEGR mass flow and LPEGR mass flow), the engine MAF, LPEGR fraction and total EGR rate are also included in the comparison. The detailed performance of the controller is presented through the figures below.

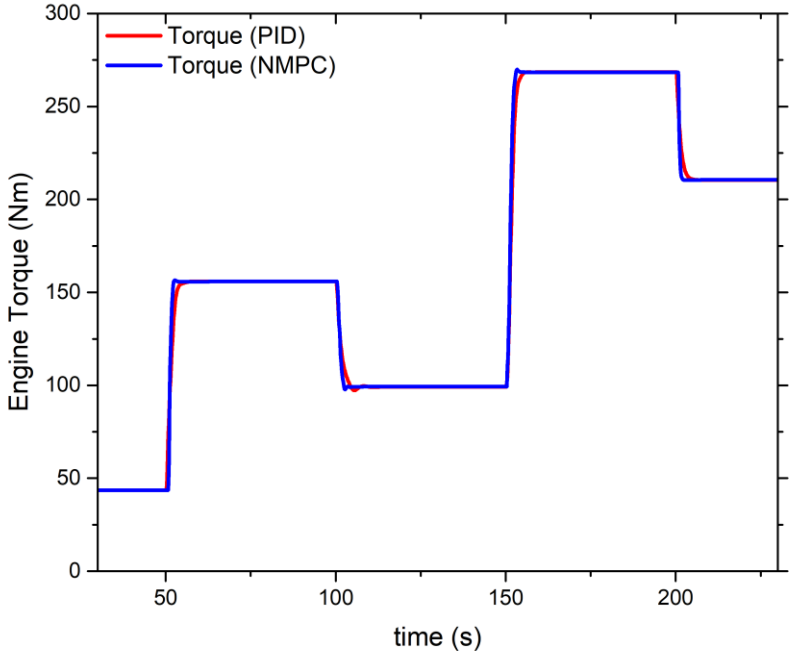

Figure 6-6 Trajectory of Engine Torque; Detailed Engine Torque Comparison under Step Increased (a) and Step Decreased (b) Fuel Injection

Figure 6-6 shows the engine torque trajectory. This sequence is identical to that shown in the previous chapter. The proposed NMPC controller achieves the same stability of engine torque as a conventional PID controller under steady states, as seen from the torque trajectory. However, the dynamic response is much quicker than that from PID controller. Based on the calculation, the accumulated torque using the NMPC controller's method is 1.2% more powerful than that using the PID method. As the mass of fuel injection follows the same trajectory, it means an improvement of fuel economy is achieved. To demonstrate the details of the controller's performance, a period (between 70s and 180s) is selected as an example, which is listed in the following figures. This period includes both a stepped increase and decrease of the engine load.

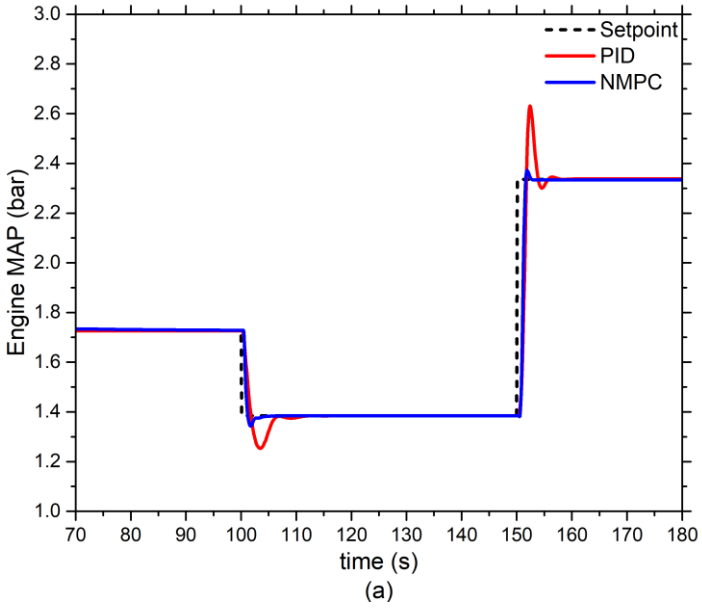
Setpoint
PID
NMPC
Engine MAP (bar)
time (s)

(a)

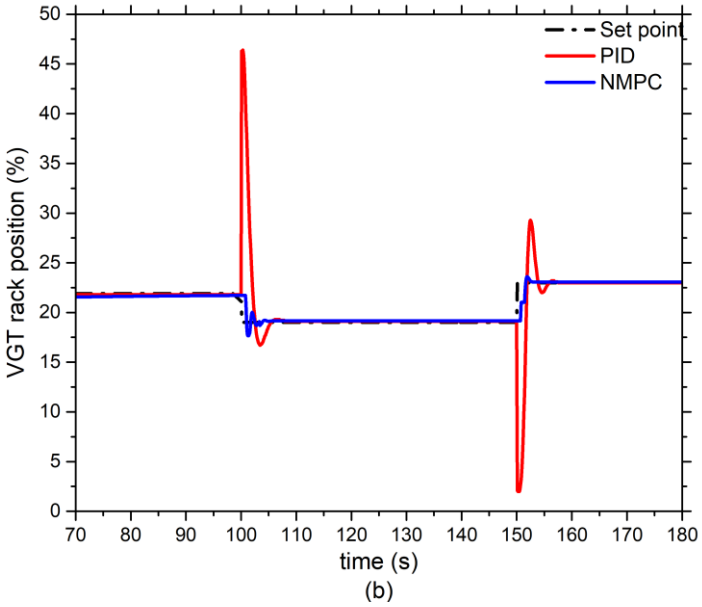
Set point
PID
NMPC
VGT rack position (%)
time (s)

(b)

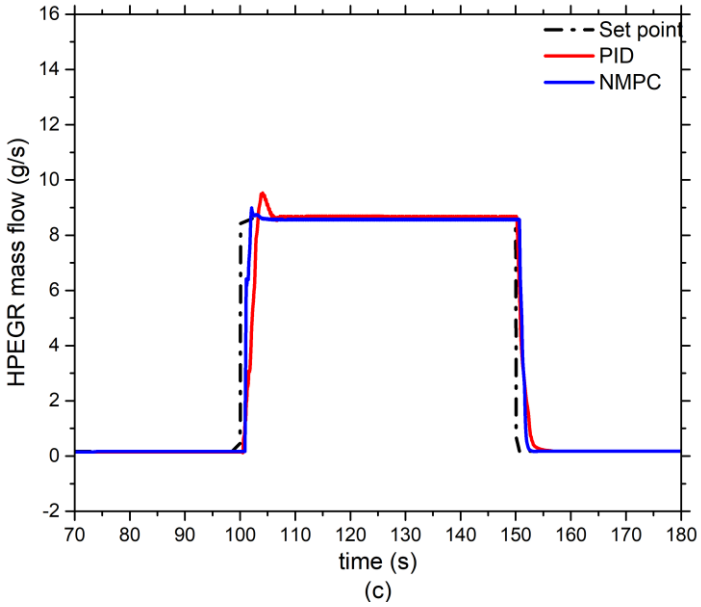
Set point
PID
NMPC
HPEGR mass flow (g/s)
time (s)
(c)

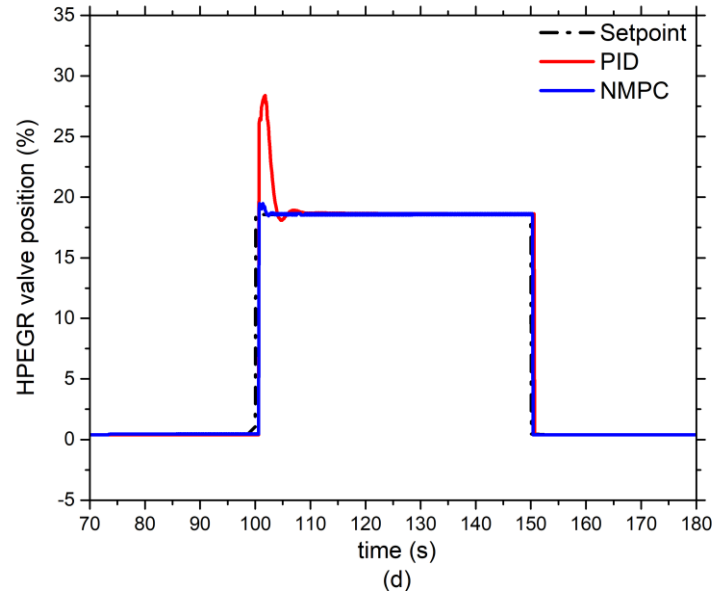
Setpoint
PID
NMPC
HPEGR valve position (%)
time (s)
(d)

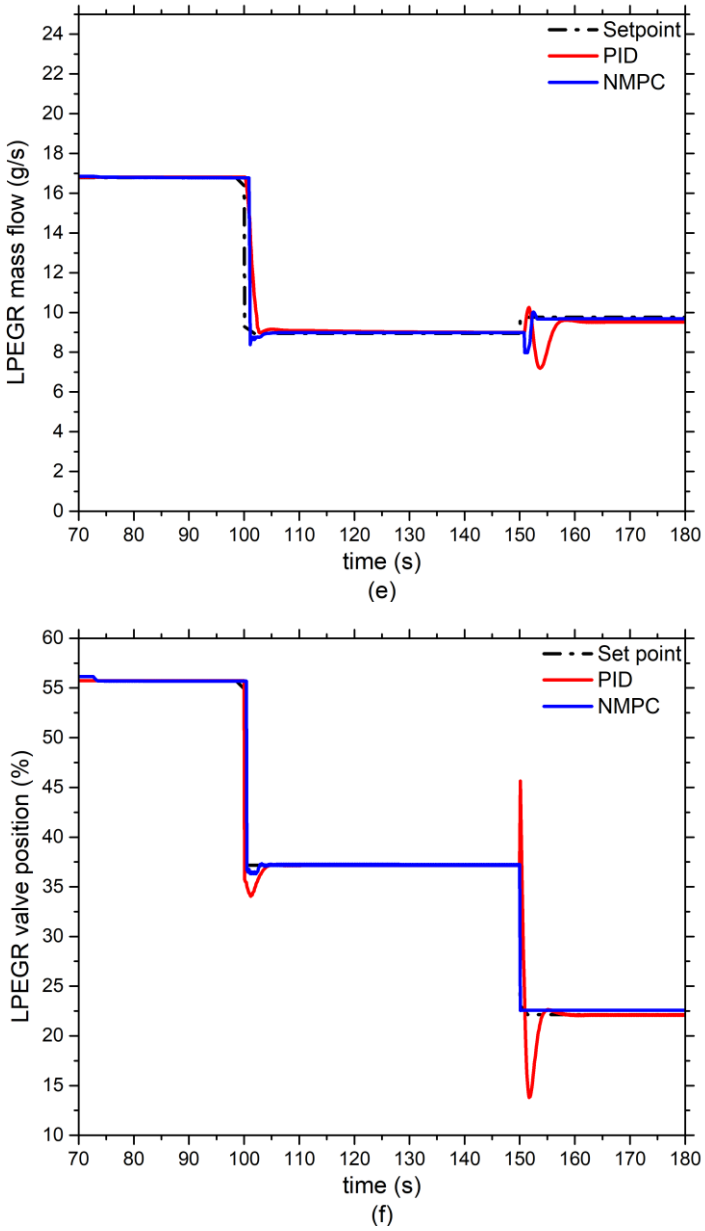

Figure 6-7 Trajectories of Engine MAP (a); VGT Rack Position (b); HPEGR Mass flow (c); HPEGR Valve Position (d); LPEGR Mass Flow (e); LPEGR Valve Position (f)

The evaluation of a controller's performance mainly focuses on the system overshoot, settling time, and rise time. As shown in Figure 6-7, the control objects' overshoot, settling time and delay are all successfully reduced by the proposed NMPC controller. The main reason behind this is the less aggressive control of the control variables. With the help of an internal prediction model, the NMPC

controller could anticipate the behaviour of the control object. The PID controller only relies on the feedback signal to modify the controller's decisions. Besides, unlike the SISO PID controller, the NMPC controller is a multiple-objective controller, which means it can overcome the coupling effect and delay inside the diesel engine's air path. The three actuators are controlled simultaneously. The quantitative comparison between the two controllers is shown in the table below. The numbers in the table are the averaged values.

Table 6-2 Quantitative Comparison between NMPC and PID Controllers

Control Object (NMPC)	MAP (bar)	HPEGR Mass Flow (g/s)	LPEGR Mass Flow (g/s)
Overshoot (%)	1.9	2.4	15.8
Settling Time (s)	3.4	4.2	4.7
Delay (s)	1.4	2.7	2.1
Control Object (PID)	MAP (bar)	HPEGR Mass Flow (g/s)	LPEGR Mass Flow (g/s)
Overshoot (%)	11.5	10.5	25.4
Settling Time (s)	6.9	6.4	6.6
Delay (s)	1.8	3.6	2.8

The diesel engine's air path also involves many other parameters. As shown in previous chapters, the control objects will also affect the engine's MAF, total EGR

rate, LPEGR fraction and engine torque. The trajectories of these parameters are shown in Figure 6-8.

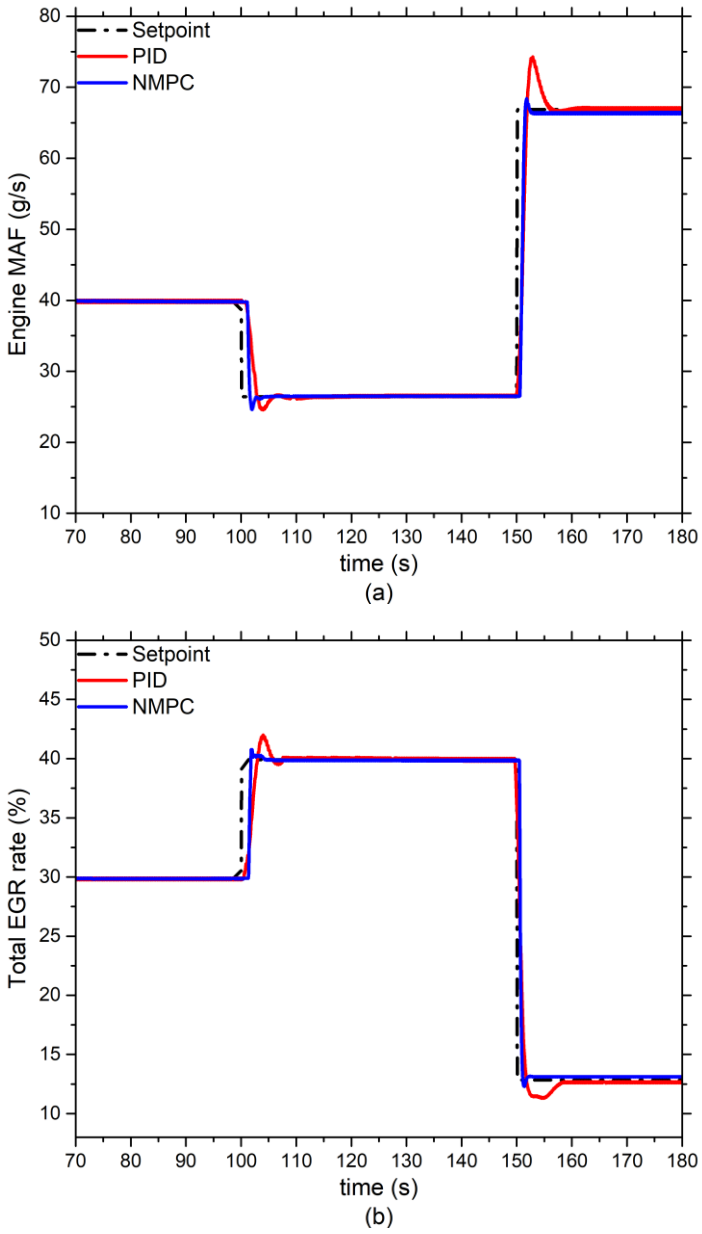

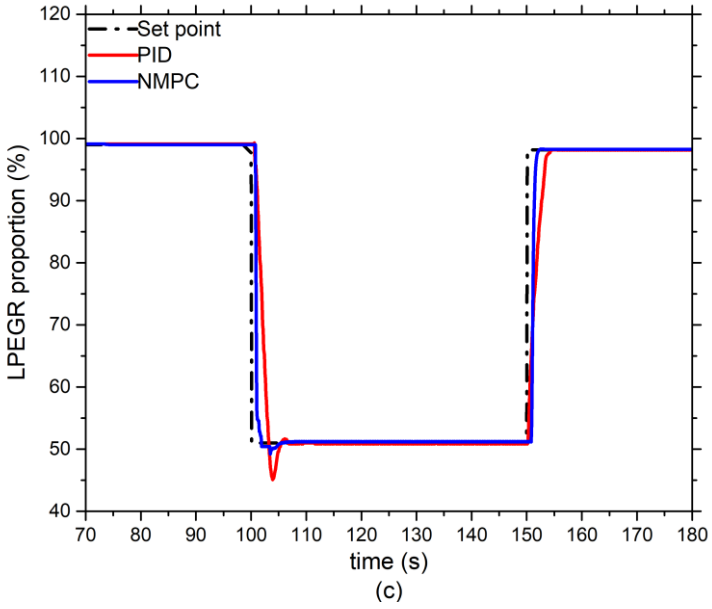
Set point
PID
NMPC
LPEGR proportion (%)
time (s)

(c)

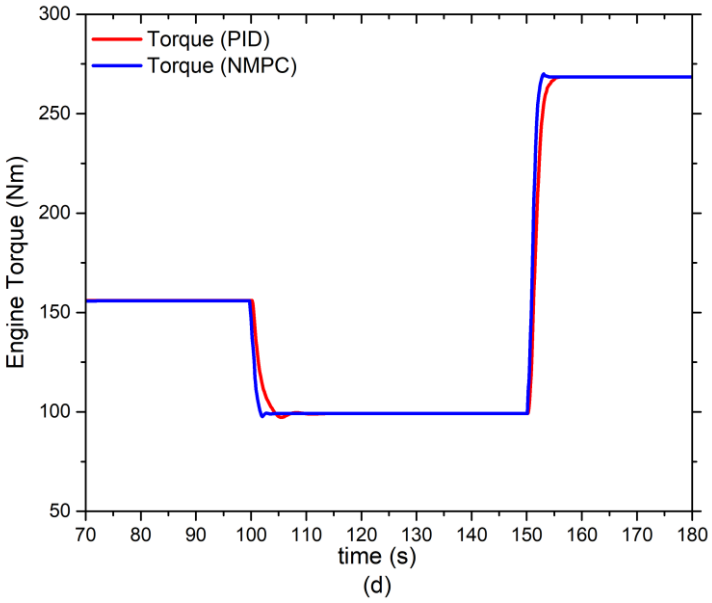
Torque (PID)
Torque (NMPC)
Engine Torque (Nm)
time (s)

(d)

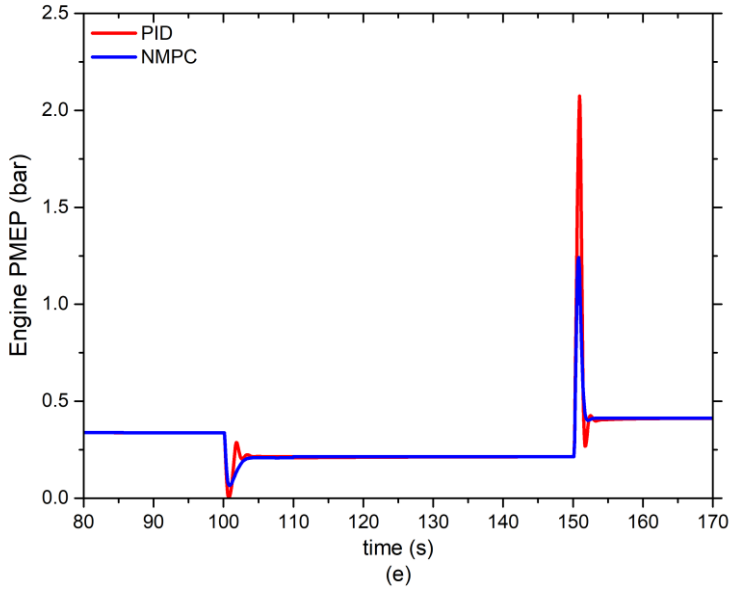

Figure 6-8 Trajectories of Engine MAF (a); Total EGR Rate (b); LPEGR Fraction (c); Engine Torque (d), Engine Pumping Loss (e)

The MAF is another important parameter in the diesel engine's air path as it regulates the amount of fresh air pumped into the cylinders. Figure 6-8(a) shows the trajectory of an engine's MAF. Under both load decrease and increase conditions, the MAF's trajectory using the NMPC controller achieves a smoother transition between the reference setpoints. Moreover, the MAF's response is much quicker than the conventional PID controller. The MAF's behaviour has a significant impact on the engine's torque performance (Heywood, 1988). The more optimal controlled MAF contributes to the trajectories in Figure 6-8(d). The torque trajectory using the NMCP controller achieves a quicker dynamic response and less overshoot, when compared with the control result using the PID controller. As introduced in the previous chapter, another reason for this is the less aggressively controlled VGT rack position; the related engine pumping loss

is reduced. The trajectory of engine pumping loss is shown by the figure 6-8 (e). When the mass of fuel injection is increased at 150s, the PID controller causes a larger spike of the engine PMEP. The dual-loop EGR control should also evaluate the trajectories of the total EGR rate and LPEGR fraction. As introduced in this Chapter 5, the larger overshoot, longer settling time and slower dynamic response will increase the spikes of the engine's emissions and the burden of the engine's VGT system. Based on the results in Figure 6-8(b) and (c), the engine parameters' overshoot, settling time and delay are all reduced by the NMPC controller. According to the references in the literature review, these improvements are beneficial to emissions' reduction. The detailed quantitative comparison between the two controllers is shown in the table below.

Table 6-3 Quantitative Comparison between NMPC and PID Controllers

Control Object (NMPC)	MAF (g/s)	Total EGR Rate (%)	LPEGR fraction (%)
Overshoot	4.4	3.5	1.6
Settling Time	2.8	4.2	3.5
Delay	3.1	3.1	1.5
Control Object (PID)	MAF (g/s)	Total EGR Rate (%)	LPEGR fraction (%)
Overshoot	8.7	10.1	11.9
Settling Time	6.6	7.4	6.7
Delay	2.3	2.6	2.9

6.4.2 Validation on the HIL Test Platform

The diesel engine's controller (NMPC and PID) is also validated on a HIL test platform.

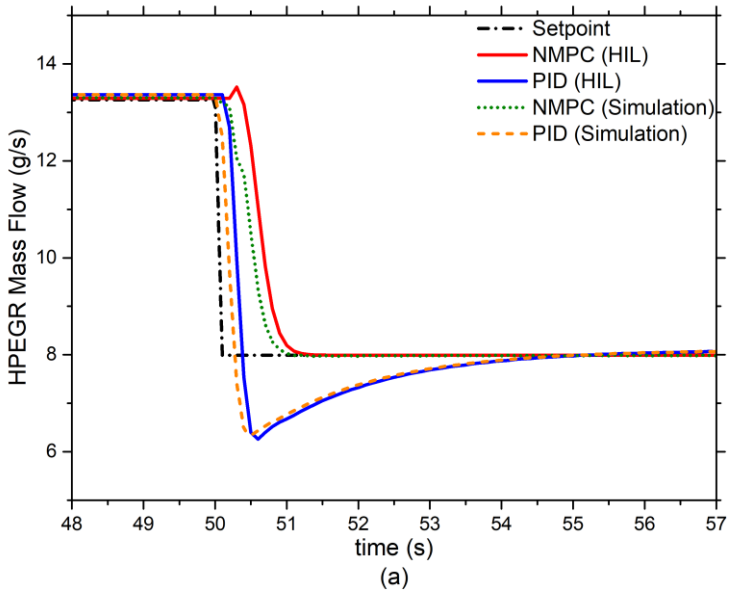
Setpoint
NMPC (HIL)
PID (HIL)
NMPC (Simulation)
PID (Simulation)
HPEGR Mass Flow (g/s)
time (s)
14
12
10
8
6
48
49
50
51
52
53
54
55
56
57

(a)

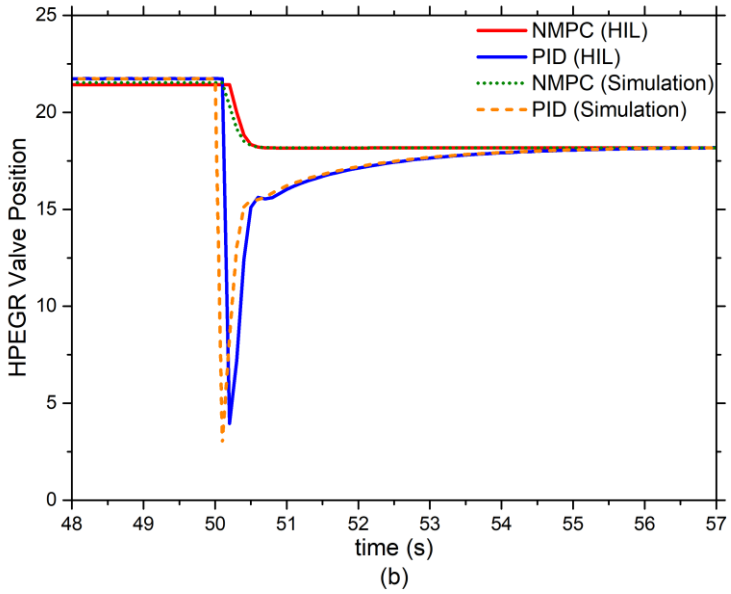
NMPC (HIL)
PID (HIL)
NMPC (Simulation)
PID (Simulation)
HPEGR Valve Position
time (s)
25
20
15
10
5
0
48
49
50
51
52
53
54
55
56
57

(b)

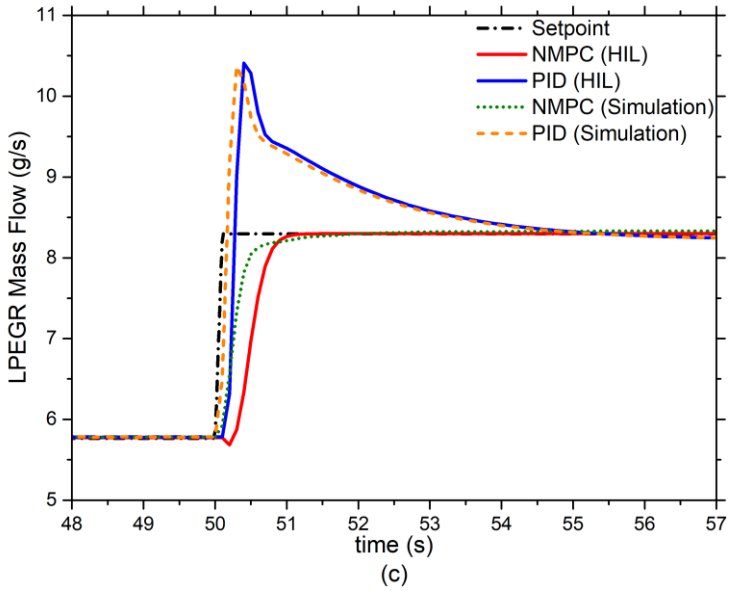
Setpoint
NMPC (HIL)
PID (HIL)
NMPC (Simulation)
PID (Simulation)
LPEGR Mass Flow (g/s)
time (s)

(c)

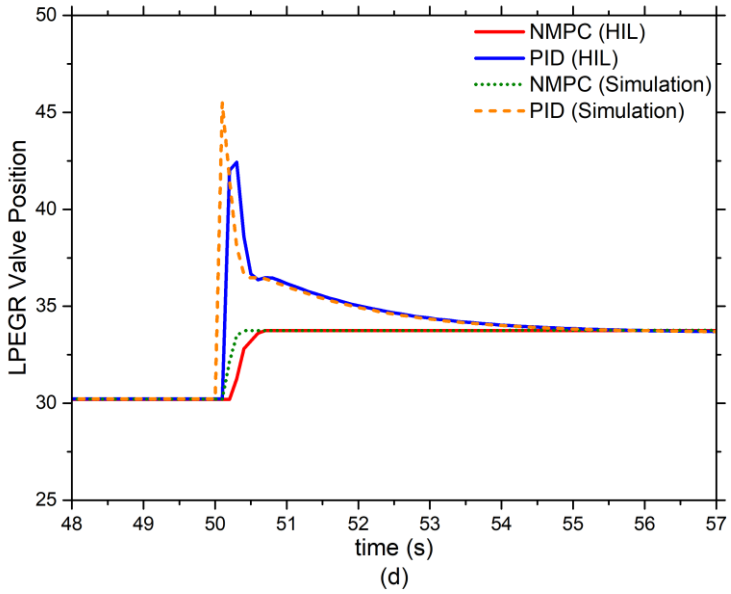
NMPC (HIL)
PID (HIL)
NMPC (Simulation)
PID (Simulation)
LPEGR Valve Position
time (s)

(d)

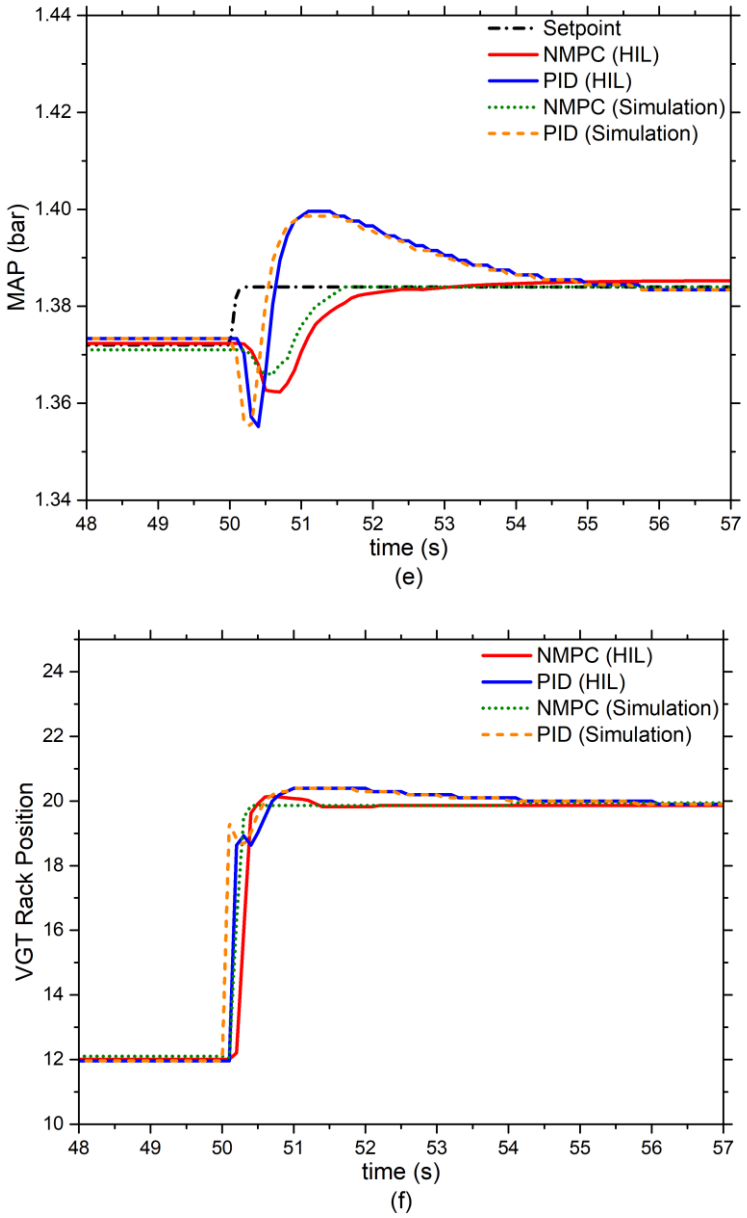

Figure 6-9 Comparison between the Simulation Results and HIL results; HPEGR mass flow (a); HPEGR Valve Position (b); LPEGR Mass Flow (c); LPEGR Valve Position (d); MAP (e); VGT Rack Position (f)

Figure 6-9 shows that the overshoot and settling time of the control objects using the NMPC controller are still smaller than those using the PID controller; which follows the same trend as results from the simulation platform. However, for both the NMPC controller and the conventional PID controller, tiny lags of HIL test

results still exist. This phenomenon could be explained from two aspects: firstly, it is the signal transmission between the ES910 and the real-time target PC, which makes the ES910 receive the signals from the real-time PC with a delay of one sample time. Even though the sample time is set to 0.1 s in this case, the trajectories of engine parameters are still affected. The second aspect is the computational requirements of the NMPC controller. Due to the mechanism of MPC-based controller, the prediction of control objects and the calculation of the optimal control sequence must be finished online. The difference of computational capability between the ES910 processor and the desktop PC processor is non-negligible. This is also reflected by the larger deviation between the simulation results and the HIL test results when using NMPC controller (Lu et al., 2016).

6.4.3 Comparison between NMPC Controller and TMPC Controller

The main advantage of the proposed NMPC controller is reducing the number of the internal prediction models by dealing with the nonlinear system directly without the system linearization process. It also provides more flexibility to develop the real-time solver and the internal prediction model. But the TMPC controller in chapter 5 has a more systematic design approach and the less controller parameters need to be calibrated. The implementation process is also less complex compared with the NMPC controller. The TMPC is a more mature

approach in the MPC control theory. The selection of TMPC and NMPC controller should be determined based on specific applications.

Table 6-4 compares the performance between the proposed NMPC controller and the TMPC controller (introduced in Chapter 5, it is developed based on linear MPC). The comparison mainly focuses on the overshoot and settling time of the control objects. In addition, the improvement of the fuel consumption between the two controllers is also evaluated. In this case, the test sequences for the NMPC and TMPC controllers are identical. The trajectories of the engine parameters have been shown in the figures in section 6.4.1 and section 5.4.1. The comparison focuses on the summarized results of the control objects.

Table 6-4 Comparison between NMPC Controller and TMPC Controller

NMPC Controller	MAP (bar)	HPEGR Mass Flow (g/s)	LPEGR Mass Flow (g/s)
Average Overshoot (%)	1.9	2.4	15.8
Average Settling Time (s)	3.4	4.2	4.7
TMPC Controller	**MAP (bar)**	**HPEGR Mass Flow (g/s)**	**LPEGR Mass Flow (g/s)**
Average Overshoot (%)	1.2	0.5	18.7
Average Settling Time (s)	5.7	6.4	4.3

It can be seen from the table, the NMPC and TMPC controllers achieve close results on averaged overshoot and settling time of the control objects. The NMPC controller has a larger overshoot value but shorter settling time. On the contrary, the TMPC controller has a longer settling time and smaller overshoot. These values are all in the same scale. In general, the NMPC controller could achieve the same controller performance as the linear TMPC controller.

In terms of the fuel economy, the proposed NMPC controller achieves a 1.3% improvement in the designed test sequence; while the TMPC controller acquires a 1.2% improvement. For pure internal combustion engine research, the results

can be regarded as the same level.

6.5 Summary

A NMPC controller for a diesel engine with DLEGR and a VGT is introduced in this chapter. The unique parts of the NMPC controller are the CAPSO-based real-time solver and NARX-based internal prediction model, which can solve the non-linear multiple-objective optimization problem directly. The proposed NMPC controller also provides a modular design structure, which means the real-time solver and internal prediction model could be replaced for various control applications. The conclusions based on the results from the designed test sequences are summarized as follows:

1. The average overshoot and settling time of the engine's MAP using the original PID controller are 9.1% and 7.3 s respectively. The NMPC controller successfully reduces them to 1.9% and 4.4 s.

2. The HPEGR mass flow controlled by a PID controller has an 8.6% overshoot and a settling time of 7.1 s; the NMPC controller could minimize them to 4.2% and 3.5 respectively.

3. The average overshoot and settling time of the LPEGR mass flow are only 15.8% and 4.7 s when controlled by the NMPC controller, but the PID control

results are 26.3% and 6.9 s respectively.

4. Compared with the conventional PID controller, a 1.2% drop of the BSFC during transient scenarios is acquired by the proposed NMCP controller. Better fuel economy is achieved by the proposed control method.

5. The comparison between the NMPC controller and TMPC controller shows that they could achieve the same level of improvements on the engine's fuel economy and dynamic response.

6. The validation results from the HIL platform present accurate reference trajectory tracking of the control objects. The results show that the actual ECU response is close to the offline simulation. The proposed controller could be applied to the real engine.

Therefore, it can be concluded that the proposed NMPC controller shows a better tracking performance on the control objects when compared with the PID controller. It overcomes the coupling effect, delay and nonlinearity of the engine's air path. These improvements are beneficial for the reduction of the engine's emissions.

CHAPTER 7 CONCLUSIONS AND FUTURE WORK

The research work in this thesis focuses on improving the transient performance of a diesel engine's air-path. The improvements are achieved by developing intelligent transient calibration algorithm based on CAPSO and advanced air-path controllers based on the MPC control theory. The main conclusions are summarized below, followed by the planned future work.

7.1 Conclusions

The conclusions in this thesis are categorized into three parts as below, in the sequence of the thesis chapters.

7.1.1 Intelligent Transient Calibration using CAPSO Algorithm

A new engine transient calibration method based on the CAPSO algorithm has been developed. The unique part of the algorithm is the chaotic mapping strategy, which contributes to locating the global optimum controller parameters. The optimized engine performance has been validated. The repeatability test is also conducted to evaluate the proposed CAPSO algorithm. The proposed intelligent calibration algorithm could optimize the transient behaviour of the engine's air-path under various working conditions. Compared with the baseline engine

calibration, the overshoot and the settling time of the controller objects are massively reduced. An improved engine fuel economy is also obtained by the more optimal calibration. The proposed CAPSO algorithm outperforms the conventional APSO algorithm. The Monte Carlo analysis shows that the CAPSO algorithm achieves a lower value of the cost function than the conventional APSO algorithm. It is found in the repeatability test that the standard deviation of the optimization object using CAPSO algorithm is much smaller than that using conventional APSO algorithm.

It should be noticed that the weighting factors in the algorithm need to be calibrated properly as it will affect the cost-function values of the control objects significantly. Besides, the intelligent transient calibration algorithm couldn't modify the existing control strategy, it could only upgrade the calibration.

7.1.2 Tuneable Model Predictive Control

The conventional PID controller is difficult to handle the system nonlinearity, coupling effects and constraint multiple objective control. To deal with this problem, a TMPC controller is developed and implemented on the air-path of a modern diesel engine. The approach mainly includes the design of controller structure, acquiring the internal prediction model via system identification and controller calibration. In various transient scenarios, the proposed TMPC controller shows better reference trajectory tracking performance than the original

PID controller. The overshoot and settling time of the control objects (MAP, EGR mass flow) are significantly reduced. The dynamic performance of the diesel engine's air-path is improved. The properly controlled engine parameters such as MAF, total EGR rate and LPEGR fraction contribute to emission abatement. Besides, a 1.3% drop of accumulated BSFC is observed from the test cycle because the VGT is under optimal control, which reduces the pumping loss of the engine.

The proposed controller is validated on the HIL test platform to evaluate its real-time capability. The results show identical tracking performance of the control objects. The delay between the pure simulation results and the actual control unit's response is tiny and acceptable, which is caused by the signal transmission. It means the TMPC controller can be utilized on real engines.

The TMPC controller has the advantages of systematic design approach and easy implementation. However, to achieve real-time control, the QP solver and linear state-space model inside the controller could not be replaced. Besides, the system linearization is still compulsory.

7.1.3 Neural Network Model Predictive Control

An NMPC controller is also presented, it provides an alternative solution for the multiple objective control issue instead of the TMPC method. The unique parts of

the NMPC controller are the CAPSO-based real-time solver and NARX-based internal prediction model, which can solve the nonlinear multiple-objective optimization problem directly. It also provides a design approach of NMPC controller. The real-time solver and the internal prediction model could be replaced or modified for different applications. Results from the simulation platform show that the proposed NMPC controller achieve better reference trajectory tracking performance than the original PID controller. The overshoot and settling time of the control objects are significantly reduced. Besides, a 1.2% drop of the accumulated BSFC is observed from the test sequence. Compared with the TMPC controller, the NMPC controller achieves close improvements of the engine's transient performance and fuel economy.

The NMPC controller also shows good trajectory tracking performance of the control objects on the HIL test platform. The results indicate that the agreement between the pure simulation and actual controller response is acceptable.

7.2 Future Work

Supported by JLR research project and the University of Birmingham, the engine test bench has been fully upgraded which provides the capability of proceeding engine calibration and developing real-time control strategies. According to the achievements in this thesis, several suggestions for the future work are provided.

7.2.1 Development of Constraint Many-objective Intelligent Optimization Algorithm

The proposed CAPSO algorithm is a type of multiple objective optimization algorithms. As the future powertrain system getting complex, more control or optimization objects will be involved. Algorithms inside the controller need to be upgraded. Conventional multiple objective optimization algorithms are no longer capable of locating the global best result. The many-objective optimization algorithm is a possible solution to this issue. Besides, the future vehicle test procedure also includes the real-world driving conditions, which means the weather condition, vehicle status, geography information and driver's behaviour etc. should be considered. The development of more advanced optimization algorithm is needed.

7.2.2 Implementation of Engine On-board Calibration

The Open-ECU has the powerful computational capability, it is possible to achieve on-board automatic calibration of the engine parameters. As a result, the proposed intelligent tuning algorithm can be utilized not only for offline model-based optimization but also online tuning of engine variables. In this way, the engine optimization environment would be close to real applications. The engine could be maintained at its optimum status among all engine conditions along with the lifetime of the engine.

7.2.3 Model Free Predictive Control

The MPC-based controller is a typical model-based controller which requires internal models to solve the control problem. In recent year, the fast development of artificial intelligence brings new ideas to the area of engine control. The controller could be shift from model-based controllers to model-free controllers. The optimization function and the real-time control function are separate. Like the on-board optimization algorithm, the model-free controller could automatically upgrade the calibration of the controller by deep-learning or reinforcement learning method. The real-time control function is then simplified into a basic neural network controller. The inputs of controller are the current system states and the required system states, the outputs then are the sequences of control variables.

APPENDIX

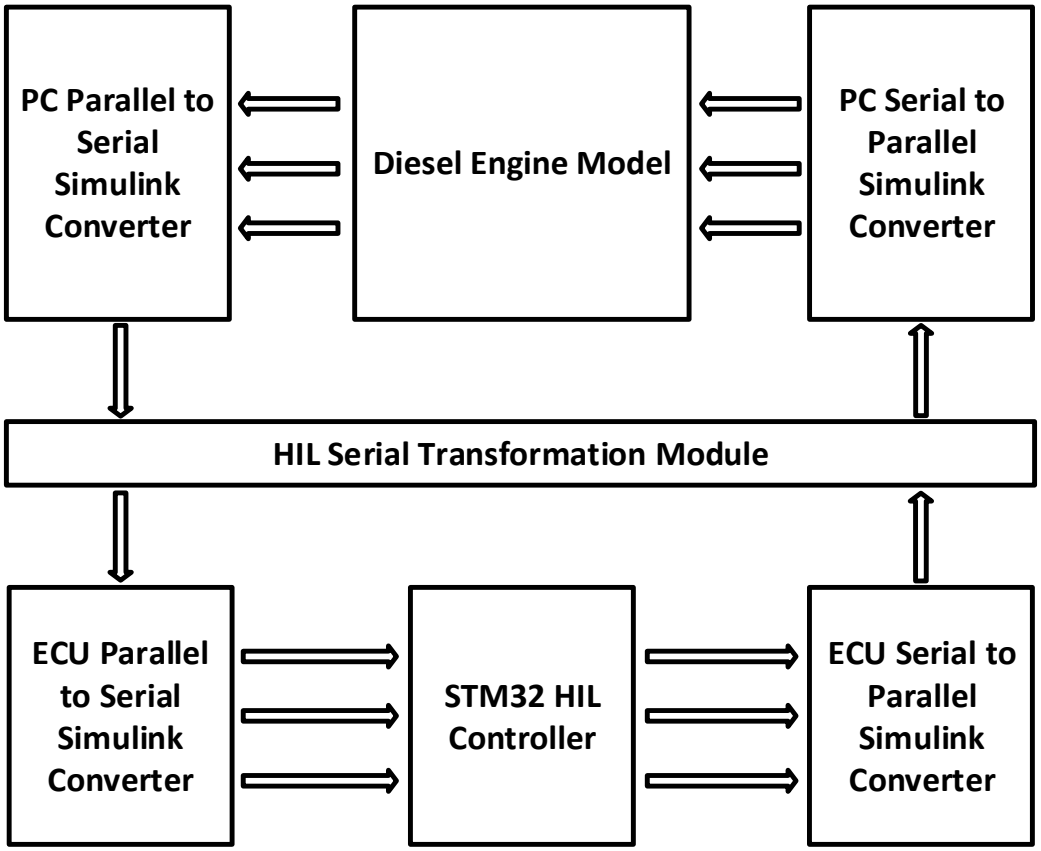

Figure A1 Block Diagram of HIL Test Platform Set-up

Figure A1 shows the set-up of the HIL simulation platform for a diesel engine's air path with an external hardware controller and the real-time diesel engine model. Firstly, the variables from the engine model, including desired values and measured values, are processed to serial signals through a PC parallel to serial convertor. Then, the serial signal is sent to the ECU serial to parallel convertor through a HIL serial transfer module. After the controller receives the parallel signal, the control algorithm is executed and the control variables such as the

EGR valve positions and the VGT rack position are converted to serial signals and sent back to the real-time model. A computer is used as the target PC to operate the engine model and real-time signal convertor. The TMPC and PID controller are compiled into the hardware controller ARM STM32F417lx. The detailed specification of the controller is shown in the table below (Zhang et al., 2017):

Table A1 Specification of the HIL Platform

Make and Model	ARM STM32F417lx
Flash memory	512 kb 1024 kb
SRAM	192 (112+16+64) kb
FSMC memory controller	Yes (1)
GPIOs	140
Channel 12-bit ADC	24
Maximum PU frequency	168 MHz
working temperature	-40 to +105℃
Package	LQFP176

REFERENCES

Abidi, I., Bosche, J., El Hajjaji, A., 2013. Air path control of a Turbocharged diesel engine: Fuzzy approach. 3rd Int. Conf. Syst. Control 401–407. https://doi.org/10.1109/ICoSC.2013.6750890

Abidi, I., Bosche, J., Hajjaji, a. El, Aguilera-Gonzalez, a., 2013. Fuzzy robust tracking control with pole placement for a Turbocharged diesel engine. 21st Mediterr. Conf. Control Autom. 1417–1422. https://doi.org/10.1109/MED.2013.6608906

Abido, M.A., 2006. Multiobjective optimal VAR dispatch using strength Pareto evolutionary algorithm. Evol. Comput. 2006. CEC 2006. IEEE Congr. 730–736. https://doi.org/10.1109/CEC.2006.1688384

Agarwal, D., Singh, S.K., Agarwal, A.K., 2011. Effect of Exhaust Gas Recirculation (EGR) on performance, emissions, deposits and durability of a constant speed compression ignition engine. Appl. Energy 88, 2900–2907. https://doi.org/10.1016/j.apenergy.2011.01.066

Alberer, D., Re, L., del Re, L., 2013. Fast Oxygen Based Transient Diesel Engine Operation. SAE Int. J. Engines 2, 405–413. https://doi.org/10.4271/2009-01-0622

Albin, T., Ritter, D., Abel, D., Liberda, N., Quirynen, R., Diehl, M., 2015. Nonlinear MPC for a two-stage turbocharged gasoline engine airpath, in: Proceedings of the IEEE Conference on Decision and Control. pp. 849–856. https://doi.org/10.1109/CDC.2015.7402335

Albin, T., Ritter, D., Liberda, N., Quirynen, R., Diehl, M., 2017. In-Vehicle Realization of Nonlinear MPC for Gasoline Two-Stage Turbocharging Airpath Control. IEEE Trans. Control Syst. Technol. 1–13. https://doi.org/10.1109/TCST.2017.2724020

Alonso, J.M., Alvarruiz, F., Desantes, J.M., Hernández, L., Hernández, V., Moltó, G., 2007. Combining neural networks and genetic algorithms to predict and reduce diesel engine emissions. IEEE Trans. Evol. Comput. 11, 46–55. https://doi.org/10.1109/TEVC.2006.876364

Armas, O., Garcia-Contreras, R., Ramos, A., 2013. Impact of alternative fuels on performance and pollutant emissions of a light duty engine tested under the new European driving cycle. Appl. Energy 107, 183–190.

https://doi.org/10.1016/j.apenergy.2013.01.064

Arnold, J.F., Langlois, N., Chafouk, H., 2009. Fuzzy controller of the air system of a diesel engine: Real-time simulation. Eur. J. Oper. Res. 193, 282–288. https://doi.org/10.1016/j.ejor.2007.08.046

Arsie, I., Cricchio, A., De Cesare, M., Pianese, C., Sorrentino, M., 2013. A methodology to enhance design and on-board application of neural network models for virtual sensing of Nox emissions in automotive diesel engines. SAE Tech. Pap. 6. https://doi.org/10.4271/2013-24-0138

Arsie, I., Pianese, C., Sorrentino, M., 2010. Development of recurrent neural networks for virtual sensing of nox emissions in internal combustion engines. SAE Int. J. Fuels Lubr. 2, 354–361. https://doi.org/10.4271/2009-24-0110

Arsie, I., Pianese, C., Sorrentino, M., 2004. Nonlinear Recurrent Neural Networks for Air Fuel Ratio Control in SI Engines Reprinted From : Electronic Engine Controls 2004. SAE Tech. Pap. 2004. https://doi.org/10.4271/2004-01-1364

Ashok, B., Denis Ashok, S., Ramesh Kumar, C., 2016. A review on control system architecture of a SI engine management system. Annu. Rev. Control 41, 94–118. https://doi.org/10.1016/j.arcontrol.2016.04.005

Assanis, D.N., Filipi, Z.S., Fiveland, S.B., Syrimis, M., 2000. A Methodology for Cycle-By-Cycle Transient Heat Release Analysis in a Turbocharged Direct Injection Diesel Engine. Sae 1–14. https://doi.org/10.4271/2000-01-1185

Åström, K.J., Hägglund, T., 2001. The future of PID control. Control Eng. Pract. 9, 1163–1175. https://doi.org/10.1016/S0967-0661(01)00062-4

Atkinson, C., Mott, G., 2005. Dynamic Model-Based Calibration Optimization : An Introduction and Application to Diesel Engines. SAE Tech. Pap. Ser. 2005-01-0026 2005. https://doi.org/10.4271/2005-01-0026

Atkinson, C.M., Long, T.W., Hanzevack, E.L., 1998. Virtual Sensing : A Neural Network-based Intelligent Performance and Emissions Prediction System for On-Board Diagnostics and Engine Control. Prog. Technol. 73, 2–4. https://doi.org/10.4271/980516

AVL DynoSpirit - Dynamometers for Engine Testing - avl.com [WWW Document], n.d. URL https://www.avl.com/-/avl-dynospir-2 (accessed 5.1.18).

AVL Fuel Mass Flow Meter and Fuel Temperature Control - Consumption Measurement - avl.com [WWW Document], n.d. URL https://www.avl.com/-/avl-fuel-mass-flow-meter-and-fuel-temperature-control (accessed 5.1.18a).

AVL Fuel Mass Flow Meter and Fuel Temperature Control - Consumption Measurement - avl.com [WWW Document], n.d. URL https://www.avl.com/-/avl-fuel-mass-flow-meter-and-fuel-temperature-control (accessed 6.23.18b).

Barrero, F., Prieto, J., Levi, E., Gregor, R., Toral, S., Durán, M.J., Jones, M., 2011. An enhanced predictive current control method for asymmetrical six-phase motor drives. IEEE Trans. Ind. Electron. 58, 3242–3252. https://doi.org/10.1109/TIE.2010.2089943

Bc. Ondrej Mikulas, 2016. A Framework for Nonlinear Model Predictive Control. Master Thesis, Czech Technical University.

Bemporad, a., Borrelli, F., Morari, M., 2002. Model predictive control based on linear programming - the explicit solution. IEEE Trans. Automat. Contr. 47, 1974–1985. https://doi.org/10.1109/TAC.2002.805688

Bemporad, A., Morari, M., Dua, V., Pistikopoulos, E.N., 2002. The explicit linear quadratic regulator for constrained systems. Automatica 38, 3–20. https://doi.org/10.1016/S0005-1098(01)00174-1

Bemporad, A., Morari, M., Ricker, N.L., 2014. Model Predictive Control Toolbox ™ User ' s Guide R2014a. The MathWorks, Inc.

Bianco-Rodriguez, D., Vagnoni, G., Holderbaum, B., 2016. EU6 C-Segment Diesel vehicles, a challenging segment to meet RDE and WLTP requirements. IFAC-PapersOnLine 49, 649–656. https://doi.org/10.1016/j.ifacol.2016.08.094

Bishop, J.D.K., Stettler, M.E.J., Molden, N., Boies, A.M., 2016. Engine maps of fuel use and emissions from transient driving cycles. Appl. Energy 183, 202–217. https://doi.org/10.1016/j.apenergy.2016.08.175

Black, J., Eastwood, P.G., Tufail, K., Winstanley, T., Hardalupas, Y., Taylor, A.M.K.P., 2007. The effect of VGT vane control on pumping losses during full-load transient operation of a common-rail diesel engine. SAE Tech. Pap. 15. https://doi.org/10.4271/2007-24-0063

Boiocchi, R., Gernaey, K. V., Sin, G., 2016. Systematic design of membership functions for fuzzy-logic control: A case study on one-stage partial nitritation/anammox

treatment systems. Water Res. 102, 346–361. https://doi.org/10.1016/j.watres.2016.06.047

Bonilla, D., Bishop, J.D.K., Axon, C.J., Banister, D., 2014. Innovation, the diesel engine and vehicle markets: Evidence from OECD engine patents. Transp. Res. Part D Transp. Environ. 27, 51–58. https://doi.org/10.1016/j.trd.2013.12.012

Borhan, H., Kothandaraman, G., Pattel, B., 2015. Air handling control of a diesel engine with a complex dual-loop EGR and VGT air system using MPC. Proc. Am. Control Conf. 2015–July, 4509–4516. https://doi.org/10.1109/ACC.2015.7172039

Boruah, D., 2016. Artificial Neural Network based Modelling of Internal Combustion Engine Performance. Sussex Res. Online 5, 568–576.

Bourouba, B., Ladaci, S., 2016. Comparative performance analysis of GA, PSO, CA and ABC algorithms for ractional PID controller tuning, in: 2016 8th International Conference on Modelling, Identification and Control (ICMIC). pp. 960–965. https://doi.org/10.1109/ICMIC.2016.7804253

Brahma, I., Chi, J.N., 2012. Development of a model-based transient calibration process for diesel engine electronic control module tables - Part 1: data requirements, processing, and analysis. Int. J. Engine Res. 13, 77–96. https://doi.org/10.1177/1468087411424376

Catania, A.E., Dongiovanni, C., Mittica, A., Negri, C., Spessa, E., 1996. Study of Automotive Diesel Injection-System Dynamics Under Control, in: SAE Technical Paper 962020. https://doi.org/10.4271/962020

Chauhdry, M.H.M., Luh, P.B., 2012. Nested partitions for global optimization in nonlinear model predictive control. Control Eng. Pract. 20, 869–881. https://doi.org/10.1016/j.conengprac.2012.05.003

Chen, H., Hu, Y., Sun, P., Chen, H., 2017. Neural Network-based Model Predictive Control for Wastegate of a Turbocharged Gasoline Engine, in: 2017 29th Chinese Control And Decision Conference (CCDC). pp. 6527–6532.

Chen, W., Li, X., Chen, M., 2009. Suboptimal Nonlinear Model Predictive Control Based on Genetic Algorithm. 2009 Third Int. Symp. Intell. Inf. Technol. Appl. Work. 119–124. https://doi.org/10.1109/IITAW.2009.46

Cieslar, D., Dickinson, P., Darlington, A., Glover, K., Collings, N., 2014. Model based approach to closed loop control of 1-D engine simulation models. Control Eng. Pract.

29, 212–224. https://doi.org/10.1016/j.conengprac.2014.01.021

D'Ambrosio, S., Finesso, R., Fu, L., Mittica, A., Spessa, E., 2014. A control-oriented real-time semi-empirical model for the prediction of NOx emissions in diesel engines. Appl. Energy 130, 265–279. https://doi.org/10.1016/j.apenergy.2014.05.046

Darby, M.L., Nikolaou, M., 2012. Control Engineering Practice MPC : Current practice and challenges. Control Eng. Pract. 20, 328–342. https://doi.org/10.1016/j.conengprac.2011.12.004

Davis, P., Peckham, M., 2007. The Analysis of Gasoline Transient Emissions Behaviour Using Fast Response Gas Analysers. https://doi.org/10.4271/2007-26-015

De Cesare, M., Covassin, F., 2011. Neural network based models for virtual NOx sensing of compression ignition engines. SAE Tech. Pap. https://doi.org/10.4271/2011-24-0157

Deb, K., Jain, H., 2013. An Evolutionary Many-Objective Optimization Algorithm Using Reference-point Based Non-dominated Sorting Approach, Part I: Solving Problems with Box Constraints. Ieeexplore.Ieee.Org 18, 1–1. https://doi.org/10.1109/TEVC.2013.2281534

DELPHI, 2017. Worldwide Emissions Standards: Passenger Cars and Light Duty.

Deng, C., Colin, G., Chamaillard, Y., Gruel, D.N., 2012. Sequential robust control design methodology application to the MIMO air path of a diesel engine. IECON Proc. (Industrial Electron. Conf. 2138–2143. https://doi.org/10.1109/IECON.2012.6388796

Deng, J., Stobart, R., Winward, E., 2014. Explicit Model Predictive Control of the Diesel Engine Fuel Path 2014. https://doi.org/10.4271/2012-01-0893.R

Design Time Series NARX Feedback Neural Networks - MATLAB & Simulink - MathWorks United Kingdom [WWW Document], n.d. URL https://uk.mathworks.com/help/nnet/ug/design-time-series-narx-feedback-neural-networks.html (accessed 5.8.18).

Dezong Zhao, Cunjia Liu, Stobart, R., Jiamei Deng, Winward, E., 2013. Explicit model predictive control on the air path of turbocharged diesel engines, in: 2013 American Control Conference (ACC). pp. 5213–5218.

Di, X., Huang, Y., Ge, Y., Li, G., Hu, M., 2015. Fuzzy-PID Speed Control of Diesel Engine

Based on Load Estimation. SAE Int. J. Engines 8, 2015-01-1627. https://doi.org/10.4271/2015-01-1627

Dickinson, P., Glover, K., Collings, N., Yamashita, Y., Yashiro, Y., Hoshi, T., 2015. Real-time control of a two-stage serial VGT diesel engine using MPC. IFAC Proc. Vol. 48, 117–123. https://doi.org/10.1016/j.ifacol.2015.10.017

Dimaratos, A., Tsokolis, D., Fontaras, G., Tsiakmakis, S., Ciuffo, B., Samaras, Z., 2016. Comparative Evaluation of the Effect of Various Technologies on Light-duty Vehicle CO2 Emissions over NEDC and WLTP. Transp. Res. Procedia 14, 3169–3178. https://doi.org/10.1016/j.trpro.2016.05.257

Dishy, A., You, T.H.H., Iwashiro, Y., Nakayama, S., Kihara, R., Saito, T., 1995. Controlling Combustion and Exhaust Emissions in a Direct-Injection Diesel Engine Dual-Fueled with Natural Gas. SAE Tech. Pap. 952436 1–13. https://doi.org/10.4271/952436

Dittrich, P.A., Peter, F., Huber, G., Kuehn, M., 2010. Thermodynamic potentials of a fully variable valve actuation system for passenger-car diesel engines, in: SAE Technical Papers. https://doi.org/2010-01-1199

Donateo, T., Giovinazzi, M., 2017. Building a cycle for Real Driving Emissions. Energy Procedia 126, 891–898. https://doi.org/10.1016/j.egypro.2017.08.307

E.Zitzler, L.Thiele, 1998. An evolutionary algorithm for multiobjective optimization:The strength Pareto approach, Computer Engineering and Communication Networks Lab.

El Hadef, J., Olaru, S., Rodriguez-Ayerbe, P., Colin, G., Chamaillard, Y., Talon, V., 2013. Nonlinear model predictive control of the air path of a turbocharged gasoline engine using Laguerre functions. 2013 17th Int. Conf. Syst. Theory, Control Comput. 193–200. https://doi.org/10.1109/ICSTCC.2013.6688959

Elsisi, M., Soliman, M., Aboelela, M.A.S., Mansour, W., 2016. Bat inspired algorithm based optimal design of model predictive load frequency control. Int. J. Electr. Power Energy Syst. 83, 426–433. https://doi.org/10.1016/j.ijepes.2016.04.036

Emekli, M.E., Güvenç, B.A., 2016. Explicit MIMO Model Predictive Boost Pressure Control of a Two-Stage Turbocharged Diesel Engine. IEEE Trans. Control Syst. Technol. 25, 521–534.

Enang, W., Bannister, C., 2017. Modelling and control of hybrid electric vehicles (A comprehensive review). Renew. Sustain. Energy Rev.

https://doi.org/10.1016/j.rser.2017.01.075

Fang, H., Chen, L., Shen, Z., 2011. Application of an improved PSO algorithm to optimal tuning of PID gains for water turbine governor. Energy Convers. Manag. 52, 1763–1770. https://doi.org/10.1016/j.enconman.2010.11.005

Fessler, H., Genova, M., 2004. An electro-hydraulic lost motion VVA system for a 3.0 liter diesel engine. SAE Trans. 113, 1639–1649. https://doi.org/10.4271/2004-01-3018

Filipi, Z., Wang, Y., Assanis, D., 2001. Effect of Variable Geometry Turbine (VGT) on Diesel Engine and Vehicle System Transient Response. SAE 2001 World Congr. 1–19. https://doi.org/10.4271/2001-01-1247

Finesso, R., Misul, D., Spessa, E., 2014. Development and validation of a semi-empirical model for the estimation of particulate matter in diesel engines. Energy Convers. Manag. 84, 374–389. https://doi.org/10.1016/j.enconman.2014.04.053

Finesso, R., Spessa, E., Venditti, M., Yang, Y., 2015. Offline and Real-Time Optimization of EGR Rate and Injection Timing in Diesel Engines. SAE Int. J. Engines 8, 2015-24–2426. https://doi.org/10.4271/2015-24-2426

Fonseca, C.M., Fleming, P.J., 1993. Genetic Algorithms for Multiobjective Optimization: Formulation, Discussion and Generalization. Icga 93, 416–423. https://doi.org/citeulike-article-id:2361311

Fontaras, G., Ciuffo, B., Zacharof, N., Tsiakmakis, S., Marotta, A., Pavlovic, J., Anagnostopoulos, K., 2017a. The difference between reported and real-world CO2 emissions: How much improvement can be expected by WLTP introduction?∗. Transp. Res. Procedia 25, 3937–3947. https://doi.org/10.1016/j.trpro.2017.05.333

Fontaras, G., Zacharof, N.G., Ciuffo, B., 2017b. Fuel consumption and CO2emissions from passenger cars in Europe – Laboratory versus real-world emissions. Prog. Energy Combust. Sci. 60, 97–131. https://doi.org/10.1016/j.pecs.2016.12.004

Friedrich, I., Liu, C.S., Oehlerking, D., 2009. Coordinated EGR-rate model-based controls of turbocharged diesel engines via an intake throttle and an EGR valve. 5th IEEE Veh. Power Propuls. Conf. VPPC ’09 340–347. https://doi.org/10.1109/VPPC.2009.5289828

Gandomi, A.H., Yun, G.J., Yang, X.S., Talatahari, S., 2013. Chaos-enhanced accelerated particle swarm optimization. Commun. Nonlinear Sci. Numer. Simul. 18, 327–340. https://doi.org/10.1016/j.cnsns.2012.07.017

Garciaa-Nieto, S., Martinez, M., Blasco, X., Sanchis, J., 2008. Nonlinear predictive control based on local model networks for air management in diesel engines. Control Eng. Pract. 16, 1399–1413. https://doi.org/10.1016/j.conengprac.2008.03.010

Garg, a. G., Diwan, P., Saxena, M., 2012. Artificial Neural Networks based Methodologies fo Optimization of Engine Operations. Int. J. Sci. Eng. Res. 3, 2–7.

Garriga, J.L., Soroush, M., 2010. Model Predictive Control Tuning Methods: A Review. Ind. Eng. Chem. Res. 49, 3505–3515. https://doi.org/10.1021/ie900323c

Ge, H.-W., Shi, Y., Reitz, R.D., Wickman, D.D., Willems, W., 2009. Optimization of a HSDI Diesel Engine for Passenger Cars Using a Multi-Objective Genetic Algorithm and Multi-Dimensional Modeling. SAE Int. J. Engines 2, 2009-01–0715. https://doi.org/10.4271/2009-01-0715

Gelso, E.R., Dahl, J., 2016. Air-Path Control of a Heavy-Duty EGR-VGT Diesel Engine. IFAC-PapersOnLine 49, 589–595. https://doi.org/10.1016/j.ifacol.2016.08.086

Gelso, E.R., Lindberg, J., 2013. Air-Path Model Predictive Control of a Heavy Duty Diesel Engine with Variable Valve Actuation. IFAC Proc. Vol. 47, 3–8. https://doi.org/10.3182/20140824-6-ZA-1003.01263

Gihun Lim, 2011. Effects of HPL and LPL EGR Gas Mixed Supply on Combustion and Emissions in Automotive Diesel Engines, in: SAE International Powertrains, Fuels and Lubricants Meeting. pp. 2011-01-1831.

Glewen, W., Meyer, C., Foster, D., Andrie, M., Krieger, R., 2011. Sources and Tradeoffs for Transient NO and UHC Emissions with Low Temperature Diesel Combustion. Sae SAE 2011 W. https://doi.org/10.4271/2011-01-1356

Global Greenhouse Gas Emissions Data | Greenhouse Gas (GHG) Emissions | US EPA [WWW Document], n.d. URL https://www.epa.gov/ghgemissions/global-greenhouse-gas-emissions-data (accessed 6.22.18).

Grahn, M., Johansson, K., Vartia, K., McKelvey, T., Vartia, C., McKelvey, T., 2012. A Structure and Calibration Method for Data-Driven Modeling of NO X and Soot Emissions from a Diesel Engine. SAE Int. 355–2012. https://doi.org/10.4271/2012-01-0355

Grondin, O., Stobart, R., Chafouk, H., Maquet, J., 2004. Modelling the Compression Ignition Engine for Control : Review and Future Trends. Sae 2004.

https://doi.org/10.4271/2004-01-0423

Guerrier, M., Cawsey, P., 2004. The development of model based methodologies for gasoline IC engine calibration. SAE Tech. Pap. 2004-01-1466 113, 981–1002. https://doi.org/10.4271/2004-01-1466

Gurney, A., Ahammad, H., Ford, M., 2009. The economics of greenhouse gas mitigation: Insights from illustrative global abatement scenarios modelling. Energy Econ. 31, S174–S186. https://doi.org/10.1016/j.eneco.2009.08.016

Guzzella, L., Onder, C.H., 2010. Introduction to modeling and control of internal combustion engine systems. Springer. https://doi.org/10.1007/978-3-642-10775-7

Haber, B., 2010. A Robust Control Approach on Diesel Engines With Dual-Loop Exhaust Gas Recirculation Systems. The Ohio State University. https://doi.org/10.1115/DSCC2010-4135

Hadef, J. El, Olaru, S., Rodriguez-ayerbe, P., Colin, G., Chamaillard, Y., 2013. Explicit Nonlinear Model Predictive Control of the Air Path of a Turbocharged Spark - Ignited Engine, in: 2013 IEEE International Conference on Control Applications (CCA). pp. 71–77.

Hafner, M., Schüler, M., Nelles, O., Isermann, R., 2000. Fast neural networks for diesel engine control design. Control Eng. Pract. 8, 1211–1221. https://doi.org/10.1016/S0967-0661(00)00057-5

Haga, H., Hashimoto, E., Nakajima, K., Matsunaga, H., Yasui, Y., 2015. New urea-SCR control system for super clean diesel. J. Robot. Mechatronics 27, 41–48. https://doi.org/10.3182/20130904-4-JP-2042.00045

Hagena, J.R., Filipi, Z.S., Assanis, D.N., 2006. Transient Diesel Emissions: Analysis of Engine Operation During a Tip-In. SAE Tech. Pap. 2006. https://doi.org/10.4271/2006-01-1151

Haiyan, W.H.W., Wang, H., Zhang, J., 2006. Control oriented dynamic modeling of a turbocharged diesel engine, Sixth International Conference on Intelligent Systems Design and Applications. Ieee. https://doi.org/10.1109/ISDA.2006.253821

Hannan, M.A., Azidin, F.A., Mohamed, A., 2014. Hybrid electric vehicles and their challenges: A review. Renew. Sustain. Energy Rev. 29, 135–150. https://doi.org/10.1016/j.rser.2013.08.097

Harder, K., Buchholz, M., Niemeyer, J., Remele, J., Graichen, K., 2017. Nonlinear MPC with Emission Control for a Real-World Off-Highway Diesel Engine. IEEE/ASME Int. Conf. Adv. Intell. Mechatronics, AIM 1768–1773. https://doi.org/10.1109/AIM.2017.8014274

Henningsson, M., Ekholm, K., Strandh, P., Tunestål, P., Johansson, R., 2012. Dynamic Mapping of Diesel Engine through System Identification. Lect. Notes Control Inf. Sci. 418, 223–239. https://doi.org/10.1007/978-1-4471-2221-0_13

Herceg, M., Raff, T., Findeisen, R., Allgowe, F., Allgower, F., 2006. Nonlinear model predictive control of a turbocharged diesel engine. Proc. 2006 Ieee Int. Conf. Control Appl. Vols 1-4 2766–2771. https://doi.org/10.1109/CACSD-CCA-ISIC.2006.4777076

Heuwetter, D., Glewen, W., Foster, D.E., Krieger, R., Andrie, M., 2014. Experimental Investigation of Transient Response and Turbocharger Coupling for High and Low Pressure EGR Systems. SAE Int. J. Engines 7, 977–985. https://doi.org/10.4271/2014-01-1367

Heywood, J.B., 1988. Internal Combustion Engine Fundementals, McGrawHill series in mechanical engineering. McGraw-Hill, Inc., New York.

Hiroyasu, T., Nakayama, S., Miki, M., 2005. Comparison study of SPEA2+, SPEA2, and NSGA-II in diesel engine emissions and fuel economy problem. 2005 IEEE Congr. Evol. Comput. 1, 236–242. https://doi.org/10.1109/CEC.2005.1554690

Honek, M., Kvasnica, M., Szucs, A., Simoncic, P., Fikar, M., Rohal'-Ilkiv, B., 2015. A low-complexity explicit MPC controller for AFR control. Control Eng. Pract. 42, 118–127. https://doi.org/10.1016/j.conengprac.2015.05.009

Hong, S., Park, I., Chung, J., Sunwoo, M., 2015. Gain Scheduled Controller of EGR and VGT Systems with a Model-Based Gain Scheduling Strategy for Diesel Engines. IFAC 109–116. https://doi.org/10.1016/j.ifacol.2015.10.016

How VW tried to cover up the emissions scandal - BBC News [WWW Document], n.d. URL https://www.bbc.co.uk/news/business-44005844 (accessed 6.21.18).

Hrovat, D., Di Cairano, S., Tseng, H.E., Kolmanovsky, I.V., 2012. The development of Model Predictive Control in automotive industry: A survey. 2012 IEEE Int. Conf. Control Appl. 295–302. https://doi.org/10.1109/CCA.2012.6402735

Hu, Y., Chen, H.H., Wang, P., Chen, H.H., Ren, L., 2018. Nonlinear model predictive

controller design based on learning model for turbocharged gasoline engine of passenger vehicle. Mech. Syst. Signal Process. 109, 74–88. https://doi.org/10.1016/j.ymssp.2018.02.012

Hu, Y., Körfer, T., Miccio, M., Schaub, J., Schnorbus, T., 2014. Reduction of engine-out emission and fuel consumption by variable EGR distribution in diesel and multi fuel engines, in: 14. Internationales Stuttgarter Symposium. Springer Vieweg, Wiesbaden, pp. 565–580. https://doi.org/10.1007/978-3-658-05130-3

Huang, M., Nakada, H., Butts, K., 2015. Nonlinear Model Predictive Control of a Diesel Engine Air Path : A Comparison of Constraint Handling and Computational Strategies. IFAC-PapersOnLine 48, 372–379. https://doi.org/10.1016/j.ifacol.2015.11.308

Jain, H., Deb, K., 2014. An evolutionary many-objective optimization algorithm using reference-point based nondominated sorting approach, Part II: Handling constraints and extending to an adaptive approach. IEEE Trans. Evol. Comput. 18, 602–622. https://doi.org/10.1109/TEVC.2013.2281534

Janakiraman, V.M., Nguyen, X., Assanis, D., 2016. An ELM based predictive control method for HCCI engines. Eng. Appl. Artif. Intell. 48, 106–118. https://doi.org/10.1016/j.engappai.2015.10.007

Janakiraman, V.M., Nguyen, X., Assanis, D., 2015. Nonlinear Model Predictive Control of A Gasoline HCCI Engine Using Extreme Learning Machines. ISSUE NEURODYNAMIC Syst. Optim. Appl. 1–15.

Jankovic, M., Jankovic, M., Kolmanovsky, I., Scientific, F., 1998. Robust ionlinear controller for turbocharged diesel engines, in: American Control Conference. pp. 1389–1394.

Ji Li, 2015. Department of Mechanical Engineering MSc Advanced Mechanical Engineering Advanced Project Application of a fuzzy logic PID controller for V6 GDI engine with supercharger. University of Birimgham.

JLR, València, U.P. de, 2015. Development of methods for evaluating real time turbocharged engine models. Valencia.

Johnson, T., 2008. Diesel engine emissions and their control: An overview. Platin. Met. Rev. 52, 23–37. https://doi.org/10.1595/147106708X248750

Johnson, T. V, 2001. Diesel emission control in review. Sae Trans. 110, 128–144.

https://doi.org/doi:10.4271/2006-01-0030

Kalghatgi, G., 2018. Is it really the end of internal combustion engines and petroleum in transport? Appl. Energy 225, 965–974. https://doi.org/10.1016/j.apenergy.2018.05.076

Kamat, S., Diwanji, V., Smith, J., Javaherian, H., Madhavan, K.P., 2006. Virtual Sensing of SI Engines Using Recurrent Neural Networks 2006. https://doi.org/10.4271/2006-01-1348

Kang, M., Shen, T., Jiao, X., 2014. Continuation/GMRES Method based Nonlinear Model Predictive Control for IC Engines ⋆. IFAC Proc. Vol. 47, 5697–5702. https://doi.org/10.3182/20140824-6-ZA-1003.00488

Kang P. V. Farrell, H., Kang P. V. Farrell, H., 2005. Experimental Investigation of Transient Emissions (HC and NOx) in a High Speed Direct Injection (HSDI) Diesel Engine. Sae Tech. Pap. Ser. 13. https://doi.org/10.4271/2005-01-3883

Karaky, H., Mauviot, G., Tauzia, X., Maiboom, A., 2015. Development and Validation of a New Zero-Dimensional Semi-Physical NOx Emission Model for a D.I. Diesel Engine Using Simulated Combustion Process. SAE Int. J. Engines 8, 2015-01-1746. https://doi.org/10.4271/2015-01-1746

Keeler, B., Shayler, P.J., 2008. Constraints on Fuel Injection and EGR Strategies for Diesel PCCI-Type Combustion. SAE Tech. Pap. 2008-01-13, 776–790. https://doi.org/10.4271/2008-01-1327

Kim, S., Jin, H., Choi, S., 2014. Pressure and Flow Based Control of a Turbocharged Diesel Engine Air-path System Equipped with Dual-loop EGR and VGT. Proc. Am. Control Conf. 1493–1498. https://doi.org/10.1109/ACC.2014.6858964

Kirchen, P., Obrecht, P., Boulouchos, K., 2009. Soot Emission Measurements and Validation of a Mean Value Soot Model for Common-Rail Diesel Engines during Transient Operation. SAE Int. J. Engines 2, 2009-01-1904. https://doi.org/10.4271/2009-01-1904

KISTLER, 2018. PiezoStar ® Pressure sensor [WWW Document]. URL www.kistler.com/en/product/type-6124a/?application=7 (accessed 4.12.18).

Kittisupakorn, P., Thitiyasook, P., Hussain, M.A., Daosud, W., 2009. Neural network based model predictive control for a steel pickling process. J. Process Control 19, 579–590. https://doi.org/10.1016/j.jprocont.2008.09.003

Kocher, L., Koeberlein, E., Stricker, K., Alstine, D.G. Van, Biller, B., Shaver, G.M., 2011. Control-Oriented Modeling of Diesel Engine Gas Exchange, in: Proceedings of the 2011 American Control Conference. pp. 1555–1560.

Kumar Pathak, S., Sood, V., Singh, Y., Channiwala, S.A., 2016. Real world vehicle emissions: Their correlation with driving parameters. Transp. Res. Part D Transp. Environ. 44, 157–176. https://doi.org/10.1016/j.trd.2016.02.001

Kumar, S., Kumar Chauhan, M., Varun, 2013. Numerical modeling of compression ignition engine: A review. Renew. Sustain. Energy Rev. https://doi.org/10.1016/j.rser.2012.11.043

Kushwaha, G., Saraswati, S., 2015. Air path identification of turbocharged diesel engine using RNN, in: 2015 International Conference on Industrial Instrumentation and Control, ICIC 2015. IEEE, pp. 1328–1332. https://doi.org/10.1109/IIC.2015.7150954

Kuzmych, O., Aitouche, A., Cheng, L., 2013. Robust nonlinear control design for turbocharged biodiesel engine. 2013 3rd Int. Conf. Syst. Control. ICSC 2013 395–400. https://doi.org/10.1109/ICoSC.2013.6750889

Kyunghan, Donghyuk Jung, M.*, Sunwoo, M., 2015. Air System Modeling of Light-duty Diesel Engines with Dual-loop EGR and VGT Systems. pp. 38–44. https://doi.org/10.1016/j.ifacol.2015.10.006

Ladommatos N, Abdelhalim SM, Zhao H, H.Z., 1997. The dilution, chemical and thermal effects of exhaust gas recirculation on diesel engine emissions- Part3: Effect of water vapor, in: SAE Technical Paper. https://doi.org/https://doi.org/10.4271/971659

Ladommatos, N., Abdelhalim, S.M., Zhao, H., Hu, Z., 1997. The Dilution , Chemical , and Thermal Effects of Exhaust Gas Recirculation on Diesel Engine Emissions - Part 2 : Effects of Carbon Dioxide. SAE Tech. Pap. https://doi.org/10.4271/971660

Ladommatos, N., Abdelhalim, S.M., Zhao, H., Hu, Z., 1996. The Dilution, Chemical, and Thermal Effects of Exhaust Gas Recirculation on Diesel Engine Emissions - Part 1: Effect of Reducing Inlet Charge Oxygen. SAE Tech. Pap. https://doi.org/10.4271/961167

Langthaler, P., Re, L., 2008. Robust Model Predictive Control of a Diesel Engine Airpath, in: Proceedings of the 17th World Congress. pp. 9485–9490.

Lee, T., Park, J., Kwon, S., Lee, J., Kim, J., 2013. Variability in operation-based

NOxemission factors with different test routes, and its effects on the real-driving emissions of light diesel vehicles. Sci. Total Environ. 461–462, 377–385. https://doi.org/10.1016/j.scitotenv.2013.05.015

Li, Y., Hu, Y., Wang, S., Chen, H., 2016. Nonlinear model predictive controller design for air system control of a gasoline engine. Intell. Control Autom. (WCICA), 2016 12th World Congr. 1600–1605.

Li, Y., Zhou, X., Hu, Y., Chen, H., 2015. Air path system control of turbocharged gasoline engine based on fuzzy PID, in: Proceedings of the 2015 27th Chinese Control and Decision Conference, CCDC 2015. IEEE, pp. 941–946. https://doi.org/10.1109/CCDC.2015.7162054

Liu, B., Wang, L., Jin, Y.-H., Tang, F., Huang, D.-X., 2005. Improved particle swarm optimization combined with chaos. Chaos, Solitons & Fractals 25, 1261–1271. https://doi.org/10.1016/j.chaos.2004.11.095

Liu, D., 2014. COMBUSTION AND EMISSIONS OF AN AUTOMOTIVE DIESEL ENGINE USING BIODIESEL FUELS UNDER STEADY AND START CONDITIONS. PhD Thesis, University of Birmingham.

Lu, G., Zhang, Y., Xu, H., Li, Z., Neaves, B., 2016. Multiple Model Predictive Control for Diesel Engines with Dual Loop Exhaust Gas Recirculation, in: 3rd Biennial International Conference on Powertrain Modelling and Control.

M670 - Pi Innovo Product Overview [WWW Document], n.d. URL http://www.pi-innovo.com/product/m670/ (accessed 7.18.17).

Ma, H., 2012. Control Oriented Engine Modelling and Engine Multi- Objective Optimal Feedback Control. PhD Thesis. University of Birmingham.

MA, H., Li, Z., Tayarani, M., Lu, G., Xu, H., Yao, X., 2017. Computational Intelligence Non-model-based Calibration Approach for Internal Combustion Engines. J. Dyn. Syst. Meas. Control 140, 1–9. https://doi.org/10.1115/1.4037835

Ma, H., Xu, H., Wang, J., Schnier, T., Neaves, B., Tan, C., Wang, Z., 2014. Model-based Multi-objective Evolutionary Algorithm Optimization for HCCI Engines. IEEE Trans. Veh. Technol. 9545, 1–1. https://doi.org/10.1109/TVT.2014.2362954

Maass, B., Deng, J., Stobart, R., 2011. In-Cylinder Pressure Modelling with Artificial Neural Networks. https://doi.org/10.4271/2011-01-1417

Maiboom, A., Tauzia, X., Hétet, J.-F., 2008. Experimental study of various effects of exhaust gas recirculation (EGR) on combustion and emissions of an automotive direct injection diesel engine. Energy 33, 22–34. https://doi.org/10.1016/j.energy.2007.08.010

Maiboom, A., Tauzia, X., Shah, S.R., Hétet, J., 2009. Experimental Study of an LP EGR System on an Automotive Diesel Engine , compared to HP EGR with respect to PM and NOx Emissions and Specific Fuel Consumption. SAE Int. J. Engines 2, 597–610. https://doi.org/10.4271/2009-24-0138

Maruyama, T., Shimura, T., Ejiri, A., Ikai, Y., Shimotani, K., 2011. Model Predictive Control Applied to a Diesel Engine Air-Path System with Dead Time. SICE Annu. Conf. 2011 2628–2633.

MathWorks, n.d. Rise time, settling time, and other step-response characteristics - MATLAB stepinfo - MathWorks United Kingdom [WWW Document]. URL https://uk.mathworks.com/help/control/ref/stepinfo.html (accessed 10.14.18).

Mattarelli, E., Perini, F., Rinaldini, C.A., 2009. Optimization of a Supercharged Single Cylinder Engine for a Formula SAE Racing Car. SAE Int. J. Engines 2, 2009-01–0309. https://doi.org/10.4271/2009-01-0309

Mercorelli, P., Werner, N., Becker, U., Harndorf, H., 2011. A robust sliding mode control of a hybrid hydraulic piezo actuator for camless internal combustion engines, in: IEEE/ASME International Conference on Advanced Intelligent Mechatronics, AIM. pp. 499–504. https://doi.org/10.1109/AIM.2011.6027099

Michiel van Nieuwstadt, 2003. Coordinated Control of EGR Valve and Intake Throttle for Better Fuel Economy. SAE 2003. https://doi.org/10.4271/2003-01-0362

Midlam-Mohler, S., Guezennec, Y., 2006. Regeneration Control for a Bypass-Regeneration Lean NOx Trap System, in: 2006 American Control Conference. IEEE, pp. 1203–1208. https://doi.org/10.1109/ACC.2006.1656381

Millo, F., Giacominetto, P.F., Bernardi, M.G., 2012. Analysis of different exhaust gas recirculation architectures for passenger car Diesel engines. Appl. Energy 98, 79–91. https://doi.org/10.1016/j.apenergy.2012.02.081

Millo, F., Rolando, L., Andreat, M., 2011. Numerical Simulation for Vehicle Powertrain Development, in: Numerical Analysis - Theory and Application. InTech. https://doi.org/10.5772/24111

Montazeri-Gh, M., Yousefpour, H., Jafari, S., 2010. Fuzzy logic computing for design of gas turbine engine fuel control system. 2010 2nd Int. Conf. Comput. Autom. Eng. 5, 723–727. https://doi.org/10.1109/ICCAE.2010.5451342

Morari, M., Lee, J.H., 1999. Model predictive control : past , present and future 23, 667–682. https://doi.org/10.1016/S0098-1354(98)00301-9

Murata Y., K.J.O.M.D.Y. et al., 2006. Achievement of Medium Engine Speed and Load Premixed Diesel Combustion with Variable Valve Timing, in: SAE Technical Paper 2006-01-0203. https://doi.org/10.4271/2006-01-0203

Murata, Y., Kusaka, J., Daisho, Y., Kawano, D., Suzuki, H., Ishii, H., Goto, Y., 2008. Miller-PCCI Combustion in an HSDI Diesel Engine with VVT. SAE Int. J. Engines 1, 2008-01–0644. https://doi.org/10.4271/2008-01-0644

Nishio, Y., Hasegawa, M., Tsutsumi, K., Goto, J., Iizuka, N., 2013. Model Based Control for Dual EGR System with Intake Throttlein New Generation 1.6L Diesel Engine. 11th Int. Conf. Engines Veh. 24-0133. https://doi.org/10.4271/2013-24-0133

Niu, X., Wang, H., Hu, S., Yang, C., Wang, Y., 2018. Multi-objective online optimization of a marine diesel engine using NSGA-II coupled with enhancing trained support vector machine. Appl. Therm. Eng. 137, 218–227. https://doi.org/10.1016/j.applthermaleng.2018.03.080

Ortner, P., Langthaler, P., Ortiz, J.V.G., Del Re, L., 2006. MPC for a diesel engine air path using an explicit approach for constraint systems. Proc. IEEE Int. Conf. Control Appl. 2760–2765. https://doi.org/10.1109/CACSD-CCA-ISIC.2006.4777060

Ortner, P., Re, L., 2007. Predictive Control of a Diesel Engine Air Path. IEEE Trans. Control Syst. Technol. 15, 449–456.

Pano, V., Ouyang, P.R., Member, I., 2014. PSO Gain Tuning for Position Domain PID Controller. 4th Annu. IEEE Int. Conf. Cyber Technol. Autom. Control Intell. 377–382.

Park, J., Choi, J., 2016. Optimization of dual-loop exhaust gas recirculation splitting for a light-duty diesel engine with model-based control. Appl. Energy 181, 268–277. https://doi.org/10.1016/j.apenergy.2016.07.128

Park, Y., Bae, C., 2014. Experimental study on the effects of high/low pressure EGR proportion in a passenger car diesel engine. Appl. Energy 133, 308–316. https://doi.org/10.1016/j.apenergy.2014.08.003

Pavlovic, J., Marotta, A., Ciuffo, B., 2016. CO2 emissions and energy demands of vehicles tested under the NEDC and the new WLTP type approval test procedures. Appl. Energy 177, 661–670. https://doi.org/10.1016/j.apenergy.2016.05.110

Plianos, A., Stobart, R., 2008. Modeling and Control of Diesel Engines Equipped with aTwo-Stage Turbo-System. SAE Tech. Pap. 2008-01-1018 2008. https://doi.org/2008-01-1018

Querel, C., Grondin, O., Letellier, C., Qurel, C., Grondin, O., Letellier, C., 2015. Semi-physical mean-value NOx model for diesel engine control. Control Eng. Pract. 40, 27–44. https://doi.org/10.1016/j.conengprac.2015.02.005

R.S.Wijetunge, C.J.Brace, J.G.Hawley, N.D.Vaughan, 2000. Fuzzy Logic Control of Diesel Engine Turbocharging and Exhaust Gas Recirculation. Control 2000 UKACC Inernational Conf. Control Univ. Cambridge.

Rahman, I., Vasant, P.M., Singh, B.S.M., Abdullah-Al-Wadud, M., 2016. On the performance of accelerated particle swarm optimization for charging plug-in hybrid electric vehicles. Alexandria Eng. J. 55, 419–426. https://doi.org/10.1016/j.aej.2015.11.002

Rakopoulos, C., Dimaratos, A., Giakoumis, E., Peckham, M., 2010. Experimental Assessment of Turbocharged Diesel Engine Transient Emissions during Acceleration, Load Change and Starting. Sae Tech. Pap. 269–285. https://doi.org/10.4271/2010-01-1287

Rakopoulos, C.D., Giakoumis, E.G., 2009. Diesel Engine Transient Operation. Springer, London. https://doi.org/10.1007/978-1-84882-375-4

Rakopoulos, C.D., Giakoumis, E.G., 2006. Review of Thermodynamic Diesel Engine Simulations under Transient Operating Conditions. SAE Int. 2006, 884. https://doi.org/10.4271/2006-01-0884

Rawlings, J.B., 1999. Tutorial: model predictive control technology. Am. Control Conf. 1999. Proc. 1999 1, 662–676 vol.1. https://doi.org/10.1109/ACC.1999.782911

Real-Time Combustion Analysis Sytem [WWW Document], n.d. URL http://www.alma-automotive.it/en/real-time-control-and-measurement (accessed 7.18.17).

ReB, J., Sturzebecher, C., Bohn, C., Marzke, F., Frase, R., 2015. Diesel Engine Model Including Exhaust Diesel Engine Engine Model Model Including Including Exhaust Exhaust Flap , Intake Throttle , LP-EGR Flap , Intake Throttle , LP-EGR and Part I :

System Modeling. 4th IFAC Work. Engine Powertrain Control. Simul. Model. E-COSM 2015 48, 52–59. https://doi.org/10.1016/j.ifacol.2015.10.008

Reifarth, S., Ångström, H.-E., 2010. Transient EGR in a High-Speed DI Diesel Engine for a set of different EGR-routings. SAE Int. J. Engines 3, 1071–1078. https://doi.org/10.4271/2010-01-1271

Reynoso-Meza, G., Blasco, X., Sanchis, J., Martínez, M., 2014. Controller tuning using evolutionary multi-objective optimisation: Current trends and applications. Control Eng. Pract. 28, 58–63. https://doi.org/10.1016/j.conengprac.2014.03.003

Rogers, S., Birge, B., 2004. Swarm Optimization Applied to Engine RPM Control. SAE Int. https://doi.org/10.4271/2004-01-2669

Samokhin, S., Zenger, K., 2014. Robust and adaptive wastegate control of turbocharged internal combustion engines. Proc. Am. Control Conf. 3219–3224. https://doi.org/10.1109/ACC.2014.6859027

Sanathanan, C.K., 1988. FREQUENCY DOMAIN METHOD FOR TUNING HYDRO GOVERNORS. IEEE Trans. Energy Convers. 3, 14–17. https://doi.org/10.1109/60.4193

Sardarmehni, T., Keighobadi, J., Menhaj, M.B., Rahmani, H., 2013. Robust predictive control of lambda in internal combustion engines using neural networks. Arch. Civ. Mech. Eng. 13, 432–443. https://doi.org/10.1016/j.acme.2013.05.003

Shah, S., Maiboom, A., 2009. Experiment Study of Inlet Manifold Water Injection on a Common Rail HSDI Automobile Diesel Engine, Compared to EGR with Respect to PM and Nox Emissions and Specific Consumption, in: SAE Technical Paper. https://doi.org/10.4271/2009-01-1439

Shayler, P.J., Darnton, N.J., Ma, T., 1997. Factors influencing drive cycle emissions and fuel consumption. SAE Tech. Pap. https://doi.org/10.4271/971603

Shen, L., Xu, L., Wei, R., Cao, L., 2016. Multi-swarm Optimization with Chaotic Mapping for Dynamic Optimization Problems, in: Proceedings - 2015 8th International Symposium on Computational Intelligence and Design, ISCID 2015. IEEE, pp. 132–137. https://doi.org/10.1109/ISCID.2015.173

Shi, X., Liu, B., Zhang, C., Hu, J., Zeng, Q., 2017. A study on combined effect of high EGR rate and biodiesel on combustion and emission performance of a diesel engine. Appl. Therm. Eng. 125, 1272–1279.

https://doi.org/10.1016/j.applthermaleng.2017.07.083

Sileghem, L., Bosteels, D., May, J., Favre, C., Verhelst, S., 2014. Analysis of vehicle emission measurements on the new WLTC, the NEDC and the CADC. Transp. Res. Part D Transp. Environ. 32, 70–85. https://doi.org/10.1016/j.trd.2014.07.008

Sources of Greenhouse Gas Emissions US EPA [WWW Document], n.d. URL https://www.epa.gov/ghgemissions/sources-greenhouse-gas-emissions (accessed 6.22.18).

Srinivasan, S., Tanner, F.X., 2011. Computational Optimization of Split Injections and EGR in a Diesel Engine Using an Adaptive Gradient-Based Algorithm 2006. https://doi.org/10.4271/2006-01-0059

Stewart, G., Borrelli, F., 2008. A Model Predictive Control Framework for Industrial Turbodiesel Engine Control, in: Chaouki T. Abdallah, Thomas Parisini (Eds.), 47th IEEE Conference on Decision and Control. Cancun, Mexico, pp. 5704–5711. https://doi.org/10.1109/CDC.2008.4739384

Stone, R., 1999. Introduction to Internal Combustion Engines, 3th editio. ed. Macmillan Press. https://doi.org/10.1017/CBO9781107415324.004

Study, T.M.C., Pachner, D., Herceg, M., Pekaˇ, J., 2016. Towards ECU-Ready Nonlinear Model Predictive Control :, in: IEEE 55th Conference on Decision and Control (CDC).

Stürzebecher, C., Reß, J., Bohn, C., Märzke, F., Prase, R., 2015. A diesel engine model including exhaust flap, intake throttle, LP-EGR and VGT. Part II: Identification and validation, in: IFAC-PapersOnLine. Elsevier B.V., pp. 60–65. https://doi.org/10.1016/j.ifacol.2015.10.009

Takashi Suzuki, 1997. The Romance of Engines. SAE International.

Tan, C., 2015. Model Based Control for a Modern Automotive. PhD Thesis,University of Birmingham.

Tan, D., 2012. Chaos Particle Swarm Optimization Algorithm for Multi-Objective Constrained Optimization Problems. Springer Berlin Heidelberg, pp. 469–476. https://doi.org/10.1007/978-3-642-27326-1_60

Tan, Q., Hu, Y., 2016. A study on the combustion and emission performance of diesel engines under different proportions of O2 & N2 & CO2. Appl. Therm. Eng.

108, 508–515. https://doi.org/10.1016/j.applthermaleng.2016.07.151

Tan, R., Lin, C.-Y., Tomizuka, M., 2015. Approximate nonlinear model predictive control of a gasoline engine with EGR. Control Conf. (ECC), 2015 Eur. 1414–1419.

Tang, H.C., 2007. An analysis of linear congruential random number generators when multiplier restrictions exist. Eur. J. Oper. Res. 182, 820–828. https://doi.org/10.1016/j.ejor.2006.08.055

Taraza, D., Henein, N.A., Ceansu, R., Bryzik, W., 2008. Complex diesel engine simulation with focus on transient operation. Energy and Fuels 22, 1411–1417. https://doi.org/10.1021/ef700472x

Tayarani, M.H.N., Yao, X., Xu, H., 2015. Meta-Heuristic Algorithms in Car Engine Design: A Literature Survey. IEEE Trans. Evol. Comput. 19, 609–629. https://doi.org/10.1109/TEVC.2014.2355174

Technical Data ES910 [WWW Document], 2010. URL https://www.etas.com/en/products/es910_rapid_prototyping_module-technical_data.php (accessed 4.24.18).

Terdich, N., Martinez-Botas, R., 2013. Experimental Efficiency Characterization of an Electrically Assisted Turbocharger, in: 11th International Conference on Engines & Vehicles. p. 122. https://doi.org/10.4271/2013-24-0122

Thangaraja, J., Kannan, C., 2016. Effect of exhaust gas recirculation on advanced diesel combustion and alternate fuels - A review. Appl. Energy 180, 169–184. https://doi.org/10.1016/j.apenergy.2016.07.096

Thiel, M.P., Klingbeil, a E., Reitz, R.D., 2002. Experimental Optimization of a Heavy-Duty Diesel Engine Using Automated Genetic Algorithms, in: SAE 2002 World Congress & Exhibition. p. 7191.

Thomas, J., 2014. Particle swarm optimization based model predictive control for constrained nonlinear systems. 2014 11th Int. Conf. Informatics Control. Autom. Robot. 01, 397–403.

Tian, J., 2015. Particulate Emission Characteristics of a Light Duty Diesel Engine under Transient Operation Conditions. PhD Thesis,University of Birmingham.

Tian, J., Xu, H., Arumugam Sakunthalai, R., Liu, D., Tan, C., Ghafourian, A., 2014. Low Ambient Temperature Effects on a Modern Turbocharged Diesel engine running in

a Driving Cycle. SAE Int. J. Fuels Lubr. 7, 2014-01-2713. https://doi.org/10.4271/2014-01-2713

Turkson, R.F., Yan, F., Ali, M.K.A., Hu, J., 2016. Artificial neural network applications in the calibration of spark-ignition engines: An overview. Eng. Sci. Technol. an Int. J. 19, 1346–1359. https://doi.org/10.1016/j.jestch.2016.03.003

Turner, J.W.G., Popplewell, A., Patel, R., Johnson, T.R., Darnton, N.J., Richardson, S., Bredda, S.W., Tudor, R.J., Bithell, C.I., Jackson, R., Remmert, S.M., Cracknell, R.F., Fernandes, J.X., Lewis, A.G.J., Akehurst, S., Brace, C.J., Copeland, C., Martinez-Botas, R., Romagnoli, A., Burluka, A.A., 2014. Ultra Boost for Economy: Extending the Limits of Extreme Engine Downsizing. SAE Int. J. Engines 7, 2014-01-1185. https://doi.org/10.4271/2014-01-1185

van Aken, M., Willems, F., de Jong, D., 2007. Appliance of High EGR Rates With a Short and Long Route EGR System on a Heavy Duty Diesel Engine. SAE Tech. Pap. 2007-01-0906 2007. https://doi.org/10.4271/2007-01-0906

Wahlstr, J., 2008. Robust Nonlinear EGR and VGT Control with Integral Action for Diesel Engines. Oil &Gas Sci. Technol. – Rev. IFP Energies Nouv. 66, 2057–2062.

Wahlstr, J., Eriksson, L., 2006. Modeling of a Diesel Engine with VGT and EGR including Oxygen Mass Fraction. Department of Electrical Engineering, Linkopings universitet.

Wahlström, J., Eriksson, L., 2011. Modelling diesel engines with a variable-geometry turbocharger and exhaust gas recirculation by optimization of model parameters for capturing non-linear system dynamics. Proc. Inst. Mech. Eng. Part D J. Automob. Eng. 225, 960–986. https://doi.org/10.1177/0954407011398177

Wahlstrom, J., Eriksson, L., Wahlström, J., Eriksson, L., 2011. Modelling diesel engines with a variable-geometry turbocharger and exhaust gas recirculation by optimization of model parameters for capturing non-linear system dynamics. Proc. Inst. Mech. Eng. Part D J. Automob. Eng. 225, 960–986. https://doi.org/10.1177/0954407011398177

Walker, K., Samadi, B., Gerhard, J., Butts, K., 2016. Design Environment for Nonlinear Model Predictive Control, in: SAE 2016 World Congress and Exhibition. p. 627. https://doi.org/10.4271/2016-01-0627.Copyright

Wang, H.P., Bosche, J., Tian, Y., El Hajjaji, A., 2011. Two loop based dynamical feedback stabilization control of a diesel engine with EGR and VGT. Proc. IEEE Conf. Decis. Control 1596–1601. https://doi.org/10.1109/CDC.2011.6160792

Wang, S.W., Yu, D.L., Gomm, J.B., Page, G.F., Douglas, S.S., 2006. Adaptive neural network model based predictive control for air-fuel ratio of SI engines. Eng. Appl. Artif. Intell. 19, 189–200. https://doi.org/10.1016/j.engappai.2005.08.005

Wang, Y., 2018. Control and Calibration of Vehicle Systems For Real World Fuel Economy & Emissions, in: Advaned Powertain Conference. p. 22.

Wang, Z., Su, Q., Luo, X., 2016. A novel HTD-CS based PID controller tuning method for time delay continuous systems with multi-objective and multi-constraint optimization. Chem. Eng. Res. Des. 115, 98–106. https://doi.org/10.1016/j.cherd.2016.09.025

Watson, H.C., Ratnawera, A., Halgamuge, S., 2006. Optimization of all SI engine combustion control and related events for efficiency. SAE Tech. Pap. https://doi.org/10.4271/2006-01-0045

Watson, N., Janota, M.S., 1982. Turbocharging the Internal Combustion Engine. Macmillan Education UK, London. https://doi.org/10.1007/978-1-349-04024-7

Watson, N., Marzouk, M., 1977. A non-linear digital simulation of turbocharged diesel engines under transient conditions, in: 1977 International Automotive Engineering Congress and Exposition. https://doi.org/10.4271/770123

Wei, L., Yan, F., Hu, J., Xi, G., Liu, B., Zeng, J., 2017. Noxconversion efficiency optimization based on NSGA-II and state-feedback nonlinear model predictive control of selective catalytic reduction system in diesel engine. Appl. Energy 206, 959–971. https://doi.org/10.1016/j.apenergy.2017.08.223

Wickman, D.D., Senecal, P.K., Reitz, R.D., 2001. Diesel Engine Combustion Chamber Geometry Optimization Using Genetic Algorithms and Multi-Dimensional Spray and Combustion Modeling, in: SAE 2001 World Congress. https://doi.org/10.4271/2001-01-0547

Wijetunge, R.S., Brace, C.J., Hawley, J.G., Vaughan, N.D., Horrocks, R.W., Bird, G.L., 1999. Dynamic Behaviour of a High Speed Direct Injection Diesel Engine. https://doi.org/10.4271/1999-01-0829

Xin, Q., Xin, Q., 2013. 13 – Diesel engine air system design, Diesel Engine System Design. https://doi.org/10.1533/9780857090836.4.860

Xu, F., Chen, H., Gong, X., Mei, Q., 2016. Fast nonlinear model predictive control on FPGA using particle swarm optimization. IEEE Trans. Ind. Electron. 63, 310–321. https://doi.org/10.1109/TIE.2015.2464171

Xu, F., Chen, H., Hu, X.G.Y.F., 2013. Engine Idle Speed Control Using Nonlinear Model Predictive Control. IFAC Proc. Vol. 46, 171–176. https://doi.org/10.3182/20130904-4-JP-2042.00119

Xue, X., Caton, J. a., 2012. Detailed multi-zone thermodynamic simulation for direct-injection diesel engine combustion. Int. J. Engine Res. 13, 340–356. https://doi.org/10.1177/1468087411435206

Xue, X., Rutledge, J., 2017. Potentials of Electrical Assist and Variable Geometry Turbocharging System for Heavy-Duty Diesel Engine Downsizing. SAE Tech. Pap. 2017-01-10. https://doi.org/10.4271/2017-01-1035

Yang, J., Zhang, Z., chen, L., Wang, Y., 2013. Optimization of a High Speed Gasoline Engine Using Genetic Algorithm 2–7. https://doi.org/10.4271/2013-01-1626

Yang, X.-S., 2014. Chapter 1- Nature-Inspired Optimization Algorithms, in: Nature-Inspired Optimization Algorithms. pp. 1–21. https://doi.org/10.1016/B978-0-12-416743-8.00001-4

Yang, Z., Yang, Y., Yang, H., Zhang, L., 2014. An improved particle swarm optimization method based on chaos, in: 2014 10th International Conference on Natural Computation (ICNC). IEEE, pp. 209–213. https://doi.org/10.1109/ICNC.2014.6975836

Yang Zifei, 2014. Improving the conversions between the various passenger vehicle fuel economy/CO2 emission standards around the world | International Council on Clean Transportation [WWW Document]. URL http://www.theicct.org/blogs/staff/improving-conversions-between-passenger-vehicle-efficiency-standards (accessed 8.15.17).

Ye, Y., Yin, C.-B., Gong, Y., Zhou, J., 2017. Position control of nonlinear hydraulic system using an improved PSO based PID controller. Mech. Syst. Signal Process. 83, 241–259. https://doi.org/10.1016/j.ymssp.2016.06.010

Yokomura, H., Kouketsu, S., Kotooka, S., Akao, Y., 2004. Transient EGR Control for a Turbocharged Heavy Duty Diesel Engine. SAE 2004 World Congr. Exhib. 1–120.

Zacharof, N., Tietge, U., Franco, V., Mock, P., 2016. Type approval and real-world CO2and NOxemissions from EU light commercial vehicles. Energy Policy 97, 540–548. https://doi.org/10.1016/j.enpol.2016.08.002

Zamboni, G., Capobianco, M., 2013. Influence of high and low pressure EGR and VGT

control on in-cylinder pressure diagrams and rate of heat release in an automotive turbocharged diesel engine. Appl. Therm. Eng. 51, 586–596. https://doi.org/10.1016/j.applthermaleng.2012.09.040

Zamboni, G., Capobianco, M., 2012. Experimental study on the effects of HP and LP EGR in an automotive turbocharged diesel engine. Appl. Energy 94, 117–128. https://doi.org/10.1016/j.apenergy.2012.01.046

Zhang, F., 2013. SPRAY , COMBUSTION AND EMISSION CHARACTERISTICS OF DIESELINE FUEL. University of Birmingham.

Zhang, Q., Pennycott, A., Burke, R., Akehurst, S., Brace, C., 2015. Predicting the Nitrogen Oxides Emissions of a Diesel Engine Using Neural Networks. https://doi.org/10.4271/2015-01-1626.Copyright

Zhang, W., Chen, Z., Li, W., Shu, G., Xu, B., Shen, Y., 2013. Influence of EGR and oxygen-enriched air on diesel engine NO-Smoke emission and combustion characteristic. Appl. Energy 107, 304–314. https://doi.org/10.1016/j.apenergy.2013.02.024

Zhang, X., Wang, H., Zheng, Z., Reitz, R.D., Yao, M., 2016. Effects of late intake valve closing (LIVC) and rebreathing valve strategies on diesel engine performance and emissions at low loads. Appl. Therm. Eng. 98, 310–319. https://doi.org/10.1016/j.applthermaleng.2015.12.045

Zhang, X.D.Z.L.J., 2015. PSO based on chaotic Map and Its Application to PID Controller Self-tuning, in: 16th International Conference on Electronic Packaging Technology (ICEPT). IEEE, pp. 1470–1476. https://doi.org/10.1109/ICEPT.2015.7236860

Zhang, Y., Lu, G., Xu, H., Li, Z., 2017. Tuneable model predictive control of a turbocharged diesel engine with dual loop exhaust gas recirculation. Proc. Inst. Mech. Eng. Part D J. Automob. Eng. https://doi.org/10.1177/0954407017726944. https://doi.org/10.1177/0954407017726944

Zhang, Y., Zhou, Q., Li, Z., Li, J., Xu, H., 2018. Intelligent transient calibration of a dual-loop EGR diesel engine using chaos-enhanced accelerated particle swarm optimization algorithm. Proc. Inst. Mech. Eng. Part D J. Automob. Eng. https://doi.org/10.1177/0954407018776745. https://doi.org/10.1177/0954407018776745

Zhao, D., Liu, C., Stobart, R., Deng, J., Member, S., Winward, E., Dong, G., 2014. An Explicit Model Predictive Control Framework for Turbocharged Diesel Engines.

IEEE Trans. Ind. Electron. 61, 3540–3552.

Zheng, M., Irick, D.K., Hodgson, J., 2002. Stabilizing Excessive EGR With an Oxidation Catalyst on a Modern Diesel Engine. SAE Int. 119–125. https://doi.org/10.1115/ICES2002-455

Zheng, M., Reader, G.T., Hawley, J.G., 2004. Diesel engine exhaust gas recirculation - A review on advanced and novel concepts. Energy Convers. Manag. 45, 883–900. https://doi.org/10.1016/S0196-8904(03)00194-8

Zheng, Y., Qiu, H., Niu, R., Li, S., Member, S., 2011. Horizon-Varying Model Predictive Control for Accelerated and Controlled Cooling Process. IEEE Trans. Ind. Electron. 58, 3–6.

Zhou, F., Peng, H., Zeng, X., Tian, X., Peng, X., 2017. RBF-ARX model-based robust MPC for nonlinear systems with unknown and bounded disturbance. J. Franklin Inst. https://doi.org/10.1016/j.jfranklin.2017.10.002

Zhou, J., Fiorentini, L., Canova, M., 2014. A Softly Switched Multiple Model Predictive Control of A Turbocharged Diesel Engine, in: 2014 American Control Conference.

Zhou, J., Fiorentini, L., Canova, M., Wang, Y.-Y., 2015. Coordinated Performance Optimization of a Variable Geometry Compressor With Model Predictive Control for a Turbocharged Diesel Engine. IEEE Trans. Control Syst. Technol. 1–1. https://doi.org/10.1109/TCST.2015.2468085

Zhou, Q., Zhang, W., Cash, S., Olatunbosun, O., Xu, H., Lu, G., 2017a. Intelligent sizing of a series hybrid electric power-train system based on Chaos-enhanced accelerated particle swarm optimization. Appl. Energy 189, 588–601. https://doi.org/10.1016/j.apenergy.2016.12.074

Zhou, Q., Zhang, Y., Li, Z., Li, J., Xu, H., Olatunbosun, O., 2017b. Cyber-Physical Energy-Saving Control for Hybrid Aircraft-Towing Tractor based on Online Swarm Intelligent Programming. IEEE Trans. Ind. Informatics 3203, 1–1. https://doi.org/10.1109/TII.2017.2781230

Zhou, X., Li, Y., Hu, Y., Chen, H., 2015. Torque tracking control of turbocharged gasoline engine using nonlinear MPC, in: 2015 European Control Conference, ECC 2015. pp. 2958–2963. https://doi.org/10.1109/ECC.2015.7330987

Zhu, Q., Koli, R., Feng, L., Onori, S., Member, S., Prucka, R., 2017a. Nonlinear Model Predictive Air Path Control for Turbocharged SI Engines with Low Pressure EGR

and a Continuous Surge Valve, in: American Control Conference. pp. 4741–4746. https://doi.org/10.23919/ACC.2017.7963688

Zhu, Q., Onori, S., Member, S., Prucka, R., 2017b. An Economic Nonlinear Model Predictive Control Strategy for SI Engines : Model-Based Design and Real-Time Experimental Validation. IEEE Trans. Control Syst. Technol. 1–15.

Zitzler, E., Laumanns, M., Thiele, L., 2001. SPEA2: Improving the Strength Pareto Evolutionary Algorithm, Evolutionary Methods for Design Optimization and Control with Applications to Industrial Problems. https://doi.org/10.1.1.28.7571